Feedback-Controlled Functional Electrical Stimulation to Restore Upper Extremity Functions

. . .

Improving the Clinical Feasibility of Elaborated Neuroprosthetic Devices by Automatic Adaptation and Feedback of Muscle-Recruiment

vorgelegt von
Dipl.-Ing. Christian Klauer
geboren in Bad Kreuznach

von der Fakultät IV – Elektrotechnik und Informatik
der Technischen Universität Berlin
zur Erlangung des akademischen Grades

Doktor der
Ingenieurwissenschaften
– Dr.-Ing. –

genehmigte Dissertation

Promotionsausschuss:
Vorsitzender: Prof. Dr.-Ing. Friedel Gerfers
Gutachter: Prof. Dr.-Ing. Jörg Raisch
Gutachter: Dr. Chris Freeman (University of Southampton)
Gutachter: Prof. William Holderbaum (University of Reading)
Tag der wissenschaftlichen Aussprache: 25. Januar 2018

Berlin, 2019

ABSTRACT

This thesis considers Neuro-prosthetic systems using Functional Electrical Stimulation (FES) to restore or support motor functions in neurologically impaired patients. An often encountered difficulty is the precise control of limb motion by adjusting the stimulation intensity. The musculoskeletal systems involving muscle mechanics, limb motion dynamics, and muscle recruitment due to FES and possibly volitional activity are highly complex and non-linear. Hence, the stimulation effect is hard to model and predict. An intensive effort during a calibration phase would be required to adapt models describing such systems to the full extent, which is unfeasible in clinical environments or at home. Further, many parameters vary under the rapid progression of muscle fatigue with FES. Hence, most practically relevant devices focus on simple open-loop strategies that trigger pre-defined stimulation patterns on different events caused by the user. This thesis presents new methods to improve the applicability and movement precision of closed-loop FES systems and applies them to practically relevant applications to support or to restore functional arm reaching movements in entirely or partially paralyzed patients.

The compensation of muscle fatigue and the linearization of the highly non-linear process of muscle recruitment is addressed in this thesis. Electromyography (EMG)-measurements can give insight into the muscular recruitment process. Therefore, a feedback of the stimulation-evoked EMG (eEMG) enforcing the desired recruitment level is presented. Because of this enforcement, a more predictable behavior is obtained such that muscles are much easier to model and control using this method as an underlying feedback loop. The positive effects on the predictability are shown in a study involving five healthy subjects. Further, the applicability of this approach was successfully tested in two stroke patients.

In partially paralyzed patients it is often beneficial to take account the residual volitional activity to, e.g., realize a user-control of the neuroprosthesis. Devices exist that control FES based on a measurement the volitional EMG (vEMG). The low signal to noise ratio, however, typically leads to many restrictions in control performance. Hence, a different approach based on angular measurements is presented: An arm weight relief is realized by a FES-activation proportional to the elevation angle. This FES-activation reduces the required volitional effort significantly as demonstrated in five healthy subjects. In two acute stroke patients, arm function could be partially and fully restored, respectively, as long as the controller was active.

For patients who have a complete paralysis of the upper extremity, the functional restoration of movements is difficult due to the numerous degrees of freedom (DoF). Hence, a system using a combination of a passive, light-weight exoskeleton with FES is proposed, wherein each DoF can be locked by brakes to reduce muscle fatigue during holding-postures and to guide movements. FES is feedback controlled, and the movement precision was evaluated in five healthy subjects showing a sufficient performance for performing simple reaching tasks.

Further considered aspects include the improvement of motor precision by artificially introducing co-activations in antagonistic muscle pairs and the potential reduction of muscle fatigue by varying the stimulation frequency as desired for the contrary objectives "motor precision" and "muscle fatigue." For the former aspect, a non-linear system inversion based approach is developed to realize desired joint torques and co-activation levels and, further, applied to joint angle control yielding good results in a healthy subject. For the latter, a time-discretization method for linear time-invariant systems is presented that also considers variable sampling rates. Further, a system linearization approach is suggested allowing to apply standard discrete-time controllers for variable sampling rate systems.

KURZFASSUNG

Diese Dissertation beschäftigt sich mit der Erforschung von Algorithmen zur Regelung von Neuroprothesen, die Funktionelle Elektrostimulation (FES) verwenden, um motorische Funktionen in neurologisch beeinträchtigten Patienten wiederherzustellen oder zu unterstützen. Die Generierung von feinmotorischen Bewegungen mittels einer Regelung der Stimulationsintensität ist oftmals schwierig. Da die involvierten biomechanischen Systeme sehr komplex und nichtlinear sind, ist der Effekt der Stimulation nur schwierig durch Modelle beschreibbar. Es wäre ein sehr hoher Zeitaufwand notwendig, um die Parameter eines solchen Modells für die jeweiligen Patienten anzupassen. Mit der schnell fortschreitenden Muskelermüdung bei Anwendung von FES ändern sich diese Parameter typischerweise im Laufe der Zeit so stark, dass nach kurzer Zeit eine neue Anpassung vorgenommen werden muss. Die meisten praktisch relevanten Ansätze konzentrieren sich deshalb auf einfache aber robuste Steuerstrategien ohne die Rückführung von Messgrößen und die Verwendung von komplexen Modellen. Hierbei werden oftmals fest einprogrammierte Stimulationsverläufe verwendet, die durch den Benutzter initiiert werden.

Ein wichtiger Teil der Dissertation beschreibt eine neue Methode, mit der sich der Bedarf eines komplexen Modells bei der FES-Regelung zum großen Teil erübrigt. Eine Reduzierung der Komplexität wird hierbei durch eine unterlagerte Regelung der Muskelrekrutierung erreicht, welche durch eine Messung des FES-evozierten Elektromyogramms (EMG) bestimmt wird. Damit verbessert sich die Anwendbarkeit und die Feinmotorik mittels geregelter FES. In einer Studie mit fünf gesunden Probanden wurde gezeigt, dass dadurch z.B. der Einfluss muskulärer Ermüdung kompensiert wird und das nichtlineare muskuläre Ansprechverhalten teilweise linear wird. Dieser neue Ansatz der Rekrutierungsregelung wurde in praktisch relevanten Systemen zur Unterstützung/Wiederherstellung von Armbewegungen bei teilweise/komplett Gelähmten im Rahmen meiner Dissertation angewandt.

Bei teilweise gelähmten Patienten ist es sinnvoll, die noch vorhandene Restaktivität des Patienten zur Steuerung der Neuroprothese zu verwenden. Hierzu gibt es bereits Geräte, die die FES anhand einer Willkür-EMG-Messung steuern. Allerdings beschränkt das schwache Signal zu Rauschverhältnis des Willkür-EMG die erzielbare Feinmotorik der Bewegungen. In der Dissertation wurde deshalb ein anderer Ansatz zur Unterstützung der Armhebung vorgestellt, welcher mittels einer Messung des Gelenkwinkels die Willkürаktivität indirekt einbezieht. Hierbei wird eine Armgewichtsunterstützung durch Generierung einer mit dem Winkel proportional ansteigenden Muskelrekrutierung erzielt. Bei fünf gesunden Probanden konnte gezeigt werden, dass dies die willkürliche Armhebungen erleichtert. Bei zwei Schlaganfallpatienten konnte der Bewegungsumfang im einen Fall teilweise und im anderen Fall vollständig wiederhergestellt werden.

Bei Patienten mit einer kompletten Lähmung der oberen Extremität ist die Wiederherstellung von Armfunktionen mittels FES durch die hohe Anzahl an Freiheitsgraden in der Bewegung sehr schwierig. Um dieses Problem zu lösen, wird eine Kombination aus geregelter FES mit einem leichten passiven Exoskelett zur Führung der Bewegungen und zur partiellen Gewichtsentlastung vorgeschlagen. Die einzelnen Freiheitsgrade können dafür mit Bremsen blockiert werden, was auch stabile Armhaltungen bei abgeschalteter FES ermöglicht. Die Positioniergenauigkeit der Hand mit dem System wurde bei fünf Probanden untersucht und ist ausreichend genug, um funktionelle Bewegungen des täglichen Lebens durchzuführen.

Eine weitere Untersuchung der Dissertation beinhaltet die Verbesserung der Feinmotorik durch eine künstliche Koaktivierung in antagonistischen Muskelpaaren. Hierzu wird ein Regelungsansatz vorgestellt, der gewünschte Momente und Koaktivierung einstellt. Dieser wurde in einer Gelenkwinkelregelung an einem gesunden Probanden erfolgreich erprobt.

ACKNOWLEDGEMENTS

First and foremost, my gratitude belongs to my advisors Prof. Jörg Raisch and Dr. Thomas Schauer for hosting and continuously supporting me and my research. Further, acknowledgments go to the evaluators of my doctoral thesis Dr. Chris Freeman and Prof. William Holderbaum and, further, to Prof. Friedel Gerfers for chairing the doctoral committee.

Furthermore I'd like to thank my colleagues, especially Holger Nahrstaedt for providing support for his Physiosense EMG-measurement device that allowed first investigations on recruitment control, Markus Valtin for the support with the RehaMove Pro EMG measurement device that was used in the meantime, Constantin Wiesener for sharing his expertise in Simulink realtime code generation, Dr. Thomas Seel for proofreading of various publications and valuable discussions on numerous topics, and Dr. Thomas Schauer for proofreading this thesis, sharing his scientific expertise, and the support in controller design and numerous experiments. I like to thank Astrid Bergman for technical support and building electronic items during the past ten years.

I, further, would like to acknowledge Mirjana Ruppel for her assistance in clinical trials, and the realization of various computer-animations, Maximilian Irmer, who greatly contributed to the implementation of the model for hybrid muscle activations described in Appendix A, and Arne Passon, who strongly contributed to the pre-investigations in potential control schemes to realize an arm-weight relief control system. I further acknowledge Stefan Ruppin and Sven Knuth for implementing a generic graphical interface (PaPI), with which the performed experiments were controlled. Steffen Schäperkötter contributed to the very first investigations in recruitment control. Finally, I like to acknowledge Clara Menzen, Lars Hichert, Constantin Wiesener, Mirjana Ruppel, Lilli Kuen, Holger Nahrstaedt, Markus Valtin, Thomas Seel, and Lia Strenge for proofreading and numerous suggestions for the improvement of readability.

From the beginning, back in 2010, my research was accompanied by the research group NearLab, Politecnico Milano. Especially, I like to thank Emilia Ambrosini and Simona Ferrante, who tirelessly supported me within numerous hours spent in the laboratory and the clinic to develop and test the hybrid system for the restoration of reaching functions (Chapter 5). Further, Alessandra Pedrocchi for coordinating the surrounding research project and many useful discussions on the control concept. Moreover, they gave many fruitful pieces of advice to the evaluation of the recruitment control presented Chapter 3.

The investigations on the control of antagonistic muscle pairs (Chapter 6) are based on previous investigations performed by Pierfrancesco Spagnol. Thanks for his contributions to the development the model and the identification routine, the design of the controller was made possible.

The clinical evaluation of recruitment control (Chapter 3) and the arm weight relief control (Chapter 4) were made possible by Uri Shiri, Sebastian Böttcher, Dr. Frank Dähne, and Prof. Ingo Schmehl from Unfallkrankenhaus Marzahn (ukb), Berlin. They performed the screening of patients suitable to participate in the studies and contributed in the investigations in stroke patients.

TABLE OF CONTENTS

ACRONYMS

ADL	activities of daily living
ANN	artificial neural network
AP	action potential
ARAT	action research arm test
ARX	autoregressive exogenous
BCI	brain computer interface
CNS	central nervous system
CV	conduction velocity
EMG	electromyography
eEMG	evoked EMG
vEMG	volitional EMG
DoF	degree of freedom
DS	direct stimulation
FET	functional electrical therapy
FES	functional electrical stimulation
ILC	iterative learning control
IMU	inertial measurement units
LLM	local linear model
LTI	linear time invariant
MAV	mean absolute value
MDF	median frequency
MNF	mean frequency
MIMO	multiple input multiple output
MMAC	multiple-model adaptive control
NRMSE	normalized root mean squared error
P-control	proportional control
PD-control	proportional, derivative control
PID-control	proportional, derivative, and integral control
RC	recruitment control
RMS	root mean squared
SCI	spinal cord injury
SISO	single input single output
SMC	sliding-model control

1

INTRODUCTION

Neuroprosthetic systems are technical devices that electrically connect to the nervous system to obtain and influence sensory information or to induce motor functions. For the latter case, Functional Electrical Stimulation (FES) is a commonly used method that applies electrical pulses to the motor-nerves to trigger action potentials that generate muscle contractions. The application of the electricity is typically performed via surface electrodes but also implanted electrodes may be used [154].

For many neurological impairments, e.g., caused by stroke or Spinal Cord Injury (SCI), the restoration of motor functions by FES is feasible. To obtain or support functional movements, the stimulation intensity must herein be carefully adjusted by control algorithms. The restoration of precise motor functions, however, is difficult to achieve as the musculoskeletal system is of high complexity and uncertainty: The stimulation effect is commonly difficult to model and predict due to the highly non-linear, uncertain, and time-varying behavior of the muscle and, hence, is difficult to control. There is a strong variance of the muscle's response to FES depending on the positioning of electrodes and across different subjects [114, 112]. Compared to the lower extremities, motor functions are complex in case of the upper extremities due to the higher number of Degrees of Freedom (DoF) and the number of involved muscles.

Successful applications of FES, e.g., include cycling in SCI patients, the generation of wrist and finger extension movements in stroke patients and the support of foot elevation movements in patients suffering from the drop-foot syndrome. Further, Functional Electrical Therapy (FET) [141] is used in the rehabilitation of stroke patients to train reaching and grasping functions. For these purposes, several commercial, multi-purpose stimulation devices are available on the market, whereby products targeting clinical environments can often be programmed by clinicians to fulfill specific rehabilitation tasks. These systems focus on reliable, commonly simple open-loop strategies often using pre-defined stimulation patterns that are triggered by the user, for example, utilizing switches. In the more elaborate case, the residual volitional activity is detected by evaluating Electromyography (EMG)-measurements (cf. Sec. 2.5) from the stimulated or another muscle and then utilized for user-control, for example, StiWell, MED-EL Medical Electronics, Innsbruck, Austria. All these devices typically require a precise tuning of stimulation intensity and timing parameters.

As the main advantage of the open-loop approach, a reliable operation and a fast donning procedure feasible to daily-use are achieved. However, due to the open-loop nature, changes in muscle conditions, e.g., the fast progression of muscle fatigue under FES, cannot be automatically detected and compensated. This fact commonly leads to an increased effort of required manual intervention as the complexity of the task to perform increases. Further, the potential regarding motor precision and complexity is limited.

To overcome the limits of the open-loop control approaches as typically found in clinically relevant solutions, feedback control may be used that is expected to have a high potential. Such

approaches often incorporate a feedback of the generated movement for compensating deviations from desired movement paths by performing a real-time adjustment of the intensity of FES. Because of the rapid progression in the development of small-sized Inertial Measurement Units (IMUs), it became feasible to measure limb motion in real-time with small effort (e.g., [127]). This measurement renders the implementation of motion controllers feasible concerning the effort spent for attaching devices to the human body.

Closed-loop FES control is still difficult to realize, however. The variety of encountered difficulties includes, among others, the complexity of the musculoskeletal system, which makes the effects of FES, e.g., in terms of joint angles, difficult to model and predict. Herein, a huge problem is the reliable prediction of the muscle force that depends on many factors, e.g., the number and frequency of recruited motor units, fiber length, and contraction speed.

The field of control engineering provides answers in form of sophisticated control approaches to the treatment of the mentioned difficulties of complexity, fatigue, uncertainty, and variance. Nonlinear feedback control with elaborate system identification algorithms and adaptive control approaches to adapt the control system to the individual patient, electrode placement, and muscle condition could be used, however. These approaches rely on detailed mathematical models of the complex musculoskeletal system [148].

Adapting such models to the individual subject and muscle condition typically introduces a high effort in the application of the neuroprosthesis due to long-lasting calibration procedures that must be applied to the patient each time the electrodes are attached. Once calibrated, they may become unreliable under the fast progression of muscle fatigue caused by FES. This fact renders such approaches unfeasible for usage in clinical applications. Further, as the complexity of feedback-controlled FES increases it becomes harder to keep the susceptibility to errors within reasonable limits, as many special conditions (e.g., the patient's interaction with the device suddenly changing) need to be considered. Finally, the huge amount of uncertainty in the musculoskeletal system that cannot be captured in models renders most elaborate control approaches infeasible to apply. In practice, this significantly hinders the development of feedback-controlled neuro-prosthetic systems that can involve many degrees of freedom actuated by more than one muscle to restore precise motor functions [114, 112]. In general, feedback-controlled FES – even for the lower limbs – remains a technology that has been investigated in laboratories for over four decades up to now without any significant breakthrough leading to commercial devices.

- A first approach to consider uncertainty is the application of robust control schemes. They are designed to tolerate deviations in the assumed model parameters or even in the model structure. The main cost of the robustness is, however, often paid by a lower control performance (e.g., achieved movement speed) see [155, 129].

  For the restoration of simple motor tasks, the situation is more relaxed. For example, for the foot elevation [115], feedback control seems clinically feasible. Often, there is still room for improvement concerning the automatic tuning to the individual and the adaptation to muscle fatigue, though.

- As a second approach, if the intended purpose of the specific neuroprosthesis allows, it is often helpful to reduce the complexity of the motion that shall be realized. This reduction may be achieved by an external mechanical device (e.g., an exoskeleton) that performs a guidance of movements by reducing the degrees of freedom (e.g., [147]). Such an approach

will be considered in this work: For the restoration of reaching functions in completely paralyzed patients, e.g., after a high-level spinal cord injury, the combination of FES with a passive, lightweight exoskeleton to guide movements has been evaluated. The main drawback is, however, a potentially reduced mobility of the resulting support system.

- This thesis presents a third approach to treat the high amount of uncertainty without relying on mechanical devices or robust control. Joint angle feedback in form of traditional (non-linear) control alone is often not sufficient to obtain a satisfying control performance. To deal with the uncertainty, an approach is presented that introduces additional measurements of the internal state of the muscle. Therefore, a feedback of the stimulation-evoked EMG (eEMG) is proposed to estimate and control the level of muscle recruitment. This approach lowers the influence of a large class of uncertainty and further compensates for the effects of muscle fatigue. Neuroprosthetic applications that are based on this approach, therefore, have lower requirements on complex models and, hence, the calibration effort can be reduced.

As one application that relies on the eEMG feedback approach, a neuroprosthesis for stroke patients suffering from a paresis in the arm elevation is presented. Herein, the compensation for the effects of muscle fatigue is not possible by solely measuring joint angles. This neuroprosthesis restores precise, user-controlled movements by amplifying residual volitional activity. To further improve FES, joint angle control with co-activations to increase motor precision in antagonistic muscle pairs and the variation of the stimulation frequency to reduce muscle fatigue are considered.

1.1 Contributions to the State of the Art

Thesis contributions to the state of the art are:

1. A method to estimate the muscular recruitment level using the FES-evoked EMG and a control scheme to control the recruitment level (Chapter 3),
2. A control strategy to amplify weak volitional activity by FES yielding the effect of a weight compensation (Chapter 4),
3. An assistive neuroprosthetic system combining a passive light-weight exoskeleton and FES to artificially restore upper-arm function in patients with complete paralysis in the arm (Chapter 5),
4. A control strategy for joint angle control in antagonistic muscle pairs based on a non-linear exact inversion controller that generates co-activations when the direction of movement changes (Chapter 6), and
5. A variable sampling rate stimulation to reduce muscular fatigue (Chapter 7). Herein, an analytical method for the time-discretization of irregularly sampled and actuated linear time-continuous systems is derived.

Additionally, a potential extension to the control system described in Chapter 4 is presented in the appendix of this thesis:

6. A dynamic model to describe the joint angle for volitionally and FES activated (hybrid) muscles. (Appendix A).

Future work is, however, required to adapt and integrate the proposed model into the methods presented in this thesis.

1.2 Related Publications by the Author

The following publications, in which I was involved, are related to the work presented in this thesis.

Recruitment control, arm weight support & hybrid muscle activation

- [85] C. Klauer, J. Raisch, and T. Schauer. "Linearisation of electrically stimulated muscles by feedback control of the muscular recruitment measured by evoked EMG". in: *Proc. of the 17th International Conference on Methods and Models in Automation and Robotics 2012*. Międzyzdroje, Poland: IEEE, 2012, pp. 108–113. ISBN: 978-1-4673-2124-2. DOI: 10.1109/MMAR.2012.6347902.
- [84] C. Klauer, J. Raisch, and T. Schauer. "Feedback Control of the Electrical Stimulation Induced Muscular Recruitment Determined by the Evoked Electromyogram". In: *Biomedical Engineering / Biomedizinische Technik* 57.Suppl. 1, Track-F (2012), pp. 639–639. ISSN: 1862-278X. DOI: 10.1515/bmt-2012-4417.
- [83] C. Klauer, J. Raisch, and T. Schauer. "Advanced Control Strategies for Neuro-Prosthetic Systems". In: *Proc. of the 4th European Conference on Technically Assisted Rehabilitation - TAR 2013*. Berlin, Germany, 2013.
- [82] C. Klauer, A. Passon, J. Raisch, and T. Schauer. "Virtual Weight-Compensating Exoskeleton using λ-Controlled FES". in: *Proc. of Automed 2013*. Dresden, Germany, 2013.
- [81] C. Klauer, M. Irmer, and T. Schauer. "A muscle model for hybrid muscle activation". In: *Current Directions in Biomedical Engineering* 1.1 (2015), pp. 386–389. ISSN: 2364-5504. DOI: 10.1515/cdbme-2015-0094.
- [8] E. Ambrosini, T. Schauer, C. Klauer, A. Pedrocchi, G. Ferrigno, and S. Ferrante. "Control system for neuro-prostheses integrating induced and volitional effort". In: *IFAC-PapersOnLine*. 9th IFAC Symposium on Biological and Medical Systems BMS 2015, Berlin, Germany, 31 August-2 September 2015 48.20 (2015), pp. 327–332. ISSN: 2405-8963. DOI: 10.1016/j.ifacol.2015.10.160.
- [80] C. Klauer, S. Ferrante, E. Ambrosini, U. Shiri, F. Dähne, I. Schmehl, A. Pedrocchi, and T. Schauer. "A patient-controlled functional electrical stimulation system for arm weight relief". In: *Medical Engineering & Physics* 38.11 (2016), pp. 1232–1243. DOI: 10.1016/j.medengphy.2016.06.006.
- [93] C. Klauer and Schauer T. "Two-Channel Muscle Recruitment (λ)-Control using the Evoked-EMG". in: *Proc. of the 20th Annual International FES Society Conference 2016*. La Grande Motte, France, 2016.

- [88] C. Klauer and T. Schauer. "Adaptive Control of a Neuroprosthesis for Stroke Patients Amplifying Weak Residual Shoulder-Muscle Activity". In: *Proc. of the 20th World Congress of the International Federation of Automatic Control, 9-14 July 2017*. Toulouse, France, 2017.
- [125] P. Meyer-Rachner, A. Passon, C. Klauer, and T. Schauer. "Compensating the effects of FES-Induced Muscle Fatigue by Rehabilitation Robotics During Arm Weight Support". In: *Current Directions in Biomedical Engineering, Proc. of the 6th European Conference on Technically Assisted Rehabilitation – TAR 2017*. Berlin, Germany, 2017. DOI: 10.1515/cdbme-2017-0007.
- [87] C. Klauer, M. Ruppel, and T. Schauer. "FES-based arm weight relief: First investigations in stroke patients". In: *Abstract in Proc. of the 6th European Conference on Technically Assisted Rehabilitation – TAR 2017*. Berlin, Germany, 2017.

Control under complete paralysis

- [90] C. Klauer, T. Schauer, J. Karner, W. Reichenfelser, E. Ambrosisni, S. Ferrante, and J. Raisch. "Design of feedback control strategies for an arm neuroprothesis combined with an exoskeleton". In: *Converging Clinical and Engineering Reseach on Neurorehabilitation - Part II, ICNR 2012*. Springer, 2012, pp. 1189–1193. ISBN: 978-3-642-34545-6.
- [135] A. Pedrocchi, S. Ferrante, E. Ambrosini, M. Gandolla, C. Casellato, T Schauer, C. Klauer, J. Pascual, C. Vidaurre, M. Gfoehler, et al. "MUNDUS project: MUltimodal Neuroprosthesis for daily Upper limb Support". In: *Journal of neuroengineering and rehabilitation* 10.66 (2013), pp. 1–20. DOI: 10.1186/1743-0003-10-66.
- [92] C. Klauer, T. Schauer, W. Reichenfelser, J. Karner, S. Zwicker, M. Gandolla, E. Ambrosini, S. Ferrante, M. Hack, A Jedlitschenka, A. Duschau-Wicke, M. Gföhler, and A. Pedrocchi. "Feedback Control of arm movements using Neuro-Muscular Electrical Stimulation (NMES) combined with a lockable, passive exoskeleton for gravity compensation". In: *Frontiers in Neuroscience* 8.262 (2014). DOI: 10.3389/fnins.2014.00262.

Modelling, identification & control of antagonistic muscle pairs

- [174] P. Spagnol, C. Klauer, F. Previdi, J. Raisch, and T. Schauer. "Modeling and Online-Identification of Electrically Stimulated Antagonistic Muscles for Horizontal Shoulder Abduction and Adduction". In: *Proc. of the European Control Conference 2013*. Zürich, Switzerland: IEEE, 2013, pp. 3979–3984. ISBN: 978-3-033-03962-9.
- [86] C. Klauer, J. Raisch, and T. Schauer. "Nonlinear Joint-Angle Feedback Control of Electrically Stimulated and Lambda-Controlled Antagonistic Muscle Pairs". In: *Proc. of the European Control Conference 2013*. Zürich, Switzerland: IEEE, 2013, pp. 3101–3107. ISBN: 978-3-033-03962-9.
- [184] C. Vidaurre, C. Klauer, T. Schauer, A. Ramos-Murguialday, and K.R. Müller. "EEG-based BCI for the Linear Control of an Upper-Limb Neuroprosthesis". In: *Medical Engineering & Physics* 38.11 (2016), pp. 1195–1204. DOI: 10.1016/j.medengphy.2016.06.010.
- [153] M. Ruppel, C. Klauer, and T. Schauer. "Towards a High Motor-Precision Neuroprosthesis by Recruitment-Controlled Antagonistic Muscle Co-activation Strategies". In: *Abstract*

in Proc. of the 6th European Conference on Technically Assisted Rehabilitation – TAR 2017. Berlin, Germany, 2017.

- [152] M. Ruppel, C. Klauer, and T. Schauer. "Enhancing the smoothness of joint motion induced by functional electrical stimulation using co-activation strategies". In: *Current Directions in Biomedical Engineering* 3.2 (2017), pp. 155–159. ISSN: 2364-5504. DOI: 10.1515/cdbme-2017-0033.

Variable stimulation rates

- [89] C. Klauer and T. Schauer. "Discretisation & Control of Irregularly Actuated and Sampled LTI-Systems". In: *Proc. of the 19th International Conference on Methods and Models in Automation and Robotics, IEEE*. Międzyzdroje, Poland, 2014. ISBN: 978-1-4799-5081-2. DOI: 10.1109/MMAR.2014.6957394.

1.3 Theses Supervised by the Author

- Master Thesis: Upper-Limb Neuroprosthesis for Weight-Support via Feedback-Controlled Multichannel Functional Electrical Stimulation, Dirk Reinhardt, 2016
- Master Thesis: Untersuchung des Informationsgehalts der beim elektrisch stimulierten Muskel hervorgerufenen EMG-Antwort, Christian Jaenicke, 2015
- Bachelor Thesis: Modelling, Identification and Control of the Hysteresis occurring in the Recruitment Function of Electrically Stimulated Muscles, Erick Ersada, 2013
- Master Thesis: A Hybrid Model for Joint Angle Prediction of Electrically and Voluntarily Activated Muscles Using EMG-Measurements, Maximilian Irmer, 2012
- Master Thesis: Weight Compensation for the Upper Limb by Evoked EMG-Controlled Electrical Stimulation, Arne Passon, 2012
- Bachelor Thesis: Modellbildung der Beziehung zwischen Stimulationsstärke und eEMG-Signal elektrisch stimulierter Muskeln, Steffen Schäperkötter, 2011
- Master Thesis: Comparison of Decoupling Strategies for Use in Multivariable Motion Control Systems applied to the Human Limb, Yeqin Gong, 2011

1.4 Outline of the Thesis

This thesis presents a variety of methods and applications contributing to the control of FES-based neuroprostheses for upper-limb function support and restoration. Presented are fundamental theoretical methods, approaches to reduce difficulties in the control of FES-activated muscles and complete neuroprosthetic systems ready to be applied to patients. In this section, an overview is given on how the individual parts are related.

Recruitment control To enable an automatic adaptation of the FES system and a reliable operation, an approach that uses a feedback of the stimulation effect at muscular level is presented in

Chapter 3. The amount of artificially recruited motor units by the FES is assessed by analyzing the evoked electromyogram. Exploiting this information enables the control of the muscle activation and, thereby, compensates, e.g., for the effects of muscle fatigue. As a major achievement, the approach enforces a simple linear relationship between the commanded activation level and the muscular stimulation effect. The resulting feedback-controlled muscle behavior is then much easier to model and control and simplifies the design of on-top movement or posture controllers. The effectiveness of this method is shown for the upper limbs in a pilot study involving five healthy subjects and two stroke patients. The approach has been incorporated into the control systems presented in Chapter 4 and 6.

Amplification of residual volitional activity To effectively support arm elevation movements in partially paralyzed patients, it is desirable to incorporate the potentially weak residual volitional activity into the control of FES. By performing an amplification of the residual muscle activity using FES, a completely patient-driven control of movements is possible. This is important in the rehabilitation of stroke patients, as it has been shown that the synchronous application of FES to the patient induced movements enhances the process of motor re-learning [17, 167, 52]. Further, such systems could be applied to support stroke and SCI patients in daily-live activities by extending the achievable range of motion. In the past, several approaches on volitional control (as compared in Sec. 2.8.1) were presented. Many rely on electromyography measurements to detect the volitional muscle activity which is then used to control FES. As it is difficult to obtain EMG during active stimulation, only imprecise control is possible leading to jerky movements. An improved concept to support the shoulder elevation is therefore presented in Chapter 4. Herein, based on the measured elevation angle, a FES-induced muscle recruitment is generated that yields a pre-specified percentage (support factor) of this angle – yielding an arm weight relief. The developed system has no limitations on the type of supported motor tasks as the entire movement is entirely controlled by the patient, and it has similar effects as realized by external mechanical devices (e.g., spring-based mechanisms) for arm weight support. The control system internally uses the developed recruitment control method to enable long-term operation without the need of a re-calibration.

In tests involving five healthy subjects, a significant reduction of the required volitional activity was achieved, while a precise positioning of the arm elevation by the user was possible. Further, in a stroke patient with an almost complete paralysis in the shoulder elevation, the maximal arm-elevation level could be significantly increased. In a second patient who had a milder paresis, however, still hindering functional movements, arm functions could be fully restored while applying the system.

As the already tested control system requires the manual tuning of the support level, an adaptive control strategy, that automatically adjusts the support factor, was developed. Herein, the volitional EMG is used during repetitive trials to realize the optimal amount of FES support such that the full range of the volitional activity is available to control the neuroprosthesis. This automatic tuning was tested in two experiments on one healthy subject.

The presented system is suitable for patients if at least weak residual volitional muscle activity is present (e.g., stroke, incomplete SCI or traumatic brain injury).

Combining FES and volitionally evoked muscle activations In the presented weight compensation controller, the muscle is activated volitionally and by FES at the same time (hybrid muscle activation). In the design of the control system, a static linear model is used, although the actual behavior is non-linear and dynamic. To further improve the controller performance, a model based on an Artificial Neural Network (ANN) is proposed in Appendix A to describe hybrid muscle activations in terms of the joint angle.[1] Tunable parameters are adapted to the individual subject by a system identification approach using previously recorded I/O data. The model has been validated in two healthy subjects yielding RMS values well sufficient for the desired application. It is strongly expected that the use of such a model can further improve the interplay between residual volitional activity and FES support.

Assistive system for SCI-patients with a complete paralysis In the case of SCI patients with complete paralysis, the restoration of reaching function using FES is difficult due to the high number of degrees of freedom in the upper extremity.

In Chapter 5, a feedback-controlled system to restore arbitrary arm movements using a combination of FES and a passive, gravity compensating, exoskeleton is presented. The developed system allows to automatically move the patient's hand to an arbitrary position given in 3D coordinates. Using the light-weight exoskeleton, all degrees of freedom can be locked by brakes, enabling the patient to maintain postures without the need of active FES. Further, a spring-based mechanism is used to effectively reduce the arm weight. This weight reduction significantly reduces FES-induced muscle fatigue and hence enlarges the applicability of the proposed system. To confirm this statement, a study involving five healthy subjects was performed.

Co-activation strategies In the natural generation of movements, motor precision is achieved by a simultaneous contraction of multiple contrary acting muscles. This phenomenon leads to an increase of the mechanical stiffness in the joints and, therefore, enhances motor precision and stability of postures.

Co-activation, allowing the modulation of the mechanical impedances, can also be artificially induced using FES and a great potential to improve FES-induced motion is expected [26]. Indeed, more than twenty years ago it was demonstrated, that the involvement of co-contractions can significantly increase the performance of control systems using FES for actuation [36].

As muscle fatigue progresses, the level of co-activation is likely to gradually decrease in time for the same stimulation levels. Further, most commonly, the individual contribution of each involved muscle cannot be estimated as only measurements of the summation of all individual muscle contraction effects are typically available. Therefore, a reliable generation of a desired level of co-activation is difficult to realize by FES. Further, a periodically repeated re-calibration of the control system is then required to adapt the generation of co-activation to the current muscle fatigue state.

However, the recruitment control method introduced in Chapter 3, now allows overcoming the present difficulties in co-activation control. Therefore, a joint angle control approach using exact

[1] The developed model is listed in the appendix of this thesis as it – in its current state – cannot be directly used in combination with the methods, e.g., recruitment control proposed in this thesis. The required adjustments are minor, though, and consider the model's input variables (a change from the stimulation intensity to the estimated muscle recruitment must be performed).

linearization is presented in Chapter 6 that introduces co-activations as a result of the exact inversion of the model equations. The co-activation strength can be externally adjusted so that in situations with a high demand on motor precision the joint stiffness can be temporarily increased.

Variable stimulation frequencies Compared to voluntary activation, FES activated muscles are subjected to a fast progression of muscle fatigue Sec. 2.2. This fact can severely hinder functional tasks in the long term. For achieving the same resulting muscular force, a higher stimulation frequency (and smaller intensity) leads to a faster proceeding of muscular fatigue, compared to a lower stimulation frequency (and higher intensity) [78]. However, more frequently applied pulses typically enable a better performance in time-discrete control systems. Therefore, typically a compromise between the progressing of muscular fatigue and control performance is chosen. Herein, fixed frequencies ranging from 20 to 60 Hz are used, whereby the stimulation intensity remains the only actuation variable. For temporarily increasing the control performance, an obvious approach could be to increase the actuation rate for periods during which it is beneficial (e.g., during fast movements), while for periods of low activity (e.g., holding a position) the actuation rate may be lowered. However, the effect of continuously adjusting the actuation times must be included in the discretized model. Therefore, in Chapter 7, a general framework for discretizing LTI systems with variable times for sampling and additionally actuation is presented, and a general linearizing controller for the obtained discrete-time models is proposed that compensates the effects introduced by the irregular time intervals.

2

FUNDAMENTALS & STATE OF THE ART

This chapter introduces the reader to the fundamentals relevant to the neuro-prosthetic systems developed in this thesis. This includes the basics of muscle fiber activation, Functional Electrical Stimulation (FES), and Electromyography (EMG). Further, the commonly used approach to model the behavior of FES-activated muscles is presented.

In the second part of this chapter, the state of the art in controlled FES is reviewed, whereby the focus lies on the upper extremity. This part is separated into the restoration of reaching functions and, second, model-based control of FES.

2.1 Background

Spinal Cord Injury (SCI) and stroke are significant causes of neurological impairments often leading to reduced motor capabilities. Per year, more than one million people in Europe suffer from a stroke according to the World Health Organization (WHO) [181]. This number is expected to even rise in the future due to demographic changes and the increase of life expectancy leading to an increased demand in rehabilitation-techniques and assistive devices for use at home.

A SCI causes, depending on the level of the lesion, a loss of motor and sensory functions, and results in the immobilization of the patient [24]. Cervical (neck) injuries usually result in a full or partial tetraplegia (paralysis of the arms, legs, and trunk). Individuals with a complete lesion at the C7 level or above usually depend on attendant care for all daily-live activities. In some cases, the paralysis is incomplete so that residual volitional activity might be partially present. SCI at the high C3 and C4 level result in a significant loss of function at elbow and shoulder level. Deltoid and the biceps muscles are innervated from the C5 and C6 level of the spinal cord. These muscles may be also denervated (lower motor neuron lesion), especially in case of C4 tetraplegia. However, the extent of denervation is likely to vary across individuals.

Stroke patients often suffer from a reduced volitional muscle activity that may hinder functional movements, whereby compared to SCI patients, the impairment is typically only present in one side of the body (hemiplegia) [62]. In this case, it is often possible to regain motor functions for the impaired extremities because of the plasticity of the central nervous system. This can be achieved by an intensive repetitive training of individual motor functions in a manually assisted therapy. Herein, the basic concept is to perform training sessions in which the patient is supposed to repeatedly perform arm movements that mimic functional movements from daily life. Since the voluntary activity is often not sufficient to fulfill the desired training-tasks, typically a therapist assists. Sometimes also passive rehabilitation devices for guiding movements or even active robotic devices are used (under the supervision of a therapist).

For severe impaired arm functions where no residual voluntary activity is present, the rehabilitation progress in a manual therapy is commonly minor. Therapy concepts in which patients

perform an active training without assistance cannot be applied because of the lack of residual voluntary motor functions. Hence, in the past, for the corresponding patients, manual therapy typically concentrated not on the motor relearning, but instead on the rehabilitation of Activities of Daily Living (ADL) by using the unimpaired hand to perform ADL and on the mobility.

Devices used in rehabilitation To lower the effort of the manual assistance in guiding movements, many devices have been invented that allow patients to train without assistance given by the physiotherapist. In this case, also the rehabilitation of motor relearning seems feasible in patients suffering from severe impaired arm functions as it is reasonable to apply training sessions more often.

The broad range of available devices [99, 116] starts with passive mechanical devices in which the guidance of the (partially) paralyzed side is performed by the unimpaired side (e.g. RehaSlide, Reha-Stim Medtec GmbH, Berlin, Germany). More elaborate devices (In the sense of technological effort) use spring-based mechanisms (e.g. Armeo Spring, Hocoma AG, Switzerland) or motor-actuated wires connected to the upper limb (Diego, Tyromotion, Austria) to perform an arm weight relief. This leads to a reduced volitional effort required to perform movements. A robotic device (Armeo Power, Hocoma AG, Switzerland) that performs a complete guidance of all degrees of freedom of the upper extremity using impedance-controlled motors is the most technologically elaborate device so far with respect to the effort spent on motorization and control. Such devices allow patients to perform their training mostly on their own. Further, an on-screen biofeedback is often used to motivate the patient. However, such devices are often complex, immobile, and last but not least expensive. Further, the benefit concerning the rehabilitation outcome in comparison to manual therapy is questionable [99].

Functional Electrical Stimulation In the case of stroke and SCI patients, by the application of Functional Electrical Stimulation (FES), muscle contractions can be artificially induced, even if muscles are completely paralyzed. This enables the potential to restore and support limb functions. To obtain precise functional movements, the amount of stimulation must be precisely adjusted by means of an automatic control-system.

FES has been successfully applied in the rehabilitation of stroke patients as well as in Spinal Cord Injury (SCI) for daily-live support of motor functions [131]. Electrical Stimulation (ES) can be further used in a therapy to treat spastic co-activations [100] and shoulder pain [96, 41]. For these purposes, a number of commercial devices – some targeted to special FES-applications (e.g. drop-foot compensation, hand and finger extension, FES-cycling) – are available on the market.

As another rehabilitation approach for stroke patients, FES can be used in repetitive training movements to guide and support movements in a therapy yielding a similar potential as given by active robotic devices. This may have beneficial effects on the process of motor re-learning, if the volitional training movements are synchronously supported, meaning the movement induced by FES-support goes into the same direction as the voluntarily intended [52, 17, 167]. This is typically exploited by Functional Electrical Therapy (FET) [141].

Other typical clinical applications of FES include the correction of drop foot in stroke patients [115] in daily-life and the support of wrist and finger extension.

Table 1: *Motor unit / muscle fiber classification and their properties.*

fiber type	resistance to fatigue	conduction velocity of enervating axon / nerve	axon diameter	time to contract	size of motor unit	intensity of the evoking stimuli
Type-I	resistant	slow	small	long twitch	small, less fibers	high
Type-II-A	resistant	intermediate	intermediate	fast twitch	intermediate	high
Type-II-B	fast fatigable	fast	large	fast twitch	large, many fibers	low

Combinations of robotic devices / orthosis and FES Such hybrid approaches were developed for rehabilitation purposes as well as for daily-live support. Many systems for the realization of reaching functions were presented in which mechanical surroundings perform a weight compensation and a guidance of movements that are induced by FES. The benefits include a slower progression of muscle fatigue due to the weight compensation and simplified requirements for the control of FES due to the guidance of movements. Additionally, many commercially available devices for stroke rehabilitation were extended with FES [147] with the aim to exploit the beneficial impact of FES on motor relearning. Many of these approaches are subject to to ongoing research. In the case of active devices, the surrounding actuation may take over the generation of training-movements initially generated by FES as muscle fatigue increases, hence, allowing a longer and more intensive training. A review of currently available approaches is given in Sec. 2.7.

2.2 Muscle Fiber Types, Motor Units, and Recruitment

Each muscle in the human body is made of a large number of muscle fibers. Herein, each fiber is assigned to a motor unit, which forms the lowest instance in the generation of motor function and involves many further muscle fibers. All fibers belonging to one motor unit are connected to one lower motoneuron (alpha motoneuron) via enervating axon / nerve fibers as illustrated in Fig. 1. The number of motor units per muscle may range from 100 in small, e.g., hand muscle to 1000 in, e.g., limb muscles. Almost all motor units and, further, their enervated muscle fibers belong to one of three main classes Type-I, Type-II-A and Type-II-B subjected to different properties as shown in table 1 [101, 70, 124].

The main distinctive feature that differs among these classes is the resistance to the fatigue and the time required to develop a contraction in response to a stimulus. Fibers of Type-I require a longer time to contract than fibers of Type-II. The latter class is further subdivided into Type-II-A that is more resistant to fatigue and Type-II-B that is subjected to fibers suffering from a faster progression of fatigue. However, the fatigue resistant classes (Type-I and Type-II-A) require a higher intensity of the evoking stimuli. The size of the motoneuron varies and increases with the number of muscles fibers belonging to the motor unit.

The lower motor neuron is connected to the upper motor neuron located in the brain via one nerve fiber. It spreads the activation stimuli to the individual muscle fibers in the form of action

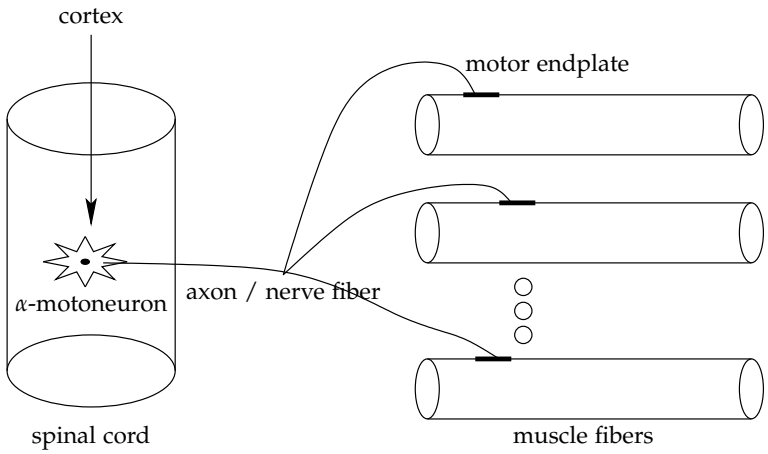

FIGURE 1: *Schematic illustration of one motor unit. (Figure adapted from [101])*

potentials transmitted via the axon (cf. Fig. 1). The conduction velocity (CV), i.e., the propagation velocity of the depolarization along the axon, is different for each type of motor unit.

Each time a motor unit is recruited by a single stimulus, all muscle fibers are activated for a certain duration (in the order of 80 ms) [124]. By repetitive application of stimuli, the individual responses superpose to a smooth muscle activation. Dependent on the fiber extension and, further, on how fast the fibers are extended or compressed, a muscle torque is generated in response to the muscle activation.

To achieve a continuous muscle contraction, potentially involving multiple motor units, the activation stimuli must be applied successively at a rate greater than approximately 10 Hz such that the individual effects of each applied stimuli superpose to a smooth contraction.

To develop muscle forces, different combinations of firing rates, the number and type of activated motor units, and the firing rate are possible. The central nervous system uses rules to determine how to adjust the individual parameters depending on the desired force to, e.g., retard the onset of muscle fiber fatigue. Herein, in one principle, called spatial recruitment or Henneman's size principle, the smaller, slow twitching and fatigue-resistant motor units are activated first to induce slight muscle tension. To further increase the contraction strength, the larger, fast twitching, and fast fatiguing motor units are activated additionally [101]. Herein, the larger motor units (involving more muscle fibers) generate more force for one single stimulus than smaller motor units. This principle does not fixate the firing rate (temporal recruitment) or the number of recruited motor units; hence, further rules are involved by the central nervous system that determines these two remaining parameters unambiguously. For example, typically the firing rate is further modulated by the central nervous system.

2.3 Functional Electrical Stimulation (FES)

Functional Electrical Stimulation (FES) is a technique in which artificially generated electrical stimuli, commonly in form of successive pulses, are applied to motor nerves [154]. They induce an artificial recruitment of motor units by inducing action potentials in the corresponding

motoneurons. The application of the electricity is typically performed via surface electrodes but also implanted electrodes may be used – however, suffering from an intensive invasive effort.

The common strategy of applying the electrical current[2] is in form of bi-phasic stimulation pulses as illustrated in Fig. 2. Herein, the generated force can be modulated by the current amplitude and/or pulse width of the applied stimuli (spatial recruitment) or by the rate of stimuli (temporal recruitment). In spatial recruitment, the delivered charge, i.e., the product of current amplitude and pulse width is affecting the amount of recruited motor units and, hence, also the muscular activation.

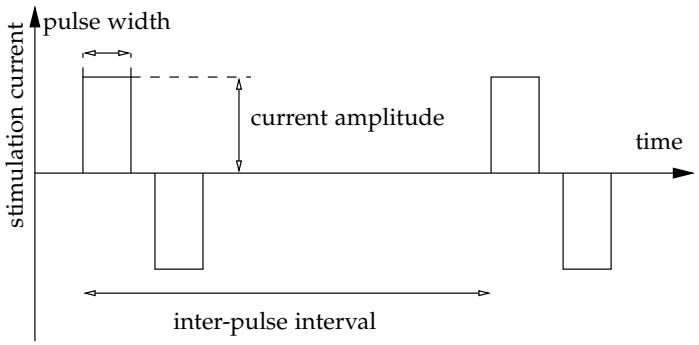

FIGURE 2: *Biphasic stimulation pulses: Two rectangular shaped pulses are applied one after the other, whereby the second one is applied with an opposite current direction to minimize galvanic effects in combination with the material of the stimulation electrodes. This aims to prevent tissue damages [136].*

Because of their larger axon diameter of the corresponding motor unit (cf. Table 1), Type-II-B muscle fibers are activated at lower intensities of external electrical pulses compared to fibers of Type-I and Type-II-A. Hence, for low levels of FES-induced muscle contraction, mostly fast fatiguing fibers (Type-II-B) are involved. This is in contrast to the natural recruitment as formulated by Henneman's size principle in which smaller motor units (fewer muscle fibers and smaller axon diameters) of Type-I and Type-II-A are activated at first. Because of the primary activation of the fast fatiguing Type-II-B fibers, a more rapid progression of muscle fatigue in FES-activated muscles is observed.

For constant stimulation intensities, the same motor units are recruited for each stimulus. This is contrary to natural recruitment in which motor unit activations are distributed over all available units in a timely alternating fashion to generate a resulting torque that is uniformly caused by all available muscle fibers. Herein, the individual motor unit is recruited less often in time compared to FES activation. This contradiction further contributes to changing muscle-response properties to FES. Because of these reasons [154], the treatment of muscular fatigue forms another challenge in the control of FES.

In stroke as well as SCI patients the neural pathway from the Central Nervous System (CNS) to the muscles may be interrupted leading to a complete or partial paralysis. The muscles themselves retain their ability to contract and produce force when the muscle is not denervated, i.e., the lower motor neuron is still intact. FES applied to the lower motor neurons can replace the lacking

[2]The electrical current passing the stimulation electrodes is commonly controlled within the stimulation device by adjusting the voltage in-between the electrode pair.

signals from the CNS [167] such that, e.g., arm movements can be artificially introduced. Hence, FES is long proven technique for inducing muscular contractions in patients suffering from upper neuron motor lesion and is often used for rehabilitation purposes or in neuroprosthesis for restoring lost motor functions [133]. Typically, stroke patients and people with spinal cord injury can benefit from FES. If, however, the lower motoneuron is damaged and the corresponding muscle denervated, e.g., due to other neurological diseases, the artificial muscle activation by FES is difficult – however possible with sufficiently high stimulation intensities [119].

This thesis focuses on the application of FES to the upper limbs to restore and support arm functions.

2.4 Charge Control

To modulate the intensity of FES, three parameters (pulse width, current amplitude, and stimulation frequency) may be adjusted. Therefore, multiple degrees of freedom are available to influence the level of muscle activation. The most common approach is to modulate (or dynamically adjust) the pulse width within a range of 0 to 500 μs and to fixate the current amplitude to a level ranging from 0 to 120 mA. In almost every application, the stimulation frequency is kept constant between 20 to 60 Hz.

All experiments and control systems presented in this thesis use the charge control-method [166] in which the current amplitude I and the pulse width pw are adjusted to realize a given charge $Q = pw \times I$ for one sub-phase of the bi-phasic stimulation pulse as shown in Fig. 3.

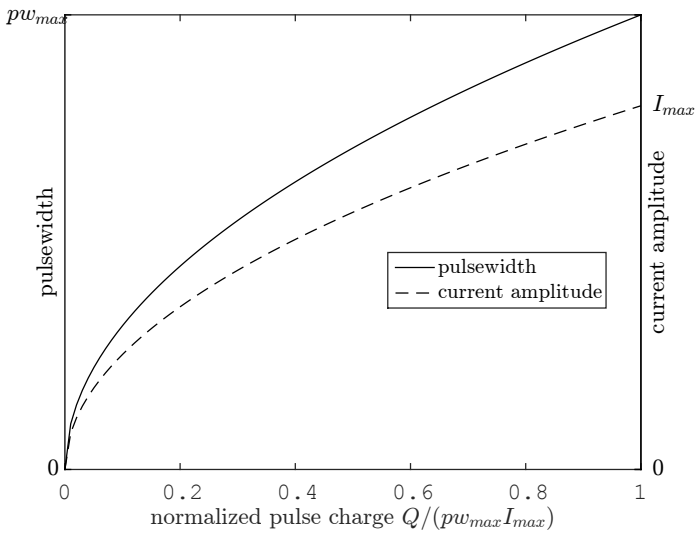

Figure 3: *Current amplitude and pulse width of the bi-phasic stimulation pulses as a function of the pulse charge Q.*

Herein, a given charge Q is equally distributed to pulse width and current amplitude as follows:

$$pw = \sqrt{\frac{Q\, pw_{\max}}{I_{\max}}}, \quad I = \sqrt{\frac{Q \times I_{\max}}{pw_{\max}}}, \quad 0 \leq Q \leq (I_{\max}\, pw_{\max}),$$

wherein $pw_{\max}$ and $I_{\max}$ are the maximal values of pulse width and current amplitude, respectively.[3]

The pulse charge Q is limited by a maximal level Q_{max} in the individual application. This maximum may be chosen such that the stimulation intensity does not go beyond the linear region of the muscle recruitment function (cf. Sec. 2.6) or such that the stimulation pulses do not become unpleasant in case of subjects with remaining sensation. In case of adaptive control schemes, a value going beyond the linear region may be used such that there is some room left for the compensation of fatigue.

Stimulation intensities in form of pulse charges are commonly inconvenient for visualization or parameter adjustment purposes. To simplify the handling of the numeric values, a normalized stimulation intensity in form of a percentage value $v \in [0, 1]$ is introduced as follows

$$v = Q/Q_{\max},$$

so that 0 % means no stimulation and $v = 1$ refers to the maximally tolerated stimulation level.

2.5 Electromyography (EMG)

Electromyography (EMG) [124] is a technique to measure the electrical responses produced during muscle contractions. During motor unit recruitment, the command signal is transmitted from the lower motor neuron to the associated muscle fibers by electrophysiological and electrochemical processes. Each activation of the nerve fibers causes an electrical depolarization called Action Potential (AP) that is spread within the tissue surrounded by the muscle as explained in Sec. 2.2. The activation of multiple motor units causes a superposition of the individual action potentials. Please note that this activation can be caused volitionally or due to FES. Even a combination of both activation types (hybrid muscle activation) is visible in the EMG.

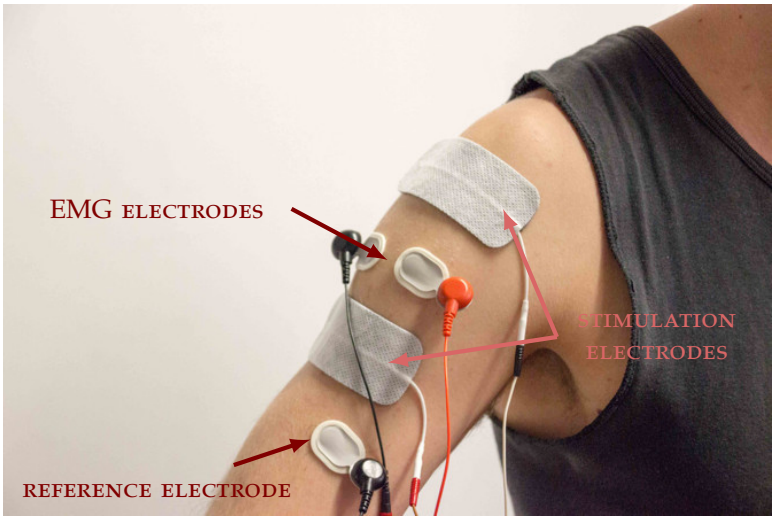

Figure 4: *Exemplary placement of stimulation- and EMG electrodes on the shoulder deltoid muscle.*

[3] In the experiments described in this thesis, these values were fixed to the maximal values that the used stimulation device (RehaStim Pro, HASOMED GmbH, Germany) can generate: $pw_{max} = 500\,\mu$s and $I_{max} = 120\,$mA.

When recording EMG, this superposition is measured by a pair of electrodes (typically Ag/AgCl-electrodes) attached to the surface of the skin above the muscle (as illustrated in Fig. 4). Alternatively, percutaneous needle electrodes might be used that also allow intra-muscular measurements. Typically, if the estimation of the volitional EMG (vEMG) is the primary focus, the electrode pair is placed in the fiber direction in between the stimulation electrodes with an interelectrode distance of 20 mm if no FES is applied to the muscle. In case vEMG is obtained from a stimulated muscle, the electrode pair may be placed orthogonal to the direction of the electrical current to reduce the influence of the stimulation pulse on the acquisition device. This potentially reduces disturbances in the measurement of EMG.[4] Most commonly, an additional reference electrode is used with which the EMG-acquisition device can compensate external electrical disturbances. This electrode is typically placed in electrically inactive areas (i.e., on bony parts). The electrical signal is then sampled at a rate from 1 to 4 KHz.

In case of a voluntary activation, multiple motor units are activated asynchronously at different times. The electrical potentials obtained via the EMG-electrodes are then the superposition of the individual responses yielding a signal that is similar to band-limited white noise (vEMG). Herein, the intensity in terms of the noise amplitude relates to the number of recruited motor units. This amplitude is commonly estimated by calculating the low-pass filtered absolute value of the vEMG-signal or the Mean Absolute Value (MAV) in case of block-wise signal processing.

In contrast to a voluntary activation, the artificial electrical stimulation pulse activates a set of motor units closely synchronously leading to the so-called electrically evoked EMG (eEMG). Herein, the measured EMG additionally includes the potential caused by the electrical stimulation pulses leading to a pulse-shaped artifact in the EMG measurement. A few milliseconds after this artifact the superposition of multiple, closely synchronously caused APs is visible forming a wave-shaped signal that is hence called m-wave. The intensity of this wave depends, among other factors, on the number of the activated motor units and the conduction velocity of the nerve fibers. Exemplary data sampled at 2 KHz for a healthy person is shown in Fig. 5 and Fig. 6.

In digital signal-processing of EMG-data, it is beneficial to evaluate this data block-wise, meaning EMG-data for each inter-pulse interval between the stimulation pulses is combined into a vector $\boldsymbol{EMG}[k]$ for each interval k. In this thesis, it is assumed that the m-wave, as well as the volitional EMG contain information on the recruitment state of the muscle. By appropriate digital filters, a separation and the intensity-estimation of both activation types are possible. An approach to performing this separation and evaluation is presented in Sec. 3.2.2 and 3.2.3.

On the technological side concerning amplifier design, much progress has been made in the previous three decades. In the early investigations, e.g. [172], analog high-gain (up to 200 000) amplifiers were used to measure EMG. The application of FES during an active EMG measurement typically causes these amplifiers to saturate and the subsequent recovery time hinders measurement of the actual EMG-signal. Today, high-resolution analog to digital converters are available on the market. With them, only small amplification factors are required, as the EMG-signals in the range of a few mV are well captured by the resolution of these converters.

[4] Despite these recommendations, the commonly used positioning of EMG-electrodes in the experiments presented in this thesis is outside of the stimulation electrodes as discussed in Sec. 3.1. Experience obtained in previous experiments lead to the conclusion that the stimulation-evoked EMG (eEMG), as introduced in this section, is less dependent on joint movements in this case.

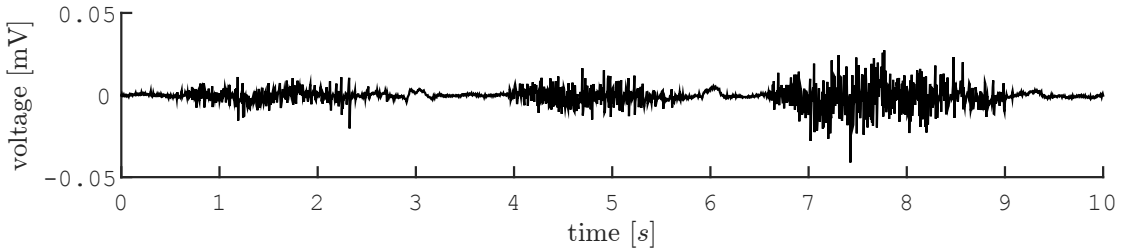

FIGURE 5: *EMG data obtained in the absence of FES only showing three volitional activation periods from the medial deltoid of a healthy subject with a sampling frequency of 2048 Hz.*

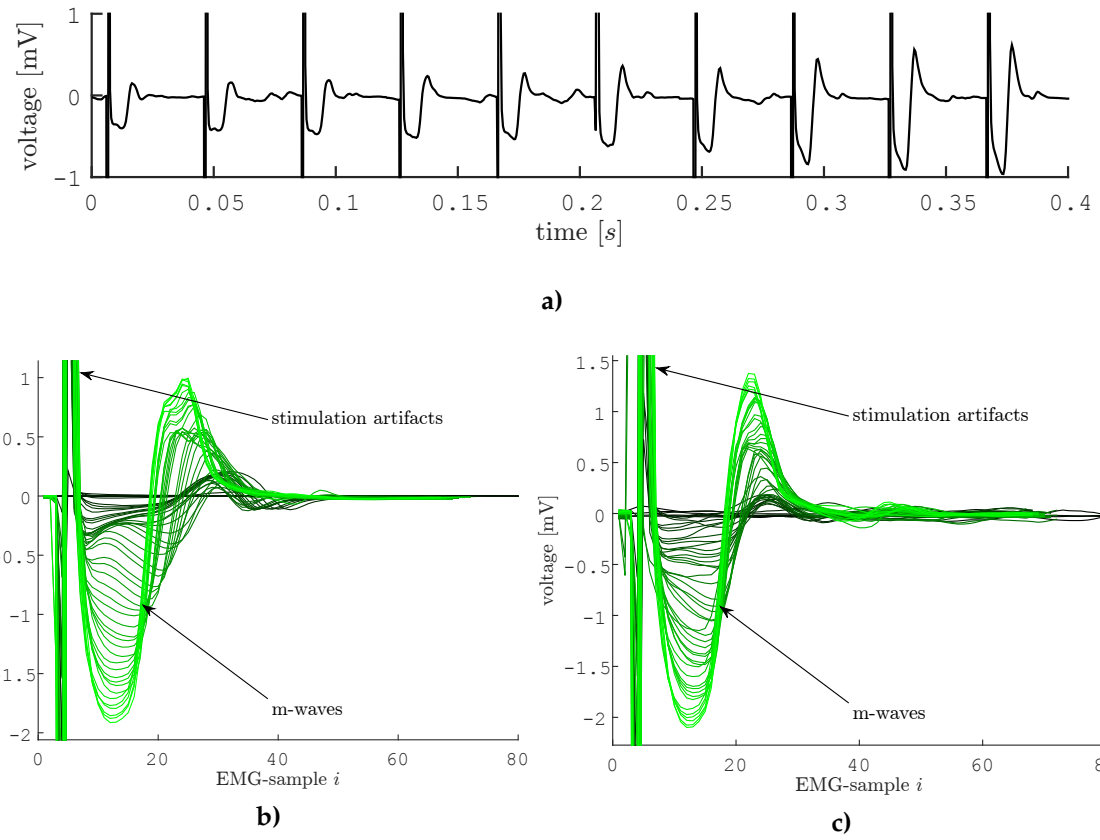

FIGURE 6: *In **a)** sample EMG data obtained during active FES including the stimulation artifacts from the medial deltoid of a healthy subject with a sampling frequency of 2048 Hz are shown. In **b)** and **c)** EMG-data $\boldsymbol{EMG}[k]$ for multiple inter-pulse intervals k are aligned. In **b)** data for the absence and in **c)** for the presence of additional volitional activity are shown.*

Most recently, a 24-bit converter directly suitable for biopotential measurements in form of an integrated circuit[5] became available.

2.6 Muscle Models

To describe FES-induced motions, e.g., in terms of a joint angle, typically a Hill-type model as shown Fig. 7 is assumed [73, 67, 188]. Herein, a Hammerstein structure[6] is used to describe the muscle activation σ, succeeded by a second-order mechanical system is assumed. The internal muscle recruitment state λ is given by the non-linear muscular recruitment function $rc(v)$ which is related to the number of motor units activated by FES[7] which depends on the stimulation intensity v. This static function usually includes a threshold, a saturation and a rise in-between that typically is assumed to be linear as illustrated in Fig. 8 [38]. Ideally, this function only depends on the stimulation intensity. In reality, however, there may be a dependence on fiber length and the speed of its change (directly related to joint angle and angular velocity) because of tissue deformation below the electrodes as indicated by the dashed line as illustrated in in Fig. 7. Additionally, hysteresis effects can be observed [1]. However, in the design of control systems, these dependencies are typically not considered as an intensive identification effort would be required. Additionally, a strong dependency on the progression of muscle fatigue is present.

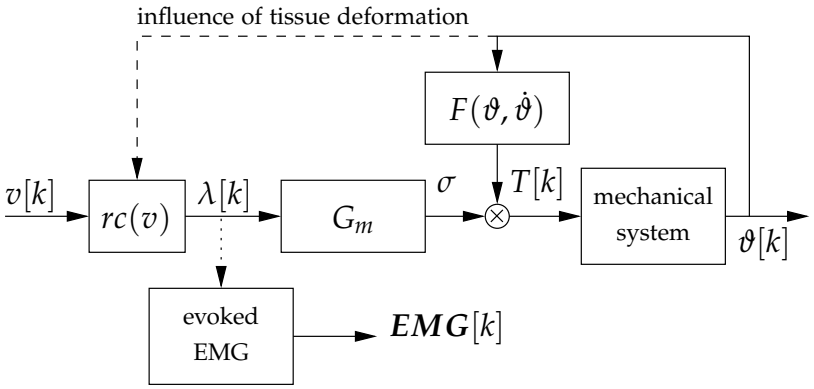

Figure 7: *Assumed neuro-musculoskeletal system for one FES-activated muscle under the absence of volitional activity.*

To describe the dynamic process of muscle activation inside the muscle fibers, a second-order transfer function G_m without transmission zeros is often used yielding the muscle activation σ. It typically consists of a time delay of 0.02 s and a low-pass filter with a rise time around 0.04 s [149]. The muscular torque T is then obtained by the product of the muscle activation and the output of a non-linear function that depends on the joint angle ϑ, and its time-derivative. The function F captures the effect of muscle length and contraction velocity on the contractile force of the muscle.

In addition to the occurrence of a mechanical force, the electrical response $\boldsymbol{EMG}$ is generated (cf. 2.5).

[5] part number ADS1294, Texas Instruments Inc., Dallas, USA

[6] A static non-linear function to which the input(s) are applied in series to a linear time-invariant system.

[7] In this thesis – especially in Chapter 3 – a value proportional to the level of muscle recruitment, i.e., the number of recruited motor units is assumed to be estimated. The factor describing this proportional relationship is unknown. However, it is not required in the methods presented in this thesis.

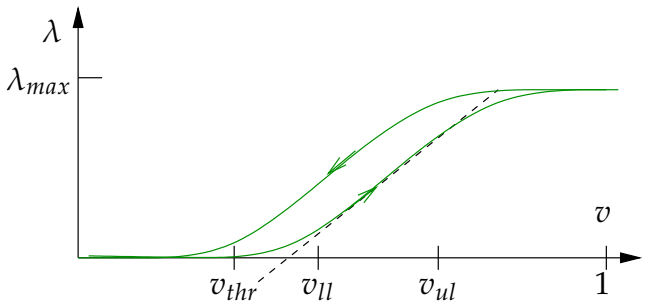

FIGURE 8: *Recruitment function and the commonly used linear approximation within the stimulation range $[v_{ll}, v_{ul}]$. To generate limb movements not acting against gravity, only low muscle forces are required and, hence, low stimulation intensities close to v_{ll} and, hence, also close to v_{thr} are sufficient to generate feasible movements. Therefore, the parameter v_{thr} must be known well in the design of such control systems. For movements acting against gravity, e.g., elevation movements, typically, the whole linear range of the recruitment function is exploited.*

The model presented above implies strong simplifications, as the process of motor unit recruitment and fiber activation is highly complex. However, it is commonly used and has proven to be feasible to the design of control algorithms for FES. A more realistic model was developed by Riener and Quintern [150].

Hybrid muscle activation In addition to FES, the muscle can still be volitionally activated. The volitional and FES-induced activation at the same time is called hybrid muscle activation in this thesis. The process of motor unit recruitment increases in complexity as illustrated by a black-box model in Fig. 9.

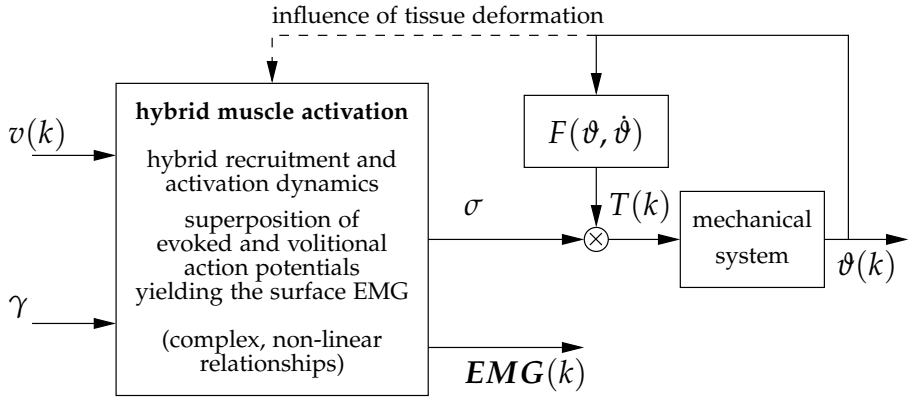

FIGURE 9: *Assumed neuro-musculoskeletal system for one muscle in case of a hybrid muscle activation. Herein the motor units are recruited volitionally (described by the volitional activity γ) and, further, by FES at the same time. The involved neuro-physiological processes are complex and non-linear.*

2.7 Systems to Support Arm Reaching Functions

In the upper extremity, the degree of paralysis – in SCI as well as in stroke patients – varies within a broad range. Often, not all muscles involved in the arm function are affected by a paralysis meaning some muscles remain functional while others are affected. Muscles may also be partially paralyzed, e.g., in stroke patients. Often extensive movements, e.g., the elbow joint extension or the shoulder elevation, may be affected by spasticity hindering the volitional control.

Compared to the application of FES to the lower extremities it seems that less attention has been paid to the upper limbs, especially arm and elbow movements. This narrowed attention might be because motor tasks are harder to accomplish in the upper extremity [191]. Nevertheless, within the past two decades, a couple of neuroprosthetic systems for the restoration or the support in the rehabilitation of upper arm reaching functions were presented. For stroke patients, an overview is given in [94]. The number of stimulated muscles varies in a broad range starting from a simple triceps stimulation to an almost full activation of the most important muscles in the upper extremity including hand functions using transcutaneous or implanted electrodes. Such systems apply to stroke and SCI as well as completely and partially paralyzed patients.

A recent trend is to combine FES with robotic or passive mechanical devices to, e.g., realize a guidance of movements and to reduce muscle fatigue by applying a weight support [147]. The former often yields a simplification of the required control approach to realize the arm motion. Hybrid approaches that combine FES with exoskeleton-like mechanical devices were also presented for SCI patients that are subjected to daily-live support.

Though hand functions also belong to the upper extremity, devices and methods for their restoration are not considered in the ongoing review of the literature, as they form an entire research topic on their own and may be separately treated in parallel to the restoration of reaching functions. An available neuroprosthesis is, e.g., the Freehand system [176].

To be beneficial in daily live environments, the FES-induced arm movements must be triggered or controlled by the user's intention. This intention is typically obtained by voice control, mechanical recordings of unaffected body parts, eye-trackers or the residual volitional activity through EMG obtained from the affected or unaffected body parts. Very recent investigations consider the control of FES to restore reaching and grasping controlled by Brain-Computer Interface (BCI) technology in tetraplegic patients. Often – especially in the case of BCI or eye-tracker technology – a classification is performed yielding to the execution of predefined movement-commands is used. A continuous control, e.g., by adjusting the stimulation intensity proportional to a measured volitional activity (through EMG) is typically difficult to realize.

2.7.1 Systems only relying on FES

In the upper extremity, the actuation of several degrees of freedom using FES, e.g., the inner shoulder rotation, is difficult to achieve as muscles affecting different degrees of freedom of the arm motion are layered over each other. Hence, a selective stimulation is difficult or practically infeasible via surface electrodes. A full restoration of upper extremity function is, therefore, difficult to realize by only using surface electrodes. When using implanted electrodes, the

selectivity improves and a full restoration becomes easier to achieve as demonstrated by, e.g., [161, 160, 76].

As often only some muscles of the upper extremity are affected by a paralysis, the application of FES to these affected muscles is often sufficient to restore reaching – in combination with an appropriate control strategy. The remaining degrees of freedom may still be controlled by the patient's volitional activity. For example, in some approaches, only the triceps muscle is stimulated to support elbow-joint extension movements, while shoulder elevation movements are assumed to remain under volitional control [55, 54].

Stroke Around 2002, Functional Electrical Therapy (FET) has been introduced by Popovic [140, 142] to mimic reaching functions. Herein, Electrical Stimulation (ES) is applied to the partially paralyzed upper limbs of subacute stroke patients. Repetitive training of simulated functional tasks using FES is herein performed that is typically applied in daily 30 minutes sessions over multiple weeks. The applied pre-defined stimulation patterns are triggered by a user-switch.

In more elaborate therapy approaches, Electromyography (EMG)-controlled FES (cf. Sec. 2.8.1) has been applied, e.g., to the biceps or triceps muscle [61]. Herein, FES is controlled by the residual volitional activity of the partially paralyzed muscle, which is assumed to be advantageous for the rehabilitation outcome (cf. 2.1).

Goffredo et al. [56] proposed a FES-assisted rehabilitation system for reaching. A feedforward control algorithm based on an Artificial Neural Controller calculates the stimulation intensities for the flexors and extensors at the shoulder and the elbow. The arm position is observed by a camera set-up and estimated by an image processing algorithm. In this publication, the FES-controller was tested in simulation only.

Spinal Cord Injury (SCI) The feasibility to restore shoulder and elbow functions at least partially by FES was demonstrated by Acosta et al. [2] in persons with C_3/C_4 tetraplegia using percutaneous stimulating electrodes and by Bryden et al. [25] in persons with C_5/C_6 tetraplegia using a fully implanted stimulation system. However, the generated force in individuals with C_3 and C_4 SCI was not sufficient to hold the arm against gravity. In this context, it should also be noted, that a long-lasting electrical stimulation of shoulder and arm muscles typically leads to a significant reduction of the reachable range due to the fast progression of fatigue in electrically stimulated muscles.

In 1994, Popovic et al. [139] proposed a synergistic control approach to realize FES-induced reaching. They found synergies between the shoulder horizontal rotation and the elbow-joint motion in the natural generation of reaching movements. Later, they presented an approach [138] to support reaching movements by applying FES to support elbow extension movements. Reaching is initiated by volitional shoulder movements. Herein, the triceps-stimulation is adjusted on-line based on a continuous joint-angle velocity measurement of the shoulder and elbow joint to detect voluntary movements. Herein, synergies between elbow and shoulder movements were exploited. Tests were performed in eight healthy subjects that were instructed to perform reaching movements volitionally. However, FES was not applied herein. The obtained data was used to determine the present synergies.

To support elbow flexion in C5/C6 tetraplegia, Giuffrida et al. [55] proposed a control system in which the stimulation of the biceps is decreased in a reciprocal way to the volitional activity (determined through EMG) of the biceps. The approach was successfully tested in four tetraplegic patients. A few years later, they proposed a synergistic controller that used volitional activity feed to an ANN to support the elbow extension [54]. Herein, EMG is obtained from eight muscle or muscle portions of the upper extremity except for the triceps that is stimulated. This data forms the inputs of the ANN yielding the stimulation intensity for the triceps. This control concept was successfully evaluated in two patients.

An approach involving the stimulation of an increased number of upper extremity-muscles was presented by Kameyama et al. [76] in the late nineties. They used implanted electrodes to stimulate a total number of 12 muscles responsible for upper extremity function. Fixed stimulation patterns have been previously calculated using a statistical analysis of EMG-data obtained from multiple subjects. The system was tested in six patients – including partial and complete paralysis of the upper extremity – and could successfully restore simple arm-postures in most cases.

Pure FES-induced reaching for completely paralyzed SCI-patients was investigated by Schearer et al. starting around 2014 [161, 160]. They considered an implanted 12-channel FES neuroprosthesis applied to the upper extremity. Their research concentrated on the development of a model and system identification tequnics to be used to implement feedforward controllers. Recently they proposed an approach that uses a quasi-stationary relationship between the stimulation intensities and the resulting arm posture / hand position to implement a feedforward controller to realize reaching movements in presence of paralysis [162]. The controller maps desired shoulder and elbow joint positions to stimulation intensities. In preliminary investigations, a good tracking of the hand position in the lateral direction was achieved. Tracking performance of forward- and backward movements was less, however.

Liao et al. [107] developed a control strategy to restore reaching. However, the concept was only validated in a computer simulation so far.

Jagodnik et al. [74] consider feedback-controlled reaching in a planar plane by optimized PD-controllers. Their investigations, however, focus on simulation studies to determine the robustness of the proposed approach.

To detect the user's intention, Chadwick et al. [29] investigated the feasibility of using human intracortical Brain-Computer Interface (iBCI). Using their set-up, a tetraplegic participant successfully controlled virtual arm movements in a computer simulation that were displayed on a screen. In this simulation, movements were generated by a FES-based muscle activation wherein the stimulation intensities were adjusted by feedback-control.

Most recently, Ajiboye et al. [3] presented the first experimental results on the restoration of reaching and grasping functionality using implanted FES that is user-controlled by an implanted BCI. In this proof-of-concept demonstration involving one tetraplegic, the neural activity in the motor cortex was translated into command signals to control FES that is applied via a total amount of 36 electrodes. They are implanted in the shoulder and the upper- and forearm. Additionally, an active mechanical support for the forearm (also controlled by iBCI) was used to support FES-induced humeral abduction and adduction.

2.7.2 FES combined with mechanical devices

Hybrid approaches that combine FES with passive mechanical or even robotic devices have emerged in the past years [147]. In the rehabilitation of stroke patients, an increased outcome due to the advantages of both approaches is expected. In case of SCI, exoskeleton-like devices were presented. Typically, a weight compensation and a guidance of movements are realized by the mechanical component. Due to the weight compensation, typically lower stimulation intensities are required yielding in a slower progression of muscle fatigue.

Stroke In stroke rehabilitation, often elbow extension movements were considered in the past, e.g., [16, 189, 72]. Systems that also apply FES to the support of shoulder-induced movements are recently emerging, however.

Barker et al. [16] studied the combination of an existing low-cost, nonrobotic training device and FES for rehabilitation. Herein, a passive linear guidance is combined with FES applied to the triceps. FES is triggered by a detection of the volitional EMG and an open-loop control scheme is used to ajust the stimulation intensity. This combination was tested in 10 stroke patients and compared to the training without FES. In both cases, significant improvements in all impairments and activity measures were demonstrated. However, there was no significant improvement by the additional application of FES compared to the results without FES.

The system presented by Wu et al. [189] is similar to [16], however, it adds one more degree of freedom to the guidance, such that arbitrary movements within a horizontal plane become possible. FES is controlled in an open-loop fashion and triggered on the basis of the positioning error. Preliminary results of a study showed that the additional use of FES yields benefits to the rehabilitation process.

Recently, Meyer-Rachner et al. [125] presented a hybrid approach that combines an active, cable-driven robotic system (Diego, Tyromotion GmbH, Austria) and FES applied to shoulder-deltoid muscle to support arm elevation movements. Herein, recruitment control and the arm-weight relief controller presented in this thesis in the chapters 3 and 4, respectively, are used. In addition to FES, the robotic system also performs an arm-weight relief by applying an adjustable, motor-controlled force to the forearm via the wires. The level of weight support is adjustable for FES and the robotic, as well. The system aims at repetitive arm elevation movements. As the progression of muscle fatigue leads to an insufficient support of the arm elevation due to FES, the level of weight support performed by the robotic device is increased while the FES-support level is decreased. The approach was tested in healthy subjects, so far.

Using the same robotic device like the one used in [125], Passon et al. [132] presented an approach that compensates the arm weight by the cable-driven robotic system and, further, applies FES to the anterior- and posterior deltoid, biceps, and triceps. This system aims at breaststroke swimming movements for rehabilitation purposes, wherein horizontal arm movements are generated by FES. In the proposed concept, receptive movements shall be realized, wherein FES is feedback-controlled by an iterative learning vector field. By this vector field, the stimulation intensities are calculated dependent on the joint angles such that the desired movement path is realized. To compensate for deviations, the vector field is updated after each completed trial. The system was evaluated in four healthy subjects.

The group surrounded by Freeman investigated iterative learning control for FES reaching in stroke rehabilitation to realize feedback-controlled positioning in repetitive movements. Compared to the commonly used open-loop, pattern-based strategies, the introduction of iteratively learning feedforward control (ILC)-based learning control forms an elaborate approach to control FES. This control concept relies on repetitive movements. After each trial, the sequences of the actuation variables (i.e., stimulation intensities) are updated such that deviations from the desired arm movement are smaller in the next trial. Starting in 2009, Freeman et al. and Hughes et al. [45, 72] investigated an approach combining a robotic device that performs a guidance of the hand position within a horizontal plane and feedback-controlled FES. They used a combination of a closed-loop controller and iteratively learning feedforward control applied to determine the intensity of a triceps stimulation. The user can initiate the movements by a switch. This approach relies on a mathematical description of the musculoskeletal system whose numerous parameters must be determined by a previously applied system identification procedure, however. Later on, they continued studying iterative learning control in their numerous investigations [72, 121, 120, 48, 97, 98]. Due to iterative learning control, the error between a positioning target trajectory and the achieved movement path could be reduced within a few repetitive trials. The restriction to repetitive movements renders ILC unambiguous to apply for activities of daily life.

More advanced rehabilitation systems consider not only the stimulation of the triceps to support the elbow extension but additionally apply FES to the shoulder deltoid.

The SAIL (stimulation assistance through iterative learning) system presented by Meadmore, Freeman et al. in [121, 46] combines a passive exoskeleton device (Armeo Spring, Hocoma AG, Switzerland) with feedback and feedforward controlled FES. Herein, also an iterative adaptation of the feedforward component is performed. Again, FES is button-triggered.

In a feasibility study involving five stroke patients, Meadmore et al. [120] investigated the GO-SAIL (goal-oriented stimulation assistance through iterative learning) system [48, 97, 98] for stroke rehabilitation. This system combines a passive SaeboMAS arm support (Saebo Inc., Charlotte) with FES applied to the deltoid, triceps and the wrist / finger extensors (cf. Fig. 10). Their results showed an improvement of motor capabilities in case of hybrid FES and the passive arm support alone.

Westerveld et al. [186] used a robotic device (Demcon, Enschede, The Netherlands) to realize reaching. Herein, FES was only used for grasping, however.

Recently, Resquin et al. [146] combined a passive exoskeleton (Armeo Spring, Hocoma AG, Switzerland) with FES applied to the shoulder, the triceps, and the anterior deltoid. The intensities are controlled by two decoupled control loops for shoulder and elbow motion, respectively. They involve feedback in form of a PID-controller combined with a feedforward path based on an artificial neural network (ANN). The ANN is learning the non-linear inverse dynamics of the musculoskeletal system during active motion yielding a Feedback Error Learning strategy. First tests on healthy subjects were successful and showed the learning behavior of the ANN. Tests on stroke patients have not been performed so far. However, questions regarding the interpolation behavior were not answered so far: Likely, for different reaching movements a trial-based learning has to be carried out for each movement though. Maybe in case of only slight derivations from the desired reaching trajectory, the ANN is still feasible to calculate valid control signals. This improved flexibility about the desired trajectory would be a clear advantage over control

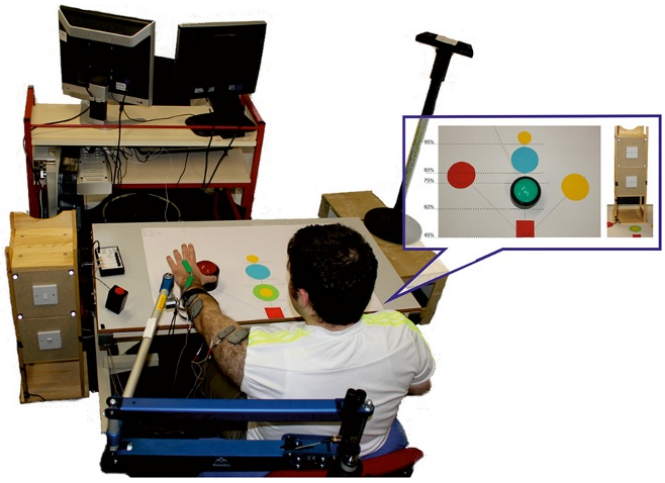

FIGURE 10: *The experimental set-up used in [120]: The impaired arm is connected to an arm weight-support device, while FES is applied to the anterior deltoid, triceps and wrist and finger extensors. The picture was taken from [120] with permission of the author.*

approaches relying on ILC. In case of completely different desired movements, this extrapolation probably fails, however.

Spinal cord injury (SCI) To enable reaching functions in individuals with SCI at C_3 and C_4 level, FES-hybrid orthoses have been investigated.

In the late eighties Hoshimiya et al. [71] presented a hybrid system to restore elbow extension, wrist extension/flexion and grasping functions in C_4 SCI-patients by using implanted electrodes. A balanced forearm orthosis (BFO) was used for inducing the arm motions from weak shoulder movements. Pre-defined stimulation patterns that are previously obtained by EMG recordings in healthy subjects were applied. User control was realized by volitional respiratory commands. The device was successfully tested in one C_4 patient and allowed sophisticated movements.

Nathan et al. followed a similar approach [128] using surface electrodes for up to 12 muscles. Mechanical splinting was used to guide movements, and the system integrates volitional shoulder girdle movements. By voice commands, several FES-induced motor functions are triggered. This device has been successfully tested in pilot clinical trials.

Smith et al. [169] developed an open-loop control system for the upper extremity enabling FES-support of grasping, elbow extension and flexion as well as shoulder elevation. A suspended sling was used to provide shoulder joint stability. The induced movements were continuously user-controlled utilizing a position transducer attached to the contralateral shoulder. The obtained position was then normalized and used to apply stimulation by pre-programmed stimulation patterns that depend on this normalized position.

Schill et al. [163] developed the system OrthoJacket - an active FES-hybrid orthosis for the paralyzed upper extremity. The system combines FES controlled grasping with an electrical / pneumatic actuation of shoulder movements and a flexible fluid actuator for support of elbow-joint movements. To control the orthosis, arm EMG-signals were acquired. This means that only individuals with some residual arm/hand functions could use this system. Furthermore, FES

was not used for movement generation at the shoulder or elbow joint. A clinical evaluation has not been reported by now.

Within the EU project TOBI, a further FES-hybrid orthosis was developed to support both grasping and elbow-joint movements by FES [151]. However, this system requires sufficient residual shoulder function to be provided by the user. To avoid an excessive stimulation of the biceps muscle during holding tasks, an in-flexion direction self-locking and electrically de-lockable elbow-joint is used within the orthosis. A Brain-Computer Interface (BCI) and a shoulder joystick at the non-supported side are provided as interfaces for the control of the orthosis.

2.7.3 Summary

In many existing systems, FES was applied in an open-loop manner using pre-defined stimulation patterns. Movements are often triggered, e.g., by a user-switch, through EMG signals of preserved muscles or recently by Brain-Computer Interface technology. Continuous control is also achieved by a position transducer attached to the contralateral shoulder. Stimulation levels and the timing of patterns are typically adapted manually to the individual, and the corresponding effort increases as the number of stimulated muscles increases. A feasible treatment of muscle fatigue using open-loop approaches only is difficult as an adaptation to the current fatigue-level is impossible due to the missing feedback information.

In contrast, closed-loop control has the potential to correct position deviations in reaching. Investigations on this topic that also include tests in healthy subjects or patients were mainly performed by the group around Freeman. They successfully applied iterative learning control combined with direct feedback control starting in 2009. This control concept is restricted to repetitive movements, which is very feasible in stroke rehabilitation, however. In their numerous investigations on this topic, they developed systems for stroke rehabilitation of arm and hand functions (e.g., SAIL, GO-SAIL) and tested them in stroke patients.

Further, more recently in 2016, also Resquin et al. realized feedback-controlled positioning [146]. They claim that due to the use of an online-learning artificial neural network the effort required to be spent for initial calibration procedures is significantly reduced. Instead, the adaptation is performed during the initial phase of active control. Further, no detailed mathematical model of the musculoskeletal system is needed. Their approach applies real-time feedback control for the correction of positioning errors in a real FES setting (in contrast to simulation-only studies), without requiring trial-based learning. In contrast to the open-loop strategies, this theoretically enables the automatic positioning of the hand at arbitrary positions in the reachable workspace. However, tests in stroke patients have not been performed yet.

2.8 Automatic Control Strategies for FES

To realize limb motions using FES, feasible automatic control strategies to adjust the stimulation intensity of each FES-activated muscle are required to build autonomous neuroprosthetic devices. Herein, two goals are possible: a) The FES-based support of movements caused by the residual volitional activity that is harmed by paresis to a certain degree, and b) The generation of purely FES-induced motion to restore movements in case of a paralysis.

In case a), control systems were invented that measure the intensity of the remaining volitional activity using EMG and in turn adjust the stimulation intensities such that the currently present volitional activity is supported by FES. An overview of this topic is given in Sec. 2.8.1.

In case b), often feedforward or open-loop strategies are applied (cf. Sec.2.7.3). To compensate for errors between the generated motion and the planned trajectory or a target position, position feedback is required [34], however. Numerous approaches including, e.g., PID, model-based, and many more were investigated in the past as reviewed in Sec. 2.8.2. Many potential applications of FES, e.g., the restoration of reaching functionality can benefit from closed-loop FES. However, due to difficulties in the prediction of the muscular behavior in response to FES caused, e.g., by delays, non-linearities, and cross couplings, feedback-controlled FES is difficult to realize [114, 112, 191].

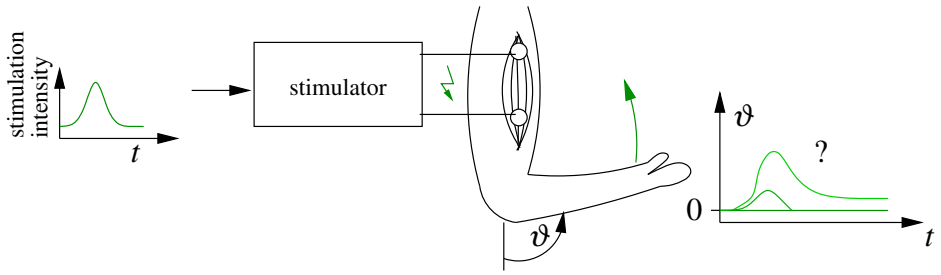

FIGURE 11: *Illustration of the typically observed uncertain (highly variant) muscle response to FES.*

In advance to position measurements, further information describing the current muscle condition may be obtained via stimulation-evoked EMG (eEMG). Herein, potential to assess the state of muscle fatigue and the level of muscle recruitment is expected. The exploitation of eEMG forms an upcoming topic in research that is reviewed in Sec. 2.8.5.

As outlined above, FES-based control typically uses the intensity of the stimulation pulses to modulate the level of muscle recruitment and the consequential effects on limb motion. The modulation of the rate of the applied stimulation, however, forms a less often considered actuation variable that may have the potential to improve feedback-controlled FES by, e.g., reducing muscle fatigue. This topic is considered in Sec. 2.8.6.

2.8.1 FES CONTROLLED BY VOLITIONAL EMG MEASUREMENTS

Different strategies to control FES based on the residual EMG of the stimulated muscle were proposed in the literature, e.g., [59, 122, 22, 58, 166].

In early investigations, pre-determined stimulation sequences, which are triggered by the presence of volitional activity as detected by EMG, are applied in an open-loop modality. This concept was, e.g., applied to support wrist and finger extension in [27] and to support the finger and thumb extension in [156]. Such systems are easy to implement, feasible to the application in clinical environments, and yielded some commercial devices, e.g., [Neuromove 900, Stroke Recovery Systems Inc., Littleton, CO, USA] that consider the wrist and finger extension. However, these approaches do not assure the synchronization of FES to the intended voluntary movement after the trigger as the intensity of the volitional activity could only be detected when FES is not active.

This is because the acquisition of EMG during active FES was difficult to implement in the past cf. Sec. 2.5.

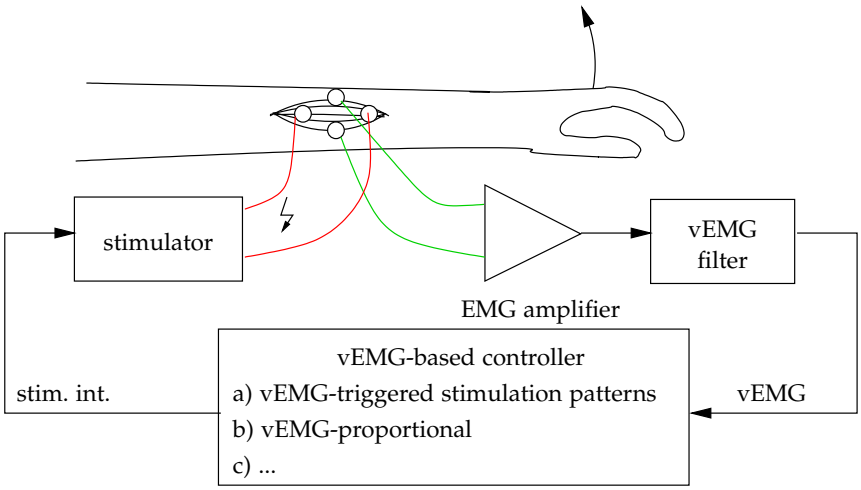

FIGURE 12: *Control of FES based on the volitional activity determined from the stimulated muscle. This principle is often applied to support the wrist and finger extension.*

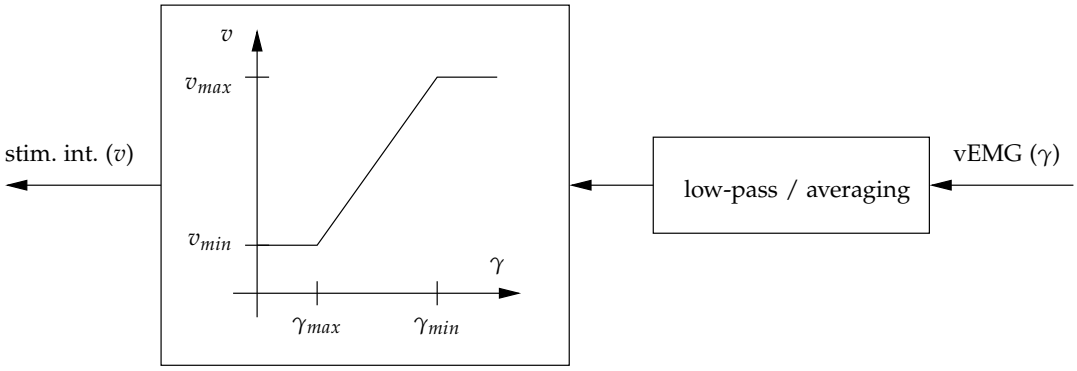

FIGURE 13: *Proportional control of the intensity of FES (v) based on the volitional activity (γ). The parameters $v_{min}, v_{max}, \gamma_{min}, \gamma_{min}$ are usually tuned in a trial and error approach to match the patient's requirements.*

This drawback can be overcome by EMG-proportional controllers (cf. Fig. 13), which modulate the stimulation proportionally to the volitional EMG e.g. [51, 180, 60, 7, 166]. This type of control relies on the measurement of EMG from the stimulated muscle (cf. Fig. 12). This measurement requires a higher effort regarding signal processing and amplifier design because the volitional EMG component is disturbed by high-voltage artifacts of the electrical stimulation pulses (cf. Sec. 2.5). As a benefit to the user, however, such control schemes allow to instantaneously amplify weak residual activity so that – in contrast to EMG-triggered approaches – continuous movements can be realized by the user controlling the neuroprosthesis.

Using this kind of proportional control, Thorsen et al. [180] performed tracking tests in six SCI-patients (five C5 and one C7) to support the wrist extension and thumb extension, respectively. Their results show that EMG-proportional control is feasible to assist in rehabilitation. However,

the movements may suffer from oscillations [180, 166]. Later on, in a larger study involving SCI patients (C_5 to C_7), they used the standardized ARAT-test (Action Research Arm Test) to evaluate the functional benefits of EMG-proportional control to enhance the tenodesis grip [179]. The approach was found to be clinically relevant for the daily-live support as well as for therapeutic effects.

EMG-proportional control to support the finger and wrist extension in therapy for stroke patients has further been investigated in clinical studies by Hara et al. [60] and little later by Fujiwara et al. [51]. Hara et al. found significant improvements in the volitional control and also improvements concerning the motor functions, spasticity, and functional scores after the therapy. Further, they applied EMG-proportional to the biceps and triceps muscle [61]. Fujiwara et. al found similar improvements in upper-extremity functions.

To support reaching functions in SCI-patients, Ambrosini et al. applied EMG-proportional control to the biceps muscle. In addition to FES, a passive exoskeleton is used to guide movements and to perform a weight compensation for the shoulder elevation [7].

While aiming at physiological movements, the main difficulty in EMG-proportional control might be caused by the low signal-to-noise ratio of the estimated volitional activity signal: Typically, a low-pass filter is required, which introduces a delay in the respective closed loop and thus causes limitations with regard to the desired movement [180]. Another effect that may hinder the determination of the volition EMG during active FES (e.g., when stimulating the tibialis anterior) is the occurrence of f-waves caused by spinal reflexes. These waves occur in the electromyogram during the phases in which the volitional activity is evaluated [178] and, therefore, hinder the estimation of the volitional activity.

A slightly modified approach was presented by Giuffrida et al. [55]. To support the elbow-flexion, they proposed a control system in which the stimulation of the triceps is decreased in a reciprocal way to the voluntary activity obtained from the biceps. In three SCI-patients, torque- and angle tracking tests were performed. Herein, a comparison to a constantly active triceps stimulation was carried out. The tracking performance of the presented control system was comparable to the case of constant triceps stimulation. However, the average stimulation level is reduced. This approach is expected to introduce an increased joint-stiffness due to co-activated muscles, i.e., the biceps and triceps are activated at the same time. This increased stiffness might be beneficial as it may improve motor precision (cf. Sec. 2.8.4). The main drawback, however, is that at least one muscle in this antagonistic muscle pair must be contracted. Further extensions are required that allow the user to enter a rest position in which muscles can relax.

Based on their previous experience in EMG-proportional control [7], Ambrosini et al. recently proposed an on/off non-linear control system [6] to support elbow flexion movements. This device allows even patients with reduced muscle contractions to autonomously activate and deactivate the stimulation support controlled by their residual muscle activity. However, due to the switching-based strategy, no continuous movements can be controlled.

An approach that does not belong to the category of EMG-controlled FES also enables volitional control was presented by Riener et al. [149]. They proposed a control strategy only relying on joint angle measurements to support standing up. Not relying on vEMG measurements, patients can control the system by their residual volitional activity. Herein, the stimulation intensities are continuously adjusted utilizing an inverse model of the musculoskeletal system

that maps joint angles to stimulation intensities. This concept realizes a positive feedback loop. However, questions regarding the closed loop's stability remain unanswered – the closed loop might perform an overcompensation of the body's weight. As standing-up movements are considered, this fact might be less important or even beneficial in this special case, though. However, the application to, downward movements might require modifications of the proposed control strategy. Further, numerous models parameters need to be identified. This approach is similar to the arm weight compensation controller presented in Chapter 4 that ensures a slight under compensation, in contrast.

Conclusion The estimation of the volitional activity by signal processing of the raw EMG during active FES typically yields noisy signals. Herein, the noise amplitude is commonly too high to drive the stimulation intensity directly in a proportional control scheme. For this reason, commonly some kind of averaging or low-pass filtering is applied (cf. Fig. 12) that, however, also introduces a delay or phase shift in the signal path. This delay significantly influences the ability to control the level of FES by the user's volitional activity. Such delays might be one of the reasons for the oscillating movements observed in experiments (e.g., [180, 166]), though other, currently unknown, causes are likely. Further, in presence of f-waves in the obtained electromyography measurement, the estimation of the volitional activity becomes more challenging and, therefore, also the control of FES [178]. Control schemes that trigger on the presence of volitional activity tend to be more robust in their operation. However, the obtained movements are limited.

Despite all these reasons, the control of FES based on EMG-measurements seems feasible at least in a rehabilitation context. Concerning the use in a daily-live scenario in form of a supportive aid, the resulting motor precision might be improved, though simple functional tasks may be achieved.

A promising approach is introduced that allows continuous movements by an indirect detection of the volitional activity through joint angle measurements. Such an approach is applied to the support of the arm-elevation in Sec. 4.

2.8.2 Difficulties in traditional control concepts solely relying on position measurements

Artificial control of human limb movements or the support of residual movements in neuroprosthetic systems using FES forms a challenging task especially if movements according to a given reference trajectory or at least a given ending position shall be realized [114, 112]. The typical bandwidth of upper body movements ranges between 0.3 and 3.5 Hz for typical body movements and does not exceed 10 Hz [175]. FES applied in an open-loop fashion using predefined stimulation patterns was successfully applied for the correction of drop foot in stroke patients or the restoration of grasping. However, many applications of FES (e.g., the recovery of reaching functionality as described in Sec. 2.7) may benefit from more elaborate real-time control and closed-loop strategies to compensate uncertainties in modeling and perturbations [112, 191]. Indeed, in the mid-nineties, a certain amount of enthusiasm was present to solve FES-based movement generation by exploiting sophisticated control approaches, e.g., adaptive control and artificial neural networks [34]. However, some practical limitations emerged that are outlined in this section. The variety of approaches on the topic of controlled FES is illustrated in Fig. 14.

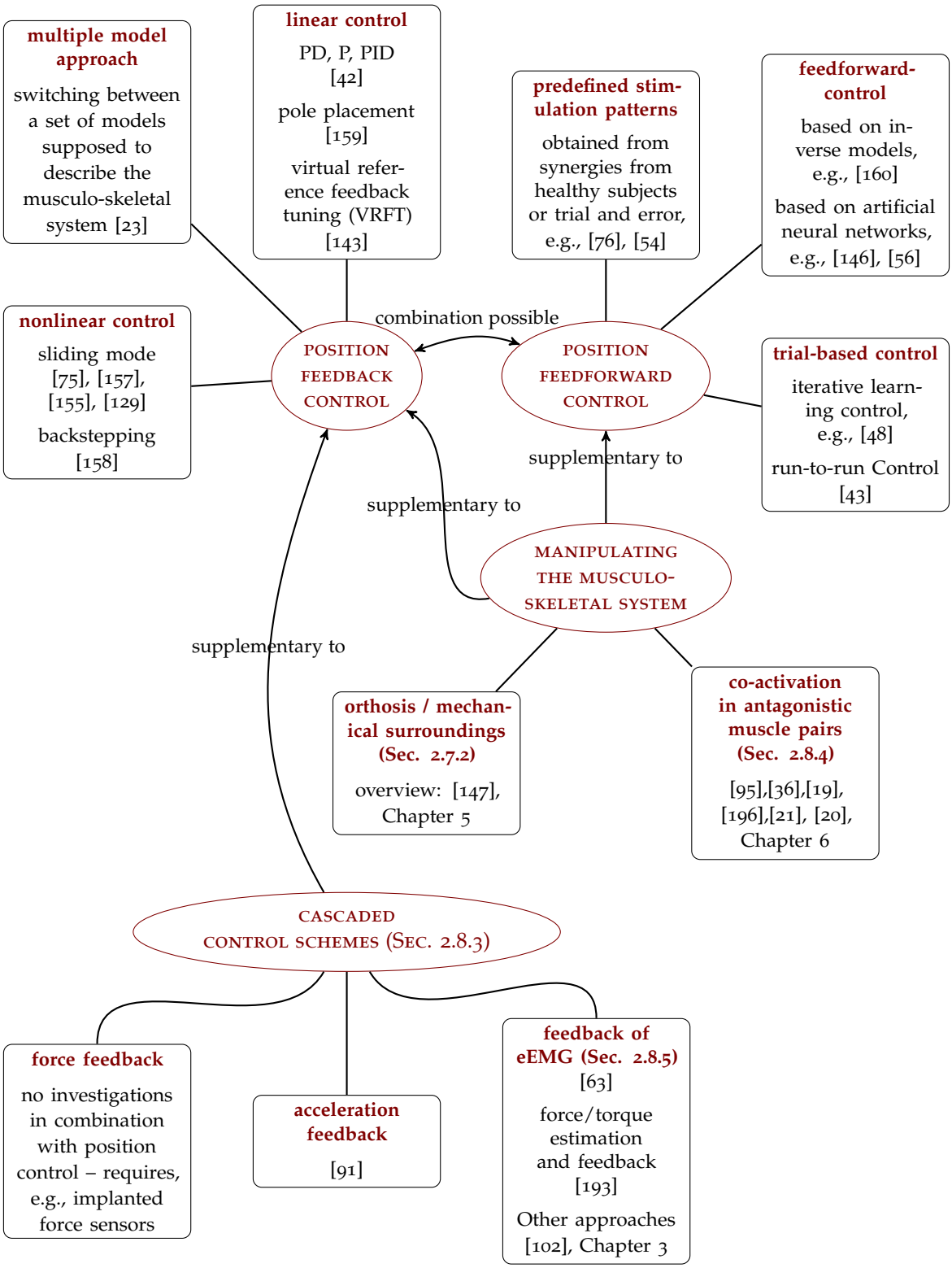

FIGURE 14: *Overview of control strategies used for limbs' positioning.*

Many control schemes based on the traditional approach that includes the steps of modeling, system identification, and controller design have been proposed. Commonly, the assumed models must be adapted to the individual user and muscle condition. These adaptation procedures become harder to perform on humans as the number of tunable parameters increases – typically if the complexity of the desired motion (e.g., regarding the number of degrees of freedom) increases. Hence, they often become clinically unfeasible as too much time for preparation must be allocated [146]. Nevertheless, a wide range of different control strategies including, e.g., PD, PID, pole-placement, and many non-linear control techniques have been investigated that are sometimes adapted on-line using adaptive control schemes [191, 112].

In case of basic control concepts like P-, PD- or PID-control or even pole-placement, a parameter tuning based on easy to accomplish recordings of step responses is successful in case of simple motion generation tasks, e.g., [30, 159] or as applied in Sec. 5.5.2. Herein, the performance can be significantly increased by combining feedforward- and feedback control (e.g., [30, 42])

To obtain better performing feedforward, feedback, and adaptive controllers, usually intensive effort to identify models that describe the musculoskeletal system is required [148] whereas the obtained models are still approximative since musculoskeletal properties typically involve many details that may be captured by such models [191]. Furthermore, the modeling of muscular fatigue and hysteresis effects in motor unit recruitment is difficult, and a fast model adaptation to the individual subject is hard to achieve.

An important model component is the nonlinear, spatial recruitment curve as illustrated in Fig. 8. Even though it is possible to obtain estimates of the curve through several methods, the obtained results are typically vague and vary even among different identification methods [38]. Under isometric and stationary conditions, the output of a force transducer can be considered proportional to the muscle recruitment (cf. 2.6). However, the estimation of this function is very time-consuming and unfeasible in practically relevant set-ups that mostly rely on non-isometric conditions. Even worse, the effects of muscle fatigue render these estimations obsolete within a few minutes of active FES.

The second difficulty in feedback-controlled FES is the delay and the low-pass dynamics G_m between muscle recruitment and muscle activation σ or muscle force (cf. Fig. 7). This is caused by metabolic processes that are also part of the closed loop. As a result of this, the achievable closed-loop bandwidth and hence control performance is limited.

Finally, the influence of muscle length and contraction velocity on the predicted torque F is difficult to model and to identify. If considered in the control design, complex – in terms of the number of parameters – non-linear functions are employed (e.g., [158], [44]). In many cases, this dependency is neglected, however.

Under the progression of muscle fatigue, a model adapted to the initial muscle condition may not reflect the current state sufficiently well and, hence, control performance and stability properties may get increasingly worse. Performing a re-calibration as the system properties change, is cumbersome and would be impractical in most applications.

If movements against gravity are performed by controlling one joint-angle, integral control typically compensates for the effects of muscle fatigue. However, the closed-loop dynamics may change potentially leading to a reduced controller performance. Many researchers investigated the use of adaptive control strategies to perform an online-identification of model parameters

(e.g., using non-linear Kalman Filters [158] or online-learning neural networks [146]). It is unclear, however, how such adaptation systems behave in presence of spontaneously occurring external perturbations like contact forces or temporarily increased loads (e.g., when manipulating objects in grasping). Such perturbations may be misinterpreted by the adaptation loops, potentially causing them to change the position controller's parameters maliciously. In case of hybrid muscle activations (volitional und FES-induced activity at the same time), the estimation of fatigue parameters becomes difficult, as the volitional contribution to the muscle contraction is typically unknown to the observer. Even if volitional EMG measurements are available, the situation is difficult as a detailed model of the hybrid recruitment process would be required (cf. Fig. 9).

Concerning the calibration routines, typically the time constraints for donning devices to patients are tightly limited as patients may get, e.g., demotivated. Further, the fraction of time spent for donning in relation to the total amount of time designated to a typical training session should not be too large. Calibration routines involving an intensive effort that cannot be automated are, therefore, commonly unfeasible (e.g., [112, 146, 114]). Further, it is advantageous if the chosen procedures also tolerate unexpected responses to FES, e.g., unexpected volitional activity or displacements of the overall body's posture and, of course, the huge variance of muscle responses across different subjects, muscle conditions, and electrode positionings.

The majority of calibration routines for elaborate closed-loop systems do not fulfill these requirements. For this reason, nearly all commercial FES systems employ a simple and easy to tune open-loop control strategy [112, 114]. Of course, pure open-loop control has many shortcommings, e.g., concerning the movement precision and repeatability.

Investigations on joint angle control In the research of feedback-controlled FES, a common benchmark to compare controller performances is to control the knee joint angle against gravity. Therefore, although this thesis focuses on the upper limbs, these investigations are also included in this review.

Among the numerous investigations in joint-angle control, are linear control techniques like PI, PID, and pole placement controllers. They are often extended by a feedforward path containing an inverse plant model because a significant improvement in tracking performance can be observed. For example, in [42] a comparison between such basic control concepts is given. Herein, a comparison between feedforward and closed-loop PID control is carried out and further compared to a combination of both. Besides, an adaptive feedforward controller is investigated. Results were obtained in two trained SCI patients showing that the combination of PID and feedforward control gives the best results regarding the positioning error. The significant increase in control performance when using a feedforward component is due to inherent delays in the response of the neuro-musculoskeletal system (cf. 2.6) that limit the achievable control performance of the feedback portion. Therefore, a combination of feedback and feedforward control is often preferred. Such combinations are naturally included in the design of RST-controllers [14] (pole-placement). An example is given in [159], wherein a linear ARX (autoregressive exogenous) model is identified based on data obtained from a simple open-loop stimulation test. The RST-controller based on this model was successfully tested with a healthy subject. A similar approach based on virtual reference feedback tuning (VRFT) is given in [143] that allows designing linear and even some classes of non-linear controllers directly based on I/O data.

The achievable performance of linear PID-control may potentially be improved by more elaborate approaches as the musculoskeletal system (cf. 2.6) is non-linear, time-variant, and subjected to unpredictable perturbations. The full variety of investigations in this field includes the use of detailed physiologic models and the application of different control approaches like, e.g., neural networks, non-linear control, adaptive control, predictive control, H_∞-, optimal control, and many further approaches [191]. Hence, only a brief overview of the most relevant investigations is given.

An approach that combines an online adapted neural network in the feedforward path with PID-control is evaluated in [30]. Like in [42], a comparison between different combinations of feedforward and feedback control is carried out in a healthy subject. A huge improvement of the tracking performance was observed when the adaptive feedforward path is activated. In [144], a gain scheduling approach is employed wherein a switching between multiple linear controllers based on the joint angle is performed. The controller was tested in a simulation using a biomechanical knee model [150] and showed accurate performance.

The sliding-mode control (SMC) approach is known for its strong robustness concerning model parameter uncertainties. Such an approach was presented in [75] and tested in simulations as well as in two paraplegic patients. In patient-tests, the RMS error was quite acceptable. However, the joint-motion tends to suffer from a continuously oscillating movement. Similar results on sliding mode are presented in [157] for one healthy subject. They conclude that sliding mode yields a robust controller without requiring complex models. The tracking performance, however, is limited due to sampling (in contrast to continuous control) and the delays in the musculoskeletal system. Further, a strongly chattering control signal is accompanied by increased demands on tracking performance. In [155] a combination of SMC and an ANNs is used, wherein the ANN is trained using data obtained during a phase in which SMC is activated. A comparably good tracking performance has been achieved in tracking tests. These tests were performed using intramuscular electrodes in three rats, however. The transfer of the results to human muscles is not clear.

In [158] an approach using an on-line identification of numerous model parameters based on an extended Kalman-filter and a nonlinear backstepping control system is presented and tested in a simulation with good results.

In case of periodic or trial-based movements, e.g., repeated reaching, cycling or drop-foot correction, run to run control, e.g., [43] or iterative learning control, e.g., [48] can be used. In these approaches, no online feedback control is performed during the individual trial. However, the resulting movements of a finalized trial are used to optimize the stimulation for the next trial to reduce positioning errors. A combination with feedback controllers is possible, in any case.

Recently, a control approach in which a switching between multiple models (all describing the same system) and corresponding controllers (one for each model) is performed was presented by Brend et al. [23]. While the control system is activated, a continuous analysis is carried out to check which model describes the system's behavior the best. In turn, the corresponding controller[8] is activated to maximize control performance. This approach is called Multiple-Model Adaptive Control (MMAC) and requires only minimal effort in the calibration as an automatic

[8]The controller that has been designed using the currently best matching model is used.

adaptation to the individual subject might be performed online[9]. These investigations form initial research and tests of this control system were performed under isometric conditions on healthy subjects yielding good force tracking results. The application to position control is subjected to future research. However, the results obtained so far are very promising.

Many examples given in this section apply to the control of the knee joint angle, whereby the subject is seated with the leg free to swing. Herein, FES is commonly applied to the quadriceps acting against gravity. The antagonist-muscles are typically not involved in the control. Hence, this forms a more academic problem, however, as it might be difficult to transfer these results to clinically relevant problems, e.g., the support of human gait.

Investigations on control systems for multi-joint configurations Most investigations for more complicated multi-joint and multi-muscle set-ups only rely on simulation studies that were seldom transferred to the real world. Among them are optimal control strategies for walking [137], [192] or the upper limbs [74] (only simulation) and [18]. Recently Freeman et al. [47, 48] applied mimo ILC to the upper extremities connected to robotic devices for rehabilitation purposes. In the design of the control systems, complex non-linear models are used that must be identified in advance to the training sessions, however.

To control multi-joint angle FES-systems, e.g., in human walking, Nekoukar and Erfanian [129] suggest decentralized control (a dedicated controller for each joint) to simplify the requirement on complex biomechanical models describing the interaction of multiple degrees of freedom. In their framework, the individual controllers are based on a combination of sliding mode-, fuzzy logic-, and adaptive control. The controller identifies the plant dynamics during active control and does not require an intensive initial calibration. This set-up was tested in three paraplegic patients to restore walking. A comparably good tracking performance could be achieved.

Recently Schearer et al. presented an open-loop control approach to induce full arm positioning using a mapping between desired arm positions and their corresponding stimulation intensities [162]. Herein, a static, data-driven model is used to describe the relationship between the stimulation intensities and the obtained arm position. Further details are given in Sec. 2.7.2.

2.8.3 Cascaded control schemes

The control of FES, especially when a position feedback shall be realized, may be potentially enhanced by incorporating further information that allows assessing more details of the current state of the musculoskeletal system. Such information may be gathered, for example, by measurements of force, limb acceleration or the state of muscle recruitment as illustrated in Fig. 15. This information can be exploited to enhance control performance by cascaded control schemes. Herein, in an inner loop, some non-linear and typically uncertain properties of the muscle's behavior can be linearized by a fast feedback loop that enforces the desired behavior. Then, in an outer loop, the resulting, more predictable behavior is easier to model and control.

The feedback of muscle-induced forces is difficult to realize as force sensors are required – preferably implanted ones, e.g., [68]. In some cases, the limbs acceleration is related to the muscle induced force or may serve as further information describing the current motion state.

[9]The model parameters may be updated during active control, while a continuous model validation is performed.

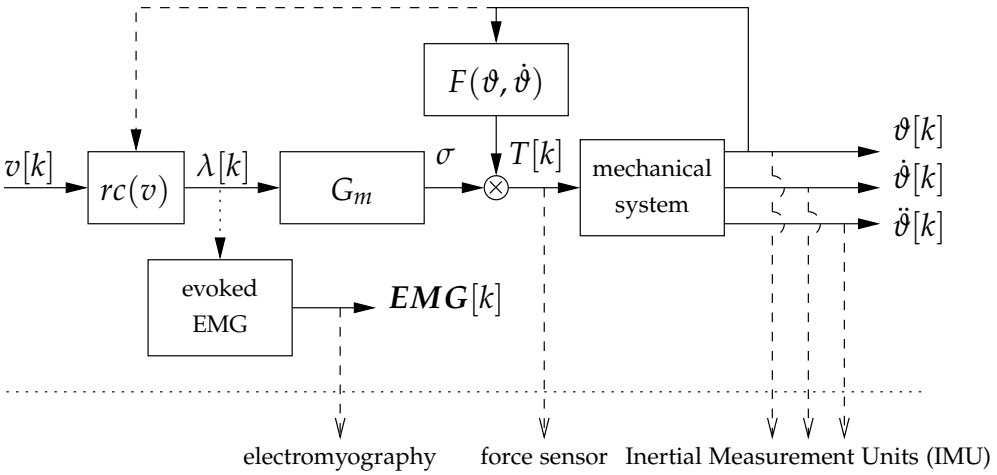

FIGURE 15: *The muscle model as introduced in Sec. 2.6 and possible information to be obtained in advance to position / joint angle measurements to enhance feedback control of FES are shown. This information includes measurements of the evoked EMG, the muscle force or joint torque, and joint angle or limb acceleration or velocity. The latter may be efficiently obtained by, e.g., Inertial Measurement Units (IMU).*

Joint-angle acceleration measurements obtained by Inertial Measurement Units (IMU) were exploited to enhance the control of the elbow joint angle in a cascaded control scheme in previous investigations (not part of this thesis) as described in [91] and illustrated in Fig. 16. The estimation of properties related to the muscular recruitment level by evaluating the evoked EMG is an upcoming field of research and reviewed in Sec. 2.8.5.

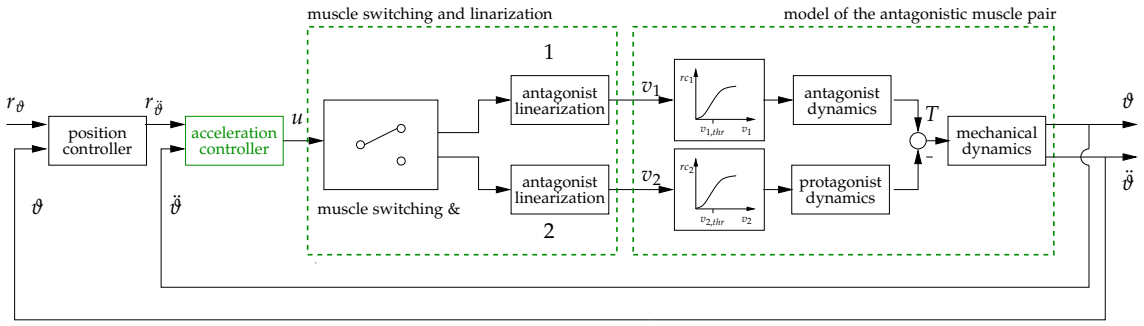

FIGURE 16: *A cascaded position control scheme involving a feedback of the joint acceleration in an inner loop. This loop is applied to an antagonistic muscle pair as proposed in [91]. A linearization controller is, further, applied to each muscle while a switching control law distributes the virtual control signal u to both muscles. In an outer loop, the joint angle is controlled.*

2.8.4 ANTAGONISTIC MUSCLE PAIRS AND CO-ACTIVATION STRATEGIES

A special case of MIMO control is given by joint angle control using antagonistic muscle pairs as illustrated in Fig. 17). Typical examples are given by the control of the elbow-/knee joint angle or the shoulder horizontal flexion/extension.

Commonly, the control of antagonistic muscle pairs is realized by a switching strategy that distributes a one-dimensional actuation variable to two stimulation intensities, respectively for each muscle (e.g., [4, 36], or the control scheme illustrated in Fig. 16). Herein, typically only one muscle is activated at the same time, meaning the activation is alternating between muscles. In [18], a controller for the upper extremities using a mixed feedforward/feedback approach is presented that is applied to an antagonistic muscle pair. In the feedforward path, an artificial neural network (ANN) is used.

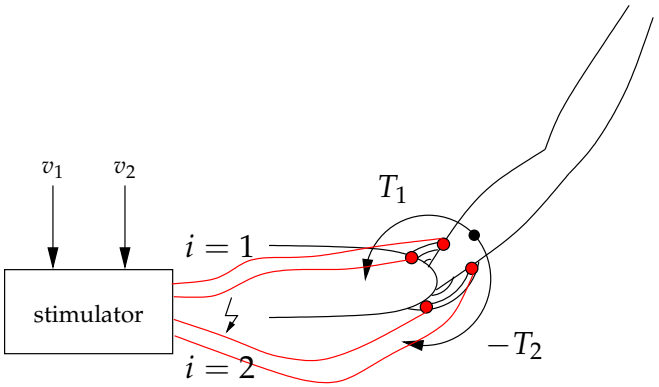

FIGURE 17: *Artificial generation of horizontal shoulder movements in an antagonistic muscle pair formed by the application of FES to the anterior (protagonist muscle, simulation intensity v_1) and posterior deltoid (antagonist muscle, simulation intensity v_2) as investigated in Chapter 6. In this example, a weight compensating exoskeleton surrounds the arm to keep a certain level of arm elevation. The protagonist produces the joint torque $T_1 \geq 0$, while the antagonist causes a torque directed into the opposite direction $T_2 \leq 0$. The resulting torque can then be defined by $T := T_1 + T_2$ and the level of co-activation by $T_{cc} := \min(T_1, -T_2)$ (the portion of both torques acting against each other).*

For natural limb movements, however, it has been shown that the involved muscles are not limited to be actuators that solely induce pulling forces into their pre-defined directions. Instead, an important property for the natural control of posture and movement is the ability to modulate the mechanical impedances by the simultaneous activation of the contrary-acting muscles, which is called co-activation. Naturally, they are modulated by the central nervous system [69] to exploit beneficial effects like increased mechanical stability accompanied by an increased motor precision [26].

To show the presence of co-activations, many investigations in which neurologically unimpaired subjects had to perform repeated movements (e.g., cycling, ...) were carried out. During these experiments, muscle activation was recorded by EMG to investigate the natural behavior of muscle activation (e.g., Fu and Wang [50] and Lynch et al. [113]). They showed the natural presence of co-activation. Milner [126] investigated muscle activations in wrist-joint movements. Herein, the wrist was connected to a motor-driven artificial load that simulated negative viscosity utilizing a positive feedback of the joint angle. As the negative viscosity increased in its amplitude, which can be considered as an increased degree of instability of the simulated mechanical system, the naturally present co-activation also increased.

For artificial muscle activation by FES, Durfee showed in 1989 that an intentionally induced co-activation in antagonistic muscle pairs yields significant performance increases in the control of

the joint angle [36]. Further, in [95] a sliding-mode controller is applied to control the ankle-joint using antagonistic muscle pairs. This approach induces co-activations that are the result of the chosen control mechanism.

In the mid-nineties, Zhou et al. [196] investigated different co-activation strategies under isometric conditions to realize sinusoidal and linear shaped joint torques. Their results show an improved torque tracking performance as the level of co-activation increased.

Recently, Bo and Moura [21] investigated PID joint angle control applied to the elbow-joint with additionally introduced co-activations. Further, a comparison between PID control with and without co-activation was carried out. The obtained results show an oscillating control behavior which is contrary to [36], however. In ongoing research, using a simulation model, they calculated the joint stiffness and damping dependent on the level of co-activation and, further, performed experiments on PI elbow joint angle control in two healthy subjects [20]. In the experimental results, the control performance was, again, worse when using co-activations. The reasons for this contrary behavior are unclear, however.

Liao et al. [107] considered the application of co-activations to FES-induced reaching functions, however in a computer simulation only.

In a system for actively damping tremor-movements, the positive effects of co-contractions are exploited as described in [19].

Most recently, Passon et al. [132] exploited co-activations in the control of the elbow-joint angle in a set-up involving a cable-driven robotic system combined with FES applied to the deltoid, triceps, and biceps (more details are given in Sec. 2.7.2). They reported an improved joint-movement by applying a simultaneous activation of both muscles when switching between muscles occurs (an approach suggested in [196]). However, they also reported difficulties in the determination of controller parameters that were obtained in a trial and error approach. Notably, the parameters describing the stimulation intensity to produce the onset of muscle contraction might be challenging to fixate.

None of the presented systems consider the difficulty of properly maintaining the level of co-activation also under the presence of muscle fatigue: As fatigue progresses, the level of the activation thresholds, and the slopes of the linear ranges in the muscle recruitment functions as well as change. These changes are not observable by existing control systems as only the cumulative stimulation effect of both muscles (indicated by the resulting torque T) can be obtained through joint-angle or joint-torque measurements. Hence, also the relationship between the desired and the actual co-activation strength T_{cc} changes that is difficult to observe (cf. Fig 17). This topic has not been considered in current research.

Therefore, feasible strategies for controlling the co-activation level require the measurement of the individual contributions T_1 and T_2 to the joint torque T or (at least) measurements directly related to them e.g. the muscular recruitment level λ of each muscle (cf. Fig. 15). The former option is difficult to implement as force sensors for the individual muscles are required. The latter case will be considered in this thesis in Chapter 6.

2.8.5 Using the evoked EMG to improve feedback-controlled FES

As presented above, the majority of control systems for joint angle control using FES are based on motion feedback only. As already stated in Sec. 2.8.2, measurements that describe the stimulation-effect (e.g., joint angles) suffer from a delay and, hence, fast feedback loops are difficult to achieve. Feedback variables suffering from less delay w.r.t to the stimulation intensity (e.g., muscle recruitment) may yield better controller performance when used in addition to a joint angle feedback. Naturally, the Golgi tendon apparatus performs a torque feedback to control the contraction strength of the motor units [101]. Baratta et al. [15] investigated the performance of a feedback control loop controlling the muscular torque[10] with outstanding results. However, the described experiments were performed under isometric conditions, and an external force transducer was used to measure the muscle torque. In some cases, implanted force sensors (e.g., [68]) are thinkable, but this will remain difficult in the foreseeable future.

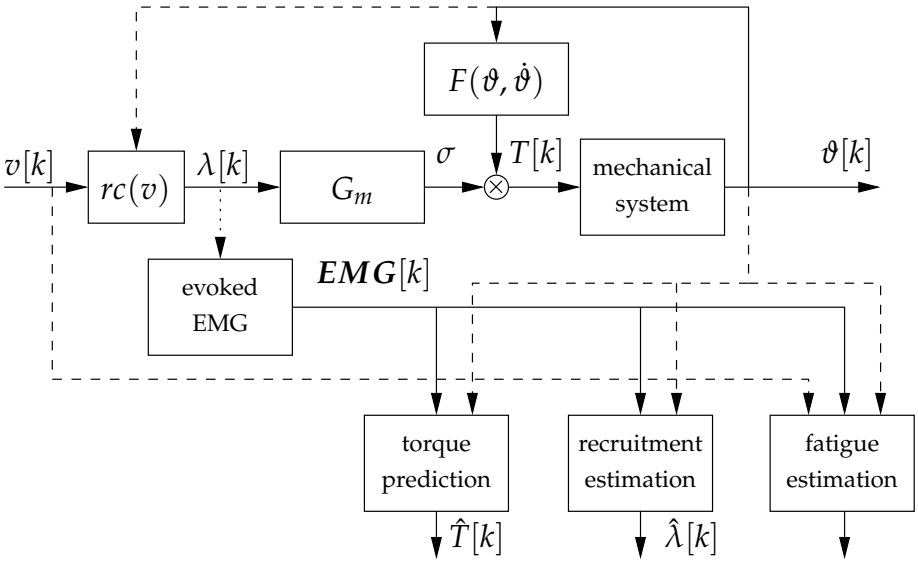

Figure 18: *The muscle model as introduced in Sec. 2.6 and information that may potentially be extracted from the eEMG are shown. In case of isometric conditions (ϑ constant), the model greatly simplifies because F is constant in this case. As a result of this, the joint torque is caused to be proportional to the muscle activation σ. Therefore, torque predictions by evaluating the eEMG are simpler to achieve in isometric conditions compared to the non-isometric case.*

In case of FES, motor units are recruited synchronously by the stimulation pulse, whereby each motor unit generates an individual action potential. The cumulative effect yields the m-wave appearing in the evoked EMG, whose intensity increases as the number of recruited motor units increase and, therefore, strongly relates to the total level of FES-induced muscle contraction. The shape, especially the duration of the m-wave is influenced by the muscle fiber conduction velocity that is different for each type of motor unit. The velocity is known to decrease during strong sustained contractions [123]. Further, changes in the m-wave's frequency characteristics are caused as a result of this which becomes visible, e.g., in a decreasing median frequency. Hence, a promising approach to gain insight into the effectiveness of a stimulation pulse (concerning the

[10] The generation of muscle force/torque is also subjected to delays in the process of muscle activation. However, at least the phase-shift introduced by the mechanical system is not present in torque feedback loops.

number of recruited motor units) is to evaluate the m-wave's intensity, frequency characteristics or other suitable indicators. Some of them are illustrated in Fig. 19.

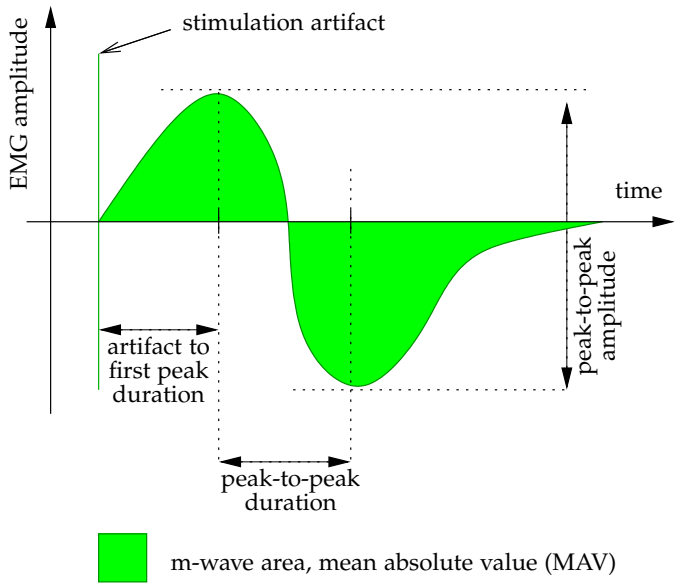

FIGURE 19: *Metrics for determining the m-wave's intensity.*

Especially the amplitude and width (area) may be related to the amount of recruited motor units[11], and the power spectrum contains information on the progression of muscle fatigue [123, 124].

Three possibilities to exploit the m-wave's characteristics are illustrated in Fig. 18. One approach to improve controlled FES is to adapt the controller to the progression of muscle fatigue automatically. Therefore, some research has been carried out that considers the estimation of the level of fatigue by evaluating the evoked EMG. Others try to estimate the muscle force from eEMG measurements. In this thesis, it is investigated whether the evoked EMG serves as a measurement and feedback variable for the stimulation induced muscle recruitment. An overview of the investigations performed so far on the exploitation of eEMG is outlined in Fig. 20. These approaches are reviewed in this section.

Estimating muscle fatigue by evaluating the m-wave To obtain information on the progression of muscle fatigue, open loop approaches that use a model (e.g., [35] or [108]) for predicting the level of fatigue are also thinkable. However, such models have to be adapted to the individual subject and muscle by a calibration procedure. Further, as these approaches do not involve a feedback of the actual muscle condition, the ability to predict the level of muscle fatigue with small errors in the long-term is questionable as the internal states of the model and the muscle are likely to diverge.

A great potential for the estimation of muscle fatigue using characteristic parameters of the m-wave was expected in the past. This expectation was motivated by the fact that the distribution of the power spectrum of the EMG signal indicates muscle fatigue in form of a more compressed

[11] An assumption made in this thesis.

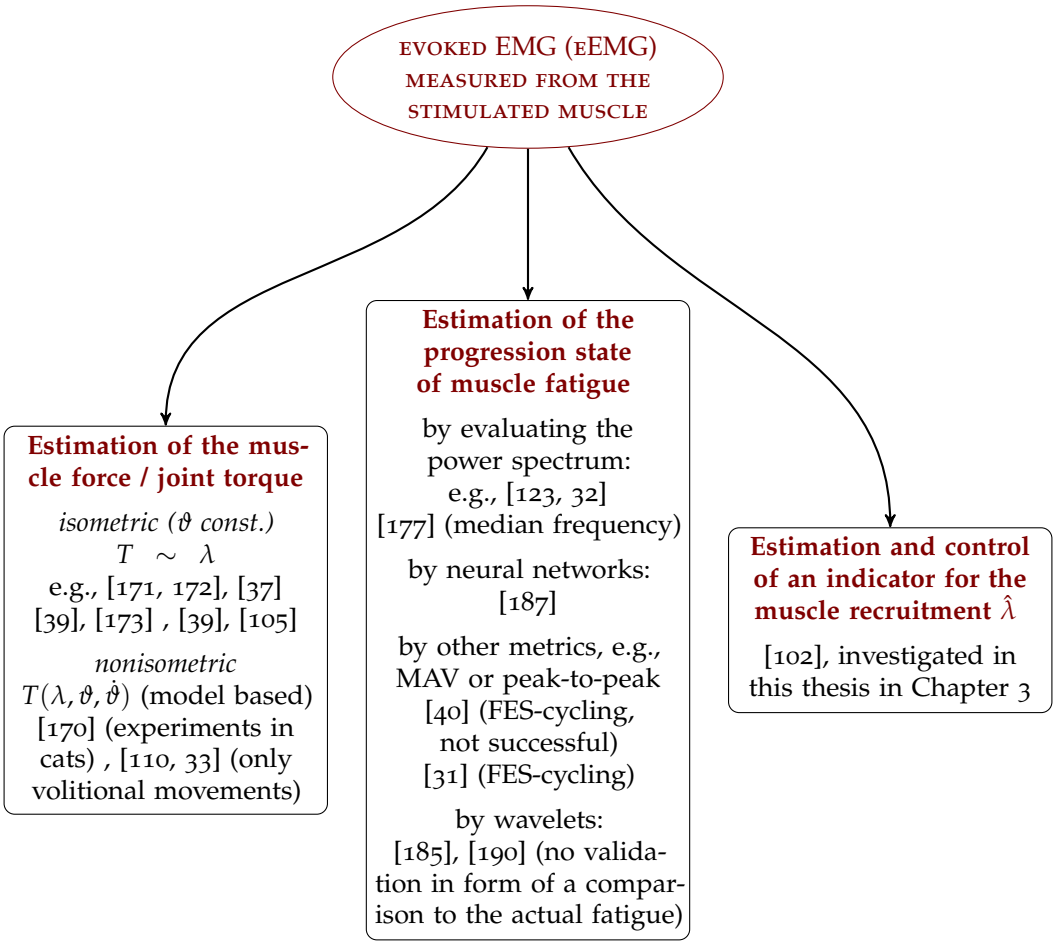

FIGURE 20: *Possibilities to extract and use information contained in the evoked EMG (eEMG).*

spectrum [123] meaning the Mean Frequency (MNF) and Median Frequency (MDF) depend on the level of muscle fatigue.

Chesler and Durfee 1997 [32] investigated the influence of muscular fatigue to the m-wave for the quadriceps. Multiple indicators, the RMS-values of the EMG and the median frequency of the EMG's spectrum, were compared. In case of healthy subjects, their experimental time-series data showed a more or less unrelated behavior between the torque and each indicator, however. In one dataset for a paraplegic subject, a clear correlation between both the median frequency and the RMS-values and muscle torque is shown, however. The reasons are unknown. In healthy subjects, there might be an unobserved interaction with volitional muscle activity that is not present in paralyzed muscles.

Winslow et al. [187] used an ANN to detect muscle fatigue and to a obtain a fatigue compensation control signal from the EMG measurements. Tests were performed either on the biceps or the quadriceps. Herein, the samples acquired for each inter-pulse interval were the inputs to the ANN, while the output was a command-signal that is used to compensate for fatigue. The application in neuro-prosthetic systems is, however, questionable as the ANN must be trained using data obtained in an experiment in which muscle fatigue must be caused by long-running FES.

Chen and Yu [31] investigated the ability to use the peak-to-peak (PtP) value (cf. Fig. 19) of the m-wave as a fatigue indicator in FES-cycling. Stimulated muscles were the quadriceps and the hamstring in paralyzed subjects. The obtained PtP-values are averaged over each cycling period and compared to the measured torque. They found that the PtP-values are significantly influenced by the cycling speed. For constant cling speeds, the PtP-value may serve as a fatigue indicator.

Further investigations in FES-cycling were performed by Erduardo et al. [40]. Tests with eight SCI subjects were performed wherein stimulation was applied to the quadriceps. They calculated several potential fatigue-indicators (peak-to-peak amplitude, peak-to-peak time, m-wave area (MAV), and the time between the stimulus artifact and the positive peak). However, no correlation to the measured torque was found.

Tepavac and Schwirtlich [177] investigated the correlation between FES-induced torque and seven indicators derived from the evoked EMG under isometric conditions. FES was applied to the wrist flexor muscles in six SCI subjects. The best correlation was obtained for the median frequency.

More recently, Yochum et al. [190] considered the estimation of muscular fatigue during FES applied to the biceps utilizing a Wavelet analysis. In their approach, an initial m-wave is memorized. For the ongoing m-waves, a comparison of the memorized to the currently measured m-wave is performed by applying a scaling in the timescale as well as in the amplitude. The scaling parameters leading to an optimal fit serve as a fatigue indicator. In their experiments involving two subjects, the assumed indicator for fatigue showed an exponential decrease within approximately nine minutes of constant stimulation. However, no reference value, e.g., muscle force was recorded and compared to the calculated indicator.

EMG-based muscle force/torque prediction The prediction of muscle force or joint torque by processing eEMG was investigated by many researchers in the past and recently. Beginning in the late 80s, Solomonow et al. investigated the relationship between the MAV of the eEMG and the

measured force [171], [172]. Second-order static polynomial models are used to describe the MAV vs. force relationship and parameters are identified using the least squares method. A few years later, also Durfee and Dennerlein [37] investigated this relationship with the aim to develop a force-prediction method that can be used as a feedback parameter in a FES-control system. Both investigations were performed only under isometric conditions, meaning that the joint angle was fixed. Further, in [173], they investigated the median frequency of the power spectrum and showed the relation to the average conduction velocity.

A few years later, the relationship between the MAV of eEMG and the force was investigated again, this time for variable joint angles, by Solomonow et al. [170]. They performed experiments in anesthetized cats in which they stimulated legs muscles to obtain extension movements. They found that for strongly extended postures, the relationship was more linear compared to a flexed joint. In the latter case, the observed relationship showed a more non-linear characteristic. In the late 90s, finally, the first algorithm for predicting joint torques using a Hammerstein-model was presented by Erfian et al. [39]. Herein, only isometric conditions were considered, however.

Zhang et al. [194, 195] developed a model based on a Hammerstein-structure to describe the muscle force produced by the triceps surae muscle group (yielding an extension of the ankle joint) under isometric conditions. The MAV of the evoked EMG was the input to the model and the generated torque the output. They stated that the model parameters are time-variant – likely caused by muscle fatigue. Hence, they further implemented a Kalman filter to perform an online adaptation. In tests with SCI-patients, the obtained torque prediction was accurate. As the online adaptation for the prediction of the joint torque required a measurement of the generated torque itself, the benefits are not quite clear. Potentially, the torque prediction becomes available a few sampling instances before the actual torque belonging to the current input is generated. In their ongoing investigations [104], an ANN was used instead of the Kalman Filter for joint-torque prediction – still under isometric conditions. In comparison to the method described in [195, 103] prediction accuracy could be improved. Most recently, the proposed methods were tested in a larger group of participants consisting of three healthy subjects and three SCI patients [105].

In [110], a model for describing voluntary muscle activations in terms of the knee joint angle based on the volitional EMG is proposed. The typical constraint to isometric conditions – limiting the practical application – was not assumed in this research. However, no FES has been applied herein because of the restriction to volitional activation. Similar investigations were performed by Clancy et al. [33].

To summarize, most investigations in predicting the muscle torque using EMG focus on isometric conditions and, hence, their relevance to practical applications is limited. Further, commonly much effort is required for the calibration procedures to perform the adaptation to the individual muscle. Up to now, no investigations were found that consider the prediction of muscle torque in FES- and volitionally activated muscle contractions. Such a prediction is of particular importance in neuroprosthesis that should incorporate with the volitional activity, e.g., in patients with incomplete paralysis. The development of such a model is considered in Appendix A: An ANN-based approach to model this kind of hybrid muscle activation is presented.

eEMG used as a feedback variable First ideas on a feedback of the evoked EMG were already proposed in the mid-eighties by Solomonow et al. [171], [172] and some years later also by Durfee

and Dennerlein [37]. At that time, an urgent difficulty was the suppression of stimulation artifacts in the data evaluation. Further, such control loops were only proposed without any further details, and no implementation and tests have been performed, however.

Solomonow et al. [171] investigated the feasibility of an eEMG feedback by estimating muscle torque from it and, herein, compared three different approaches for evaluating the m-wave's intensity to obtain a feedback variable. Investigated were the MAV, the RMS and the Median Frequency. They recommended using the MAV in a feedback control loop. The investigated filters were implemented using analog circuits that performed an averaging over multiple m-waves. In a feedback control loop, however, such an averaging introduces a delay limiting the controller's performance. This drawback can nowadays be improved by digital filter approaches as commonly used in EMG signal processing today. Herein, each m-wave is typically evaluated separately, yielding the MAV for each m-wave respectively such that a discrete-time signal is obtained. At that time, the computational power of computers or other devices suitable to perform digital signal processing tasks was low and, hence, analog filters were preferred suffering from the mentioned drawbacks.

Recently, Zhang et al. tested a feedback control system based on their previous investigations on eEMG-based torque prediction in simulation and two healthy subjects [193]. FES was applied to the proximal tibialis anterior, and the torque tracking controller yielded good results. This approach is limited to isometric conditions, however.

Similar to the approach of recruitment control presented thesis, Li et al. [102] controlled the intensity of the m-wave (measured in terms of the MAV). In contrast, their control scheme involves a Kalman-filter to perform an on-line identification of a Hammerstein-model and predictive control. The results in terms of tracking performance, however, do not show any significant improvement over the much simpler integral control approach investigated in this thesis. Further, in their approach, the used Hammerstein-model included more degrees of freedom to describe the dynamics than actually necessary, which compromises the risk of improper parameter estimation.

Conclusion In summary, the exploitation of eEMG measurements seems feasible to improve neuroprosthetic devices. However, all approaches seen so far are subjected to ongoing research and are not ready to be applied in currently available neuroprostheses. Three major directions were considered in research as illustrated in Fig. 20.

Research that focused on the estimation and eventually the compensation of muscle fatigue mostly concentrates on isometric muscle conditions. Herein, several groups were seeking for possible correlations between metrics of the m-wave and the FES-induced muscle force/torque yielding partial success. Further, FES-cycling was considered as a special non-isometric case. Herein, the periodicity of the task allows computing potential fatigue indicators for each completed cycle.

Another direction considers the estimation of muscle force/torque via a model. Such models could be used to realize closed-loop muscle-force/torque control in a cascaded control scheme. Investigations on the prediction of stimulation-induced muscle force/torque were presented very early back in the mid 80's and are still considered in current research. However, similar to the estimation of muscle fatigue, only isometric conditions were considered. Further, the required effort for parameter-identification of such models hinders the application in a neuroprosthetic device.

In a third direction, the mean absolute value of the m-wave is used as the feedback variable. Though this has also been proposed very early, real tests on subjects were only performed recently for the first time. In this context, it has to be said that the recent availability of powerful devices for digital signal processing greatly enlarges the capabilities to gain useful information from the m-wave. In contrast, at the time of the early investigations by, e.g., Durfee et al. or Solomonow et al., algorithms had to be implemented using analog signal processing made of electric circuits.

In Chapter 3, a feedback of the evoked EMG is presented to control the muscle recruitment level under fatigue and uncertain muscle activation. An estimate of this level is determined by calculating the mean absolute value (MAV) of the FES-evoked electromyogram. In contrast to the previous approaches (e.g., [102]), the MAV is only calculated within a specific region of the m-wave whose position and length is described by two parameters. These parameters are adapted the individual muscle and electrode placement, by an optimization that that aims to obtain a linear relationship between the calculated MAV and the resulting joint angle. Further, a good signal-to-noise ratio in the calculated MAV is rewarded.

The MAV-based feedback control approach described in [102] has been published in 2015 and is similar to the approach presented in this thesis. The latter goes even further, however, because of the optimization procedure mentioned above. Additionally, the control approach presented in this theses is much simpler, while the tracking performance is still comparable. Further, first results were already obtained in a simpler version of recruitment control presented three years before (2012) in [85].

Most recently, the importance and the currently rising interest in eEMG-controlled FES to compensate time-variant effects is reviewed in [63].

2.8.6 Variable stimulation frequencies

FES relies on the application of short electrical pulses whose intensity described by the pulse charge can be modulated, while the time intervals between the stimulation pulses form a second control input. Because the pulses are applied at discrete times instants, discrete-time control systems are predestinated for the control of such neuro-prosthetic systems. As FES activated muscles are subjected to a fast development of muscular fatigue, the range of motion of functional tasks can be limited in the long term requiring time for motor unit recovery. It has been found, that for achieving the same resulting muscular force, a higher stimulation frequency (and smaller intensity) leads to a faster proceeding of muscular fatigue, compared to a low-frequency stimulation (and higher intensity) [78, 79]. However, more frequently applied pulses typically enable a better performance in time-discrete control systems. Therefore, typically a compromise between the proceeding of muscular fatigue and control performance is chosen. Herein, fixed frequencies ranging from 20 to 60 Hz are used, whereby the stimulation intensity remains the only actuation variable. Though variable stimulation frequencies are commonly not used to control FES, Kesar et al. suggest considering this strategy to improve muscle performance [79].[12] For temporarily increasing the control performance, an obvious approach could be to increase the actuation rate for periods during which it is beneficial (e.g., during fast movements), while for

[12] Some stimulation devices allow the generation of doublet or triplet pulses (multiple stimulation pulses in a row) that cause a different recruitment behavior (commonly an innervated response to the stimulus). It should be noted that the developed framework does not address this.

periods of low activity (e.g., holding a position) the actuation rate may be lowered. However, the effect of continuously adjusting the actuation times must be included in the discretized model.

Typically, most methods in sampled-data systems rely on periodic sampling [57], however, and typical time-discretization methods [57] require a fixed duration of actuation- and sampling intervals rendering them unfeasible to the use case described above. Hence, a more general method is required that takes variable sampling and actuation times into account.

Irregular sampling times are typically considered in the analysis of Networked Control Systems (NCS) by considering, e.g., random time delays for the arrival of a sensor measurement at the controller [66]. An application for NCS is e.g. [5]. Such approaches typically consider variations in the sampling time to be external disturbances. In [164] stability properties for switching between multiple sampling rates are investigated, however only for a finite number of different rates. There are some approaches for determining an optimal sampling rate for each control loop, respectively, in large-scale control systems to optimize the usage of resources, e.g., [65], [106]. Stability under random sampling rates is e.g. investigated in [53]. Applications that use variable sampling rates are e.g. [118], [168]. In event-based control [13], typically a control step is triggered by a condition on the plant's states that may cross defined borders or tolerance bands leading to irregular sampling times. In [111] a control scheme is presented that updates the control variable as a sensor measurement becomes available. In [28] several issues in event-based sampling in the context of non-linear filtering are discussed e.g. anti-aliasing filters. An event-based PID-controller is proposed in [11] without a formal analysis. First results for analyzing event-based systems are presented in [64], whereby the focus is on regularly sampled control systems in which actuation variable updates can be skipped. In [10] the stability of a classically designed state-feedback controller applied to a plant is analyzed, whereby the time for the next update of the controller output is decided online by an event generator.

In contrast to the above investigations, in Chapter 7, an easily usable, general framework for discretizing LTI-systems with variable times for sampling and additionally actuation is presented. To design control systems based on the obtained discrete-time models, a general linearizing controller is proposed compensating the effects caused by the irregular time intervals yielding a virtual plant that can be controlled by any discrete-time controller that assumes regular sampling.

2.9 Conclusions on the State of the Art

FES has been successfully applied for rehabilitation purposes and in some areas of daily-live support in stroke as well as spinal cord injury. Many clinical applications of FES have emerged. The most successful and popular ones include drop-foot correction and the support of the wrist and finger extension. They come in form of ready-made, commercial devices suitable for daily use. Further, FES-cycling is quite popular. In the upper extremity, grasping and reaching functions are typically considered. The generation of functional tasks using FES becomes harder, as they involve multiple degrees of freedom in the movement and a larger number of muscles involved in reaching and grasping. Nevertheless, electrical stimulation is successfully applied for rehabilitation purposes to mimic functional tasks, e.g., in Functional Electrical Therapy (FET) without the requirement of precise positioning capabilities. Devices that react to residual volitional activity by measuring EMG are present in clinical practice. However, the herein used control

strategies are simple approaches typically combining one or more of the following strategies: Triggered open-loop control, pre-defined stimulation patterns, and state-machines. User control is often based on triggered stimulation realized with a switch or by EMG-measurements from the stimulated or other non-paretic muscles. An elaborate approach aiming at arbitrary movements in which the level of stimulation support is proportionally adjusted to the intensity of the volitional activity is prone to result in movements suffering from oscillations. Despite this drawback, for rehabilitation purposes success has been reported.

In all FES applications, a basic requirement is the reasonable control of the stimulation intensity to obtain motion feasible for the specific application. Often, this forms a challenging task as the muscular response to FES is typically difficult to predict and varies in time. Hence, active research on finding feasible (feedback) control strategies has been performed in the past four decades. The often-cited difficulty of muscle fatigue could be treated (involving some effort) by control approaches like robust control, multiple model control, learning control or the use of cascaded control schemes. Problematic is, however, the feasibility of most approaches with respect to parameter tuning and the consequential time duration that has to be spent for controller preparations.

FES applications for the upper extremity (e.g., reaching) are still difficult to implement because of the complexity regarding the number of involved muscles. Therefore, often hybrid approaches are used that perform a guidance of movements and, further, support the arm weight. Most control approaches are open-loop and based on fixed stimulation patterns.

2.9.1 Restoration of reaching functions

In functional electrical therapy, reaching functions are mimicked by FES activation in stroke rehabilitation, wherein the precision of the obtained motion is less important. In daily life support, however, e.g., the interaction with objects, a higher motor precision is essential. Because of a large number of degrees of freedom and the many involved muscles, such demands for the generation of upper-limb motion by FES are hard to achieve. In case of a partial paralysis, the user can still correct postures by his residual volitional activity meaning FES is supporting the reaching task. Many approaches that provide support of the elbow extension and arm elevation were presented. Herein, FES is often triggered through, e.g., user switches, motion measurements combined with a classification algorithm, and by the measured volitional muscle activity.

In case of a complete paralysis, the full restoration of arm-functions is not possible today by FES only and without a surrounding exoskeleton. Beneficial are implanted electrodes and orthosis or other mechanical surroundings that support the arm weight or perform a guidance of movements. Hence, FES was combined with such surroundings to overcome issues with the fast progression of muscle fatigue, to reduce movement complexity, and to deal with insufficient muscle forces. Sometimes the mechanical surrounding also performs an active generation of joint movements.

To correct positioning errors, a position feedback is required, which was, however, applied rarely – most probably because of the difficulty of the control task. Two approaches based on feedback-control must be mentioned: The first one is based on iterative learning control that is used to correct iteratively performed movements. This strategy is optimally suited to the rehabilitation of stroke patients, wherein typically the same movement is repeated. A successful reduction of deviations from desired movement trajectories could be achieved. In the second approach, the

application of online-learning neural networks was investigated to generate reaching functions by FES in combination with a weight-compensating exoskeleton. By now, this approach was investigated in healthy subjects and looks promising as also less preparation effort regarding controller calibration is required. The reduction in calibration effort is made possible by the online-learning approach that adapts to the arm's response to FES utilizing the neural network. However, questions regarding the extrapolation behavior remain unanswered so far.

2.9.2 Feedback-controlled FES

Up to today, the majority of neuroprosthetic devices feasible to clinical environments employ open-loop stimulation strategies, commonly by, e.g., applying pre-defined stimulation patterns that may be triggered by the user. In seldom cases, a continuous feedback of the stimulation effect, e.g., using joint angles is applied. This situation may be because open-loop strategies tend to be simpler, easier to certify, and often do not require a complex tuning procedure. Feedback, however, requires advanced tuning, bears the risk of instability, and the produced control signals might be unpleasant to patients with remaining sensation.

In research, the complexity of the investigated approaches is significantly increased – however, most commonly in an academic context meaning for control tasks not (directly) applicable to daily life support or rehabilitation purposes. Often single joint movements, e.g., the control of the knee joint angle against gravity were considered and, further, the more elaborate controllers were often only tested in one or more healthy subjects.

In single joint angle control, feedback control strategies ranging from simple PID- to nonlinear control systems were tested. As the control system's complexity increases, commonly elaborate models to describe the musculoskeletal system are required. Hence, the effort spent on the adaptation of such control system to the individual subject commonly also increases. Robust control schemes that have lower model-requirements may yield a lower control performance (e.g., sliding mode may cause oscillations). Alternatively, cascaded control schemes may be used to perform a linearization by feedback of certain parts of the musculoskeletal system. They, however, were seldom investigated and require more effort in measuring adequate variables like torque or acceleration in addition to position measurements.

More complex control tasks, such as the control of multi-joint systems as present in walking were often considered only in simulation studies in the past. More recently, though, feedback control in complex settings, e.g., reaching or the restoration of walking was tested – often in combination with learning control that relies on repetitive motion or online-learning artificial neural networks.

An important topic is the automatic adaptation to changing muscle conditions. This topic has been treated by approaches in which system parameters are continuously estimated by observers, e.g., Kalman-filters. However, these approaches required detailed knowledge of the system's behavior in form of mathematical models. It is questionable if such approaches are still feasible in – even more complex – multi-muscle and multi-joint configurations. The application of online-learning neural networks to explore the behavior of the musculoskeletal system might be a solution to incorporate uncertain responses better, to compensate for time-varying effects, and potentially to reduce preparation time. Iterative learning control performs an automatic adaptation, too, however, settled to repetitive movement tasks, which is still feasible to stroke rehabilitation, in any case. In case of hybrid muscle activations, meaning a muscle is activated volitionally, and by

FES at the same time, it is difficult to distinguish between the contribution of stimulation and the volitional activity to the movement. Therefore, the observation of muscle fatigue becomes difficult.

In the past years, an increased interest in the use of the evoked EMG for estimating joint forces or muscle fatigue that could be used as a feedback variable in cascaded control schemes can be observed. In the presented approaches, still, complex models are used that must be adapted to the individual muscle. Hence, they are still difficult to be applied in clinical practice.

The majority of control schemes are designed under the assumption of the absence of volitional muscle activity. The interaction with potentially present activity in stroke or SCI patients may cause undesired closed-loop behavior. Other approaches, nevertheless, use the measured volitional muscle activity to control the stimulation intensity allowing a direct user interaction. However, the low signal-to-noise ratio of the measurement limits the performance.

To improve motor-precision of artificially generated movements in antagonistic muscle pairs, co-activation strategies – as present in the natural generation of motion – were proposed. Their transfer to FES is difficult, however, as the generated co-activation level cannot be measured and is subjected to unobservable variations due to changing muscle conditions.

2.9.3 Discussion

In this section, the current state of the art as presented in the previous sections is compared to the methods and applications developed and investigated in this thesis.

Restoration of reaching functions To restore reaching functions, FES is typically applied in an open-loop manner, often employing pre-defined stimulation patterns. These strategies do not allow an arbitrary hand-positioning, wherein remaining errors are automatically corrected. In some approaches, the user can modulate the positioning linearly. Approaches for the rehabilitation of stroke patients were presented that allow a position feedback, however, only supporting repetitive movements. The work by Resquin et al. [146] has to be mentioned as it introduces a new feedback-control scheme for positioning that does not rely on trials. However, there are remaining questions regarding the learning and extrapolation behavior of the used ANN.

In addition to the open-loop control schemes, this thesis presents a system for FES-based and feedback-controlled positioning of the hand in Chapter 5. This system aims to enable reaching functions using FES in patients who have a complete paralysis of arm and shoulder functions due to high-level spinal cord injury. To reduce muscle fatigue, a weight-compensating exoskeleton is used that further allows locking three degrees of freedom of the arm movement individually. Herein, the weight-compensation increases the reachable space and the brakes allow to hold postures so that the general amount of FES required is reduced. In contrast to previous approaches, the brakes are integrated with the positioning controller to simplify the control concept and thus lower model requirements and calibration effort, while still allowing position feedback control. Further, in Chapter 4, a feedback-controlled arm-weight compensating neuroprosthesis to support weak residual activity in the arm elevation is presented.

Muscle fatigue, linearization, and artificial control of co-activation Although control schemes able to compensate or tolerate muscle fatigue or other time-varying muscle properties were presented, cases exist in which these approaches fail. These cases include at least the generation of FES-induced co-activations and some cases involving hybrid muscle activation – like the one presented in this thesis (cf. Chapter 4). To compensate for the effects of muscle fatigue – also in the cases in which current control schemes typically fail – this thesis presents recruitment control (cf. Chapter 3) as a solution.

To reduce the complexity of models required for control system's design – and thus to reduce calibration effort, the recruitment control scheme, further, performs an enforced linearization of some non-linear parts of the musculoskeletal system by a feedback of the stimulation-evoked EMG.

Similar approaches to that were already investigated. However, they were mostly constrained to isometric conditions or require torque sensors. A newer approach presented in 2015 also controls muscle recruitment by a feedback of the m-wave's mean absolute value. However, much effort is introduced by the control algorithm, and the benefits of this increased effort are not quite clear. In contrast, the approach presented in this thesis uses a simple integral controller, which has found to be well sufficient. Further, an optimized strategy for evaluating the m-wave is used that enhances the noise level and the meaningfulness of the feedback variable.

In the past, only few control concepts involving co-activation strategies were investigated. Mostly, the focus was on fundamental research, and no approach can compensate for the effects of muscle fatigue. In contrast, this thesis presents a joint angle control scheme that uses underlying recruitment control to compensate for the effects of muscle fatigue in Chapter 6. An increased level of co-activation is generated when switching in-between the muscles of the antagonistic pair occurs.

Support of volitional muscle activities To allow a user-control by the residual volitional activity, approaches that measure EMG from the stimulated muscle were proposed. Some of them trigger pre-defined stimulation patterns, and others perform a linear modulation of the stimulation intensity according to the intensity of the volitional activity. Triggered approaches do not support arbitrary movements. Hence, proportionality-based approaches were proposed that, however, tend to cause oscillations in the movements. To overcome these issues, this thesis presents (Chapter 4) an approach that indirectly uses joint angle measurements to detect the volitional activity and applies it to the support of weak arm elevation movements. Because of the hybrid muscle activation, as described in the paragraph before, this control concept requires recruitment control to compensate for the effects of muscle fatigue. A similar approach was already presented for FES supported standing up before, however, relying on detailed models and without the adaptation to muscle fatigue. Further, questions regarding the closed loops' stability remain unanswered.

Mathematical models that describe the muscle activation by FES- and a volitional contribution at the same time (hybrid muscle activation) were not investigated by now. However, such models might enhance the control of neuroprostheses that involve volitional contributions in combination with FES. This thesis, therefore, presents a first attempt of such a model in Appendix A.

Variable stimulation rates According to fundamental research, by a reduction of the stimulation rate, the progression of muscle fatigue may be retarded. However, almost no control system, neither feedback nor closed-loop, applies a modulation of the stimulation rate. One reason may be the fact that changes in the stimulation frequency also require the control system to adapt its update frequency. However, variable rate control is quite uncommon – also in other applications of automatic control. As a starting point, this thesis, therefore, presents a basic framework for the control of linear systems under variable sampling rates in Chapter 7.

3

MUSCLE RECRUITMENT CONTROL (λ-CONTROL)

As described in the introduction of this thesis, the effect of FES in terms of, e.g., joint torque and angle, is difficult to model and to predict (cf. Sec. 2.8). However, there is a direct / strong relation between these values (torque/angle) to the muscular recruitment level that can be described by a model (cf. Sec. 2.6). Thus, the main difficulty remains in modeling and predicting the muscle recruitment level that strongly depends on muscle fatigue and many other factors. The relation between the stimulation intensity and the muscle recruitment is typically described by a nonlinear static function that is often identified (or parts of it) in advance to any further calibration or control activities. However, parameters do change as muscle fatigue progresses and a degrading model-performance is typically observed.

Instead, in the recruitment control method presented in this chapter, the stimulation-evoked EMG (m-wave) is used to obtain an indicator of the muscle recruitment level λ. This indicator is estimated by evaluating the m-wave's intensity in terms of the one-norm taken within a specific window of the EMG signal. For each stimulation pulse, this yields an estimate $\hat{\lambda}$ of the recruitment level. A closed-loop control system then adapts the stimulation intensity such that a given reference $r_{\hat{\lambda}}$ for the motor unit recruitment is tracked. This allows for the precise adjustment of the muscular recruitment. As the highly non-linear recruitment function is covered by the closed loop, its influence and hence also the influence of muscle fatigue to the actual recruitment is compensated. Only a rough estimate of the initial slope of this function within its linear part is required to design the controller.

An upper-level control system (feedback or feedforward) may then directly adjust the muscular recruitment instead of the stimulation intensity, the impact of which on contraction strength is difficult to predict. Therefore, a more precise control of the joint torque or the angular motion becomes possible.

In this chapter, a digital filter algorithm to evaluate the m-wave's intensity is presented. Filter parameters are determined by an optimization procedure that improves the overall degree of linearity between the estimated recruitment level $\hat{\lambda}$ and the stimulation effect in terms of the joint angle while keeping a good signal to noise ratio of the estimate $\hat{\lambda}$. Further, the recruitment controller and its design using sensitivity functions are presented. The control system was implemented to obtain a fully automated calibration routine without user interaction. To be able to monitor volitional activity during the calibration procedure and in other neuro-prosthetic systems presented in ongoing chapters of this thesis, a digital filter for estimating the voluntary EMG activity is further introduced.

Using the developed set-up, a study involving five healthy subjects was performed in which the calibration routine and the subject-adapted control system was statistically evaluated. Results showed a higher degree of linearity for the controlled recruitment level – angle relationship in

comparison to the non-controlled stimulation intensity – angle relationship. The fact also holds true in the presence of muscle fatigue whose effects were compensated. Further, significantly smaller errors were obtained in generating desired angles.

Additionally, the automated calibration routine and the controller were successfully tested in two stroke patients with an incomplete paralysis in the shoulder elevation. Further, like in healthy subjects, an increased degree of linearity was observed.

The methods and results presented in this chapter have been previously published as listed below.

- The initial idea of recruitment control along with first results and an application wherein the elbow joint angle was controlled is presented in

  [85] C. Klauer, J. Raisch, and T. Schauer. "Linearisation of electrically stimulated muscles by feedback control of the muscular recruitment measured by evoked EMG". in: *Proc. of the 17th International Conference on Methods and Models in Automation and Robotics 2012*. Międzyzdroje, Poland: IEEE, 2012, pp. 108–113. ISBN: 978-1-4673-2124-2. DOI: 10.1109/MMAR.2012.6347902.

- First results showing the characteristics of the recruitment function as well as the compensation of muscle fatigue are presented in

  [84] C. Klauer, J. Raisch, and T. Schauer. "Feedback Control of the Electrical Stimulation Induced Muscular Recruitment Determined by the Evoked Electromyogram". In: *Biomedical Engineering / Biomedizinische Technik* 57.Suppl. 1, Track-F (2012), pp. 639–639. ISSN: 1862-278X. DOI: 10.1515/bmt-2012-4417.

- Further results on the compensation of muscle fatigue along with an application to control the foot elevation to be used in a drop foot correcting neuro-prosthesis [115] are given in

  [83] C. Klauer, J. Raisch, and T. Schauer. "Advanced Control Strategies for Neuro-Prosthetic Systems". In: *Proc. of the 4th European Conference on Technically Assisted Rehabilitation - TAR 2013*. Berlin, Germany, 2013.

- The ability of recruitment control to reliably produce joint angles for the arm elevation is demonstrated in one healthy subject. Further, a control system to be used in therapy for the rehabilitation of stroke patients involving voluntary and FES-induced muscle contractions is presented. This work was mainly performed by third-party researchers who applied and verified the proposed recruitment control method:

  [9] E. Ambrosini, T. Schauer, C. Klauer, A. Pedrocchi, G. Ferrigno, and S. Ferrante. "Control system for neuro-prostheses integrating induced and volitional effort". In: *IFAC-PapersOnLine*. 9th IFAC Symposium on Biological and Medical Systems BMS 2015, Berlin, Germany, 31 August-2 September 2015 48.20 (2015), pp. 327–332. ISSN: 2405-8963. DOI: 10.1016/j.ifacol.2015.10.160.

- A significant improvement was introduced by an optimization procedure to determine filter parameters and a design procedure for the recruitment controller yielding the ability of a fully automatic adaptation of the system to the individual subject. Further, for the shoulder abduction, the compensation of muscle fatigue effects and the improvement of the degree of linearity for the $\hat{\lambda}$ – elevation joint angle relationship were shown in a study involving five healthy subjects. Further, recruitment control was successfully verified in one stroke

patient with an almost complete paralysis in the shoulder elevation in

[80] C. Klauer, S. Ferrante, E. Ambrosini, U. Shiri, F. Dähne, I. Schmehl, A. Pedrocchi, and T. Schauer. "A patient-controlled functional electrical stimulation system for arm weight relief". In: *Medical Engineering & Physics* 38.11 (2016), pp. 1232–1243. DOI: 10.1016/j.medengphy.2016.06.006.

- To improve recruitment control for two muscles or muscle parts close to each other (e.g., in antagonistic muscle pairs), an extension to two-channel recruitment control was presented and tested in one healthy subject in

  [93] C. Klauer and Schauer T. "Two-Channel Muscle Recruitment (λ)-Control using the Evoked-EMG". in: *Proc. of the 20th Annual International FES Society Conference 2016*. La Grande Motte, France, 2016.

Copyright statement The text and the pictures in this section are based, with slight modifications, on the following publications: Sec. 3.1 to Sec. 3.6 are based on [80] slight modifications of the text and the figures were performed. Further, results for a second stroke patient were added.

Sec. 3.7 is partially based on [93]. The text describing the calibration procedure was added.

3.1 System Overview

The experimental set-up used to develop the recruitment control method is shown in Fig. 21. Herein, FES is applied to the medial part of the deltoid muscle using a current-controlled stimulator (Rehastim I, Hasomed GmbH, Germany) and self-adhesive electrodes (ValuTrode® CF4090 (4x9 cm), Axelgaard Manufacturing Co., USA). A stimulation frequency of 25 Hz is used and corresponds to the sampling frequency of the control system (with sampling index k). The intensities of the electrical pulses are modulated in terms of the pulse charge Q that varies between zero and the maximally tolerable charge Q_{max}. The control signal $v[k] \in [0, 1]$ is the normalized pulse charge. Current amplitude and pulse width are computed from $v[k]$ using the charge control method introduced in Sec. 2.4. The abduction angle $\vartheta[k]$ is measured at 25 Hz utilizing an inertial sensor (MTx, Xsens Technologies B.V., The Netherlands). The electromyogram (EMG) is measured from the stimulated muscle at 2048 Hz (sampling index i) using separate Ag/AgCl electrodes (Ambu Neuroline 720, Ambu A/S, Denmark) and amplified using a multi-channel signal amplifier (Porti^{TM}, TMS International, The Netherlands). The EMG electrodes are placed outside the stimulation electrodes, as indicated in Fig. 21. By filtering the EMG (sampled at 2048 Hz), the volitional muscle activity level $\hat{\gamma}[k]$ and the muscle recruitment level $\hat{\lambda}[k]$ of the preceding stimulation period are obtained at stimulation frequency (cf. Sections 3.2.2 and 3.2.3). The recruitment controller adjusts the stimulation intensity to produce a desired recruitment level $r_{\hat{\lambda}}[k]$.

On the placement of the EMG-electrodes The stimulation electrodes are placed at first such that a good shoulder elevation is obtained for stimulation intensities not leading to significant discomfort. Then, the EMG electrodes are placed outside of the stimulation electrodes within fiber direction. The upper electrode should be placed on a bony part of the shoulder joint, if possible. The lower

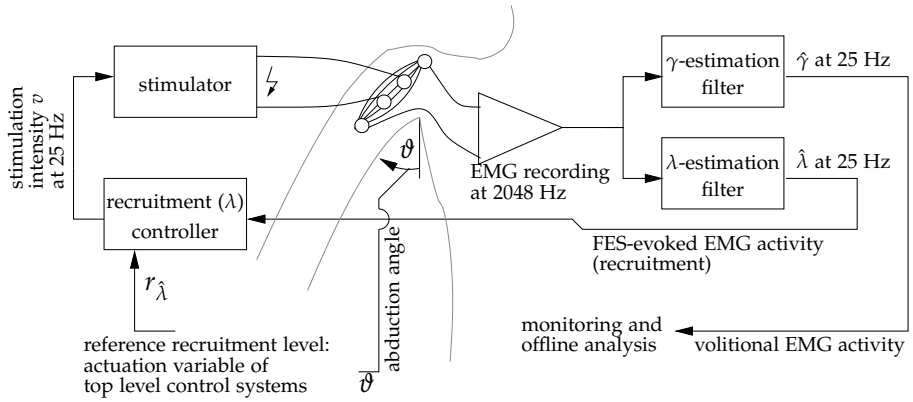

FIGURE 21: *The control scheme for recruitment control, wherein FES is applied to the medial deltoid muscle.*

should be placed below the deltoid. Herein, the assumption is that the placement of the electrodes outside of the deltoid muscle yields less dependence of the EMG-measurement on fiber shifting.

Please note that procedure described above resulted from experience and was not determined in a systematic evaluation. However, good results were obtained using this procedure.

3.2 EMG Signal Processing

The FES-evoked and the volitional muscle activities are monitored by EMG of the deltoid muscle. The EMG is sampled at 2048 Hz yielding the raw EMG vector

$$\boldsymbol{EMG}_{raw}[k] = \begin{bmatrix} EMG_{raw,1}[k] & \cdots & EMG_{raw,L}[k] \end{bmatrix}^T, L = 82,$$

for each stimulation sampling instant k. This vector captures a number of $L = 82$ EMG samples of the preceding 40 ms inter-pulse interval (corresponding to 25 Hz stimulation frequency). As indicated in Fig. 22, the beginning is aligned to the stimulation pulse and contains information about the muscle activity related to the stimulus $k-1$. It is assumed that the FES-evoked EMG component (also called m-wave) is a time-variant signal in the mV-range while the volitional EMG signal part is band-limited Gaussian noise in the μV range. To separate both information, several signal processing steps need to be performed (adapted from [6] and [85]) as detailed in the following sections.

3.2.1 Offset reduction

The offset in the raw EMG measurement is calculated by averaging the last three EMG samples of a stimulation period over the last five stimulation periods. The averaging approach makes the estimate furthermore robust with respect to volitional EMG in the same time window:

$$\hat{EMG}_{ofs}[k] = \frac{1}{5 \cdot 3} \sum_{j=k-5}^{k-1} \sum_{i=L-2}^{L} EMG_{raw,i}[j]. \tag{1}$$

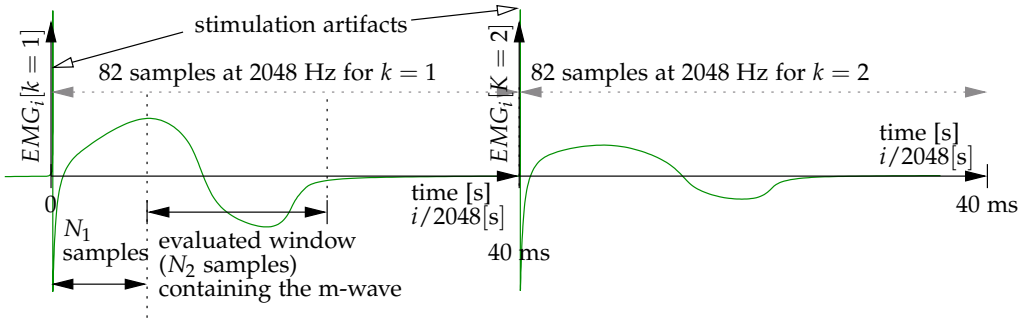

FIGURE 22: *Evaluation of the m-wave to estimate the recruitment level.*

No FES-evoked activity is expected in this time interval. Offset correction is then performed by

$$\boldsymbol{EMG}[k] = \boldsymbol{EMG}_{raw}[k] - \hat{EMG}_{ofs}[k]. \tag{2}$$

3.2.2 VOLITIONAL EMG

The estimation of the volitional EMG during active FES requires the removal of the m-wave from the EMG signal. In the chosen approach, the EMG vectors of the last six stimulation periods are memorized. The best prediction of the currently measured EMG vector by a linear combination of the previously memorized EMG vectors is then used as an estimate of the current m-wave[13]. The corresponding coefficients of the linear combination are optimized by a linear least squares approach at each stimulation period. Finally, the obtained estimate of the m-wave is subtracted from the currently measured EMG vector to determine the volitional EMG component, which is then evaluated utilizing the 1-norm. This separation approach works better for the second half of the stimulation period wherein only the tail of the m-wave is contained.

This approach is adapted from [165, 6], and a detailed description of the procedure is given below.

Initially, the first 40 entries of the EMG measurement vector $\boldsymbol{EMG}[k]$ are set to zero to blank stimulation artifacts and to remove the main part of the m-wave during each inter-pulse interval:

$$\boldsymbol{EMG}^{Vb}[k] = \begin{bmatrix} \mathbf{0}_{40}^T & EMG_{41}[k] & \cdots & EMG_{L-11}[k]. \end{bmatrix}^T \tag{3}$$

Herein, $\mathbf{0}_{40}$ is a zero vector of the dimension 40.

Then, the vector $\boldsymbol{EMG}^{Ve}[k]$, containing the FES-evoked EMG response (m-wave), for the non-blanked sampling instants is estimated by applying the adaptive filter

$$\boldsymbol{EMG}^{Ve}[k] = \begin{bmatrix} \boldsymbol{EMG}^{Vb}[k-1] & \cdots & \boldsymbol{EMG}^{Vb}[k-M] \end{bmatrix} \begin{bmatrix} \hat{p}_1^V[k] \\ \vdots \\ \hat{p}_M^V[k] \end{bmatrix}, \tag{4}$$

[13] Please note that the measured EMG does not only contain the m-wave but might also be the result of a superposition of volitional EMG activity and the m-wave. Hence the actual m-wave must be estimated.

wherein $\hat{\boldsymbol{p}}^V[k] = \begin{bmatrix} \hat{p}_1^V[k] & \dots & \hat{p}_M^V[k] \end{bmatrix}^T$ is continuously determined by solving the following least squares problem for each sampling instant k:

$$\hat{\boldsymbol{p}}^V[k] = \arg\min_{\boldsymbol{p}^V}[k] \left|\left| \boldsymbol{EMG}^{Vb}[k] - \begin{bmatrix} \boldsymbol{EMG}^{Vb}[k-1] & \cdots & \boldsymbol{EMG}^{Vb}[k-M] \end{bmatrix} \boldsymbol{p}^V \right|\right|_2 . \tag{5}$$

According to the investigations in [6], the number of previous EMG vectors is set to $M = 6$.

A scalar measure of the volitional muscle activity of the preceding 40 ms inter-pulse interval at sample k is obtained by taking the scaled 1-norm of the vector $(\boldsymbol{EMG}^{Vb}[k] - \boldsymbol{EMG}^{Ve}[k])$:

$$\hat{\gamma}[k] = 1/(L-50) \left|\left| \boldsymbol{EMG}^{Vb}[k] - \boldsymbol{EMG}^{Ve}[k] \right|\right|_1 .$$

Hence, the volitional EMG part is the residual part of $\boldsymbol{EMG}^{Vb}[k]$ that cannot be described by a linear combination of memorized blanked EMG vectors.

3.2.3 FES-evoked EMG

Similar to the approach described in Sec. 3.2.2, an estimate of the m-wave is obtained by using a linear combination of six previous EMG vectors. Then, the 1-norm is taken to obtain the intensity of the estimated m-wave in a sub-window of the inter-pulse interval. A detailed description of the procedure is given below.

To evaluate the m-wave, as shown in Fig. 22, the offset-removed EMG vector (Eq. (2)) is blanked yielding

$$\boldsymbol{EMG}^{Eb}[k] = \begin{bmatrix} \boldsymbol{0}_{N_1}^T & EMG_{N_1}[k] & \cdots & EMG_{N_1+N_2-1}[k] & \boldsymbol{0}_{L-N_1-N_2}^T \end{bmatrix}^T , \tag{6}$$

whereby the parameters N_1 and N_2 determine window position and length, respectively. Analog to the voluntary filter, the evoked EMG component is predicted by an adaptive filter

$$\boldsymbol{EMG}^{Ee}[k] = \begin{bmatrix} \boldsymbol{EMG}^{Eb}[k-1] & \cdots & \boldsymbol{EMG}^{Eb}[k-M] \end{bmatrix} \begin{bmatrix} \hat{p}_1^E[k] \\ \vdots \\ \hat{p}_M^E[k], \end{bmatrix} \tag{7}$$

where $\hat{\boldsymbol{p}}^E[k] = \begin{bmatrix} \hat{p}_1^E[k] & \dots & \hat{p}_M^E[k] \end{bmatrix}^T$ is continuously determined by solving the following least squares problem for each sampling instant k:

$$\hat{\boldsymbol{p}}^E[k] = \arg\min_{\boldsymbol{p}^E}[k] \left|\left| \boldsymbol{EMG}^{Eb}[k] - \begin{bmatrix} \boldsymbol{EMG}^{Eb}[k-1] & \cdots & \boldsymbol{EMG}^{Eb}[k-M] \end{bmatrix} \boldsymbol{p}^E \right|\right|_2 . \tag{8}$$

Then, the one-norm of $\boldsymbol{EMG}^{Ee}[k]$ yields the estimated muscular recruitment level

$$\hat{\lambda}_{N_1,N_2}[k] = \left|\left| \boldsymbol{EMG}^{Ee}[k] \right|\right|_1 .$$

The parameters N_1 and N_2 are adapted to the individual user by the optimization procedure outlined in Sec. 3.4 yielding the optimal parameters $\hat{N}_1$ and $\hat{N}_2$. In the following sections, for

simplifying the notation, the estimate of λ obtained for the optimal parameters is denoted by $\hat{\lambda} := \hat{\lambda}_{\hat{N}_1,\hat{N}_2}$.

3.3 Recruitment Control

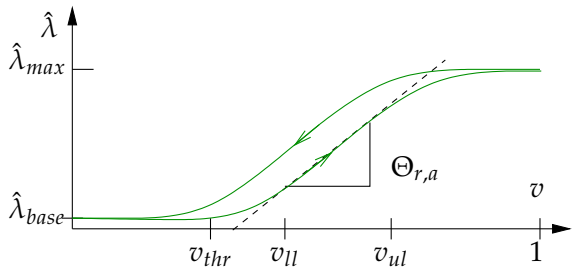

Figure 23: *Muscular recruitment function including hysteresis and the used linear approximation for the stimulation range $[v_{ll}, v_{ul}]$. Further, $\hat{\lambda}_{base}$ is the base level that occurs for stimulation not leading to a muscle contraction. The maximally obtained value for $\hat{\lambda}$ is called $\hat{\lambda}_{max}$, and v_{thr} is the stimulation intensity yielding the onset of muscle contraction.*

To design the recruitment controller, a simplified, linear discrete-time model is assumed. It describes the relationship between the stimulation intensity v and the estimated recruitment $\hat{\lambda}$:

$$\hat{\lambda}(k) = \Theta_{r,a}\, q^{-1}\, v(k) + \Theta_{r,b} + e(k), \quad \Theta_{r,a} > 0,\ v_{ll} \leq v(k) \leq v_{ul}. \tag{9}$$

Herein, q^{-1} is the backward-shift operator ($a(k)q^{-1} = a(k-1)$), and $e(k)$ is white noise (variance $\sigma^2_{\hat{\lambda}}$, expected value is zero). This equation describes the linear, rising part of the non-linear recruitment function shown in Fig. 23. The time delay of one sampling instant is introduced because the estimate $\hat{\lambda}[k+1]$ depends on the stimulation pulse $v[k]$ applied for the previous sampling instant k.

The parameters $\Theta_{r,a}$ and $\Theta_{r,b}$ are adapted by least squares to match recorded I/O data pairs describing the linear part of the recruitment function. This dataset is obtained in a calibration procedure outlined in Sec. 3.4.

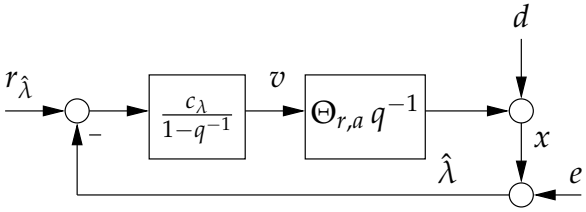

Figure 24: *Recruitment controller applied to the nominal plant.*

Frequency domain controller synthesis During control, the offset $\Theta_{r,b}$ of the linear model (9) is treated as a part of the constant disturbance d (cf. Fig. 24).

To control the nominal plant $G(q^{-1}) = \Theta_{r,a}\, q^{-1}$, a discrete-time integrating controller is chosen:

$$K(q^{-1}) = \frac{c_\lambda}{1 - q^{-1}}, \quad c_\lambda > 0.$$

The resulting closed-loop behavior (cf. Fig. 24) between the reference $r_{\hat{\lambda}}$ and the output $\hat{\lambda}$ is described by

$$T(q^{-1}) = \frac{GK}{1 + GK} = \frac{\Theta_{r,a} c_\lambda\, q^{-1}}{1 + (\Theta_{r,a} c_\lambda - 1)\, q^{-1}}.$$

The control system is asymptotically stable and well damped if the root $q_\infty = 1 - \Theta_{r,a} c_\lambda$ of the closed-loop polynomial $q + (\Theta_{r,a} c_\lambda - 1)$ fulfills $0 < q_\infty < 1$, which is equivalent to $0 < \Theta_{r,a} c_\lambda < 1$.

To be able to adjust the noise transmission of the closed loop, the tunable parameter T_n describing the noise amplification at the Nyquist-frequency is introduced. It is calculated using the complementary sensitivity transfer function T (defined as the transfer function between $-e$ and x) that is evaluated at the Nyquist frequency ($q = e^{j\Omega} = -1$, for $\Omega = \pi$)[14]:

$$T_n = |T(q^{-1} = -1)| = \frac{|-\Theta_{r,a} c_\lambda|}{|2 - \Theta_{r,a} c_\lambda|} = \frac{\Theta_{r,a} c_\lambda}{2 - \Theta_{r,a} c_\lambda}, \quad for\, 0 < q_\infty < 1. \tag{10}$$

This equation is solved w.r.t to c_λ.

$$c_\lambda = \frac{1}{\Theta_{r,a}} \frac{2T_n}{T_n + 1}. \tag{11}$$

To obtain an asymptotically stable closed loop ($0 < q_\infty < 1 \Leftrightarrow 0 < \Theta_{r,a} c_\lambda < 1$), the tunable parameter T_n must fulfill

$$0 < T_n < 1. \tag{12}$$

The tuning parameter T_n is chosen such that the amplification of high frequent measurement noise at the Nyquist-frequency with an amplitude $\sigma_{\hat{\lambda}}$ (standard deviation of the noise e estimated for the model (9) by T_n results in 1% of the maximal signal amplitude λ_{max}:

$$0.01\lambda_{max} = T_n \sigma_{\hat{\lambda}}. \tag{13}$$

By resorting Eq. (13) and inserting into Eq. (11) one obtains:

$$c_\lambda = \frac{1}{\Theta_{r,a}} \frac{2\lambda_{max}}{\lambda_{max} + 100\sigma_{\hat{\lambda}}}. \tag{14}$$

This selection gives the fastest possible closed-loop behavior for the specified SNR at the Nyquist frequency.

Anti-windup Since the actuation variable is bounded by $v \in [0, 1]$ and because of the integrating controller, an anti-windup strategy as shown in Fig. 25 is used to avoid undesired closed-loop behavior in case of saturation [12].

[14] In this equation j denotes the imaginary unit.

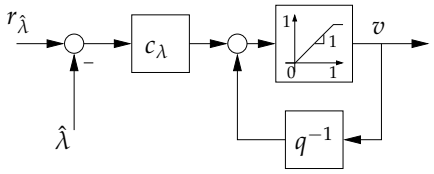

FIGURE 25: *Recruitment controller with anti-windup strategy.*

3.4 AUTOTUNING OF RECRUITMENT (λ) CONTROL

The proposed control concept needs to be adapted to the individual subject, electrode's position, and muscle condition. To minimize the requirement of manual controller tuning by the operator of the system, an automatic calibration procedure is proposed in this section. It is carried out prior to the activation of recruitment control in order to obtain the linear model of the recruitment function and to tune the filter parameters N_1, N_2 as well as the controller parameter c_λ.

3.4.1 PROCEDURE

The calibration procedure consists of two phases shown in Fig. 26, wherein the subject is asked not to intervene in the movement. During phase 1, the stimulation intensity is linearly increased from zero up to the maximum tolerated value and the EMG data, $\boldsymbol{EMG}_{p1}$, as well as the corresponding angle values, ϑ_{p1}, are recorded. From these data, the following values are calculated:

- ϑ_{min} – the minimal angle when no FES is applied.
- v_{thr} – the stimulation intensity leading to the onset of the FES-induced muscle contraction. v_{thr} is defined as the stimulation intensity corresponding to a $\hat{\lambda}$ value slightly higher than its baseline. This base-level is calculated by averaging $\hat{\lambda}$ during a period in which no FES is applied. Since the optimal parameters, $\hat{N}_1$ and $\hat{N}_2$ have not been estimated at this point of the procedure, two valid values ($N_1 = 8$ and $N_2 = 20$) that generally capture the main parts of m-waves are used to estimate $\hat{\lambda}$.
- ϑ_{sat} – the stimulation intensity above which no significant joint angle increase occurs. v_{sat} is defined as the stimulation intensity leading to an angle equal to the 95% of the maximum angle achieved, ϑ_{max}.

During phase 2, the stimulation intensity is increased from v_{thr} to v_{sat} following a stair-wise signal consisting of 10 intermediate steps and the $\boldsymbol{EMG}_{p2}$ and ϑ_{p2} data are collected. These data are used to optimize the parameters N_1 and N_2 as described in Sec. 3.4.2. After the optimal parameters $\hat{N}_1$ and $\hat{N}_2$ are found, $\hat{\lambda}$ is calculated for both phases 1,2. The data $\hat{\lambda}$ and v obtained during phase 1 are then used to identify the linear recruitment model. To assure that these data belong to the linear range of the recruitment function, two additional values of stimulation intensities are defined:

- v_{ll} (lower bound), corresponding to an angle equal to $\vartheta_{min} + 0.3 \cdot (\vartheta_{max} - \vartheta_{min})$, and
- v_{ul} (upper bound), corresponding to an angle equal to $\vartheta_{max} - 0.3 \cdot (\vartheta_{max} - \vartheta_{min})$.

The subset containing N_{recr} samples of data within the range $v \in [v_{ll}, v_{ul}]$ yields the dataset $(v_{recr,i}, \hat{\lambda}_{recr,i}, i = 1, 2, ..., N_{recr})$ that is used to identify the parameters $\Theta_{r,a}$ and $\Theta_{r,b}$ of the linear recruitment model (cf. Fig. 23) described in Sec. 3.3.

Further, datasets describing the steady-state stimulation intensity – angle and recruitment level – angle relationships are obtained from each stair during phase 2 as illustrated in Fig. 26 yielding $(\hat{\lambda}_{cal,s}, v_{cal,s}, \vartheta_{cal,s})$. Herein, $s = 1, 2, ..., 10$ corresponds to increasing and $s = 11, 12, ..., 19$ to the decreasing stairs. The obtained datasets are later used in Chapter 4 in the arm weight compensation controller to obtain a static gain of a model describing the arm elevation (cf. 4.2).

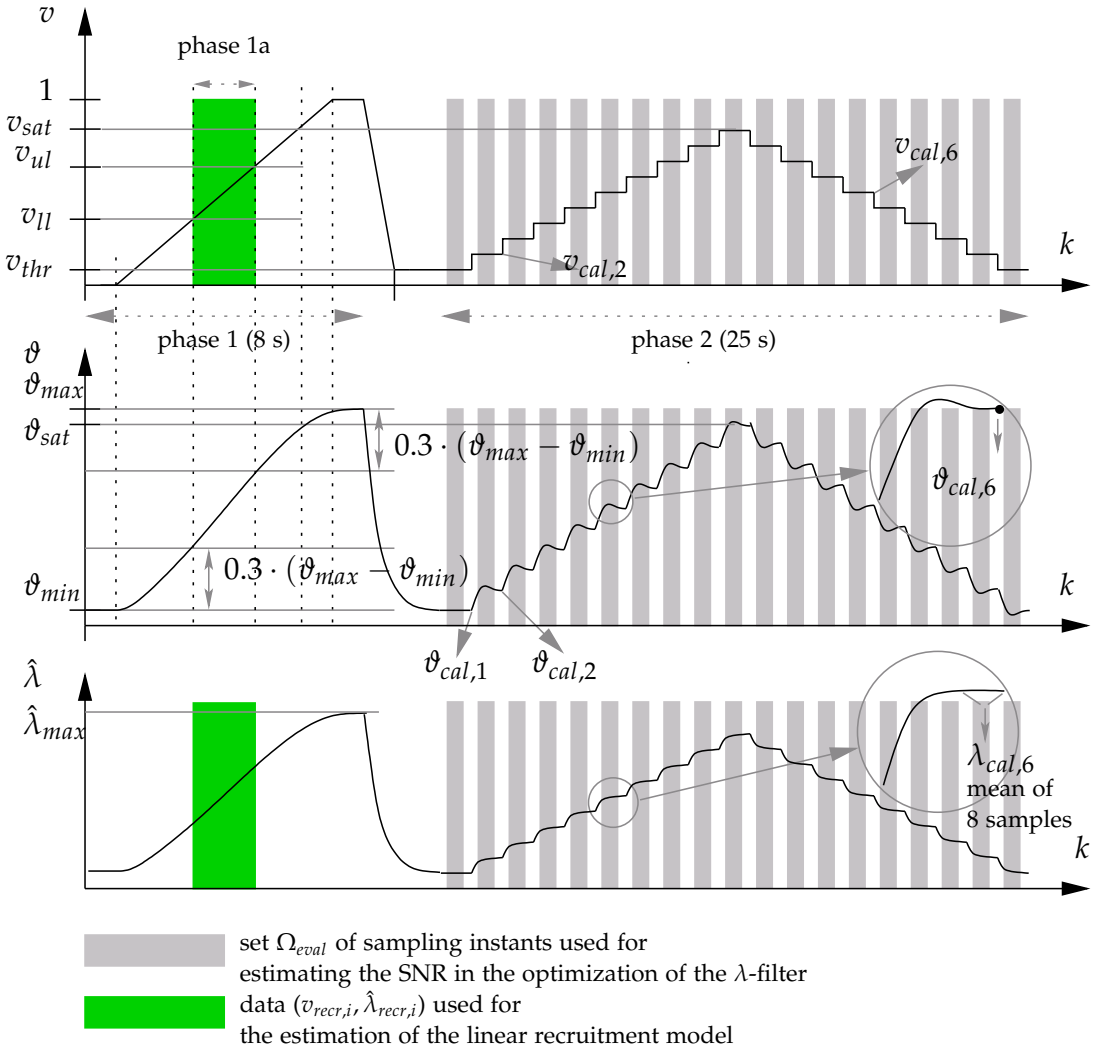

FIGURE 26: *Calibration Experiment: During phase 1, a linearly increasing stimulation intensity is applied up to the maximal tolerable intensity, and in phase 2, a staircase-wise increase and decrease of the stimulation intensity are performed. The characteristic stimulation intensities v_{thr} and v_{sat} obtained in phase 1 are used to parameterize the stimulation ranges in phase 2. The EMG and joint angle data obtained during phase 2 are used to optimize the λ-filter and afterward $\hat{\lambda}$, the output of the optimal filter, is calculated. Finally, the dataset $(v_{recr,i}, \hat{\lambda}_{recr,i})$, used for the identification of the linear recruitment model and the dataset $(\hat{\lambda}_{cal,s}, v_{cal,s}, \vartheta_{cal,s})$, describing the static actuation to joint angle relationships, are extracted.*

3.4.2 FES-evoked EMG filter optimization

This phase aims to identify N_1 and N_2 assuring a high SNR of the estimated recruitment $\hat{\lambda}$ and a good linearity between $\hat{\lambda}$ and the purely FES induced torque. Under the assumption of small angles[15], the elevation angle can be interpreted as an indirect measure of the joint torque when the biomechanical system is in steady state.

In an optimization procedure, the estimated recruitment signal $\hat{\lambda}_{p_2,N_1,N_2}$ is calculated from the EMG dataset $\boldsymbol{EMG}_{p_2}$ recorded during phase 2 for each possible combination of $N_1 \in [2,20]$ and $N_2 \in [1,30]$, which captures the feasible values for window positions and lengths. Then, for each signal $\hat{\lambda}_{p_2,N_1,N_2}$ the SNR and a measure of linearity with respect to ϑ_{p2} is calculated as described in this section and finally the best parameters are selected.

Linearity between $\hat{\lambda}$ and ϑ For the static relationship between $\hat{\lambda}$ and ϑ a linear model of the form

$$\vartheta = \Theta_{\vartheta\lambda,N_1,N_2,a} \cdot \hat{\lambda}_{N_1,N_2} + \Theta_{\vartheta\lambda,N_1,N_2,b} + e_\vartheta \tag{15}$$

is assumed. From the I/O dataset $(\hat{\lambda}_{p_2,N_1,N_2}, \vartheta_{p_2})$ one data pair is extracted for each stair s during the stationary phases of the biomechanical system. Therefore, at the end of the constant phase of each stair s, the joint angle $\vartheta_{cal,s}$ is obtained and further the mean value of $\hat{\lambda}_{p_2,N_1,N_2}$ over 8 samples at the end of the constant phase is calculated yielding $\hat{\lambda}_{cal,s,N_1,N_2}$ as illustrated in Fig. 26. Using this dataset, the model parameters $\Theta_{\vartheta\lambda,N_1,N_2,a}$ and $\Theta_{\vartheta\lambda,N_1,N_2,b}$ are identified by least squares. Then, the obtained model is used to compute the joint angles $\hat{\vartheta}_{s,N_1,N_2}$ for each stair s, which is then compared to the measured angles $\vartheta_{cal,s}$ by calculating the Normalized Root Mean Square Error (NRMSE) that serves as a measure of linearity:

$$NRMSE_{N_1,N_2} = \frac{\sqrt{\frac{1}{N_s}\sum_{s=1}^{N_s}(\vartheta_{cal,s} - \hat{\vartheta}_{s,N_1,N_2})^2}}{\max_s \vartheta_{cal,s} - \min_s \vartheta_{cal,s}}, \tag{16}$$

whereby $N_s = 19$ denotes the number of stairs.

Estimation of the signal to noise ratio (SNR) Since the noise-free signal for $\hat{\lambda}_{p_2,N_1,N_2}$ is not available, the signal component is estimated by applying a non-causal second-order Butterworth low-pass filter with zero phase shift ($f_{cut} = 75Hz$) to $\hat{\lambda}_{p_2,N_1,N_2}$ yielding $\lambda_{lp,p_2,N_1,N_2}[k]$.

The estimated noise signal $\hat{e}_{\hat{\lambda}}$ is then calculated by

$$\hat{e}_{\hat{\lambda},N_1,N_2} = \hat{\lambda}_{p_2,N_1,N_2} - \lambda_{lp,p_2,N_1,N_2}. \tag{17}$$

The power of the signal and the noise component are then evaluated based on the time series λ_{lp,p_2,N_1,N_2} and $\hat{e}_{\hat{\lambda},N_1,N_2}$ respectively.

Because the filter introduces transients starting from both borders of the dataset (due to uninitialized initial values of the non-causal filter), 20 samples are skipped for the computation of the signal power at each border respectively. Further, due to the steps in the excitation signal v, frequency components even beyond the cutting frequency f_{cut} are present in $\hat{\lambda}_{p_2,N_1,N_2}$ actually

[15] In the experiments performed to evaluate this control concept as described in Sec. 3.6, the maximal joint angle elevation was $52.2° \pm 21.3°$.

belonging to the signal component. No clean separation is possible with a low-pass filter for these frequency components. Hence, the sampling instants of the time-series signal close to the stepwise changes (6 samples before and after the step) are additionally not considered for the calculation of signal and noise power. Finally, the calculation is only performed in the set Ω_{eval} including $N_{\Omega_{eval}}$ samples (cf. Fig. 26). The signal power is calculated by

$$P_{s,N_1,N_2} = \frac{1}{N_{\Omega_{eval}}} \sum_{i \in \Omega_{eval}} (\lambda_{lp,p_2,N_1,N_2}[i])^2. \tag{18}$$

Similar, the noise power is then given by

$$P_{n,N_1,N_2} = \frac{1}{N_{\Omega_{eval}}} \sum_{i \in \Omega_{eval}} (\hat{e}_{\hat{\lambda},N_1,N_2}[i])^2. \tag{19}$$

Finally, the SNR is then calculated for each filter parameter variation by

$$SNR_{N_1,N_2} = \frac{P_{s,N_1,N_2}}{P_{n,N_1,N_2}}. \tag{20}$$

Quality functions Both indicators SNR_{N_1,N_2} and $NRMSE_{N_1,N_2}$ are combined in a quality function in form of a weighted sum using a tunable factor p_w to adjust the importance of the individual measures:

$$J_{N_1,N_2} := p_w \cdot \underbrace{(1 - NRMSE_{N_1,N_2})}_{J_1} + (1 - p_w) \cdot \underbrace{\frac{SNR_{N_1,N_2}}{\max_{N_1,N_2}(SNR_{N_1,N_2})}}_{J_2}. \tag{21}$$

Herein, the SNR is normalized to the observed maximum. Thus, for both sub-functions J_1 and J_2, the optimal values describing the best SNR and the best linearity are represented by $J_1 = 1$ and $J_2 = 1$, respectively. Hence, the comparison in the weighted sum is possible. A weighting factor of $p_w = 0.9$ is chosen, because a linear relationship is considered to be more important for the later introduced arm weight support controller. To find the optimal compromise, the maximum of J_{N_1,N_2} is obtained by varying the tunable filter parameters N_1 and N_2 yielding the optimal parameters

$$[\hat{N}_1, \hat{N}_2]^T = \arg\max_{N_1,N_2} J_{N_1,N_2}, \text{whereby } \hat{J} = J_{\hat{N}_1,\hat{N}_2}. \tag{22}$$

Please keep in mind that the notation of the optimal estimate is shortened to $\hat{\lambda} := \hat{\lambda}_{\hat{N}_1,\hat{N}_2}$.

3.4.3 Recruitment controller parameterization

The estimated parameters $\Theta_{r,a}$ and $\Theta_{r,b}$ of the linear recruitment model and the standard deviation $\sigma_{\hat{\lambda}}$ of the noise are used to determine c_λ by Eq. (14). Therefore, $\sigma_{\hat{\lambda}}$ is estimated from the estimated noise $\hat{e}_{\hat{\lambda},\hat{N}_1,\hat{N}_2}$ by

$$\sigma_{\hat{\lambda}} = \sqrt{\frac{1}{N_{\Omega_{noise}}} \sum_{i \in \Omega_{noise}} (\mu_e - \hat{e}_{\hat{\lambda},\hat{N}_1,\hat{N}_2}[i])^2}, \quad \mu_e = \frac{1}{N_{\Omega_{eval}}} \sum_{i \in \Omega_{eval}} \hat{e}_{\hat{\lambda},\hat{N}_1,\hat{N}_2}[i]. \tag{23}$$

3.5 Validation of the Auto-Tuned Recruitment Control

The performance of the auto-tuned recruitment control is compared to Direct Stimulation (DS). To perform this comparison, a long-term test is designed in which single trials using either the auto-tuned RC or the DS are repeated in an alternating fashion until significant muscle fatigue occurs. During each trial j, a pre-defined sequence of 19 reference joint angles with $s = 1, 2, \ldots, 19$ is used. For the first 10 references, a linearly increasing ramp between ϑ_{min} and $0.95 \cdot \vartheta_{max}$ is used, while the last 9 references are chosen to decrease back to ϑ_{min} with the same spacing. Using the calibration dataset ($\hat{\lambda}_{cal,s}$, $v_{cal,s}$, $\vartheta_{cal,s}$) the stimulation intensities v_s and the reference recruitment levels $r_{\hat{\lambda},s}$ that theoretically lead to the joint angles $\vartheta_{comp,s}$ are calculated. Successively, each of these values is constantly applied for one second using DS and RC, respectively. For each trial j, each stair s, and each control type ($type \in \{DS, RC\}$), the resulting steady-state joint angles $\vartheta_{j,s,DS}$ and $\vartheta_{j,s,RC}$ caused by v_s and $r_{\hat{\lambda},s}$, respectively, are measured directly before the next stepwise change in the actuation variable.

The following parameters were computed to compare DS and RC:

a) Linearity The degree of linearity was computed both during the RC calibration phase and during the fatigue test. During calibration, the steady-state dataset ($\hat{\lambda}_{cal,s}$, $v_{cal,s}$, $\vartheta_{cal,s}$) was analyzed comparing the degree of linearity obtained between the non-controlled direct stimulation intensity $v_{cal,s}$ and the angle $\vartheta_{cal,s}$ and between the recruitment level $\hat{\lambda}_{cal,s}$ and the angle $\vartheta_{cal,s}$. For each subject, linear models were identified for both relations and compared in terms of the fitting coefficient of determination, denoted R^2, and the normalized root mean squared error (NRMSE) between the fitted line and the dataset values. During the successive trials of the fatigue test, given that the 5 subjects performed a different number of trials before fatigue occurred, a mean degree of linearity was computed for each subject and was assessed by the coefficient of determination R^2. Only steps in which the stimulation intensity was not saturated were considered for the recruitment controller. To maximize comparability across subjects, before applying the linear fitting, the measured angles $\vartheta_{j,s,type}$ were normalized to their overall minimum $\underline{\vartheta}$ and maximum $\overline{\vartheta}$ value obtained in each subject:

$$\vartheta_{norm,j,s,type} = (\vartheta_{j,s,type} - \underline{\vartheta}) / (\overline{\vartheta} - \underline{\vartheta}). \tag{24}$$

b) Fatigue To evaluate the effect of muscle fatigue, the mean value of all normalized joint angles for the rising part[16] of the staircase is calculated:

$$M_{j,type} = 1/10 \cdot \sum_{s=1}^{s=10} \vartheta_{norm,j,s,type}, \quad \text{for } type \in \{DS, RC\}. \tag{25}$$

For both actuation types, the decaying of $M_{j,type}$ with respect to the trial number j is described by the model

$$\hat{M}_{j,type} = F_{a,type} j + F_{b,type}. \tag{26}$$

[16] The decreasing part is not considered in this analysis as hysteresis effects that are difficult to predict may be additionally present. They would introduce a higher variance to the evaluation of fatigue.

The estimated drop of the mean angle after 8 trials is given by

$$DROP_{8,type} = 1 - \hat{M}_{8,type}/\hat{M}_{1,type},\ type \in \{RC, DS\}.$$

c) Hysteresis For each trial j and for both controller types, the difference between the normalized joint angles obtained during the increasing stair-case except the last ($s = 1, 2, ..., 9$) and the respective angles caused by the same actuation level during decreasing stair-case is calculated. The absolute values of these differences were summed up and used to describe the intensity of the hysteresis as follows:

$$H_{j,type} = \sum_{i=1}^{i=9} |\vartheta_{norm,j,i,type} - \vartheta_{norm,j,10+9-i,type}| \tag{27}$$

d) Angle error For each stair s and each trial j, the error between the measured normalized angles and the desired value was calculated by

$$\vartheta_{norm,e,j,s,type} = \vartheta_{norm,r,comp,s} - \vartheta_{norm,j,s,comp,type}. \tag{28}$$

The mean value and standard deviation of $\vartheta_{norm,e,j,s,type}$ over all trials j and stairs s was then determined to describe the ability of the DS and RC in generating the desired angles for longer time periods.

To compare the performance of both approaches (DS and RC) separate Wilcoxon signed-rank tests were performed on the linearity evaluated in terms of R^2, the fatigue measured in terms of angle drop after 8 trials, the mean angle error, and the hysteresis indexes.

3.6 Results

Investigations were performed in five healthy male subjects (S1 to S5, age 32.8 ± 5.7 years). Further, two acute stroke patients P1 (81-year-old male, 6 days after infarct, with a strong paresis in the arm elevation and completely lost hand functions) and P2 (75-year-old male, 4 days after infarct, with partial paralysis) participated in the study[17]. The trials have been approved by the ethics committee of the Berlin Chamber of Physicians (Ärztekammer Berlin)[18].

Tests for the comparison of DS and RC are carried out on healthy subjects[19] who are asked not to intervene in the movement voluntarily. The test to analyze the influence of muscle fatigue and the weight compensation, tests were performed on different days for the healthy subjects, whereby the calibration procedures were performed directly before each test, respectively. Further, tests

[17] Inclusion criteria were post-stroke, degree of muscle strength ranging from M2 to M3 (incomplete movements against gravity), and Ashworth scale ranging from 0 to 2 (only slight spasticity).

[18] Ethics Approval was given by the ethics committee of the Berlin Chamber of Physicians (Ärztekammer Berlin). Eth-25/15.

[19] In the conduction of the experiments yielding the results described, later on, healthy subjects were preferred in this investigation as long-lasting tests must be performed aiming to exhaust muscle fatigue. The restriction to healthy is because, only one clinical session (Session: One continuous time-slot typically lasting from 30 to 60 minutes during which the neuroprosthesis can be donned, calibrated, and tested.) with limited time was available in the investigations with stroke patients. The feasibility of the calibration routine, the controller design, and the performance of recruitment control, however, was tested in two stroke patients

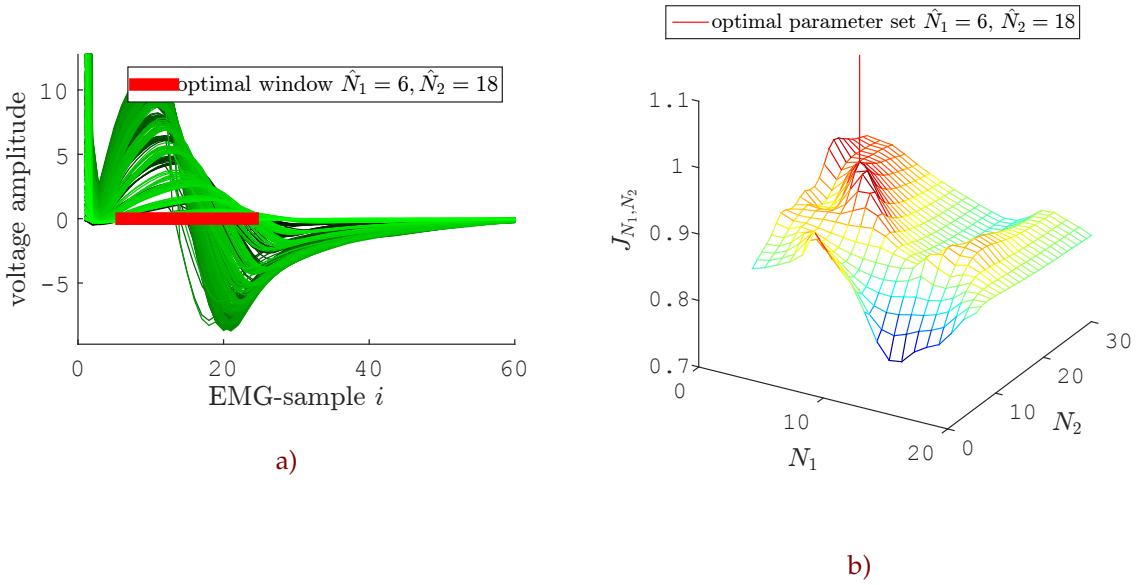

FIGURE 27: *a) Shown are the m-waves obtained during phase 2 (cf. Fig. 26) of the calibration procedure for the stroke patient P1. Further, the red bar visualizes the optimal window for the evaluation of the m-waves. To improve the visibility of the m-waves, only the first 60 samples are shown. b) A plot of the computed quality function J_{N_1,N_2} is given.*

for demonstrating the feasibility of the calibration routine and the control performance were performed in both stroke patients.

The results of the calibration procedure, directly performed before the fatigue test, are summarized in Tab. 2. For the stroke patient P1, details on the optimization procedure are shown in Fig. 27. Herein, the measured m-waves during phase 2 of the calibration experiment are shown along with the optimal window for evaluating the m-wave intensity. Further, the computed quality function J_{N_1,N_2} is shown. To demonstrate the typically achievable controller performance, a recruitment control test was performed for patient P1 in which pre-defined test patterns for the reference recruitment $r_{\hat{\lambda}}$ were applied. The time series results given in Fig. 28 show that the recruitment level closely matches the given reference, whereby only a slight delay of a few sampling-instants can be observed. Detailed results for the determined stimulation intensity – angle as well as $\hat{\lambda}$ – angle relationship are shown in Fig. 29 for the stroke patient P1 and one healthy subject, as representative. Across subjects, the optimization procedure yielded widely spread parameters N_1 and N_2 indicating the need for adaptation to the individual. In all cases, the degree of linearity in terms of the NRMSE has been significantly improved (on average by 41%) when considering the $\hat{\lambda}$ – angle relation.

Results of the fatigue test (long-term comparison of DS and RC) are summarized in Tab. 3 for all healthy subjects. Reported are the hysteresis over all trials, the drop of the mean abduction angle over eight trials (6 min of active FES)[20], the measure of linearity (R^2) for the actuation variable – angle relation, and the mean error between the desired angles and actually achieved angles.

[20]This calculation is based on a linear model approximation of the trial j – $M_{j,type}$ relation.

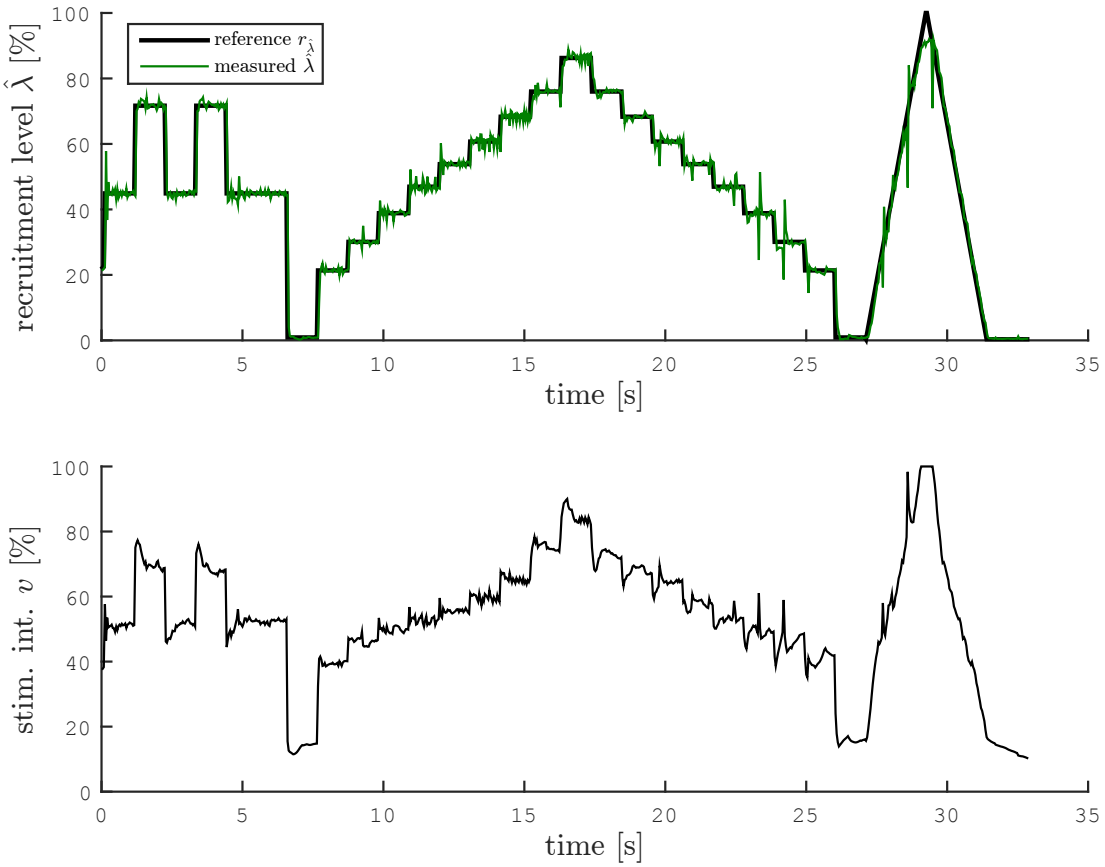

FIGURE 28: *Time series results for single channel recruitment control performed on the stroke patient P1. In some occasional instances, e.g., around* 24 *s, spikes in the recruitment time series are observable. These unwanted artifacts were caused by jitter in the USB-based data transmission from the EMG-measurement device. However, they did not harm the control systems performance to a significant degree.*

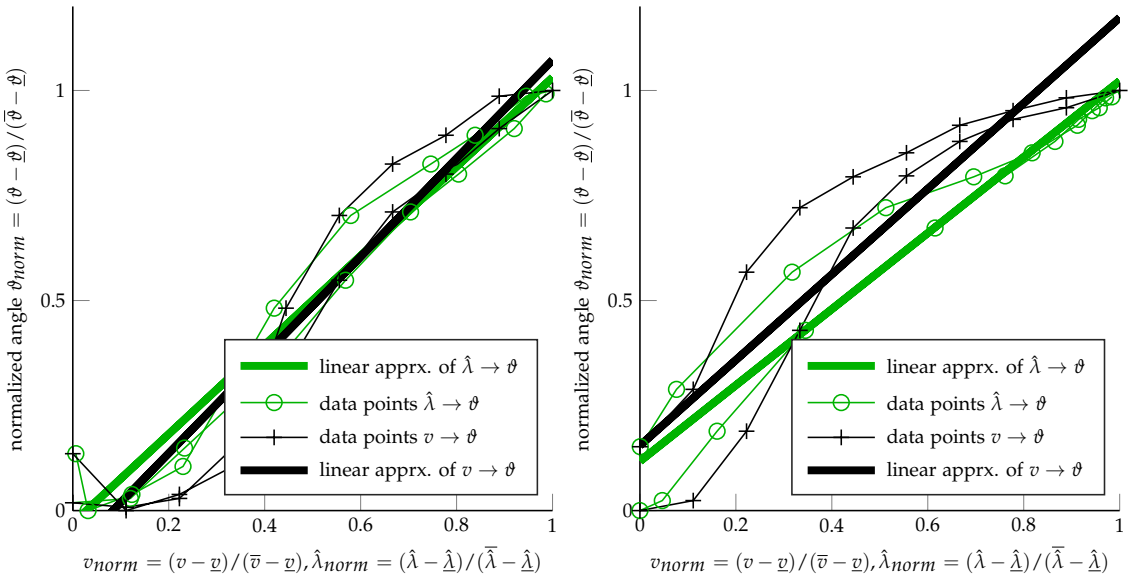

FIGURE 29: *A comparison of the achievable degree of linearity for the stroke patient P1 (left) and the subject S4 (right) is shown. The linear regressions for the $v_{cal,s} - \vartheta_{cal,s}$ and the $\hat{\lambda}_{cal,s} - \vartheta_{cal,s}$ relationship are shown. In case of the $\hat{\lambda}$ – angle relationship, the normalized RMS error has been significantly improved. All signals in the plot are normalized to the observed minima and maxima of the analyzed dataset.*

A Wilcoxon signed-rank test showed that the use of recruitment control significantly improved linearity (R^2, $Z = -2.023$, $p = 0.043$), fatigue ($DROP_8$, $Z = -2.023$, $p = 0.043$), and reduced the mean angle error ($Z = -2.023$, $p = 0.043$) with respect to the non-controlled direct stimulation.

The decrease of the mean abduction angle $M_{j,type}$ is visualized in Fig. 30 together with the identified linear models. Fig. 32 exemplarily shows the results of the first and the last trial for subject S4. A significantly reduced average joint angle due to muscle fatigue can be observed in the last trial using DS. Using DS, a rapid progression of muscle fatigue is observed. In case of RC, the effects of muscle fatigue have been well compensated. The compensation is possible until the maximally tolerable stimulation intensity is reached. Further, Fig. 31 exemplarily shows

TABLE 2: *The results of the filter optimization for neurologically intact subjects (S1 to S5) and the stroke patients P1 and P2 are shown. The linearity of the actuation variable – angle relation is captured by the NRMSE and R^2 values for v and $\hat{\lambda}$ as input arguments, respectively.*

Subject	N_1	N_2	$NRMSE$ $v \to \vartheta$	$NRMSE$ $\hat{\lambda} \to \vartheta$	R^2 $v \to \vartheta$	R^2 $\hat{\lambda} \to \vartheta$	SNR, (SNR [dB])	Angular range [°]	Max. intensity: current [mA], pulse width [μs]
S1	8	23	0.145	0.082	0.853	0.953	2798, (69)	40.23	54, 270
S2	6	8	0.128	0.082	0.89	0.954	5329, (74.5)	35.99	38, 186
S3	7	13	0.131	0.072	0.892	0.967	6966, (76.8)	73.73	38, 181
S4	3	17	0.139	0.077	0.848	0.953	10450, (80.4)	46.76	52, 272
S5	5	13	0.114	0.075	0.893	0.954	7472, (77.5)	77.94	56, 282
P1	6	18	0.116	0.071	0.914	0.968	14014, (82.9)	23.69	62, 326
P2	6	26	0.092	0.035	0.943	0.992	11485, (81.2)	71.14	59, 304
Mean	5.85	16.8	0.124	0.071	0.89	0.96	8359	52.8	51.3, 260
Std	1.57	6.2	0.018	0.016			3850	21.3	9.6, 55.9

TABLE 3: *The comparison of non-controlled direct stimulation (DC) and recruitment control (RC) is shown. Analyzed are the static stimulation intensity – angle and recruitment level – angle relations which are obtained by ramping up and down repeatedly the stimulation intensity and the desired requirement level, respectively.*

	Non-controlled direct stimulation (DS)				Recruitment control (RC)			
Subject	Hysteresis (mean±std)	Linearity (R^2)	$DROP_8$ [%]	Angle error [%] (mean±std)	Hysteresis (mean±std)	Linearity R^2	$DROP_8$ [%]	Angle error [%] (mean±std)
S1	18.08 ± 6.19	0.74	27.8	13.1±7.0	14.29 ±2.53	0.90	-4.9	-6.06±11.33
S2	8.38 ± 5.82	0.78	55.1	9.8±12.6	6.83 ±5.80	0.92	11.8	-2.71±3.84
S3	8.85 ± 5.81	0.74	57.0	13.2±14.2	7.04 ±2.45	0.93	-17.6	1.08±5.56
S4	7.29 ± 0.94	0.78	41.7	25±8.8	4.88 ±1.85	0.97	9.1	9.2±5.12
S5	3.37 ± 0.74	0.90	29.0	11.8±6.0	4.56 ±1.02	0.94	-0.5	-0.04±3.84
Mean	9.2	0.79	42.11	14.6	7.52	0.93	-0.42	0.23
Std	5.41		13.83	9.7	3.94		11.7	5.8

the positioning error (angle error) between target angle and measured angle for all trials. In case of recruitment control, a more precise and reliable positioning was possible as indicated by the smaller values for mean and variance.

Regarding the joint angle hysteresis, slight improvements can be observed in four of five subjects. However, they are not statistically significant ($Z = -1.753$; $p = 0.08$). The observed hysteresis effects are assumed to be mainly caused by nonlinear elastic joint moment effects and reflexes and only to a small extent by the FES-induced muscle activation itself. Only the latter can be compensated by the RC.

Although the effects of recruitment control on the static behavior have been intensively studied, the dynamic behavior, e.g., the reference-tracking performance, has not been statistically evaluated. However, for all tested persons, time-series plots show a precise tracking (no stationary control error) of the desired recruitment with low delay (typically rise times of 3 to 8 sampling instants have been observed), which is sufficient for the neuroprosthetic systems developed within this thesis.

Hence, the increased effort introduced by the additionally required EMG measurements (both in donning more electrodes and in using additional devices) is appropriate for the benefits achieved by the recruitment control. Furthermore, the availability of EMG measurements allows to estimate the voluntary contribution online, which can be provided as a feedback to the patient to improve his/her performance or can be used to monitor a therapy's efficacy. The set-up might be simplified when an EMG-measurement via the stimulation electrodes becomes feasible. First solutions for the assessment of volitional muscle activity are described in e.g. [166] and [183].

3.7 Two-channel Recruitment Control

The application of contemporaneous multi-channel recruitment control to muscles close to each other is difficult as strong cross-talk effects are present in the EMG measurement and the individual m-waves cannot be distinguished. To deal with the problem of crosstalk in a two-channel set-up, it is proposed to apply stimulation pulses not synchronously but alternately for both stimulation channels. In turn, the respective m-waves appear non-overlapped in the

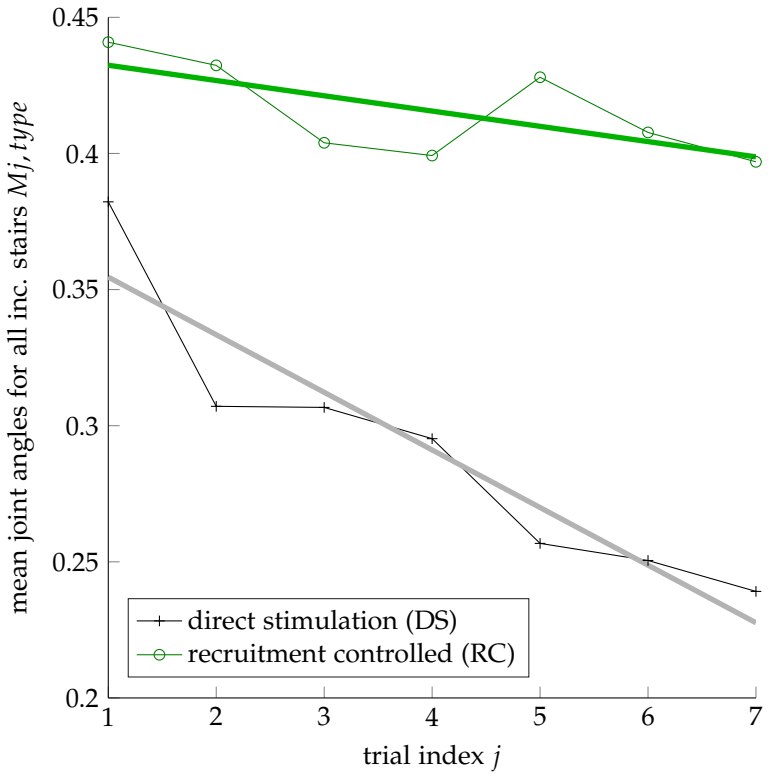

FIGURE 30: *Exemplary results of the fatigue comparison test for subject S4 are shown. For both control types and each trial j, the fatigue indicators $M_{j,DS}$ and $M_{j,RC}$ (normalized mean stationary angles of the rising part of the staircases) have been calculated respectively. As the number of trials increases, a significant decrease of the joint angle is observed, when using uncontrolled stimulation (DS). In case of λ-control, however, the effect of muscle fatigue is compensated to a large extent.*

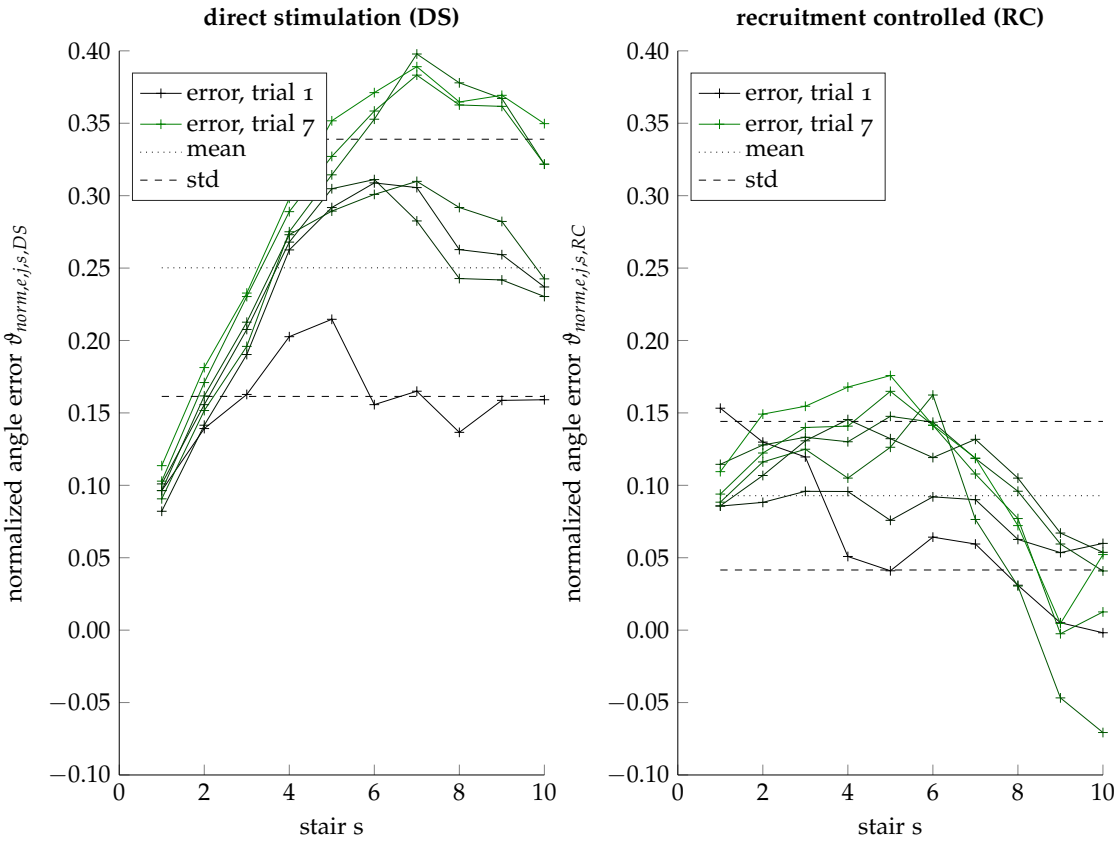

FIGURE 31: *Exemplary results of the angle error for subject S4.*

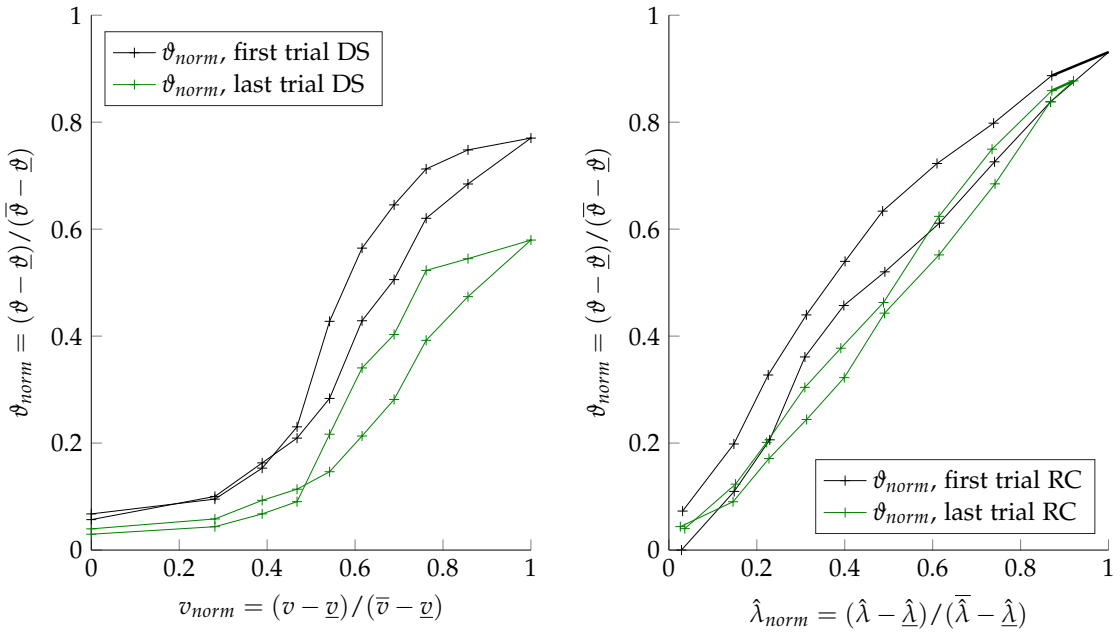

FIGURE 32: *Exemplary results of the first and the last trial of the fatigue comparison test for subject S4.*

measured EMG. This time-shifting, however, limits the maximal rate at which stimulation pulses are applied, as the time-windows during which the m-wave is evaluated may get too short for fast stimulation rates. The developed control system is exemplarily applied to the medial and anterior deltoid as it is clinically relevant to support entirely or partially paralyzed arm elevation movements.

3.7.1 Experimental set-up

The experimental set-up as used for single channel recruitment control (cf. Sec. 3.1) is extended as shown in Fig. 33. Herein, FES is applied to the anterior (channel A) and the medial (channel B) part of the deltoid muscle, and the measured EMG[21] is processed by two digital filters to estimate the normalized muscular recruitments $\hat{\lambda}^A$ and $\hat{\lambda}^B$, respectively. The stimulation intensities v^A and v^B describe the pulse-charges normalized to the respective maximal tolerated values. Two feedback controllers adjust v^A and v^B respectively, such that the desired recruitment levels $r^A_{\hat{\lambda}}$ and $r^B_{\hat{\lambda}}$ are realized.

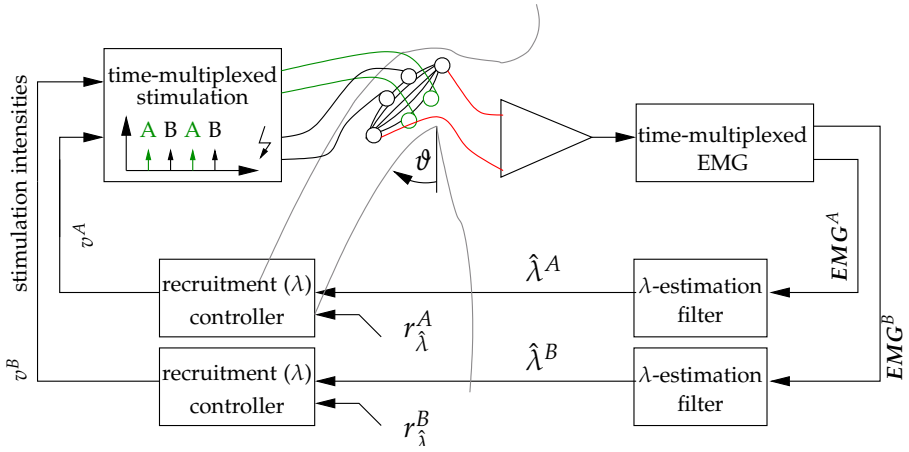

Figure 33: *Experimental set-up for two channel recruitment control.*

3.7.2 Time-multiplexed stimulation and EMG-measurement

When applying stimulation pulses to each muscle part simultaneously, both individual responses typically overlap as they are simultaneously generated by the recruited motor units of both muscle parts. A separation of the individual m-waves using decoupling strategy is difficult as, e.g., crosstalk gains must be calibrated in advance. Further, perfect decoupling is hard to achieve. To reduce calibration effort, a strategy in which both muscle parts are stimulated in an alternating fashion as illustrated in Fig. 34 is proposed: After one muscle part is stimulated, the decay of the corresponding m-wave is awaited. The duration of the individual m-waves $N^A_W[k]$ and $N^B_W[k]$ are introduced in Fig. 34. Herein, k denotes the sampling instant of the control system. Then, the other part is stimulated. This strategy causes the respective m-waves to appear in different

[21] Please note that for the recording of EMG, only one channel is required and used as the closeness of both deltoid-portions allows detecting the m-waves induced by both stimulation channels. An EMG-recording from both muscles is also possible, of course, and may improve the estimation of the individual $\hat{\lambda}$-values.

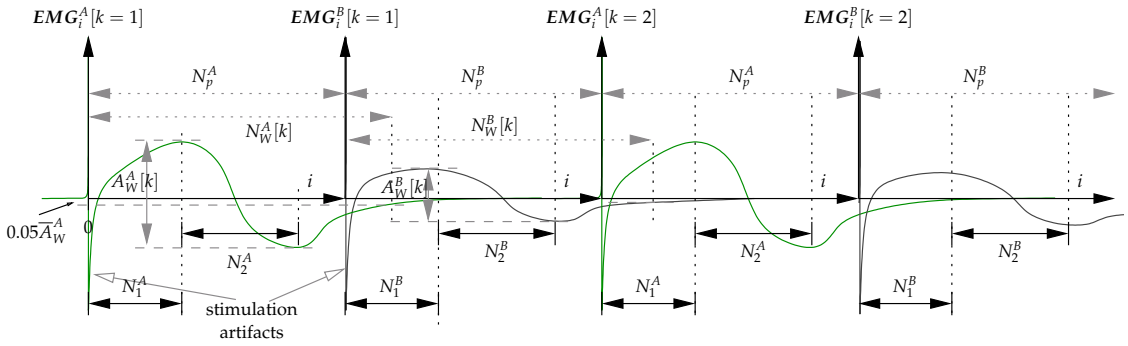

FIGURE 34: *Time-multiplex stimulation and measurement of the FES-evoked EMG. The actually measured EMG-signal is the superposition (not shown in this figure) of the individual contributions of both muscle portions shown by the black and green curves, respectively.*

time-windows and hence, overlapping is minimized. The calibration routines of the separated recruitment controllers are also performed for each channel A and B separately.

The proposed strategy then records the m-waves starting directly after each stimulus during each sampling instant k for both channels A and B. Data are stored in the EMG-measurement vectors $\boldsymbol{EMG}^A[k]$ and $\boldsymbol{EMG}^B[k]$ containing N_p^A and N_p^B EMG-samples for channel A and B, respectively. The index i denotes the sampling instance for EMG-recording $EMG_i^A[k]$ stored in the vector $\boldsymbol{EMG}^A[k]$ (analog for channel B). The calibration routines of the separated recruitment controllers are then performed for each channel A and B separately.

In this approach, the corresponding inter-pulse time-periods measured in EMG samples N_p^A and N_p^B must be large enough such that the overlap of both m-waves does not significantly influence the operation of the individual recruitment control loops. Please recap that the intensity of the m-wave is evaluated only in a window whose position and the duration is determined by the parameters N_1^A, N_1^B and N_2^A, N_2^B (cf. Sec. 3.2.3). Hence, it must be ensured that m-waves, whose durations are $N_W^A[k]$ and $N_W^B[k]$, do not overlap with the window used for the evaluation of the succeeding m-wave appearing on the other channel.

A short calibration procedure is needed to determine the maximal m-wave durations for both channels and, hence, to determine feasible inter-pulse intervals N_p^A and N_p^B that do not cause m-wave overlapping. Therefore, using fixed inter-pulse intervals $N_p^A = N_p^B = 2048/(2 \cdot 20) \approx 51$[22], two tests are performed in which is the stimulation intensity of the respective channels is increased up to the maximum. Herein, EMG data are recorded and stored in the vectors $\boldsymbol{EMG}_{\hat{p}1}^A[k]$ and $\boldsymbol{EMG}_{\hat{p}1}^B[k]$ for each channel A and B, respectively. This test equals the one performed in phase 1 of the calibration of the recruitment controllers later on. However, the inter-pulse intervals are different.[23]

Then, the amplitudes A_W^A and A_W^B between the maximum and minimum of each m-wave (cf. Fig. 26) contained in the vectors $\boldsymbol{EMG}_{\hat{p}1}^A[k]$ and $\boldsymbol{EMG}_{\hat{p}1}^B[k]$ (the datasets obtained during the calibration for each channel A and B, respectively), are calculated for each m-wave in the inter-pulse interval

[22] The dependency of the m-wave's shape, e.g., in terms of the amplitude is assumed to be independent of the duration of the inter-pulse interval. Hence, a standard stimulation frequency is applied in this first test.

[23] The muscle activation and, hence, also the arm elevation depends on the stimulation frequency. As the relation between the obtained arm elevation and the stimulation intensity is important in the calibration of recruitment control, separated tests are needed.

k:

$$A_W^A[k] = \max_i EMG_{\hat{p}1,i}^A[k] - \min_i EMG_{\hat{p}1,i}^A[k],\ A_W^B[k] = \max_i EMG_{\hat{p}1,i}^B[k] - \min_i EMG_{\hat{p}1,i}^B[k]. \quad (29)$$

Then, the maximally observed amplitudes are calculated by

$$\overline{A}_W^A[k] = \max_{\bar{k}} A_W^A[\bar{k}],\ \overline{A}_W^B[k] = \max_{\bar{k}} A_W^B[\bar{k}]. \quad (30)$$

As the decaying m-wave in the inter-pulse interval k enters a band between $-0.05\overline{A}_W^A[k]$ and $+0.05\overline{A}_W^A[k]$, the duration $N_W^A[k]$ is obtained (and analog in case of channel B). The maximal durations observed for all sampling instants are then calculated yielding $\overline{N}_W^A = \max_k N_W^A[k]$ and $\overline{N}_W^B = \max_k N_W^B[k]$.

To prevent overlapping, the durations of the inter-pulse intervals N_p^A and N_p^B are constrained to a minimum depending on the maximal durations of the m-waves $\overline{N}_W^A$ and $\overline{N}_W^B$ by the conditions

$$\overline{N}_W^A < N_p^A + N_1^B, \quad \overline{N}_W^B < N_p^B + N_1^A. \quad (31)$$

Hence, also the effective stimulation frequency

$$f_{eff} := \frac{2048}{N_p^A + N_p^B} Hz \quad (32)$$

is introduced that describes the combined inter-pulse intervals of both channels and, thus, refers to the stimulation frequency equivalent to the case of synchronous recruitment control.

The inter-pulse intervals leading to the maximally possible effective stimulation frequency f_{eff}^* are then given by

$$N_p^{A*} = \overline{N}_W^A - N_1^B, \quad N_p^{B*} = \overline{N}_W^B - N_1^A. \quad (33)$$

In further investigations in five healthy subjects (not included in this thesis), the maximally achievable effective frequency was determined for each subject [93]. Herein, f_{eff}^* was at least 26 Hz for each subject, which is well sufficient to most applications.

3.7.3 Experimental validation of two-channel control

Two-channel recruitment control was applied to one healthy subject and electrodes were placed as shown in Fig. 35.

Please note that for this first test, instead of the minimally possible inter-pulse intervals (Eq. 33), fixed timing parameters for the inter-pulse intervals $N_p^A = N_p^B = 2048/(2 \cdot 25) \approx 41$ were empirically chosen yielding the effective stimulation frequency $f_{eff} = 25$ Hz. The duration of these inter-pulse intervals is long enough to prevent overlapping in the evaluated ranges. Using the time-multiplexing stimulation and EMG-measurement, both recruitment controllers were calibrated separately following the procedure described in Sec. 3.4.1, while the stimulation intensity for the opposite channel was zero.

In a control test, the reference trajectories for $r_{\hat{\lambda}}^A$ and $r_{\hat{\lambda}}^B$ were chosen to excite both muscles concurrently. Time series results are given in Fig. 36. In case of channel B, tracking performance

is comparable to the single channel case. In case of channel A, the performance is lower – slight oscillations can be observed, though they had no significant influence on the joint angle. The reasons for this behavior are unclear, however. The oscillations may potentially be reduced by slightly decreasing the controller gain $c^A_{\hat{\lambda}}$.

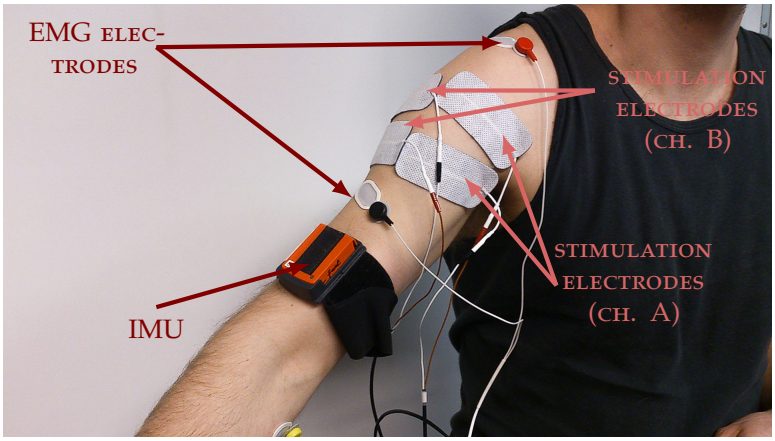

FIGURE 35: *Electrode-placement for two channels: FES is applied to the anterior- (channel A) and the medial deltoid (channel B). The acquisition of EMG is performed by one pair of electrodes placed outside of the stimulation electrodes. This one-channel measurement captures the evoked potentials by both muscle portions.*

3.8 CONCLUSIONS

To improve FES-induced muscle activation with respect to muscle fatigue and the degree of linearity, feedback control of the muscular recruitment state estimated by EMG measurements was proposed. To maximize the degree of linearity, an optimization procedure that adjusts two filter parameters in the estimation of the recruitment level has been proposed. In experimental tests in five healthy subjects, a significant improvement of linearity when comparing the stimulation intensity – angle and recruitment level – angle relationship is shown. Further, the compensation of the effects of muscle fatigue is shown: In a comparative test, after 6 minutes of active FES, the average joint angle dropped by $44\% \pm 14\%$ in case of non-controlled FES compared to $0\% \pm 12\%$ in case of recruitment controlled FES in average for all subjects. Although healthy subjects were asked to remain passive when stimulation was active, similar tests should be repeated on a significant sample of stroke patients to verify if the same results are also achieved in subjects with a compromised sensory-motor pathway. The feasibility tests performed in two stroke patients already showed encouraging results on the applicability of the proposed controller.

To allow recruitment control of two neighboring muscles, an extension of recruitment control for two-channel FES has been investigated. Normally, strong cross-talk effects are present that hinder the proper evaluation of the m-wave's intensities for synchronous stimulation. To avoid this overlapping of the individual m-waves, a time-multiplexed stimulation approach to was suggested. The control of two muscles may be performed with one pair of EMG electrodes, which is advantageous considering the effort for electrode placement. The proposed two-channel recruitment control approach was successfully tested in one healthy subject. Herein, the calibration

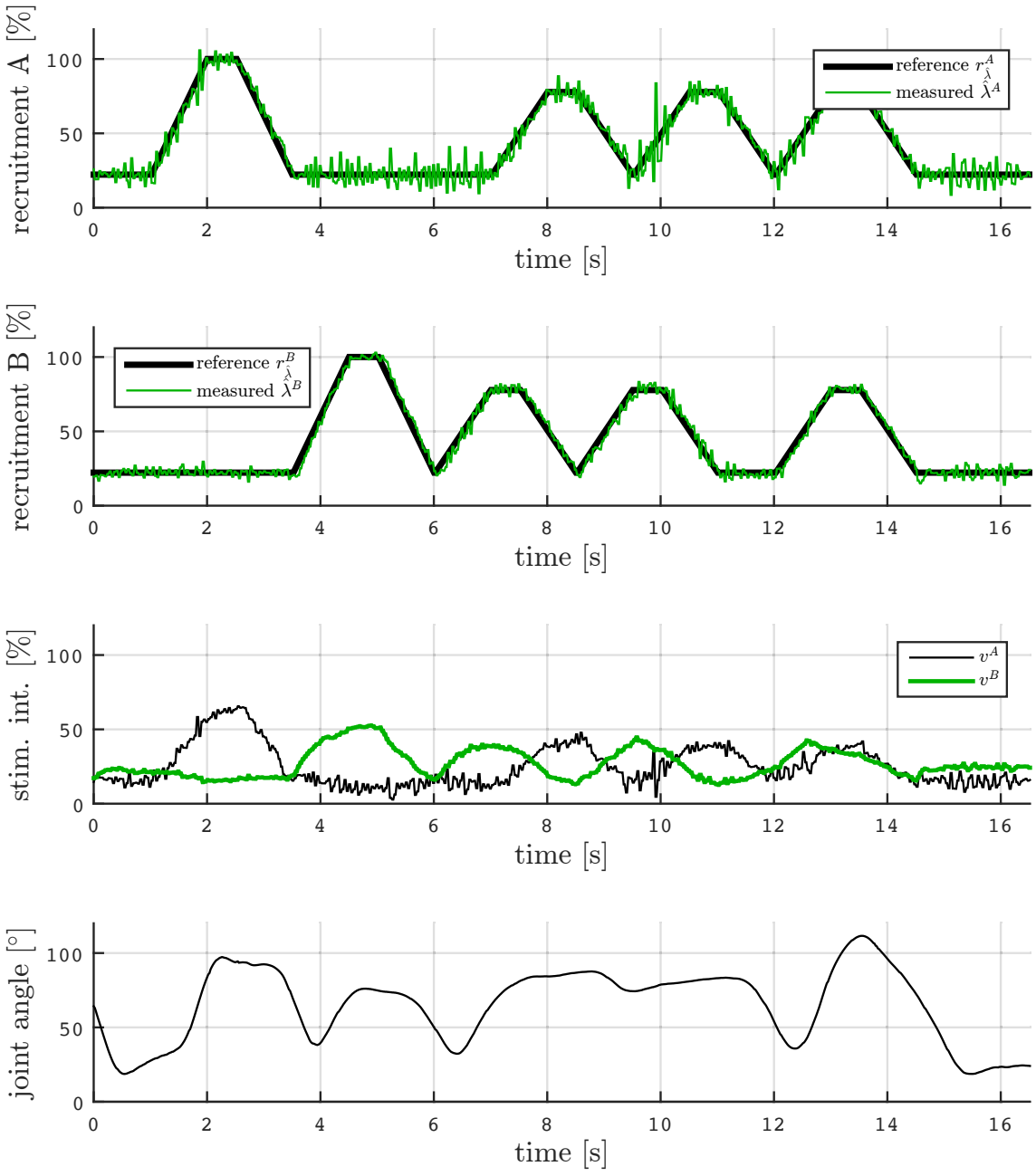

FIGURE 36: *Time series results for two-channel recruitment control in a healthy subject at* 25 *Hz are shown. Parameters are* $N_1^A = 2$, $N_2^A = 16$, $N_1^B = 7$, $N_2^B = 6$, $c^A_{\hat{\lambda}} = 0.01$, *and* $c^B_{\hat{\lambda}} = 0.0049$.

routine designed for the single-channel case can still be used by applying it to each channel separately. The feasibility of recruitment control under the maximal effective stimulation frequency obtained in the calibration procedure must be evaluated in further investigations, however. An extension to three or more channels is difficult as the maximally achievable stimulation frequency significantly degrades as the number of stimulated channels increases. The volitional component of the EMG must be evaluated in a range in which the m-wave's amplitude is low compared to the amplitude of the volitional EMG (cf. Sec. 3.2.2). Please note that in this approach, the estimation of the volitional activity becomes difficult as the inter-pulse stimulation intervals become too short (only containing the main parts of the m-wave) such that no sufficiently large range meeting the above requirement is available under reasonable stimulation frequencies.

The single channel recruitment control approach is applied to a neuroprosthesis for the support of weak residual muscle activity in the shoulder elevation in Chapter 4. As a hybrid muscle activation (volitional and stimulation evoked) is performed, the compensation of the effects of muscle fatigue relies on recruitment control (cf. Sec. 2.8.2). Further, to tune the neuroprosthesis, no additional parameter identifications routines must be performed as all needed parameters can be obtained from the data that is already collected during the calibration of RC.

Finally, RC is further applied to a control system for joint angle control in antagonistic muscle pairs described in Chapter 6. In the conducted experiments, an older revision of RC was used that does not perform the optimization of the filter parameters N_1 and N_2, however. Instead, a fixed window was chosen.

4

PATIENT-CONTROLLED NEURO-PROSTHESIS FOR ARM WEIGHT RELIEF

In patients suffering from neurological impairments, often the volitional muscle activity is weakened leading to reduced motor functions that may hinder functional movements. To support small residual voluntary forces, functional electrical stimulation (FES) can be applied to the corresponding muscles for gaining additional force. In this chapter, a patient-driven control strategy, similar to that reported by Riener and Fuhr [149], which amplifies volitionally-initiated movements, is proposed to improve stroke patients' rehabilitation and to enable daily live support. The system is intended to support movements acting against gravity and is exemplarily applied to support the shoulder elevation in stroke patients by stimulating the medial deltoid muscle.

Based on the measured elevation angle, a FES-induced muscle recruitment is generated that yields a pre-specified percentage (support factor) of this angle – yielding an arm weight relief. With that, less residual voluntary activity is required to perform functional tasks, while precise motor control is still possible. The amount of support may be adjusted by the user, the physiotherapist, or the caregiver by varying the support factor. The proposed neuro-prosthesis is intended for trial-based training for motor re-learning in therapy as well as for daily-live support in form of a wearable device.

In the proposed control system, the muscle is activated by stimulation and voluntary activity at the same time. This hybrid activation makes it difficult to determine the effect of FES by solely observing the occurring joint angle. Hence, and to obtain a system that is robust against muscle fatigue and uncertain muscle activation, underlying recruitment control as described in Chapter 3 is applied. In an outer level cascade, a proportional control with positive feedback of the joint angle is used to amplify the effects of weak voluntary contributions. The obtained weight support is theoretically investigated, and stability conditions are presented. Further, the control scheme was implemented, whereby all required parameters are derivable from the data already obtained by the calibration routine of the recruitment control system. In a study with five healthy subjects, which had to perform a tracking task for different support factors, the needed voluntary activity was obtained by EMG measurements. Results show a significant decrease of the voluntary effort as the support factor increases. Over all subjects, a maximal mean reduction of the volitional effort by 78% was achieved compared to angular tracking without FES-support.

First successful experiments with two acute stroke patients are, further, reported. For one patient, the reachable range of motion was significantly extended. For the other patient, a complete restoration of arm-functions was possible.

Further investigations consider the automatic tuning of the presented control scheme: The support-level strongly influences the closed loop's behavior especially for percentages close to 100% and, therefore, must be carefully chosen to meet the patient's requirements. Because of parameter variations, this value cannot be precisely pre-computed in an automatic calibration

procedure. Therefore, the clinician must perform a manual trial and error based approach to find out a suitable support factor. Hence, such an iterative procedure is systematically automated by an adaptive trial-to-trial based learning procedure to iteratively realize a given level of volitional amplification[24] is presented.

During each trial, the algorithm obtains measurements of the volitional activity utilizing Electromyography (EMG) and the joint angle. After the arm returns to its rest position, the achieved amplification of the volitional activity is estimated. An integral controller combined with a non-linear output transformation then updates the support factor for the next trial aiming to realize the desired volitional amplification. The closed loop with the adaptive controller is robust asymptotically stable. In two tests performed on a healthy subject, the desired level of volitional amplification was reached within 3 to 5 trials demonstrating the feasibility of the chosen approach.

The methods and results presented in this chapter have been previously published as listed below.

- The initial idea of the arm weight support control along with first results is presented in

  [82] C. Klauer, A. Passon, J. Raisch, and T. Schauer. "Virtual Weight-Compensating Exoskeleton using λ-Controlled FES". in: *Proc. of Automed 2013*. Dresden, Germany, 2013.

- The control system was evaluated in five healthy subjects showing the ability to reduce voluntary effort and, further, was successfully applied to one stroke patient with an almost complete paralysis in the shoulder elevation in

  [80] C. Klauer, S. Ferrante, E. Ambrosini, U. Shiri, F. Dähne, I. Schmehl, A. Pedrocchi, and T. Schauer. "A patient-controlled functional electrical stimulation system for arm weight relief". In: *Medical Engineering & Physics* 38.11 (2016), pp. 1232–1243. DOI: 10.1016/j.medengphy.2016.06.006.

- The adaptive controller to adjust the level of support is presented in

  [88] C. Klauer and T. Schauer. "Adaptive Control of a Neuroprosthesis for Stroke Patients Amplifying Weak Residual Shoulder-Muscle Activity". In: *Proc. of the 20th World Congress of the International Federation of Automatic Control, 9-14 July 2017*. Toulouse, France, 2017.

- The results of first clinical trials were presented in

  [87] C. Klauer, M. Ruppel, and T. Schauer. "FES-based arm weight relief: First investigations in stroke patients". In: *Abstract in Proc. of the 6th European Conference on Technically Assisted Rehabilitation – TAR 2017*. Berlin, Germany, 2017.

The following research going beyond the scope of this thesis has been performed:

- A combination of the arm-weight support controller presented in this chapter with a cable driven rehabilitation-robotics device also enabling weight support to enable continued training even when muscles fatigue occurs as described in

  [125] P. Meyer-Rachner, A. Passon, C. Klauer, and T. Schauer. "Compensating the effects of FES-Induced Muscle Fatigue by Rehabilitation Robotics During Arm Weight Support". In: *Current Directions in Biomedical Engineering, Proc. of the 6th European Conference on Technically Assisted Rehabilitation – TAR 2017*. Berlin, Germany, 2017. DOI: 10.1515/cdbme-2017-0007 .

[24] The factor that describes the amplification of the influence of volitional activity on the resulting arm elevation during active control compared to no FES-support.

Copyright statement The text and the pictures in this section are based, with slight modifications, on the following publications: Sec. 4.1 to Sec. 4.5 are based on [80]. Herein, slight modifications of the text and the figures were performed. Further, a more detailed evaluation of Jury's criteria and results for a second stroke patient were added.

Sec. 4.6 has newly been added.

Sec. 4.7 is partially based on [88]. Herein, slight modifications of the text and the figures were performed. Some parts were outlined in more details. The paragraphs "Asymptotic stability of the weight-relief control loop" and "Simulation results" were added. Further, Fig. 58 was added.

4.1 System Overview

Considering all devices as well as electrodes and IMU positioning, the used experimental set-up is the same as already described in Chapter 3. Further, as shown in Fig. 37, the underlying recruitment control is used, whereby the desired recruitment level $r_{\hat{\lambda}}$ forms a virtual actuation variable that is generated by the angle-dependent arm weight support. The estimated volitional EMG activity level $\hat{\gamma}$ is used to evaluate the performance of the arm weight support. The movement is patient-initiated by his/her weak residual muscle activity.

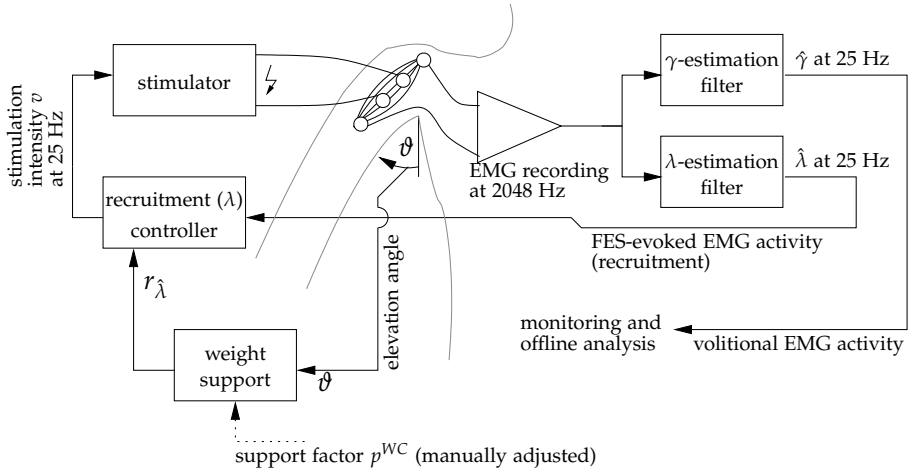

Figure 37: *Control scheme to achieve arm weight support by stimulation of the medial deltoid muscle.*

4.2 FES Arm-Weight Support Controller

The proposed control system aims to induce a fraction p^{WC} of the currently measured arm elevation by FES. As shown later in the analysis of the proposed control system, this yields to a higher influence of the volitional activity on the resulting elevation angle. Hence, the arm elevation can be easier controlled by the user. This amplification is described by the volitional amplification factor g^{WC} that is directly related to the fraction p^{WC} as outlined in this section.

The typical relationship for the $\hat{\lambda}$ – angle relation described by the dataset ($\hat{\lambda}_{cal,s}$, $\vartheta_{cal,s}$) that is obtained in the calibration of the recruitment controller (cf. Sec. 3.4.1), is shown in Fig. 38. As

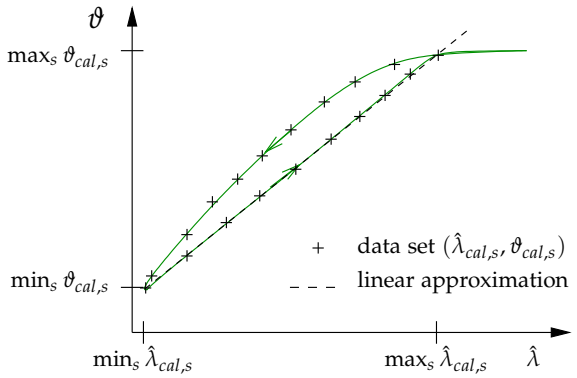

FIGURE 38: *The relation between $\hat{\lambda}$ and ϑ for the dataset $(\hat{\lambda}_{cal,s}, \vartheta_{cal,s})$ obtained during the calibration procedure of the recruitment controller as described in Sec. 3.4.1.*

known from previous experimental experience, typically, hysteresis effects may be present in this relation. In the design of the weight compensating control system, at first, an approximately linear relationship for the steady state $\hat{\lambda}$ – angle relation is assumed:

$$\vartheta = (\hat{\lambda} - \min_s \hat{\lambda}_{cal,s}) \underbrace{\frac{\max_s \vartheta_{cal,s} - \min_s \vartheta_{cal,s}}{\max_s \hat{\lambda}_{cal,s} - \min_s \hat{\lambda}_{cal,s}}}_{:=c_\lambda} + \min_s \vartheta_{cal,s}.$$

To simplify the notation, the following abbreviations are introduced (the superscript WC represents "weight compensation"):

$$\lambda^{WC}_{min} := \min_s \hat{\lambda}_{cal,s} \quad \lambda^{WC}_{max} := \max_s \hat{\lambda}_{cal,s} \tag{34}$$

$$\vartheta^{WC}_{min} := \min_s \vartheta_{cal,s} \quad \vartheta^{WC}_{max} := \max_s \vartheta_{cal,s}. \tag{35}$$

Herein, ϑ^{WC}_{min} is the minimal angle when no muscle contraction is present, ϑ^{WC}_{max} the maximum angle that is obtained for the maximal recruitment level λ^{WC}_{max} (without volitional contribution), and λ^{WC}_{min} yields the onset of muscle contraction.

The derived parameter c_λ describes the gain of the model. These parameters are experimentally obtained as described in Sec. 3.4 yielding their respective estimates $\hat{\vartheta}^{WC}_{min}$, $\hat{\vartheta}^{WC}_{max}$, $\hat{\lambda}^{WC}_{max}$ and $\hat{\lambda}^{WC}_{min}$. Please note that these estimates may slightly vary from the actual, unknown parameters. Please remember, that all estimates introduced in this work are denoted by the additional accent "ˆ".

To compensate the arm weight, a linear mapping of joint angles within a range $\Omega_\vartheta := [\hat{\vartheta}^{WC}_{min}, \hat{\vartheta}^{WC}_{max}]$ to the virtual actuation variable[25] $r_{\hat{\lambda}} \in \Omega_{\hat{\lambda}}$ in the range $\Omega_{\hat{\lambda}} := [\hat{\lambda}^{WC}_{min}, \hat{\lambda}^{WC}_{min} + p^{WC}(\hat{\lambda}^{WC}_{max} - \hat{\lambda}^{WC}_{min})]$ is performed. The controller gain $p^{WC} \geq 0$ is called support factor and describes the initially introduced percentage value. Additionally, $r_{\hat{\lambda}} \in [\hat{\lambda}^{WC}_{min}, \hat{\lambda}^{WC}_{max}]$ is saturated in case it exceeds its

[25] The virtual actuation variable is the desired recruitment level that is the reference to the underlying recruitment controller.

boundaries. The controller is then given by

$$r_{\hat{\lambda}} = sat_{\hat{\lambda}^{WC}_{min},\hat{\lambda}^{WC}_{max}} \left(p^{WC} \underbrace{\frac{\hat{\lambda}^{WC}_{max} - \hat{\lambda}^{WC}_{min}}{\hat{\vartheta}^{WC}_{max} - \hat{\vartheta}^{WC}_{min}}}_{:=1/\hat{c}_\lambda} (\vartheta - \hat{\vartheta}^{WC}_{min}) + \hat{\lambda}^{WC}_{min} \right). \tag{36}$$

Please note, that the assumed gain c_λ of the model is compensated by its estimate $\hat{c}_\lambda$.

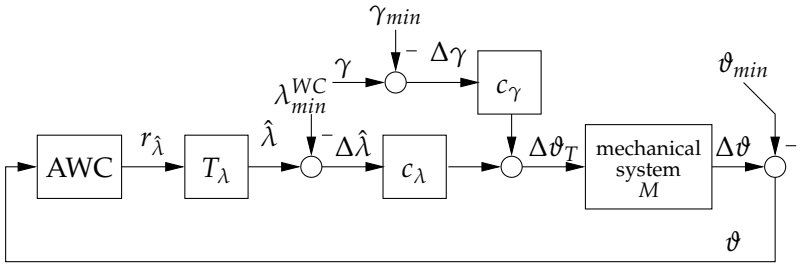

FIGURE 39: *The linear model of the closed loop. The arm-weight support controller (AWC) described by Eq. (36) adjusts the desired recruitment level $r_{\hat{\lambda}}$ of the underlying recruitment control loop. The parameter $c_\gamma > 0$ describes the influence of the volitional activity on the closed loop.*

4.3 Closed Loop Analysis

To obtain a detailed understanding of the working mechanism of the arm-weight support controller, a systematic analysis using linear systems theory is carried out. Important questions consider stability and dynamics of the positive-feedback closed-loop system as well as how the effect of force amplification is achieved. All investigations are performed using linear-time invariant system's theory for discrete-time systems. Sampling is assumed to be significantly faster than the time constants of the closed loop dynamics. A linear approximation of the non-linear biomechanical arm model is used as shown in Fig. 39. The following variables are herein introduced:

$$\Delta\vartheta := \vartheta - \vartheta^{WC}_{min}, \quad \Delta\hat{\lambda} := \hat{\lambda} - \lambda^{WC}_{min}, \tag{37}$$

$$\Delta\gamma = \gamma - \gamma_{min}, \quad c_\lambda := \frac{\vartheta^{WC}_{max} - \vartheta^{WC}_{min}}{\lambda^{WC}_{max} - \lambda^{WC}_{min}} > 0. \tag{38}$$

Herein, γ_{min} denotes an offset in the estimation of the volitional activity.

To model the mechanical behavior of the arm that acts like a second-order system with conjugate complex poles, the transfer function

$$M(z) = \frac{(1-z_1)(1-z_2)}{(z-z_1)(z-z_2)}, \tag{39}$$

$$z_1, z_2 \in \mathbb{C},\ z_1 = -\overline{z_2},\ |z_1| < 1, |z_2| < 1,\ z_1 \neq z_2 \neq 0 \tag{40}$$

is used that is assumed to be asymptotically stable. Please note that $M(1) = 1$ (unit static gain) holds. The hybrid muscle activation (volitional & FES, cf. 2.6) is modeled by the linear

combination

$$\Delta\vartheta_T = c_\lambda \Delta\hat{\lambda} + c_\gamma \Delta\gamma, \quad c_\lambda > 0,\, c_\gamma > 0. \tag{41}$$

Herein, $\Delta\vartheta_T$ describes the joint angle in which the system M is stationary.[26] The parameter $c_\gamma > 0$ describes the influence of the voluntary activity γ on the stationary joint angle $\Delta\vartheta_T$.

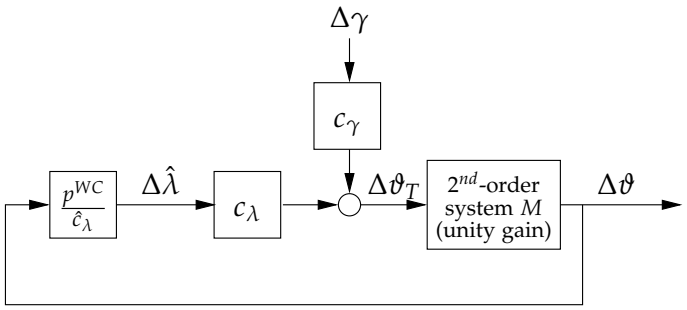

FIGURE 40: *Simplified linear model of the closed loop. The controller parameter $\hat{c}_\lambda > 0$ is an estimate of $c_\lambda > 0$.*

This model and its representation are simplified yielding the model given in Fig. 40. Herein, the arm weight support proportional controller $K = p^{WC}/\hat{c}_\lambda$, $p^{WC} \geq 0$ approximately cancels the gain factor between the actuation variable $r_{\hat{\lambda}}$ and the stationary joint angle ϑ_T and introduces the tunable factor p^{WC}. Further, as the dynamics T_λ introduced by the recruitment control loop is generally of high bandwidth compared to M, it is neglected in the ongoing analysis.

Stability of the closed loop The open-loop transfer function $L(z)$ and its static gain $L(z=1)$ are given by (cf. Fig. 40)

$$L(z) = -\frac{l_m(z)}{l_d(z)} = -\underbrace{p^{WC}\frac{c_\lambda}{\hat{c}_\lambda}}_{L(1)} \frac{(1-z_1)(1-z_2)}{(z-z_1)(z-z_2)},$$

whereby $l_m(z)$ and $l_d(z)$ are the numerator and denominator polynomials respectively. Please note that the minus sign is introduced because of the positive feedback loop. To investigate the closed-loop stability, the closed-loop polynomial is calculated:

$$\begin{aligned} q_{cl}(z) &= l_m(z) + l_d(z) \\ &= z^2 + z\underbrace{[-z_1 - z_2]}_{:=a_1} + \underbrace{z_1 z_2 - p^{WC}\frac{c_\lambda}{\hat{c}_\lambda}(1-z_1)(1-z_2)}_{:=a_2}. \end{aligned}$$

The control loop is asymptotically stable if and only if all roots of q_{cl} reside within the unit circle. To investigate the stability of the closed loop, Jury's criteria [14] is applied. The control loop is asymptotically stable if and only if the conditions

$$a_2 < 1 \tag{42}$$
$$a_2 > -1 + a_1 \tag{43}$$
$$a_2 > -1 - a_1 \tag{44}$$

[26] Hence, $\Delta\vartheta_T$ can be interpreted to be proportional to the joint torque as indicated by the index T.

hold. In this analysis, the complex conjugated poles z_1 and z_2 are written as

$$z_1 = a + jb, \quad z_2 = a - jb \quad a, b \in \mathbb{R}.$$

Please note that, additionally, the following properties

$$a > 0,\ b > 0,\ a^2 + b^2 < 1$$

are derived from (40). Further, please keep in mind that $c_\lambda > 0$ and $\hat{c}_\lambda > 0$ hold. Then, the first condition (Eq. (42)) yields[27]

$$\begin{aligned} & (a^2 + b^2) - p^{WC}\frac{c_\lambda}{\hat{c}_\lambda}((a-1)^2 + b^2) < 1 \\ \Leftrightarrow \quad & p^{WC}\frac{c_\lambda}{\hat{c}_\lambda} > \underbrace{\frac{a^2 + b^2 - 1}{(a-1)^2 + b^2}}_{<0}. \end{aligned}$$

In this application, negative support factors p^{WC} will not be considered. Hence the obtained condition can be reduced to $p^{WC} \geq 0$. Further, the second (Eq. (43)) and the third condition (Eq. (44)) yield:

$$(a^2 + b^2) - p^{WC}\frac{c_\lambda}{\hat{c}_\lambda}((a-1)^2 + b^2) > -1 - 2a \tag{45}$$

$$(a^2 + b^2) - p^{WC}\frac{c_\lambda}{\hat{c}_\lambda}((a-1)^2 + b^2) > -1 + 2a, \tag{46}$$

respectively. Please note that because of $-1 + 2a > -1 - 2a$, the first condition (45) is always fulfilled if the second (46) holds. Hence, it is sufficient to consider the second condition (46) that is equivalent to

$$p^{WC}\frac{c_\lambda}{\hat{c}_\lambda} < \frac{a^2 + b^2 + 1 - 2a}{(a-1)^2 + b^2} = 1. \tag{47}$$

To sum up, the arm-weight relief controller is asymptotically stable if[28]

$$0 \leq p^{WC}\frac{c_\lambda}{\hat{c}_\lambda} < 1. \tag{48}$$

This means the stability properties of the closed loop are independent of a and b and, hence, also independent on the dynamics of M.

Voluntary control of the joint angle The neuroprosthesis shall be designed such that the joint angle ϑ can be controlled by the patient's volitional muscle activity γ. In the traditional understanding of control loops, γ would be interpreted as a disturbance whose effects on the output are compensated. Using a positive feedback, the influence of γ on the system output is not compensated but amplified, which is the desired behavior in this case, as it allows the patient to move his arm with minimal volitional effort. Hence, γ is considered to be a command signal to drive the closed loop. The amplification effect is investigated by calculating the transfer function S_γ that describes

[27] The following properties are used: $z_1 z_2 = a^2 + b^2 < 1$, $(1 - z_1)(1 - z_2) = (a-1)^2 + b^2 > 0$, $-z_1 - z_2 = -2a < 0$.

[28] Please remind that this forms a sufficient condition only as the control loop might also be stable for some values $p^{WC} < 0$. This case, however, does not match the intention of the control system that requires $p^{WC} > 0$ to achieve an amplification of the volitional activity.

the relationship between the volitional activity $\Delta\gamma$ and the joint angle $\Delta\vartheta$:

$$S_\gamma(z) = c_\gamma \frac{M(z)}{1 - M(z)p^{WC}\frac{c_\lambda}{\hat{c}_\lambda}} = c_\gamma \frac{(1-z_1)(1-z_2)}{q_{cl}(z)}.$$

For the stationary case, a static relationship between $\Delta\gamma$ and $\Delta\vartheta$ is obtained:

$$\Delta\vartheta = s_\gamma \Delta\gamma, \quad s_\gamma = S_\gamma(1) = c_\gamma \underbrace{\frac{1}{1 - p^{WC}\frac{c_\lambda}{\hat{c}_\lambda}}}_{:=g_{WC}}. \tag{49}$$

The factor g^{WC} is called volitional amplification factor, whose dependence on the support factor is illustrated in Fig. 41 assuming perfect parameter match ($c_\lambda = \hat{c}_\lambda$). As shown in the figure, a huge amplification of the volitional activity is achieved as p^{WC} tends to one. Hence, in case of high support levels, even slight parameter variations in c_λ have a strong influence on the closed loop – especially the stability margin is sensitive to such variations. This is why an adaptation algorithm is beneficial.

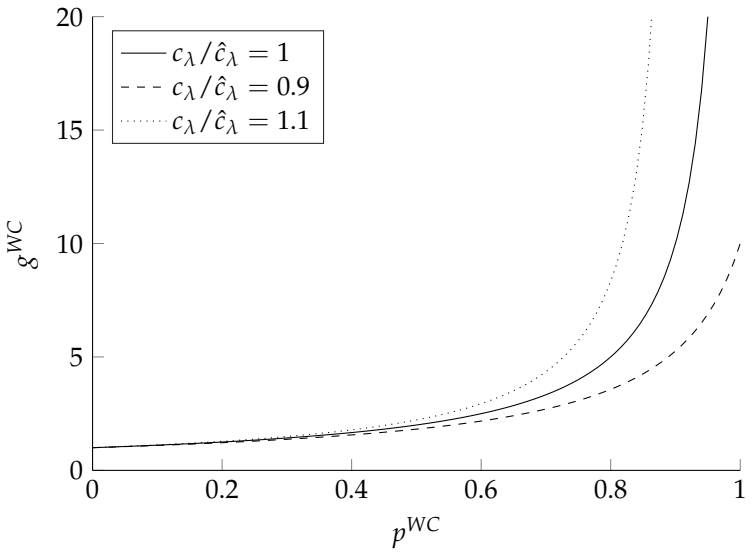

FIGURE 41: *The volitional amplification factor g^{WC} depending on the support factor p^{WC}. The solid line shows the relation in case of a perfect parameter match ($c_\lambda/\hat{c}_\lambda = 1$). In case of slight variations ($c_\lambda/\hat{c}_\lambda = 0.9$ and $c_\lambda/\hat{c}_\lambda = 1.1$), this relationship significantly changes its behavior – especially for high amplification factors g^{WC}.*

Further, the step responses of S_γ for different values of p^{WC} are shown in Fig. 42. As p^{WC} increases, the rise time of the respective step response increases. As observed, the range of motion is significantly increased for the same volitional effort. The response to changes in the volitional activity gets slower as the level of support increases. However, still continuous motor control using small volitional activities is possible. For joint angles greater than ϑ_{max}^{WC}, a linear extrapolation is performed. A more realistic simulation using a triangular input is given in Fig. 43.

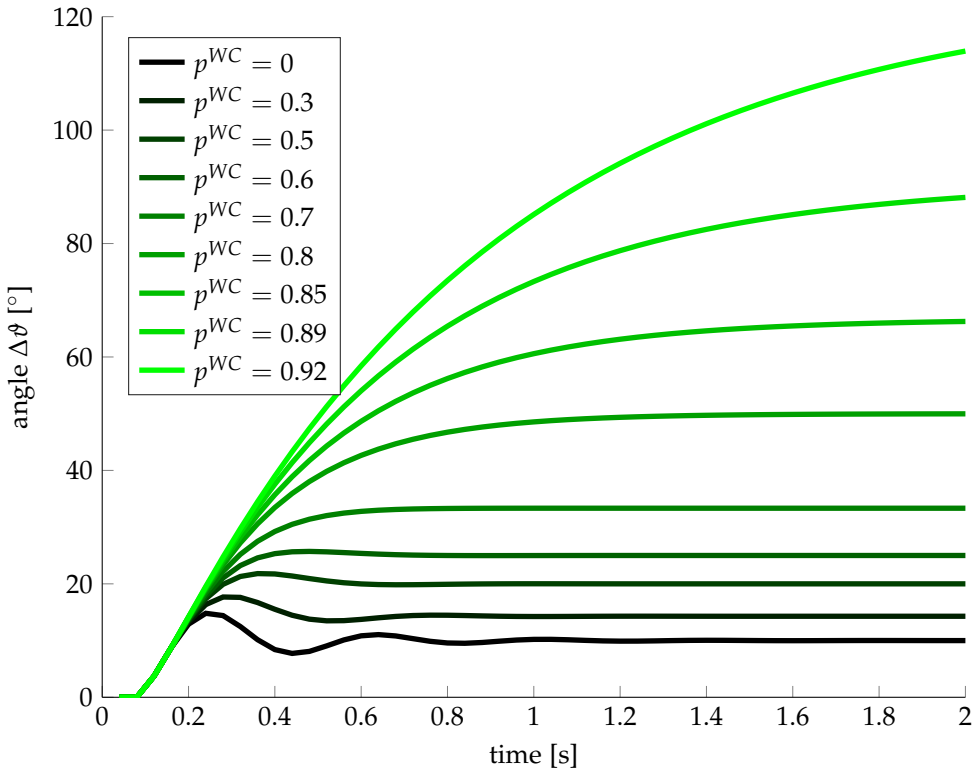

FIGURE 42: *Responses of the closed loop (transfer function S_γ) in terms of the elevation angle $\Delta\vartheta$ to a step-wise change of the volitional activity $\Delta\gamma$ from zero to one for different support factors p^{WC}. For $p^{WC} = 0$, the step response of M becomes visible. Parameters used in this simulation are $c_\gamma = 10°$, $c_\lambda/\hat{c}_\lambda = 1$, $z_1 = 0.6768 + 0.5177j$ (j-imaginary unit), $z_2 = \bar{z}_2$. The sampling time is $T_s = 1/25\,s$.*

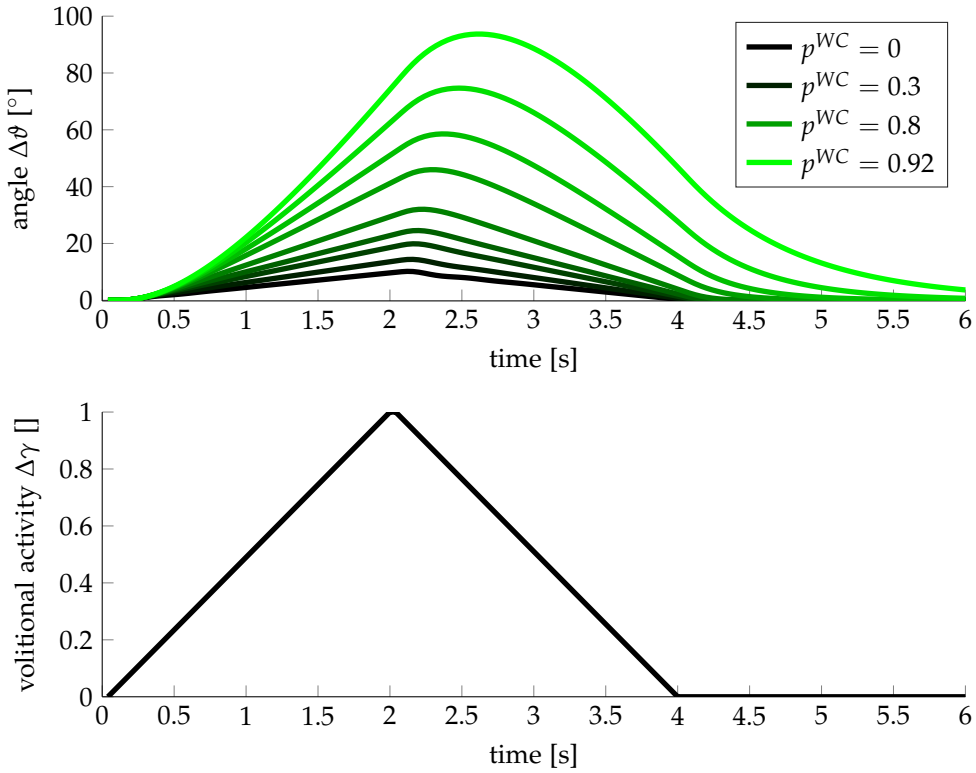

FIGURE 43: *Responses of the closed loop described by the response of the elevation angle $\Delta\vartheta$ to a triangular-shaped volitional activity. In this simulation the same parameters like in Fig. 42 are used. Further, the line colors and the different values of p^{WC} are the same like in Fig. 42.*

Conclusion To conclude, under the assumption of 2^{nd}-order linear time-invariant plant dynamics, the closed-loop system is asymptotically stable for $0 \leq p^{WC} < 1$. As p^{WC} tends to one, the required voluntary activity to realize any given joint angle trajectory theoretically tends to zero in case of perfect parameter match. For slight variations, the influence of p^{WC} significantly changes if high volitional amplification factors shall be realized.

Further, please note, that dynamical response of the joint angle to changes in the volitional activity gets slower as the level of support increases. However, continuous control is still possible, and, further, no practically relevant limitations due to the slower dynamics were observed in the experiments described in Sec. 4.5.

4.4 Experimental Validation of the Arm Weight Compensation

The support factor p^{WC} is the only tunable parameter of the weight compensation controller. In case the neuroprosthesis is applied to support daily life activities, this factor may be chosen such that a maximal support-level is achieved. This level is limited, however, by some practically relevant constraints. In any case, an overcompensation of the arm weight[29] must be prevented. Therefore, the presence of hysteresis, remaining nonlinearity, and parameter variations in the static recruitment – angle relationship, practically limits the achievable maximal support p^{WC}. One aim of this study is to determine the limits in healthy subjects.

To find out the maximal possible support factor p^{WC} and to analyze the reduction of the voluntary activity required to perform a defined joint angle tracking task in the angular range 0–60° under different levels of support, a trial-based test was carried out. While the weight compensation controller is activated, the subject is instructed to follow a staircase like angular reference trajectory (three increasing and decreasing stairs respectively) visualized on a LCD-screen along with the currently measured joint angle during each trial. When healthy volunteers were involved in these tests, they were asked to provide the minimal effort needed to track the angular reference trajectory.

As the trial number increases, the support factor p^{WC} is increased by 10% per trial starting from zero support:

$$p_j^{WC} = (j-1) \cdot 0.1, \quad j = 1, 2, ..., N_t, \quad N_t \leq 11.$$

The experiment is aborted when an overcompensation of the arm weight is observed, meaning that the subject has to actively push down to decrease the elevation level.

For all trials, the voluntary EMG $\hat{\gamma}$ is calculated as described in Sec. 3.2.2 and applied to a low-pass filter (non-causal Butterworth filter of 2^{nd}-order, with zero phase shift and a cutting frequency of $0.5Hz$) yielding $\hat{\gamma}_{lp}$. This signal is normalized to its respective minimum and maximum value yielding $\hat{\gamma}_{lp,norm}$. Finally, for each trial j, the corresponding subset is extracted yielding the signal $\hat{\gamma}_{lp,norm,j}$. Similar, ϑ_j is the signal for the measured joint angle during each trial j.

[29] Overcompensation occurs in case the open loop's static gain $L(z = 1)$ is greater or equal to one, meaning the closed loop becomes unstable or is at the margin of instability.

To assess the required voluntary activity with respect to the achieved arm elevation, the quotient A_j of the mean value $\hat{\gamma}_{mean,j}$ of the voluntary EMG $\hat{\gamma}_{lp,norm,j}$ and the mean value $\vartheta_{mean,j}$ of the measured joint angle ϑ_j is calculated for each trial:

$$A_j := \hat{\gamma}_{mean,j} / \vartheta_{mean,j}, \quad j = 1, 2, ..., N_t,$$

which is called activity level. To allow a comparison across subjects, a normalization to the maximal activity level is performed:

$$A_{norm,j} = A_j / \max_j A_j.$$

For each subject, the maximal possible support level and minimal required activity level for fulfilling the tracking task are determined.

Tests with stroke patients To demonstrate the feasibility of the weight-compensating approach in stroke patients, an observational study is performed. Herein, the system is applied to two patients suffering from a paresis in the arm elevation. In a first step, the recruitment controller is calibrated. Then, the arm-weight relief controller is activated with an initial support level p^{WC} of zero. The patient is asked to demonstrate his maximal level of volitional arm elevation multiple times. In between these trials, the support factor is manually tuned in a trial an error approach to find out the maximal possible support level that does not cause an overcompensation.

All experiments in stroke patients leading to the results described in the next section were performed in the same persons and during the same experimental session like the tests performed for the evaluation of recruitment control as described in Sec. 3.6. The ethical consent for the evaluation of recruitment control also applies to this study.

4.5 Results

Tests were carried out in healthy subjects as well as in two stroke patients. All test persons S1 to S5 were the same that also participated in the test for recruitment control in Sec. 3.6. In case of the stroke patients P1 and P2, the calibration of the recruitment controller (yielding the results described in Sec. 3.6) and the tests of the arm-weight relief controller are combined in one experimental session.

4.5.1 Healthy subjects

The weight compensation controller has been applied to each healthy subject. Detailed time-series results of all trials of S4 are shown in Fig. 44. Hereby, for increasing trial indices, the support factor has been increased from $p_1^{WC} = 0.0$ to $p_7^{WC} = 0.6$. The last trial $j = 7$ leads to some slight overcompensation of the arm weight at lower angles so that no further trial has been performed. The results of all trials for all five subjects are summarized in Fig. 45. In average, a maximal support level of $p^{WC} = 0.7$ could be achieved leading to a minimal volitional activity of 22% compared to the activity level without support (reduction by 78%).

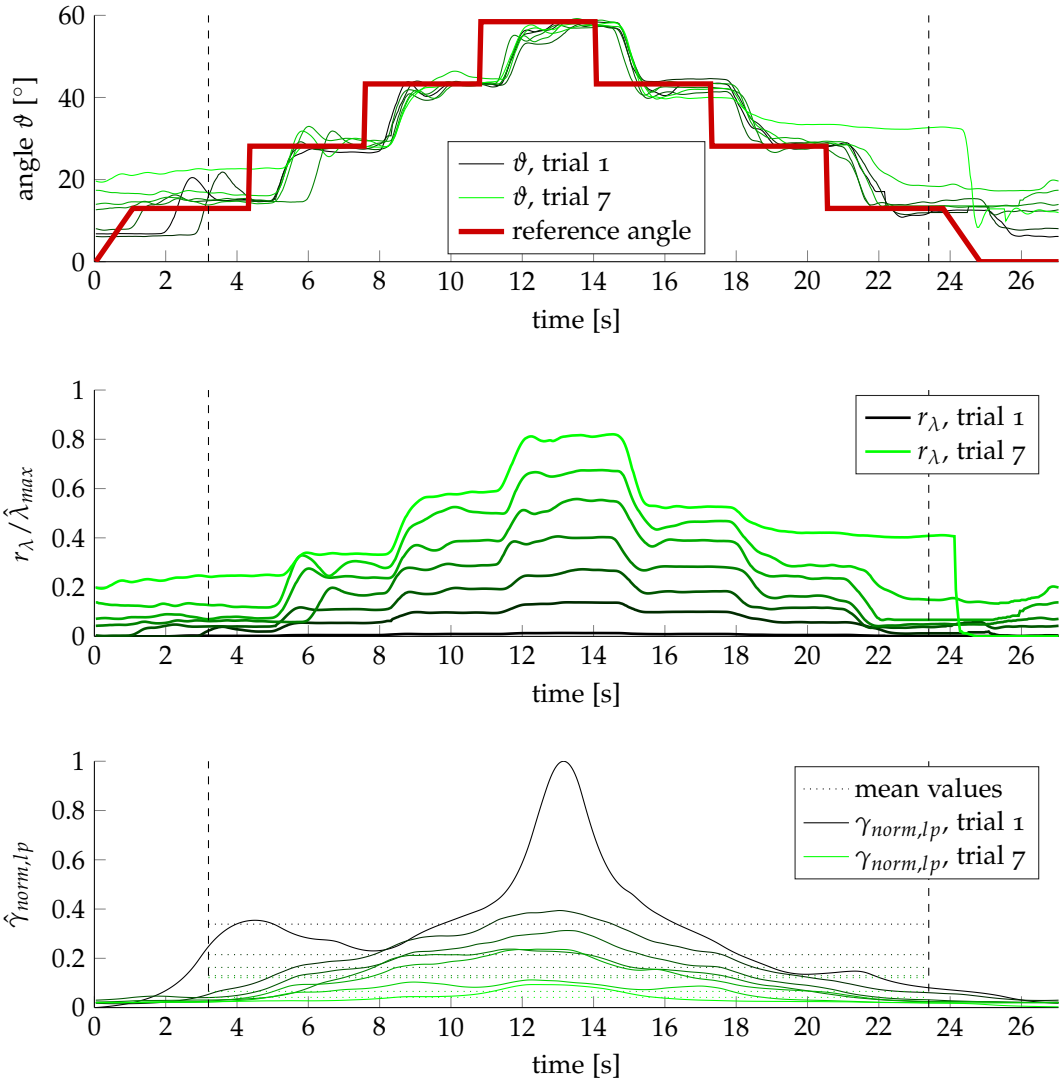

FIGURE 44: *Time series of measured signals during the tracking test with activated weight compensating controller in case of subject S4. The signals are aligned to the beginning of each trial. As the trial index increases, the support factor p^{WC} is increased leading to decreasing mean values of the volitional EMG activity $\hat{\gamma}$, while support is taken over by FES as indicated by the increasing recruitment level.*

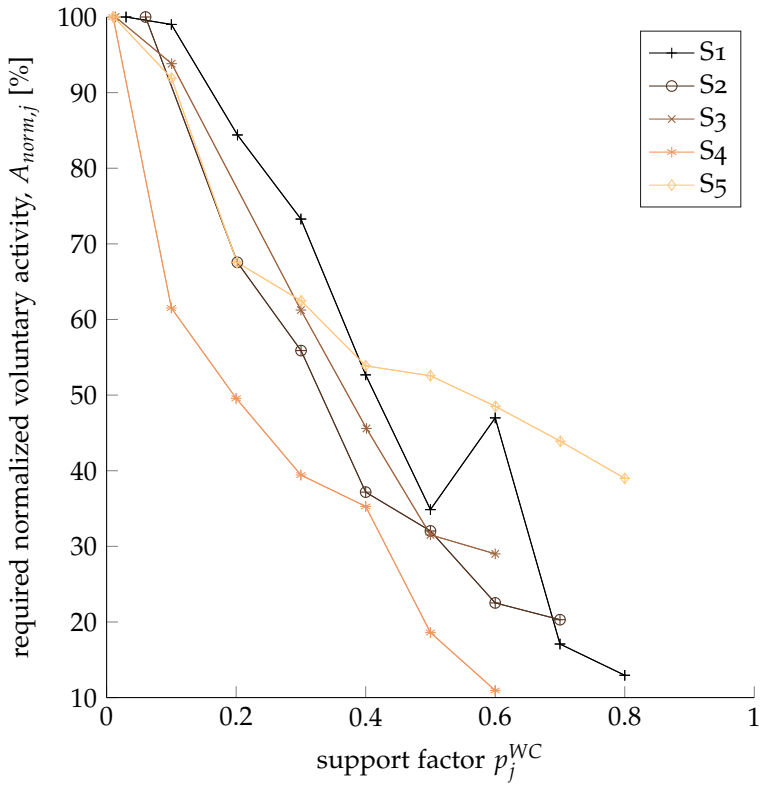

FIGURE 45: *Required voluntary activity for all healthy subjects and all tested support factors p^{WC}.*

4.5.2 STROKE PATIENTS

Patient P1 The weight compensation controller has been applied to the stroke patient P1 (details are described in Sec. 3.6) using the calibration for the recruitment controller as presented in Sec. 3.6. The achieved arm elevation is illustrated in Fig. 46. Without support, the patient could only achieve 6° shoulder elevation by himself. With arm weight support more extensive movements were possible. However, for a support factor of $p^{WC} = 1$ overcompensation of the arm weight occurred at $\vartheta = 25°$. The arm could only be lowered by decreasing p^{WC}. With a reduced support of $p^{WC} = 0.75$, he could lift, hold, and lower the arm voluntarily up to 16°.

Patient P2 A second acute stroke patient P2 (details are described in Sec. 3.6) was tested. Details for the calibration of the recruitment controller are given in Sec. 3.6. The achieved benefits of using the presented neuroprosthetic system are illustrated in Fig. 48. Compared to patient P1, P2 had much stronger volitional activity, as illustrated in Fig. 48/A, however, still significantly hindering functional movements in daily live. By applying the control system ($p^{WC} = 0.8$), the previously paretic arm elevation was almost fully restored as illustrated in Fig. 48/B. The patient had full volitional control of his arm movements and also the speed of up/down movements was comparable to healthy persons. This fact is shown in the time series plots of the experiment given in Fig. 49.

Numerous trials have been performed within 10 minutes in order to cause muscle fatigue. The maximal arm elevation by the end of the experiment ($p^{WC} = 0.8$) is illustrated in Fig. 48/C.

A B C D

FIGURE 46: *Evaluation of the arm weight compensation in a stroke patient: A – rest position, B – maximal volitional shoulder elevation without support ($p^{WC} = 0$), C – voluntary initiated shoulder elevation with maximal support factor $p^{WC} = 1$ yielding overcompensation of the arm weight (return to rest position only by decreasing p^{WC}), D – voluntary initiated and released arm lift with a support factor of $p^{WC} = 0.7$.*

Finally, also the maximal volitional activity without support was determined again at the end of the session as shown in Fig. 48/D.

4.6 Experimental Setup for Future Clinical Trials

To perform future clinical trials, a portable set-up that shall be easily operable by clinical staff was developed after the initial tests succeeded. To improve user handling, a HTML-based graphical user interface (GUI) was developed that allows the control of the neuroprosthesis via a smart device or a PC. The real-time control system is running on an embedded ARM-computer (Odroid C2, Hardkernel Ltd., South Korea) using Ubuntu 16.04 that additionally provides the HTML-content for the GUI. The connection to user interfacing devices can be achieved via USB, Wireless LAN or Ethernet. To measure EMG, the portable EMG amplifier RehaIngest (Hasomed GmbH, Germany) is used. Stimulation is applied by the stimulator RehaStim I (Hasomed GmbH, Germany). Finally, to measure the shoulder elevation angle, a wired inertial sensor (MPU 9250, InvenSense Inc., San Jose, USA) is used.

4.7 Adaptive Control

The arm-weight relief control as shown in Fig. 37 is extended by an adaptive controller. This controller acts on top and tunes the parameter p^{WC} that had to be manually tuned previously. The experimental set-up is shown in Fig. 51.

The design of this adaptive control scheme is based on the model of the closed-loop behavior introduced in Sec. 4.3. The overall scheme of the used trial-based adaption algorithm is depicted in Fig. 52 and described in the next sections.

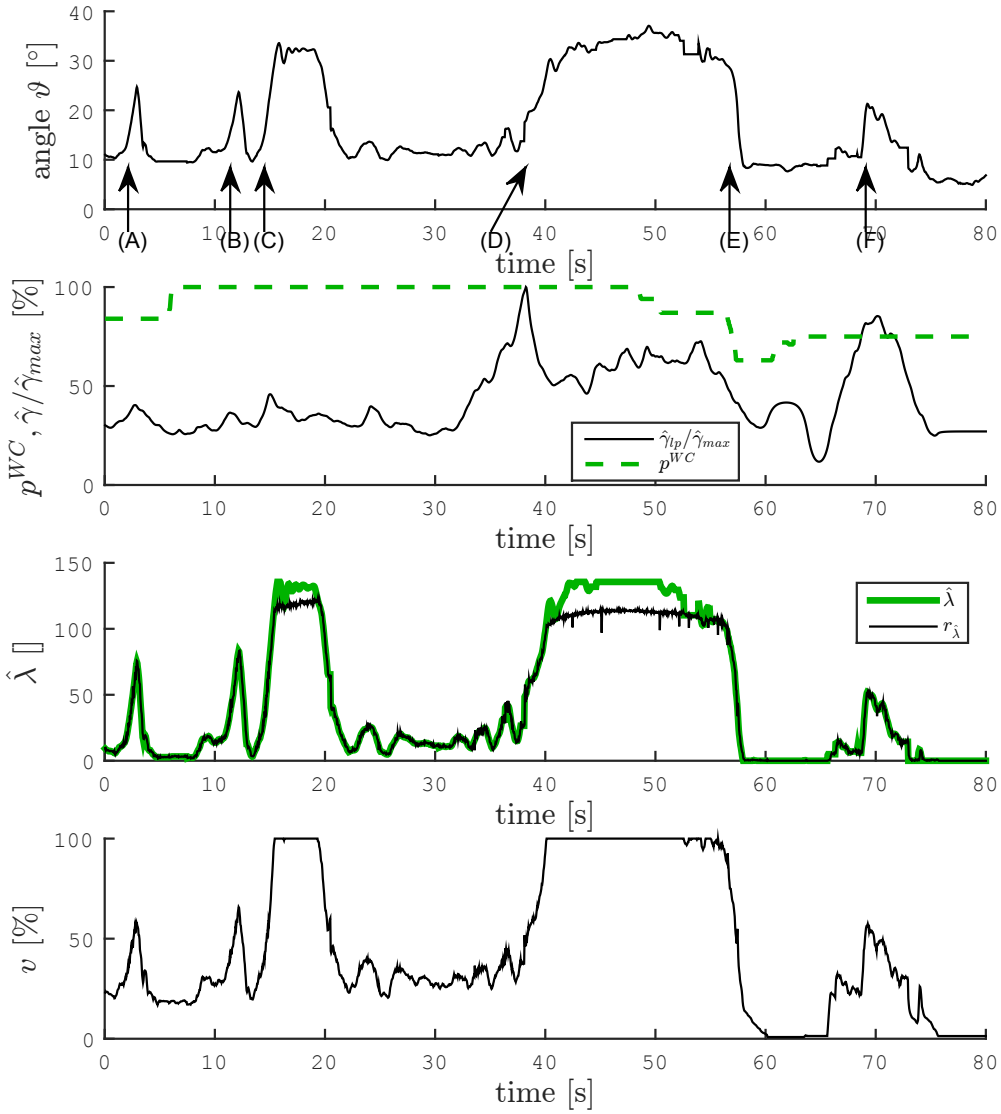

FIGURE 47: *The time-series results for the application of the weight compensation to the stroke patient P1.* ***(A)*** *are shown: With a support factor* $p_{\mathrm{WC}} = 84\%$*: The therapist has manually abducted the arm by slightly pushing. After releasing, the angle drops slowly. In* ***(B)*** *and* ***(C)*** *also manual elevation movements are performed under full weight compensation. As theoretically proposed in Sec. 4.3, due to the weight compensation, arm movements become slower, e.g., also when returning to the rest position. The smooth falling of the arm after releasing the arm took approximately* 0.5 *(A) and* 0.7*s (B). This is significantly slower than the normal drop without controller support, which is an indication of the effectiveness of the applied weight compensation. In case* ***(C)****, the effects of an overcompensation can be observed: In this case, the therapist had to push down the arm.* ***(D)*** *and* ***(F)****: The patient was able to voluntarily perform an elevation movement (no external interaction) to a significantly greater extent than without support. The voluntary contribution leading to FES-support is visible in the voluntary EMG.* ***(E)****: Due to an effective overcompensation, the support factor had to be reduced manually to decrease the elevation level.*

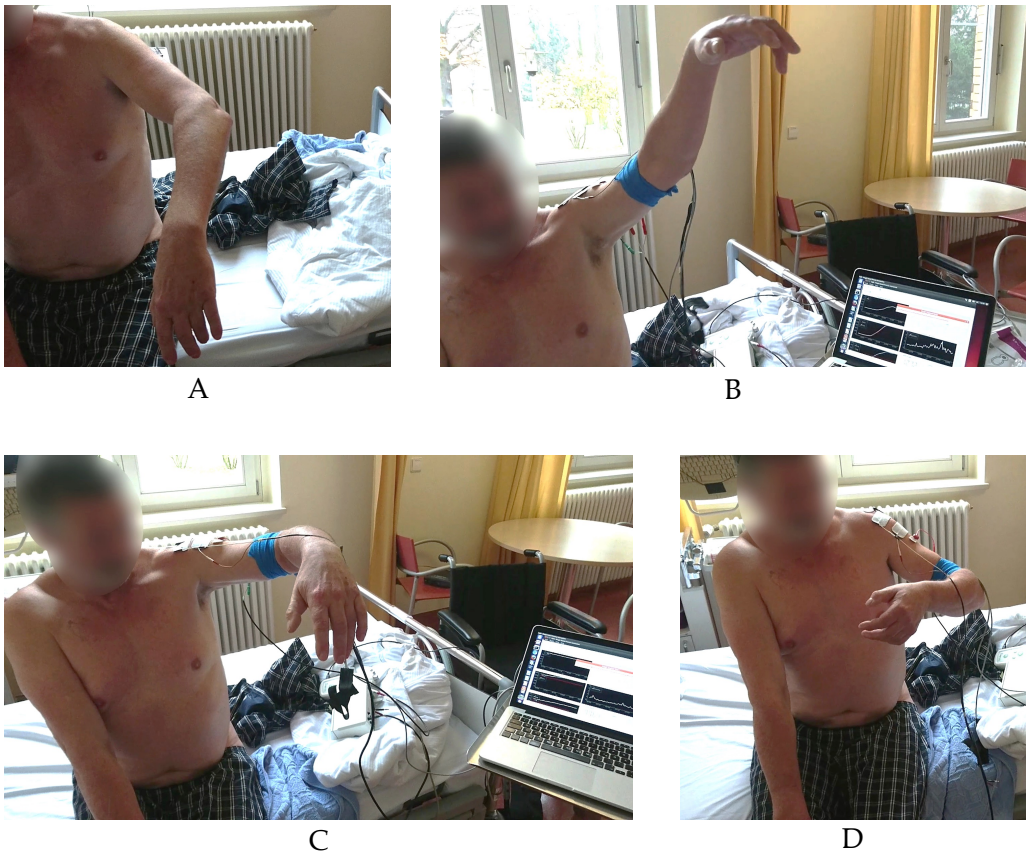

FIGURE 48: *Application of the arm-weight relief control system to a partially paralyzed stroke patient (P2). **A** The maximal residual activity before applying the device. **B** Maximal volitional shoulder elevation under a high level of support ($p^{WC} = 0.8$). **C** Maximal volitional shoulder elevation after numerous trials performed for the a constant level of support ($p^{WC} = 0.8$). **D** Maximal residual activity by the end of all trials for a deactivated FES-support ($p^{WC} = 0$). During all trials, no overcompensation was observed, and fluent movements were possible.*

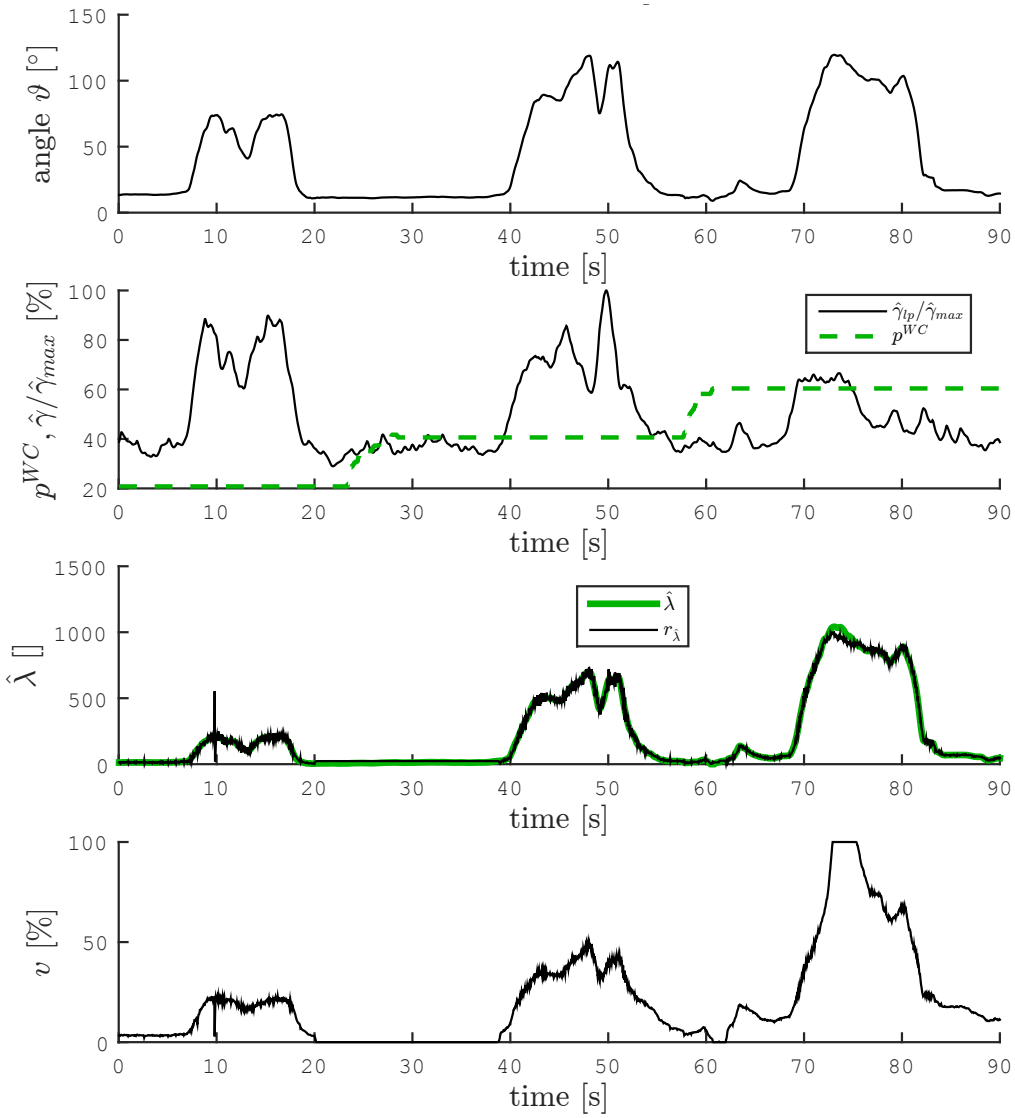

FIGURE 49: *Time series plots obtained for the activated controller applied to the stroke patient P2. Different levels of support* $p^{WC} \in [20\%, 40\%, 60\%]$ *were tested. The patient's intention fully controlled all movements.*

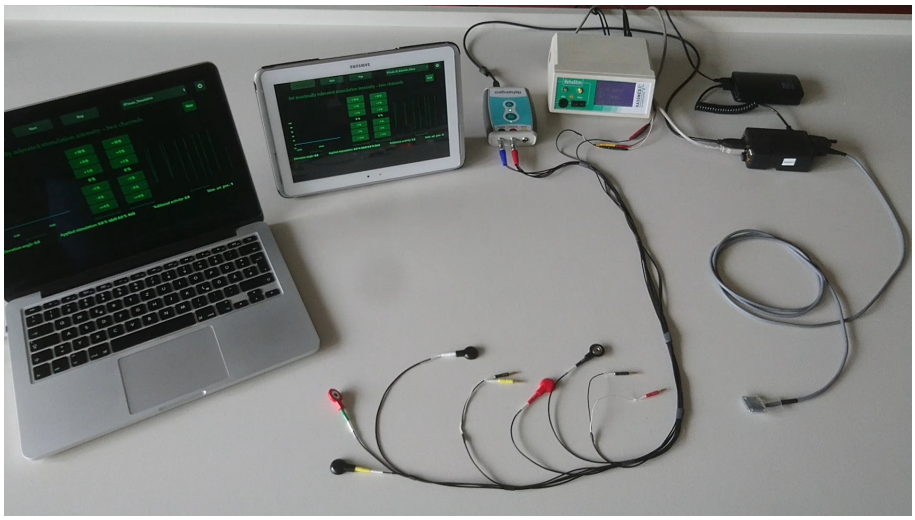

FIGURE 50: *The current set-up for experimental trials in clinical environments.*

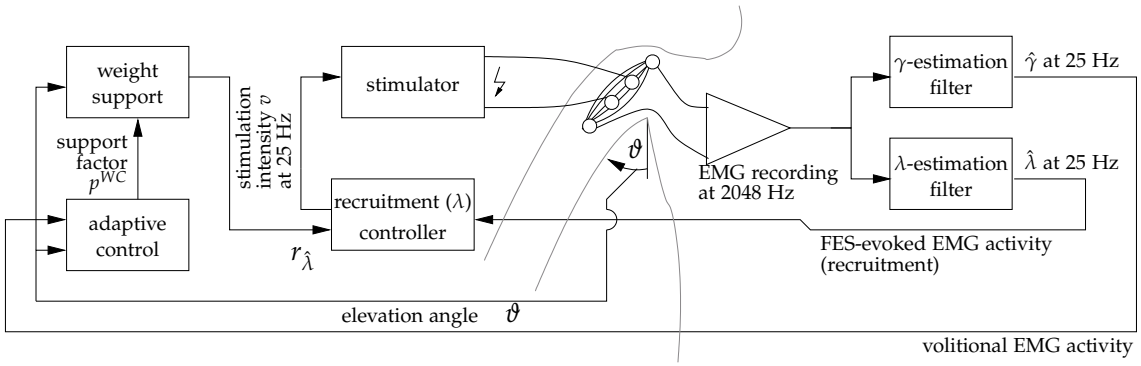

FIGURE 51: *Control scheme to achieve an arm weight relief by stimulation of the medial deltoid muscle. The controller is automatically adapted to realize the best user experience.*

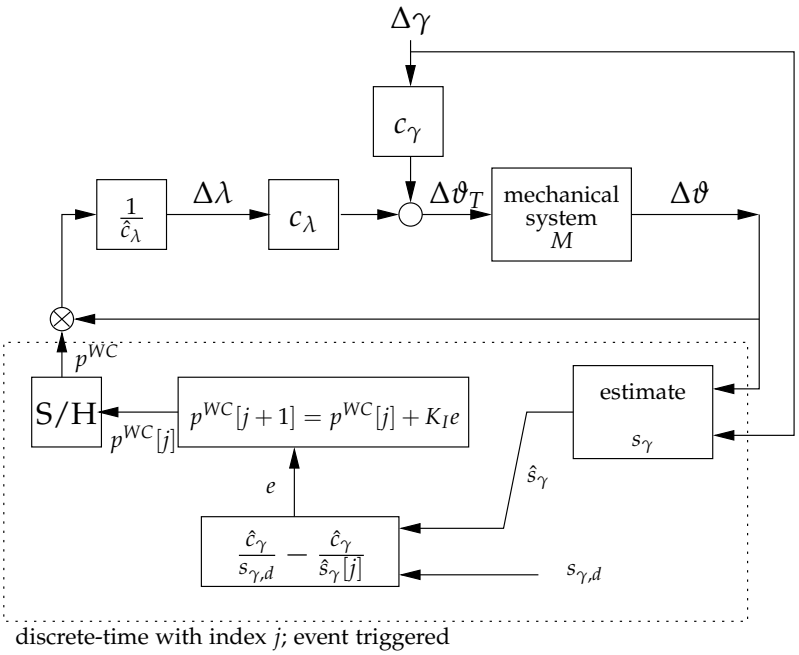

FIGURE 52: *The closed loop including the nominal model of the arm weight support that is tuned by an integral controller (Eq. (54)) adjusting p^{WC}.*

4.7.1 TRIAL-TO-TRIAL ADAPTATION

The tasks performed with the support by the neuro-prosthesis can typically be divided into short phases of active movements, e.g., for reaching and phases of complete inactivity when the upper limb stays in its rest position. To perform an automatic adaptation, a trial-based update scheme is chosen that updates the support factor p^{WC} after each phase of activity j by analyzing the closed-loop behavior during the active movement. This principle is illustrated in Fig. 53. Each trial j starts with an arm movement and finishes as the elevation returns to the rest position. For each period j, I/O data for $\hat{\gamma}$ and ϑ is obtained and stored in a separate vectors $\boldsymbol{\gamma_m}[j]$, $\boldsymbol{\vartheta_m}[j]$ for each trial j.

4.7.2 DESIRED CLOSED-LOOP BEHAVIOR

To aim of the adaptive controller is to realize a given user-experience in terms of the amplification of the required volitional activity. A pre-defined volitional amplification level g_d^{WC} (introduced in Eq. (49)) shall be realized by adjusting p^{WC}. Therefore, the desired relationship between γ and ϑ under static conditions (as described by Eq. (49)) shall be realized as illustrated in Fig. 54. This relationship is characterized by the desired slope $s_{\gamma,d}$ that is directly related the desired amplification level g_d^{WC} as described by Eq. (49). By replacing the nominal parameter c_γ by its estimate $\hat{c}_\gamma$ in this equation, the relationship for calculating the desired slope is given by

$$s_{\gamma,d} = g_d^{WC} / \hat{c}_\gamma.$$

The adaptive control scheme shall now adjust p^{WC} such that the actually present static relationship between $\hat{\gamma}$ (the estimated volitional activity) and ϑ matches its reference value given by $s_{\gamma,d}$. The

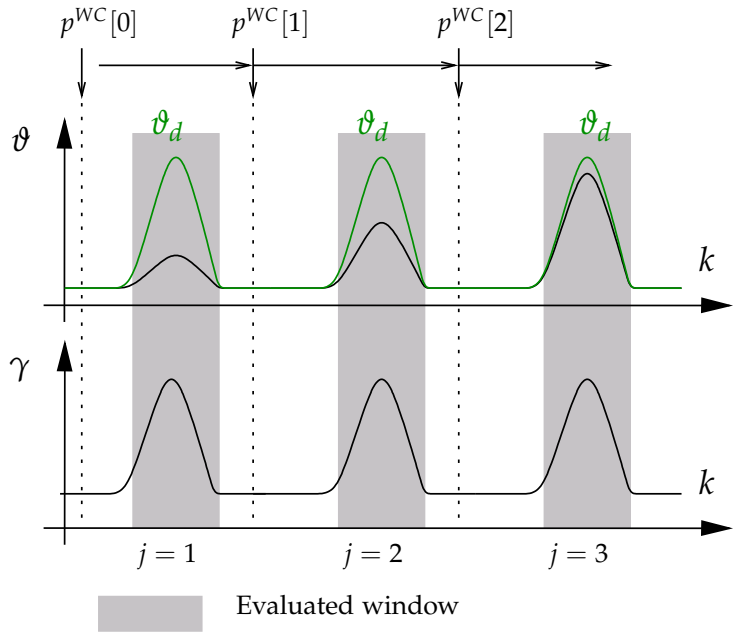

FIGURE 53: *Illustration of the trial-to-trial adaptation. The green angle trajectory named ϑ_d exemplarily describes a signal shown to the user when the control system is used for rehabilitation purposes. The user is asked to track this angle to the maximal possible extent, while the support factor p^{WC} is adapted in between trials.*

tuning of this parameter allows setting a maximally reachable joint angle that occurs for the maximal possible volitional contribution as described in Sec. 4.7.5. The adaptation procedure shall realize this behavior.

4.7.3 Estimation of the actual closed-loop behavior

After each period j, the recorded data $\boldsymbol{\vartheta_m}[j]$ and $\boldsymbol{\gamma_m}[j]$ are used to analyze the actual behavior of the closed loop. Herein, the static relationship between $\hat{\gamma}$ and ϑ shall be estimated, however, the collected data are interconnected by the closed-loop dynamics described by the transfer function $S_\gamma(z)$ (Eq. (49)). Please note that the parameter c_λ influencing the transfer function $S_\gamma(z)$ is already known approximately in form of its estimate $\hat{c}_\lambda$. Therefore, it is assumed that the dynamics in terms closed-loop poles are similar to the approximation

$$S'_\gamma(z) = S_\gamma(z)|_{c_\lambda = \hat{c}_\lambda}.$$

As illustrated in Fig. 55, a decomposition into a dynamical system F normalized to a static gain of one, and a static gain $S'_\gamma(1)$ is performed. Herein, F is given by

$$F(z) = \frac{S'_\gamma(z)}{S'_\gamma(1)} = \frac{c_\gamma}{S_\gamma(1)} \frac{M(z)}{1 - M(z)p^{WC}} \tag{50}$$

$$= \frac{M(z)(1 - p^{WC})}{1 - M(z)p^{WC}}. \tag{51}$$

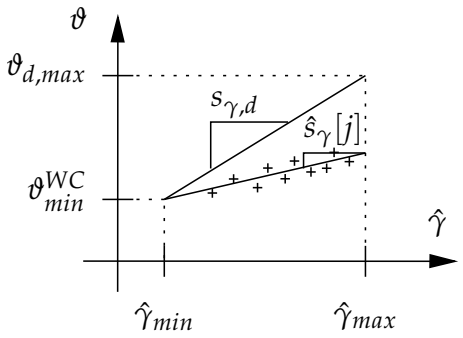

FIGURE 54: *The desired static relationship between the level of the estimated volitional muscle activity $\hat{\gamma}$ and the joint angle ϑ for stationary conditions is illustrated. The adaptive controller shall adjust the FES-support p^{WC} such that this is realized. The actual slope $\hat{s}_\gamma[j]$ is determined using measured data from trial j. Herein, ϑ^{WC}_{min} is the obtained joint angle in the absence of a muscle contraction and $\hat{\gamma}_{min}$ the belonging base-level of the estimated volitional activity. The parameter $\vartheta_{d,max}$ limits the maximally reachable joint angle that can be achieved by the maximal volitional activity $\hat{\gamma}_{max}$.*

Please note that the transfer function F does not depend on the static gain $S'_\gamma(1)$ as this gain cancels. To obtain a dataset that can be approximately described by a static relationship, the data

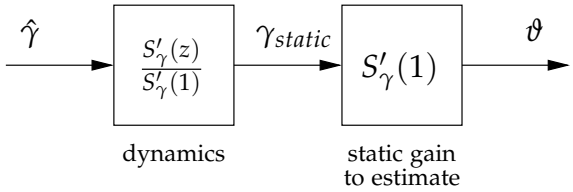

FIGURE 55: *The decomposition of the dynamical relationship between $\hat{\gamma}$ and ϑ into a dynamical part $F(z) := S'_\gamma(z)/S'_\gamma(1)$ normalized to a static gain of one, and a static gain $S'_\gamma(1)$ that shall be estimated by I/O data obtained for $\hat{\gamma}$ and ϑ. Therefore, data for $\hat{\gamma}$ is filtered by the already known function F yielding data for $\hat{\gamma}_{static}$. Then, the value of $S'_\gamma(1)$ can be directly estimated.*

$\gamma_m[j]$ are filtered by this transfer function F yielding $\boldsymbol{\gamma_{static}}[j]$, which is now assumed to relate to $\boldsymbol{\vartheta_m}[j]$ statically. Hence, the linear model

$$\boldsymbol{\vartheta_{m,i}}[j] = \hat{s}_\gamma[j] \cdot \boldsymbol{\gamma_{static,i}}[j] + \boldsymbol{\eta}_{\vartheta,i}[j], \quad \forall i \tag{52}$$

is used to describe the steady-state relationship between the volitional activity and the joint angle of the closed loop during each trial j (Fig. 40, Fig. 54, and Eq. (49)). The index i refers to the i-th vector-element (relating to the sampling instances for the recorded signal) and $\boldsymbol{\eta}_{\vartheta,i}$ describes white noise. The estimate $\hat{s}_\gamma[j]$ is then determined using a linear least squares approach after each trial j.

4.7.4 Integral control

The assumed non-linear plant including the assumed parameter variations (cf. Eq. (49)) is given by

$$\hat{s}_\gamma[j] = c_\gamma \frac{1}{1 - p^{WC}[j]\frac{c_\lambda}{\hat{c}_\lambda}}.$$

Herein, p^{WC} is the input and s_γ the variable to control (system output). By applying the output-transformation

$$y[j] := \frac{\hat{c}_\gamma}{\hat{s}_\gamma[j]} = \frac{1}{g^{WC}[j]}, \quad r[j] := \frac{\hat{c}_\gamma}{s_{\gamma,d}} = \frac{1}{g_d^{WC}}, \tag{53}$$

the virtual, linear plant

$$y[j] = \frac{\hat{c}_\gamma}{c_\gamma}\left(1 - p^{WC}[j]\frac{c_\lambda}{\hat{c}_\lambda}\right)$$

is obtained for the virtual output y and the virtual reference r. It is then feasible to apply an integral controller as follows:

$$\begin{aligned} p^{WC}[j+1] &= p^{WC}[j] + K_I(\underbrace{r[j] - y[j]}_{:=e[j]}) \\ &= p^{WC}[j] + K_I\left(\frac{\hat{c}_\gamma}{s_{\gamma,d}} - \frac{\hat{c}_\gamma}{\hat{s}_\gamma[j]}\right). \end{aligned}$$

The closed loop system is given by

$$p^{WC}[j+1] = p^{WC}[j] + K_I\left(\frac{\hat{c}_\gamma}{s_{\gamma,d}} - \frac{\hat{c}_\gamma}{c_\gamma} + p^{WC}[j]\frac{\hat{c}_\gamma c_\lambda}{c_\gamma \hat{c}_\lambda}\right) \tag{54}$$

$$\hat{s}_\gamma[j] = c_\gamma \frac{1}{1 - p^{WC}[j]\frac{c_\lambda}{\hat{c}_\lambda}}. \tag{55}$$

Feasible choices for K_I are $K_I \in]-1, 0[$ yielding as. stability under nominal conditions ($\hat{c}_\gamma = c_\gamma$, $\hat{c}_\lambda = c_\lambda$) as long as $p^{WC}[j]\frac{c_\lambda}{\hat{c}_\lambda} \neq 1$.

The steady-state value of p_{stat}^{WC} ($p^{WC}[j] = p^{WC}[j+1]$) is further given by:

$$p_{stat}^{WC} = \frac{c_\gamma \hat{c}_\lambda}{\hat{c}_\gamma c_\lambda}\left[\frac{\hat{c}_\gamma}{c_\gamma} - \frac{\hat{c}_\gamma}{s_{\gamma,d}}\right]. \tag{56}$$

By inserting p_{stat}^{WC} into Eq. (55), $\hat{s}_\gamma = s_{\gamma,d}$ is obtained meaning that the remaining control error is zero.

Asymptotic stability of the weight-relief control loop Please consider the condition ($0 \leq p^{WC} c_\lambda / \hat{c}_\lambda < 1$) (Eq. (48)) yielding as. stability of the arm-weight relief controller. It can be shown that $p_{stat}^{WC} < \hat{c}_\lambda / c_\lambda$ holds[30], meaning that the steady state of the adaptive closed loop causes the inner loop, which realizes the arm weight relief, to be asymptotically stable. To not cause instabilities of this inner loop during the automatic adaptation, the initial state $p^{WC}[0] = 0$ may be applied to the adaptive controller.

As illustrated in Fig. 56, the support factor $p^{WC}[j]$ then asymptotically converges[31] to its steady state value p_{stat}^{WC}, whereby $p^{WC}[j] < \frac{\hat{c}_\lambda}{c_\lambda}$ is guaranteed for $j \geq 0$. This condition ensures an asymptotically stable arm weight relief during each trial j.

[30] By using Eq. (56) and applying some rearrangements the following relationship is found: $p_{stat}^{WC} < \hat{c}_\lambda / c_\lambda \Leftrightarrow c_\gamma > 0$. The latter condition holds true as introduced in Eq. (41) and, hence, also the former condition is valid.

[31] Because the closed loop (Eq. (54)) is a first-order system.

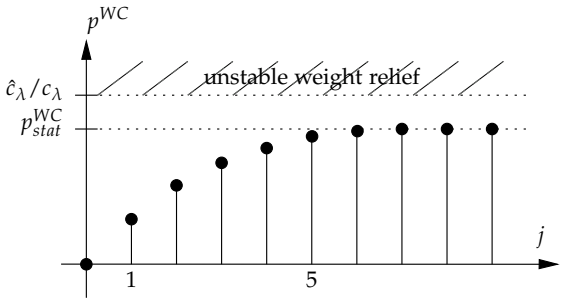

FIGURE 56: *Asymptotic convergence of the support factor p^{WC} to its steady state value p^{WC}_{stat} during the initial adaptation phase without parameter variations. Herein, $\hat{c}_\lambda / c_\lambda$ is the critical support level above which the arm weight compensation closed loop becomes unstable. It can be shown, that $p^{WC}_{stat} < \hat{c}_\lambda / c_\lambda$ holds, which means that the critical level is not crossed or reached during the initial adaptation process.*

4.7.5 TUNING PROCEDURE

The parameters $\hat{\vartheta}^{WC}_{max}$, $\hat{\vartheta}^{WC}_{min}$, $\hat{\lambda}^{WC}_{max}$, and $\hat{\lambda}^{WC}_{min}$ are determined by the calibration procedure of the recruitment controller previously performed as described in Sec. 3.4. The following steps are performed to experimentally obtain the estimate $\hat{c}_\gamma$ and the desired volitional amplification $s_{\gamma,d}$:

- For $p^{WC} = 0$, instruct the patient to perform the maximal volitionally contraction for at least 2 s and calculate the respective mean values of ϑ and $\hat{\gamma}$ for the period yielding $\hat{\vartheta}_{vol,max}$ and $\hat{\gamma}_{max}$ respectively.[32]
- For $p^{WC} = 0$, instruct the patient to not contract volitionally for at least 2 s. Record data for $\hat{\gamma}$ and calculate its mean-value during the period yielding $\hat{\gamma}_{min}$ which is the estimate of γ_{min}. Further, the minimum angle ϑ_{min} is obtained.

Then, an estimate $\hat{c}_\gamma$ of the model parameter c_γ can be easily calculated (cf. Fig. 40) by

$$\hat{c}_\gamma = \frac{\hat{\vartheta}_{vol,max} - \hat{\vartheta}_{min}}{\hat{\gamma}_{max} - \hat{\gamma}_{min}}.$$

Further, the desired static gain of $S_\gamma(z)$ (cf. Fig. 54) is given by

$$s_{\gamma,d} = \frac{\vartheta_{d,max} - \hat{\vartheta}_{min}}{\hat{\gamma}_{max} - \hat{\gamma}_{min}}.$$

Herein, the parameter $\vartheta_{d,max}$ corresponds to the maximally achievable joint angle caused by the maximal volitional activity $\hat{\gamma}_{max}$ in case the adaptive control loop reached its steady state. In the experiments in healthy subjects as described in Sec. 4.7.6, this parameter is set to the angle $\hat{\vartheta}^{WC}_{max}$ obtained for the maximal stimulation intensity. In stroke patients, this value may be set to the joint angle obtained for the maximal stimulation intensity combined with the maximal volitional contribution. However, further investigations on this topic must be performed.

The poles of the mechanical system M may be determined by a system identification experiment in which the arm is dropped while recording angle data. However, it is expected that the variations

[32] Potential changes in $\hat{\vartheta}_{vol,max}$ and $\hat{\gamma}_{max}$ due to time-variances in the muscle condition are not considered in this research.

across multiple subjects are low and, hence, a unique model might be applied to each person without significant influence on the trial-analysis as described in Sec.4.7.3.

4.7.6 Results

Simulation results To illustrate the adaptation of the closed loop to changes in muscle condition, the results of a simulation based on Eqs. (54) and (55) are shown in Fig. 57. Herein, slight step-wise variations in the system parameters c_λ and c_γ are simulated. In case of a reduction of the influence of FES on the shoulder elevation (described by c_λ), the support level p^{WC} is increased by the adaptive control loop. Further, as the influence of the volitional activity on the shoulder elevation increases, e.g., in case of a reduced muscle tone of the antagonist (flexor) muscle(s), the control loop reduces the support factor p^{WC}.

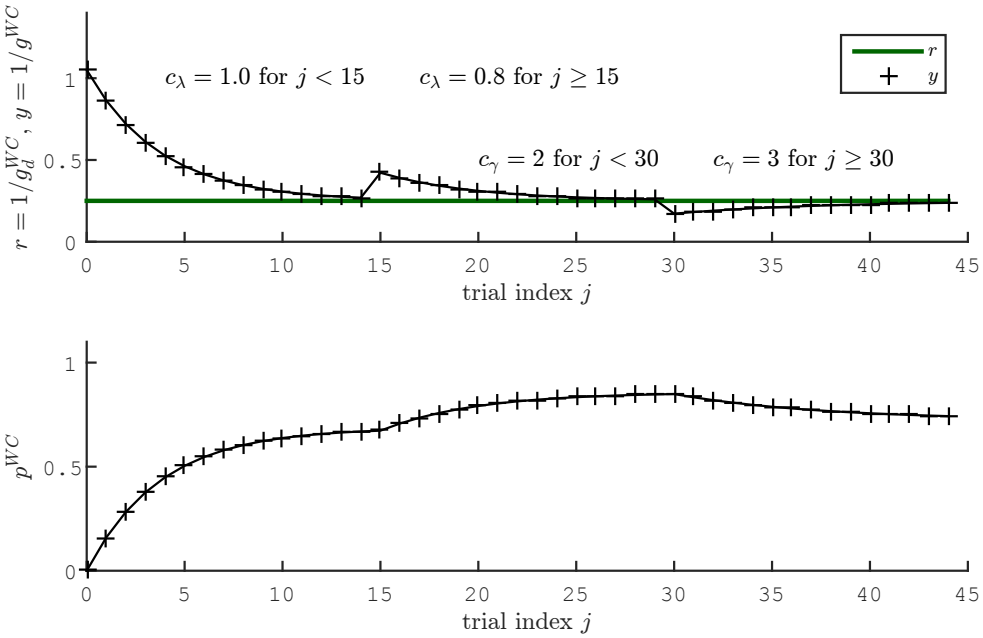

Figure 57: *Simulation results of the closed loop (Eqs. (54) and (55)). Parameters are $K_I = -0.2$, $\hat{c}_\gamma = 2.1$, and $\hat{c}_\lambda = 0.9$. At trial $j = 17$, the influence of FES on the shoulder elevation is reduced. At trial $j = 30$, the contribution of the volitional activity is increased (e.g., due to a reduced muscle tone).*

Experimental results for the automatic tuning of the support factor The developed control system was evaluated in one healthy subject. First, the recruitment controller and the arm-weight compensation controller were calibrated as illustrated in Fig. 58. The parameters of the mechanical system were experimentally identified using a test in which the arm was dropped from an angle of approximately 60 degrees, while angle data was recorded.

Then, the steps described in Sec. 4.7.5 were performed. After calibration, the adaptive control loop was applied, whereby the initial value of the integral part was set to $p^{WC}[0] = 0$. The subject then performed 24 trials in which the arm was elevated by 45 degrees, constantly held

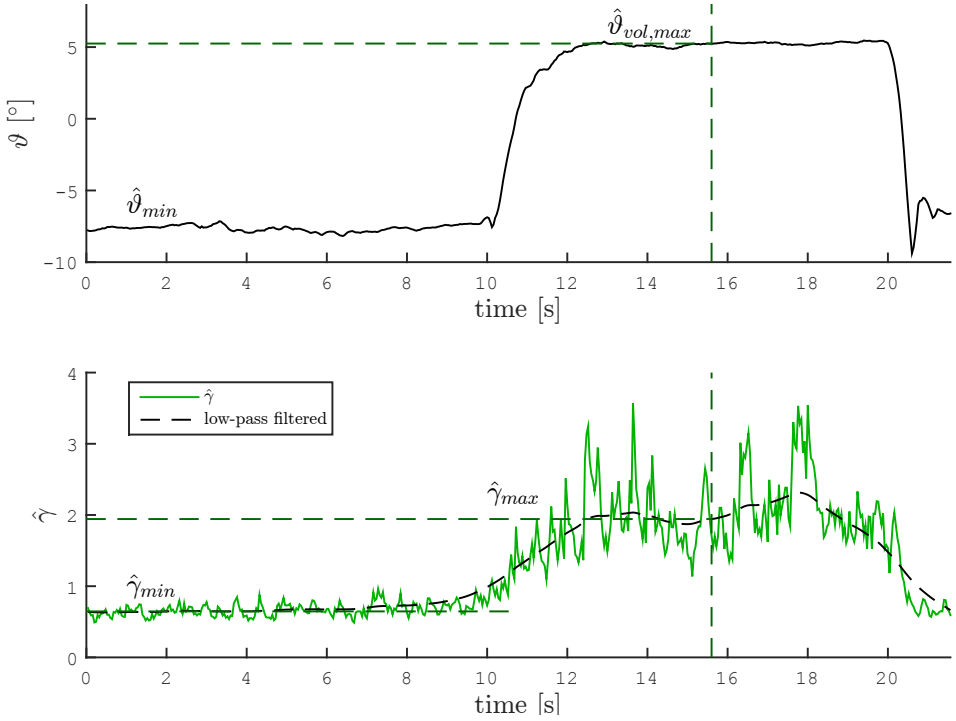

FIGURE 58: *The time series data obtained during the calibration procedure are shown. The calibration results obtained from these data were used to design the adaptive controller who's control behavior is shown in Fig. 59. The healthy subject was asked to initially relax while the parameters $\hat{\vartheta}_{min}$ and $\hat{\gamma}_{min}$ were obtained. Then, to simulate a degree of paresis, the subject was instructed to volitionally elevate his arm only by approximately 12°. In this case, the parameters $\hat{\vartheta}_{vol,max}$ and $\hat{\gamma}_{max}$ were obtained.*

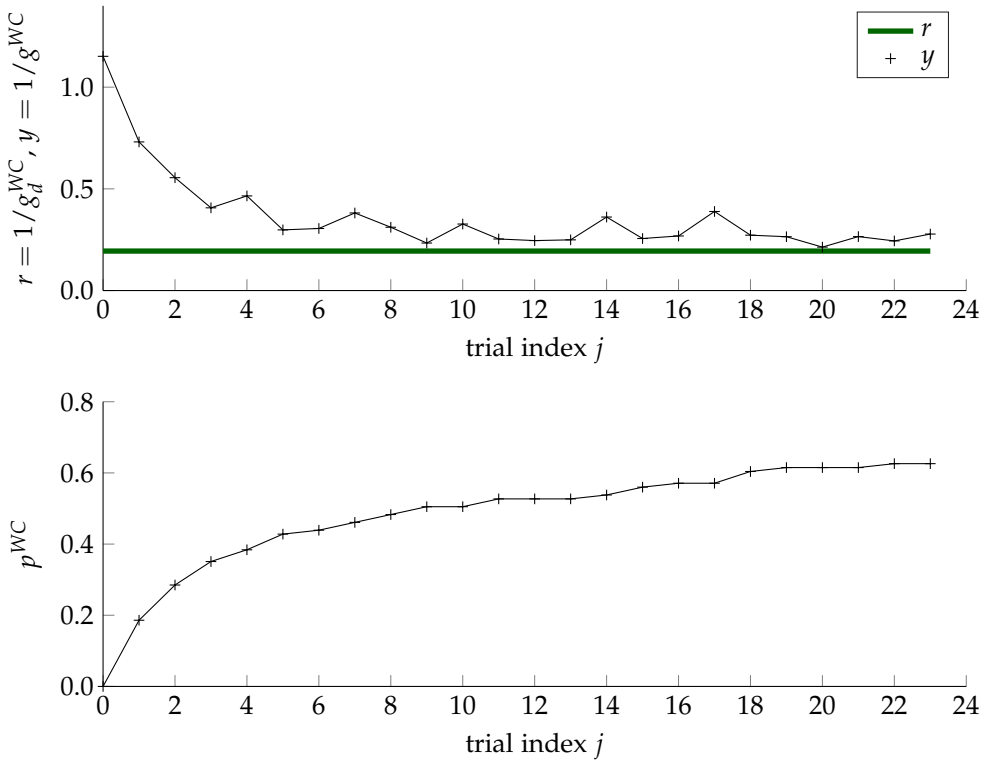

FIGURE 59: *Results for the progression of the adaptation for one healthy subject performing 14 arm elevation movements ($K_I = -0.2$). The virtual variables r and y as introduced in Eq. (53) are shown. They can be interpreted as the required volitional effort in percent. This effort is dropping as the amount of FES-support is increased by the control system.*

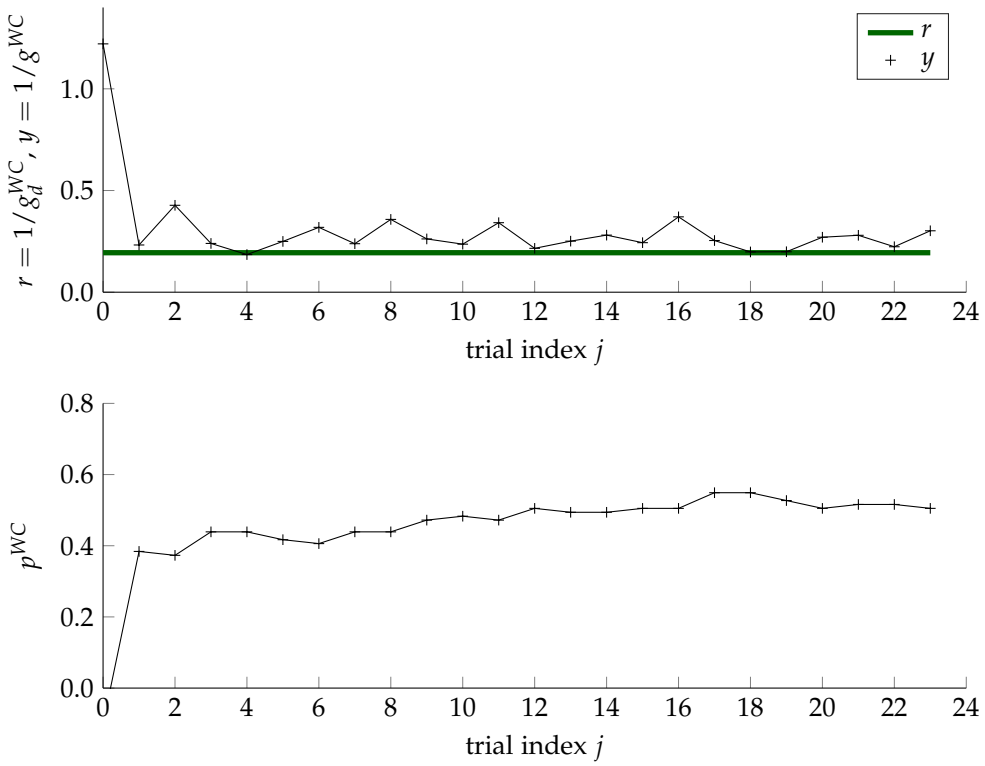

FIGURE 60: *Similar to the results shown in Fig. 59, trials with a doubled learning gain $K_I = -0.4$ were performed.*

for approximately 3 s and released again. The learning behavior across all trials for $K_I = -0.2$ is shown in Fig. 59 by the virtual variables r and y. In a second test (a complete re-calibration has been performed before), the controller gain was doubled to $K_I = -0.4$ yielding the results shown in Fig. 60. In both cases, y closely matches the reference. However, a slight remaining error was observed.

4.8 CONCLUSIONS

Arm weight support To support weak residual voluntary activity in the paretic arm elevation by FES-induced muscle activation, a proportional feedback of the joint angle to control the desired recruitment level of the deltoid muscle was proposed. The system can be parametrized by a support factor that allows the system to take over muscle activation to a certain degree. Using linear control theory, the stability of the positive feedback loop was investigated. As a further result of this investigation, the user has full control of the movement as the residual activity is amplified by the control loop. An almost completely paralyzed stroke patient was able to perform arm elevation movements to a larger extent than before. Since the maximal possible support factor is limited by hysteresis effects in the joint angle, the maximal possible support has been identified experimentally for a group of healthy subjects. A systematic approach not requiring a user-observation by the therapist would be beneficial.

The results obtained in stroke patients, strongly indicate the feasibility of the developed neuroprosthesis to increase the reachable range of motion for functional movements under a paresis. For patients suffering from a strong paresis, as demonstrated by P1, the user-control becomes more difficult. In case of such strong paresis, high levels of volitional amplification are required to restore a functionally feasible arm elevation. A high amplification, however, may bring the closed loop close to instability. In this case, even small disturbances may lead to an overcompensation of the arm weight, as it has been observed in the experiments in subject P1. Such disturbances may potentially be minimized by an enhanced angular measurement that, e.g., compensates the influence of upper-body movements. Further, the influence of hysteresis effects (cf. Fig. 38) may cause difficulties in releasing the shoulder elevation. To detect and dissolve cases in which an overcompensation occurs, a top-level classification and control system may be used that detects such situations, e.g., by taking the estimated volitional activity into account. Then, by a slight temporary reduction of the support factor, the arm elevation could be released.

In case of a slighter paresis (P2), the system performed as expected and a restoration of functional movements was possible. For both patients, the steps required to apply the system including electrode placement and calibration did not exceed more than 15 minutes, though there is still room for improvement. The time spent on electrode placement by trial and error consumed the largest amount of time. For subsequent sessions on the individual patient, the required time is expected to be reduced, because of previously obtained experience.

Because of underlying recruitment control, it is assumed that the progression of muscle fatigue does not have an influence on the weight relief control loop as long as the stimulation does not saturate. Though this assumption was not experimentally validated, it should be reasonable, as the compensation of fatigue-effects by recruitment control was experimentally demonstrated. Further, a comparison to an arm-weight relief control system that directly applies stimulation without recruitment control was not performed. From a theoretical perspective, the progression of muscle fatigue shall cause a decrease of the effective volitional amplification factor, if no fatigue compensation is present.

Adaptive control The presented adaptive control scheme was tested for two different controller gains K_I in one healthy subject. In both cases, a fast adaptation within only 3 to 5 trials was possible, demonstrating the feasibility of the chosen approach. Though an integral part is present in the control loop, a small stationary control error was observed. It is assumed that this stationary error is caused by a continuously changing time-variant parameter, whose effects cannot be compensated by a single-integrator approach. A double-integrator approach might solve this issue. However, for practical application, the results are well sufficient.

The presented adaptive control concept is primarily intended for application in rehabilitation, wherein repetitive reaching movements are performed that involve a similar trajectory in each trial. In the estimation of the actual relationship between $\hat{\gamma}$ and ϑ (cf. Fig. 54) it is assumed that this relation is linear and does not depend on the performed trajectory, which is because of the assumption of a linear model for the hybrid muscle activation. Therefore, in theory, the chosen adaptation approach does not rely on a fixed trajectory and, hence, duration and intensity of the performed arm elevation can vary without influencing the learning behavior. Under these assumptions, the chosen approach may also be feasible to be applied to support daily life activities.

It must be remarked, however, that the linear model (Eq. (41)) used to describe the hybrid muscle activation forms a strong simplification. This typically degrades the degree of linearity for the collected data pairs assumed by Eq. (52) in the trial-analysis (Sec. 4.7.3), because the closed loop that causes the observed $\hat{\gamma} - \vartheta$ relationship is then non-linear. Due to this fact, the result of the calculation of $\hat{s}_\gamma$ may additionally depend on other factors, e.g., the performed trajectory. This dependency causes a bigger variance in the calculation of $\hat{s}_\gamma$. This fact, however, becomes only visible in the progression of learning, if the performed angle trajectories differ greatly from trial to trial.

In daily life activities, reaching trajectories are typically subjected to significant variances, however. As a first approach considering this issue, a more detailed model based on artificial neural networks is presented in Appendix. A. Future investigations may, hence, also involve the integration of such a model into the adaptive control scheme.

Further investigations should also consider the influence of spastic-effects in the arm elevation (only performed in simulation in this study) and the detection and incorporation of additional loads (e.g., when grasping and releasing objects).

5

A NEURO-PROSTHETIC DEVICE TO RESTORE ARM FUNCTIONS IN COMPLETELY PARALYZED PATIENTS

This chapter presents a fully feedback-controlled arm neuro-prosthesis for individuals with no or very weak residual arm and shoulder functions (such as persons with C3/C4 tetraplegia) to restore reaching functions. In contrast to existing arm neuro-prostheses, the proposed solution allows to position the hand at arbitrary desired positions within the reachable workspace.

This arm neuro-prosthesis is a component of the modular assistive framework MUNDUS (**MU**lti-modal **N**europrosthesis for **D**aily **U**pper limb **S**upport[33]) [134] that has been developed to support and recover arm and hand functions in severely impaired people.

The arm reaching functionality can be extended by a robotic or FES-based module for grasping assistance.

To reduce the amount of required stimulation for the arm and shoulder muscles, a passive light-weight exoskeleton developed within MUNDUS by Technische Universität Wien supports the user in addition to FES. The main purpose of the exoskeleton is the gravity compensation by a passive spring mechanism. In addition to this, the exoskeleton enables to lock all joints for holding the arm at given positions without FES. Thus, only point-to-point movements under gravity compensation have to be realized through artificial muscle activation assuming no or insufficient residual motor control by the user over his/her arm and shoulder musculature.

To simplify the generation of reaching movements with FES, a sequential control of each DoF is applied: While one joint angle for one DoF is controlled by adjusting the corresponding stimulation intensity to match a pre-calculated angular reference position, the other DoFs are locked by the exoskeleton brakes. This strategy results in a fully decoupled system concerning cross-couplings between the DoFs. For this reason, a light model with few parameters can be used in the design of the controller, which dramatically reduces the effort for parameter identification.

Positions of target objects are detected in 3D space by a KINECT-based marker tracking system developed within MUNDUS by Fraunhofer IESE. The mapping between the exoskeleton angles and the position is bijective and is described by a kinematic model. Since the coordinate frame of the marker tracking system is not necessarily equal to the one used for the kinematic model, a transformation (translation and rotation) between two coordinate frames is required. The parameters of the full transformation, as well as all parameters of the kinematic model (lengths of the upper- and forearm and the inner shoulder rotation angle), are estimated by a non-linear optimization procedure using measurements from at least 12 different arm positions. Another calibration step is to acquire the maximum tolerable stimulation intensities for each muscle along

[33] http://www.mundus-project.eu; Funded by the European Commission in the 7th Framework Program, Grant agreement no.: 248326

with a calibration experiment for identifying the dynamics of the shoulder abduction movement induced by FES. The detection of the patient's intention is gathered either by an eye-tracking module or by a BCI-interface both developed within MUNDUS by Politecnico di Milano and the Machine Learning Group at TU Berlin, respectively.

The methods and results presented in this chapter have been previously published as listed below.

- An overview of the overall MUNDUS system is given in

  [135] A. Pedrocchi, S. Ferrante, E. Ambrosini, M. Gandolla, C. Casellato, T Schauer, C. Klauer, J. Pascual, C. Vidaurre, M. Gfoehler, et al. "MUNDUS project: MUltimodal Neuroprosthesis for daily Upper limb Support". In: *Journal of neuroengineering and rehabilitation* 10.66 (2013), pp. 1–20. DOI: 10.1186/1743-0003-10-66.

- Initial results have been published in

  [90] C. Klauer, T. Schauer, J. Karner, W. Reichenfelser, E. Ambrosisni, S. Ferrante, and J. Raisch. "Design of feedback control strategies for an arm neuroprothesis combined with an exoskeleton". In: *Converging Clinical and Engineering Reseach on Neurorehabilitation - Part II, ICNR 2012*. Springer, 2012, pp. 1189–1193. ISBN: 978-3-642-34545-6.

- The complete FES-control system and its statistical analysis have been published in

  [92] C. Klauer, T. Schauer, W. Reichenfelser, J. Karner, S. Zwicker, M. Gandolla, E. Ambrosini, S. Ferrante, M. Hack, A Jedlitschenka, A. Duschau-Wicke, M. Gföhler, and A. Pedrocchi. "Feedback Control of arm movements using Neuro-Muscular Electrical Stimulation (NMES) combined with a lockable, passive exoskeleton for gravity compensation". In: *Frontiers in Neuroscience* 8.262 (2014). DOI: 10.3389/fnins.2014.00262.

5.1 Control System Architecture

The entire system developed for the support of the reaching movements is depicted in Fig. 61. Potential users have no residual voluntary control of arm, shoulder, and hand muscles, but they can still control the head and gaze fixation. They usually sit in a wheelchair in front of a table.

The arm/shoulder movements are induced by FES while an exoskeleton guides the movement and supports the arm during static postures in the absence of FES. The control signals (stimulation intensities and on/off state of the exoskeleton brakes) are generated by a real-time controller that receives commands from the Central Controller (CC) implemented by a finite state machine. The central controller instructs the real-time controller to move the hand to a given target position in the reachable workspace. Sensors integrated with the exoskeleton measure joint angles that are used as feedback variables by the real-time controller. The FES control algorithm sequentially controls each joint angle while locking the other DoFs.

The user interacts with the system through an eye tracker. Therefore, a commercial system, the Tobii T60W system (Tobii Technology AB, Sweden), has been extended by a specific GUI for

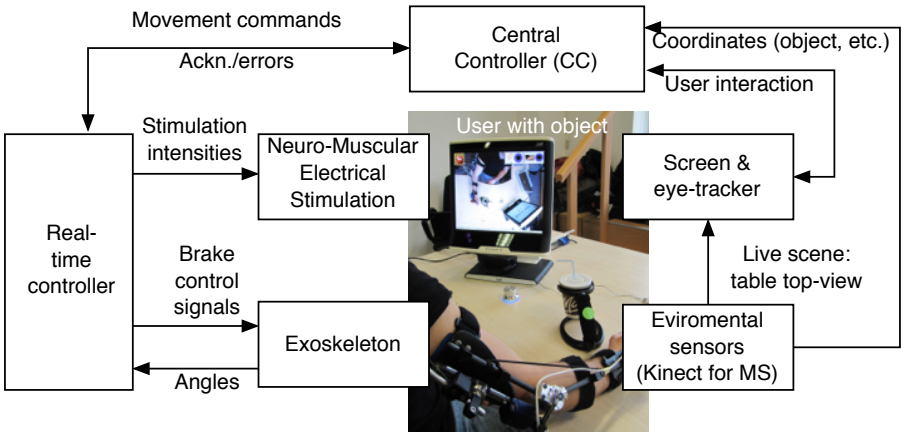

FIGURE 61: *System architecture for support of reaching function.*

the MUNDUS application. The table mounted eye tracker is integrated into a 17" TFT monitor. During tracking, the Tobii T60 uses infrared diodes to generate reflection patterns on the corneas of the user's eyes. Proper image processing is used to identify the gaze point on the screen. The three-dimensional position of the user's hand, of the objects to be manipulated, and of the user's mouth are continuously monitored by environmental sensors, two Kinect cameras by Microsoft (Microsoft Corp., Redmond, USA). Colored markers are attached to the hand and the objects to enable their tracking. The first Kinect camera projects an image of the workspace on the eye-tracking screen. To start an interaction with a specific object, the user has to visually fixate this object on the eye tracker screen for a pre-defined time duration. Once an object is selected, the corresponding Kinect coordinates are sent to the CC which transforms these coordinates into the global (exoskeleton) 3D coordinate system. The real-time controller will then use the transformed coordinates for the movement generation. The second Kinect camera is placed in front of the user and is used to track the face position.

The central controller interfaces all modules and interacts with the eye tracker and the real-time controller. For system integration, the software components of the CC and the eye tracker module have been integrated into one single MS Windows-based PC. The real-time controller and the data processing of the environmental sensor module are based on a computer system running Linux with RTAI extension[34].

Development and testing of the control system were performed in Scilab/Scicos 4.1.2[35] using the real-time framework OpenRTDynamics[36]. The communication between all modules is established via UDP and messages in the XML format are broadcasted.

5.2 EXOSKELETON

As a basis for the exoskeleton design, the previously mentioned target motions were analyzed using a motion capture system (Lukotronic, Lutz Mechatronic Technology e.U, Austria) to estimate the required ranges of motion and expected loads at the joints [77, 145]. The 3D mechanical

[34]http://www.rtai.org
[35]http://www.scilab.org
[36]http://openrtdynamics.sourceforge.net/

design was done in Catia V5R19 (Dassault Systèmes, France), focusing on modularity, simplicity, and lightweight. The developed exoskeleton with gravity compensation is shown in Fig. 62 A. The available degrees of freedom (DoF) of the exoskeleton are:

1. shoulder flexion/extension (angle ϑ_u),
2. shoulder horizontal rotation (angle φ_u),
3. elbow flexion/extension (angle ϑ_f).

The rotation of the forearm around the upper arm axis (humeral rotation) and pronation/supination of the forearm are locked by the exoskeleton as these DoFs are difficult to be controlled by FES using surface electrodes. Due to the reduced DoFs, the orientation of the hand is not freely adjustable in the workspace. Thus, to allow a safe handling of objects despite this constraint, special objects with a universal joint in the handle have been developed (e.g., cup holder shown in Fig 62 B).

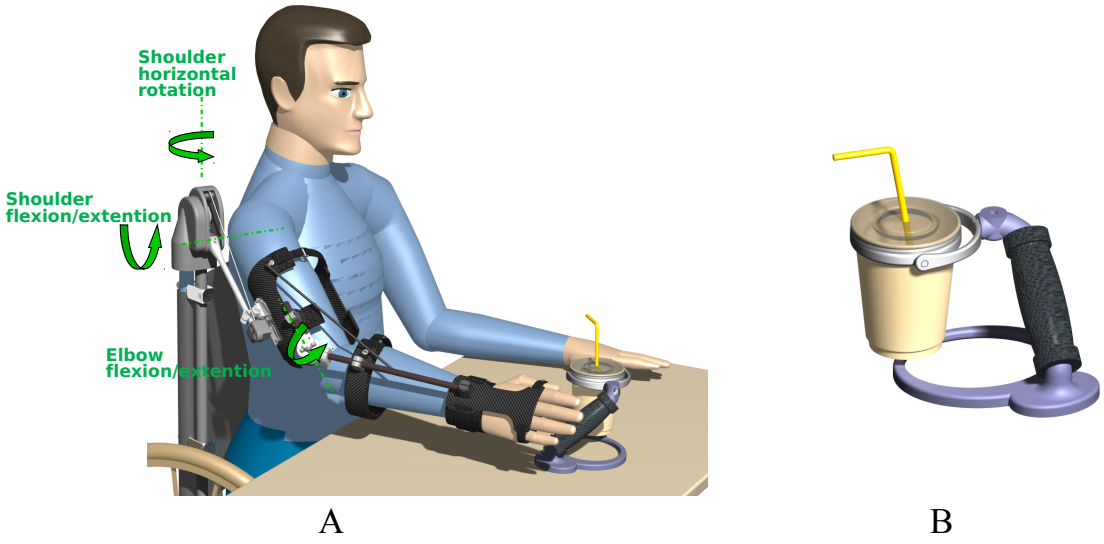

FIGURE 62: *A) Exoskeleton with spring-based gravity compensation and electromagnetic brakes mounted on a wheelchair. B) Cup holder with cardan joint in the handle.*

The exoskeleton is equipped with magnetic encoders (Vert-X, Contelec AG, Switzerland) to measure the angles for all three DoFs. Electromagnetic DC brakes (Kendrion, Germany) can lock the shoulder horizontal rotation with a torque of 2.5Nm, the shoulder flexion/extension with up to 5 Nm and the elbow flexion/extension with 1.5 Nm to hold the arm in any posture when the stimulation is switched off.

To realize gravity compensation, a pressure spring is integrated into a vertical carbon tube that can be either mounted on a wheelchair as shown in Fig. 62 or attached to a body harness for mobile use. The spring force is transferred to the elevation lever by a rope and pulley mechanism.

A slight under-compensation (spring torque smaller than gravity torque) is intended as the arm should move downwards slowly and gravity-induced when the stimulation and the brakes are turned off. The amount of compensation is adjusted manually by changing the wind-up length of

Table 4: *Stimulation channels.*

channel	activated muscle	control signal	actuated angle – movement
1	biceps	v_b	ϑ_f – elbow flexion/extension
2	deltoid, anterior head	$v_{d,a}$	positive direction of φ_u – shoulder horizontal rotation
3	deltoid, posterior head	$v_{d,p}$	negative direction of φ_u – shoulder horizontal rotation
4	deltoid, medial head	$v_{d,m}$	ϑ_u – shoulder flexion/extension

the rope at the spring adjustment module. A linear guiding provides the connection between the elevation lever and the upper arm shell and compensates misalignment of the anatomical and the mechanical shoulder joint. This guiding also minimizes the reaction forces. For the elbow-joint, an elastic band with a variable attachment point acts as weight support.

The exoskeleton has a total weight of 2.2 kg and can be quickly adjusted to different anthropometric dimensions.

5.3 Neuro-Muscular Electrical Stimulation

The desired arm movements are induced by four stimulation channels activating the anterior, posterior and medial deltoid, and the biceps muscle (cf. Table 4). By stimulating the medial deltoid, the shoulder extension can be actuated, while the anterior and posterior deltoid allow arm rotation in the horizontal plane. Stimulation of the biceps is used to flex the elbow joint. Shoulder flexion, as well as elbow extension, are induced by gravitational forces. One pair of self-adhesive hydro-gel electrodes (oval shaped with size 4x6.4 cm) is used for each stimulated muscle. The stimulation intensity described by the normalized pulse charge v_i (cf. Sec. 2.4) serves as control signal for the muscle i, while the stimulation frequency is fixed for all channels at 25 Hz. Table 4 shows the used control signal notations. Current amplitudes and pulse widths are determined from normalized stimulation intensities v_i as described in Sec. 2.4.

For the generation of the bi-phasic stimulation pulses, the current-controlled stimulator RehaStim Pro (HASOMED GmbH, Germany) is used.

In a calibration phase, that is always performed before using the MUNDUS system, the maximally tolerable pulse charge $Q_{i,max}$ of each muscle i is determined and used for the normalization of the applied charges. Then, for the medial deltoid, the stimulation intensity $\underline{v}_{d,m}$ that causes the onset of a visible muscle contraction is determined. This value is required for the implementation of the more complex shoulder flexion/extension controller described in Sec. 5.5.2.

5.4 Kinematic Model and Coordinate Transformations

To calculate the hand position from a given set of joint angles or vice versa, a kinematic model of the exoskeleton is required. Also, a transformation from the Kinect coordinate system to the global (exoskeleton) coordinate system must be determined for the following reason: Objects to interact with may potentially arbitrary located on the table in front of the user. The Kinect is required to determine the object position in the local Kinect coordinate system. To bring the hand

to objects by FES, the Kinect coordinates must be mapped into exoskeleton 3D coordinates and corresponding exoskeleton angles. The latter forms the basis for the real-time arm controller.

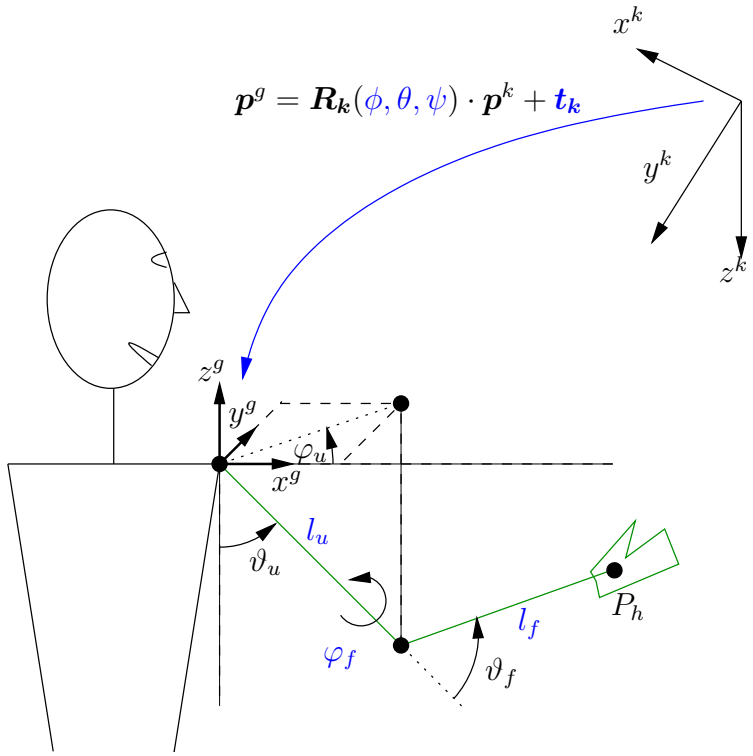

FIGURE 63: *Simplified kinematic model of the exoskeleton with coordinate systems and a transformation between these systems. Depicted is the right arm reaching forward. The parameters of the coordinate transformation ϕ, θ, ψ, and $\boldsymbol{t}_k$ as well as the kinematic model parameters l_u, l_f, and φ_f need to be identified.*

It is assumed that the placement of the Kinect, as well as the settings of the exoskeleton, may change from day to day and therefore parameters need to be determined with a simple and fast procedure through experimental system identification.

Figure 63 shows the simplified kinematic model of exoskeleton/arm with the global (exoskeleton) coordinate system (x^g, y^g, z^g) and the Kinect coordinate system (x^k, y^k, z^k). Both are Cartesian coordinate systems. Depicted is the right arm reaching forward. The model assumes that the exoskeleton is entirely rigid and that the arm is perfectly aligned to the exoskeleton.

The forward kinematics is given by

$$\boldsymbol{p}_h^g(\vartheta_u, \varphi_u, \vartheta_f) \quad = \quad -(l_u \boldsymbol{R}(\vartheta_u, \varphi_u) + l_f \boldsymbol{R}(\vartheta_u, \varphi_u)\boldsymbol{R}(\vartheta_f, \varphi_f))\boldsymbol{e}_z. \tag{57}$$

where $\boldsymbol{p}_h^g$ is hand position in the global coordinate system, $\boldsymbol{e}_z = [0, 0, 1]^T$ is a unity vector, and l_f and l_u are the lengths of the forearm and upper arm, respectively. The rotation matrix $\boldsymbol{R}$ is

defined as follows:

$$\boldsymbol{R}(\vartheta, \varphi) := \begin{bmatrix} \cos\varphi\cos\vartheta & -\sin\varphi & -\sin\vartheta\cos\varphi \\ \cos\vartheta\sin\varphi & \cos\varphi & -\sin\varphi\sin\vartheta \\ \sin\vartheta & 0 & \cos\vartheta \end{bmatrix}. \tag{58}$$

In the used set-up, the humeral rotation angle φ_f of the shoulder is constant, as it represents a fixed DoF, and its value is determined by the configuration of the exoskeleton.

Eq. (57) can be used to determine the hand position for a given set of exoskeleton angles. The inverse kinematics can be obtained by numerically solving Eq. (57) to determine the angles ϑ_u, φ_u and ϑ_f for a given hand position $\boldsymbol{p}_h^g$ within the reachable workspace and angle φ_f. The solution is unique as the humeral shoulder rotation angle φ_f is fixed and the operational space for ϑ_f is limited by the mechanical constraints to $[0, \pi]$.

The transformation from the Kinect coordinate system to the global coordinate system is visualized in Fig. 63 and can be written as

$$\boldsymbol{p}^g = \boldsymbol{R_k}(\phi, \theta, \psi)\boldsymbol{p}^k + \boldsymbol{t_k} \tag{59}$$

with $\boldsymbol{p}^g = \begin{bmatrix} x^g & y^g & z^g \end{bmatrix}^T$, $\boldsymbol{p}^k = \begin{bmatrix} x^k & y^k & z^k \end{bmatrix}^T$, and where $\boldsymbol{t_k} \in \mathbb{R}^{3\times1}$ is a translation vector, and $\boldsymbol{R_k} \in \mathbb{R}^{3\times3}$ a rotation matrix which is parameterized by the Euler angles ϕ, θ, and ψ.

Parameter identification The parameters ϕ, θ, ψ, and $\boldsymbol{t_k}$ of the coordinate transformation as well as the kinematic model parameters l_u, l_f, and φ_f are unknown and have to be calibrated for each user and system use. Therefore, a procedure that is based on a system identification approach is applied to determine the nine parameters. During the system calibration phase, the unlocked exoskeleton with the arm attached is manually placed by a third person (e.g., the caregiver) at N different positions in the reachable workspace which can be reached with the arm attached to the exoskeleton. Since nine parameters need to be identified, $N \geq 9$ must be fulfilled. The reachable workspace is at first defined by the forward kinematics of the exoskeleton. However, this space may be furthermore limited by insufficient FES-induced muscle force.

For each hand position i the corresponding joint angles ($\vartheta_{u,i}$, $\varphi_{u,i}$,$\vartheta_{f,i}$) are measured together with the hand position vector

$$\boldsymbol{p}_{h,i}^k = \begin{bmatrix} x_{h,i}^k & y_{h,i}^k & z_{h,i}^k \end{bmatrix}^T \tag{60}$$

which is recorded by the environmental sensor in the Kinect coordinate frame.

The unknown parameter vector $\boldsymbol{\Theta} = \begin{bmatrix} l_u & l_f & \varphi_f & \phi & \theta & \psi & \boldsymbol{t_k}^T \end{bmatrix}^T$ is estimated by minimizing a quadratic cost function

$$\hat{\boldsymbol{\Theta}} = \arg\min_{\boldsymbol{\Theta}} \left(\frac{1}{2} \sum_{i=1}^{N} \boldsymbol{e}_i \boldsymbol{e}_i^T \right) \tag{61}$$

wherein

$$\boldsymbol{e}_i := \underbrace{\left(-(l_u \boldsymbol{R}(\vartheta_{u,i}\varphi_{u,i}) + l_f \boldsymbol{R}(\vartheta_{u,i}, \varphi_{u,i})\boldsymbol{R}(\vartheta_{f,i}, \varphi_f))\boldsymbol{e_z} \right)}_{\boldsymbol{p}_{h,i,FK}^g} - \underbrace{\left(\boldsymbol{R_k}(\phi, \theta, \psi) \cdot \boldsymbol{p}_{h,i}^k + \boldsymbol{t_k} \right)}_{\boldsymbol{p}_{h,i,Kinect}^g} \tag{62}$$

is the error between the hand position $p^g_{h,i,FK}$, obtained by the forward kinematic model Eq. (57), and the hand position $p^g_{h,i,Kinect}$, obtained from the transformed Kinect measurements, both in global coordinates. The minimization of the cost function is achieved by the Gauss-Newton method with analytically calculated gradients.

5.5 Control System

All FES generated arm movements are initiated by commands received from the high-level control system, the Central Controller (CC), which processes among others the information collected by the eye-tracker. Possible CC movement commands are:

1. go to a desired 3D position,
2. change the angle of shoulder flexion/extension by a certain amount, and
3. change the angle of elbow flexion/extension by a certain amount.

Each command triggers a state-machine on the real-time control system to perform the actual movement.

Based on the elementary movement commands outlined above, complex movement sequences are possible by a combination of multiple commands issued in series. An example for the "Drinking" use case is outlined in Fig. 64.

In the performed experiments described in Sec. 5.6, the hand movements were performed voluntarily by the subject. In the complete MUNDUS system, two alternative solutions to support hand functions have been proposed: a hand neuroprosthesis and a robotic hand orthosis [134]. The hand neuroprosthesis deploys a new stimulation system for array electrodes [182] to produce precise finger movements.

It should be noted that the straight lines shown in the center of Fig. 64 do not represent the actual trajectories of the hand. The actual generation of a movement between two points by the real-time controller will be described in the next section.

5.5.1 Sequential real-time control strategy

The real-time control system internally controls the angles of the exoskeleton. Therefore, for all commands issued by the CC, new angular references are determined by the real-time control system in a first step. This calculation involves, if required, also stored old angular references from the last movement and the inverse exoskeleton kinematics. The resulting reference angles of the jth command are $r^j_{\vartheta_u}$, $r^j_{\varphi_u}$ and $r^j_{\vartheta_f}$ for the shoulder ab-/adduction, the shoulder horizontal rotation, and the elbow flexion/extension, respectively.

Sequential feedback control is used to adjust the normalized stimulation intensities (pulse charges) to drive the hand to desired positions in the reachable workspace. Each DoF is controlled separately, one after the other while all other DoFs are locked by the exoskeleton brakes. This sequential strategy results in an entirely decoupled system concerning crosstalk between the DoFs. For this reason, a light model with few parameters can be used for each controller design

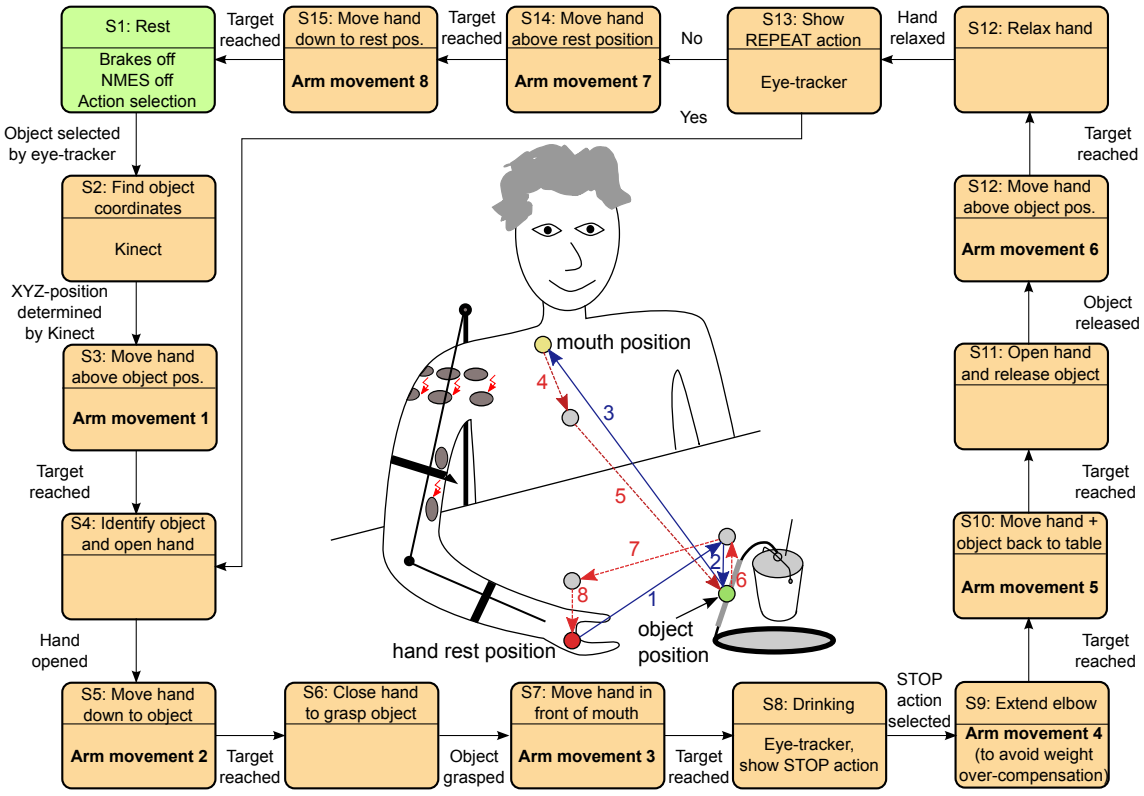

FIGURE 64: *The state automaton inside the MUNDUS Central Controller (CC) to realize the "Drinking" use case starting from an arm rest position and returning to this position again. The states (S3,S5,S7,S9,S10,S12,S14,S15), which are supposed to cause arm movements, trigger a state machine inside the real-time arm FES control module (cf. Fig. 65). The references for the rest position as well as for the mouth position may be stored in the MUNDUS CC as angular references during the system calibration phase. The Kinect system determines the object position online by tracking a green marker on the object handle.*

which dramatically reduces the effort for parameter identification. Each movement to a given 3d position is divided into three consecutive steps:

1. control of the shoulder flexion/extension,
2. control of the shoulder horizontal rotation and
3. control of the elbow flexion/extension.

The real-time arm FES controller is a hybrid control system combining a state automaton and continuous-time feedback controllers to reach the desired angle separately for each DoF (cf. Fig. 65).

5.5.2 SHOULDER FLEXION/EXTENSION CONTROL

For the shoulder flexion/extension, a discrete-time controller based on an identified pulse transfer-function model is employed. The control design uses the well-known pole-placement method in polynomial form [14]. For the jth activation of the controller, the relation between the stimulation

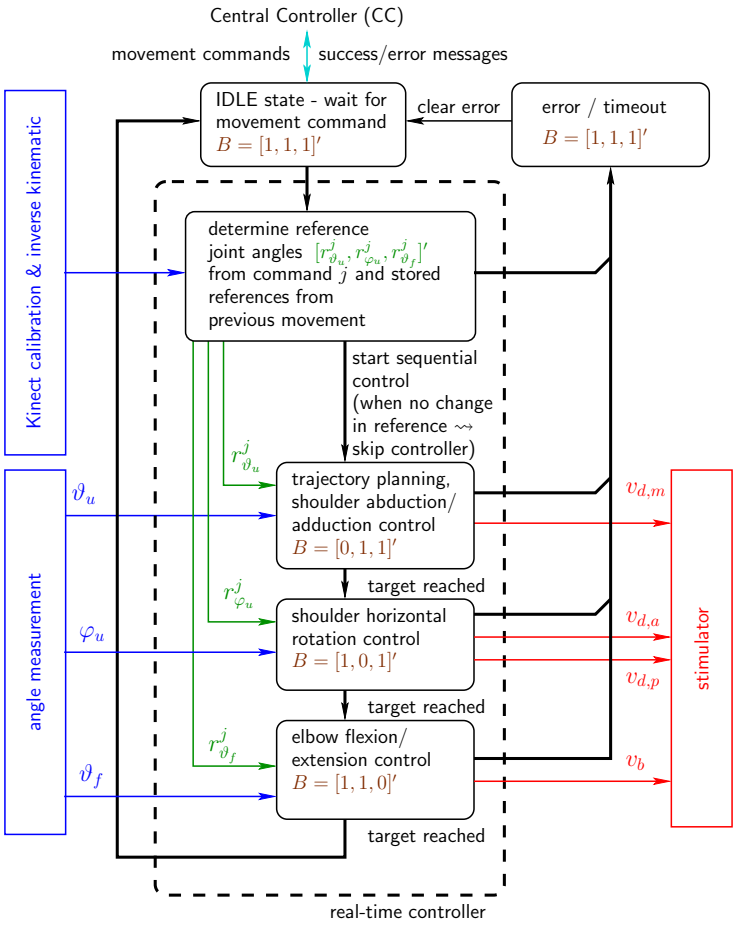

brake configuration: B=[shoulder ab-/adduction, shoulder horizontal rotation, elbow flexion/extension]'
0 - brake unlocked, 1 - brake locked

FIGURE 65: *The real-time arm FES control system shown realized as a hybrid system combining a state automaton and continuous controllers: State transitions are indicated by bold black arrows, while continuous signals are represented by colored thin arrows. Not shown are short periods (states) between the activations of the individual controllers in which all brakes are locked, and the respective initial stimulation intensities are adjusted for the next controller activation.*

intensity $v^j_{d,m}$ of medial deltoid and the shoulder elevation angle ϑ^j_u can be approximately described by a second-order *autoregressive with exogenous input model*, (ARX) model [109] of the form

$$\vartheta^j_u(k) = \frac{\mathsf{B}(q)}{\mathsf{A}(q)} v^j_{d,m}(k) + \frac{q^2}{\mathsf{A}(q)} e^j(k), \quad \underline{v}_{d,m} \leq v^j_{d,m}(k) \leq 1, k \geq 0, \tag{63}$$

wherein k is the sample index, $e^j(k)$ represents white noise, and

$$\begin{aligned} \mathsf{B}(q) &= b_0, \\ \mathsf{A}(q) &= (q^2 + a_1 q + a_2) q^4 \end{aligned}$$

are polynomials of the forward-shift operator q ($qs(k) = s(k+1)$). This model possesses an input-output time delay of six sampling instants, which can be observed in the recorded I/O

data. The used sampling frequency is 25 Hz and corresponds to the stimulation frequency. During the system calibration, the coefficients of the polynomials are estimated from a recorded input step response (changing $v_{d,m}$ from $(\underline{v}_{d,m} + 0.2(1 - \underline{v}_{d,m}))$ to $(\underline{v}_{d,m} + 0.8(1 - \underline{v}_{d,m}))$) using the instrumental variable method [109].

Based on this model, a polynomial controller of the form

$$v^j_{d,m}(k) = \frac{\mathsf{S}(q)}{\overline{\mathsf{R}}(q)(1-q)} \left(\frac{\mathsf{T}(q)}{\mathsf{S}(q)} r^j_{\vartheta_u} - \vartheta^j_u(k) \right) \tag{64}$$

is designed with the controller polynomials $\overline{\mathsf{R}}(q), \mathsf{T}(q)$ and $\mathsf{S}(q)$.

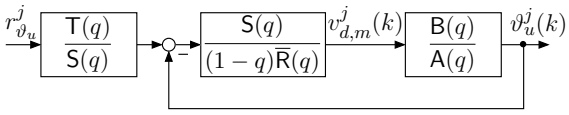

FIGURE 66: *The closed-loop system with discrete-time polynomial controller.*

Fig. 66 shows the corresponding closed-loop system. The controller has integral action (term $(1 - q)$ in (64)). This enables the rejection of constant and slowly varying disturbances and compensates the effects of muscular fatigue. The coefficients of the controller polynomials $\overline{\mathsf{R}}(q)$ and $\mathsf{S}(q)$ are chosen to obtain a desired characteristic polynomial

$$\mathsf{A}_{cl}(q) = (1-q)\overline{\mathsf{R}}(q)\mathsf{A}(q) + \mathsf{S}(q)\mathsf{B}(q) \tag{65}$$

the roots of which correspond to the closed-loop system poles and should be stable and well damped. For the given system and controller with integrator, the minimal degree controller is given by $\deg(\mathsf{S}) = 6$, $\deg(\overline{\mathsf{R}}) = 5$ and $\deg \mathsf{A}_{cl} = 12$. A common approach is to factorize $\mathsf{A}_{cl}(q)$ as follows:

$$\mathsf{A}_{cl}(q) = \mathsf{A}_{cl,1}(q)\mathsf{A}_{cl,2}(q)q^8. \tag{66}$$

Herein, $\mathsf{A}_{cl,1}(q)$ and $\mathsf{A}_{cl,2}(q)$ are second order polynomials specified via the rise-time $t_{r,i}$ and damping the factor D_i $(i = 1, 2)$ of corresponding continuous-time second-order system. Eight of the twelve closed-loop poles are located at the origin (the fastest possible mode in discrete-time). The pre-filter polynomial is set to

$$\mathsf{T}(q) = \mathsf{A}_{cl,2}(q)q^4\mathsf{A}_{cl,1}(1)/\mathsf{B}(1). \tag{67}$$

This yields a unity DC gain from the reference input $r^j_{\vartheta_u}$ to the system output ϑ^j_u . Furthermore, it cancels six closed-loop poles defined by $\mathsf{A}_{cl,2}(z)z^4$. The resulting transfer behavior of the closed-loop is then:

$$\frac{\vartheta^j_u(k)}{r^j_{\vartheta_u}(k)} = \frac{\mathsf{T}(q)\mathsf{B}(q)}{\mathsf{A}_{cl}(q)} = \frac{\mathsf{A}_{cl,1}(1)\mathsf{B}(q)}{q^4\mathsf{A}_{cl,1}(q)\mathsf{B}(1)}. \tag{68}$$

As a result, only the poles defined by the roots of $z^4\mathsf{A}_{cl,1}(z)$ influence the system behavior with respect to changes in the reference signal while the disturbance rejection and noise properties of the closed-loop system are depending on all closed-loop poles defined by Eq. (66). At first, the rise-time and damping factor for $\mathsf{A}_{cl,1}$ are selected to obtain a desired reference tracking behavior.

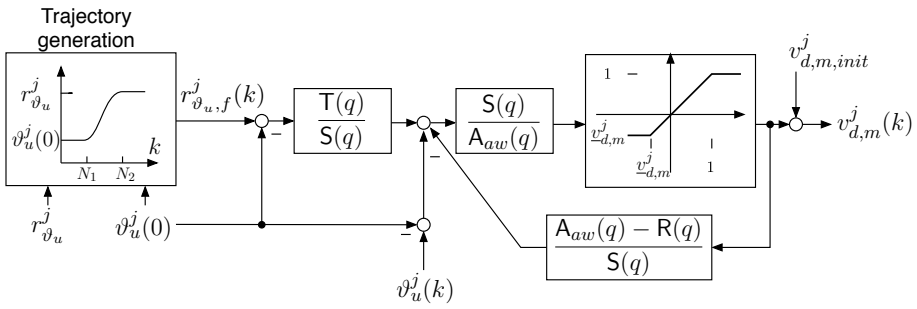

FIGURE 67: *Implementation of the shoulder extension/flexion controller including an anti-windup observer with* $\mathsf{R}(q) = (1-q)\overline{\mathsf{R}}(q)$*, a trajectory generator, and an adjustable initial stimulation intensity* $v^j_{d,m,init}$*. The parameters of the saturation function are* $\overline{v}^j_{d,m} = 1 - v^j_{d,m,init}$ *and* $\underline{v}^j_{d,m} = \underline{v}_{d,m} - v^j_{d,m,init}$ *for* $\underline{v}_{d,m} \leq v^j_{d,m,init} \leq 1$.

Then the rise-time and damping factor of $\mathsf{A}_{cl,2}$ are iteratively tuned to yield satisfactory noise sensitivity and disturbance rejection (verified by frequency response plots of the sensitivity and the complementary sensitivity function). In this study, for all subjects $t_{r,1} = 0.6\,\mathrm{s}$, $t_{r,2} = 0.5\,\mathrm{s}$ and a damping factor $D_i = 0.999$ for both polynomials was chosen.

The final controller implementation, shown in Fig. 67, takes the following additional aspects into account:

1. Controller initialization to apply a given constant initial stimulation intensity $v^j_{d,m}(0) = v^j_{d,m,init}$.
2. Generation of a smooth reference trajectory $r^j_{\vartheta_u,f}(k)$ that guides the arm from the initially measured angle $\vartheta^j_u(0)$ to the given target angle $r^j_{\vartheta_u}$ of the activation j.
3. Avoidance of integrator windup for control signals violating the constraint $\underline{v}_{d,m} \leq v^j_{d,m}(k) \leq 1$ by using the standard anti-windup scheme proposed in [14] with the anti-windup observer polynomial $\mathsf{A}_{aw}(q) = \mathsf{A}_{cl,2}(q)q^4$.

The initial stimulation intensity $v^j_{d,m,init}$ is adjusted to avoid undesired movements when the controller is activated. Thus, before the controller activation and the consequent brake release, the stimulation intensity is increased up to the value which was used before locking the DoF. The ramp-up period lasts about 1.5 seconds. Furthermore, to avoid unwanted initial transients caused by the controller transfer functions, the initial joint angle $\vartheta^j_u(k=0)$ is acquired at controller activation and then subtracted from the joint angle measurement $\vartheta^j_u(k)$ and the output of the trajectory generator.

Trajectory generation To obtain smooth shoulder flexion/extension movements, the reference trajectory $r^j_{\vartheta_u,f}(k)$ for each activation j is chosen to be a sinusoidal reference path starting at $\vartheta^j_u(0)$

and converging to the desired target angle $r^j_{\vartheta_u}$:

$$r^j_{\vartheta_u,f}(k) = \begin{cases} \vartheta^j_u(0) & \text{for} \quad 0 \leq k < N_1 \\ \frac{1}{2}\left(1 - \cos\left(\frac{\pi k - N_1}{2N}\right)\right) \cdot (r^j_{\vartheta_u} - \vartheta^j_u(0)) + \vartheta^j_u(0) & \text{for} \quad N_1 \leq k \leq N_2 = N_1 + N \\ r^j_{\vartheta_u} & \text{for} \quad k > N_2 = N_1 + N \end{cases} .$$

The parameter $N_1 = 69$ describes the number of samples (corresponding to 2.76 s) before the sinusoidal shape starts and N denotes the number of samples for the transient part of the trajectory and is set to 150 (corresponding to 3 s). After the sample $N_2 = N_1 + N$, the reference trajectory is equal to $r^j_{\vartheta_u}$ and the controller will be deactivated and the brake locked if one of the following conditions is fulfilled:

- The absolute error $|r^j_{\vartheta_u} - \vartheta^j_u(k)|$ is less than one degree.
- The control signal $v^j_{d,m}(k)$ was continuously saturated for more than two seconds.
- The controller was active for more than 15 seconds (*time-out event*).

Once the target is reached, the controller of the shoulder flexion/extension is deactivated, and the last value of stimulation used is stored.

5.5.3 Shoulder horizontal rotation control

The control of the shoulder horizontal rotation involves the stimulation of the anterior (for inward rotation) and the posterior (for outward rotation) deltoid. Thus, the following switching control law is used

$$v^j_{d,a} = \begin{cases} u^j_r & if \quad u^j_r > 0 \\ 0 & if \quad u^j_r \leq 0 \end{cases} \quad v^j_{d,p} = \begin{cases} -u^j_r & \text{if} \quad u^j_r < 0 \\ 0 & \text{if} \quad u^j_r \geq 0 \end{cases} , \tag{69}$$

which introduces a mapping of one single virtual actuation variable $u^j_r \in [-1, 1]$ to the two stimulation intensities $v^j_{d,a}$ and $v^j_{d,p}$ for the jth controller activation.

The virtual actuation variable u^j_r is the output of an integral controller with constant integration slopes, given by

$$u^j_r(k+1) = \underset{-1,1}{\text{sat}}\left(u^j_r(k) + c_r \,\text{sgn}(r^j_{\varphi_u} - \varphi^j_u(k))\right), \quad u^j_r(0) = 0$$

wherein the positive gain c_r is set to 0.033 (yielding a rise time of 83% per second in the normalized stimulation intensity) in this study. To avoid integrator windup, a saturation function

$$\underset{b_1,b_2}{\text{sat}}\,(x) := \begin{cases} b_1 & \text{if} \quad x \leq b_1 \\ x & \text{if} \quad b_1 < x < b_2 \\ b_2 & \text{if} \quad b_2 \leq x \end{cases} \tag{70}$$

is used in the integral control law. This prevents the integrator from exceeding the constraints for the actuation variable.

Conditions for the deactivation of the controller and the subsequent locking of the brake are in analogy to the ones given in Sec. 5.5.2.

5.5.4 Elbow extension/flexion control

The control of elbow extension/flexion is similar to the shoulder horizontal rotation control, but only one muscle, the biceps, is stimulated to induce elbow flexion. Gravity causes downward movements of the forearm (extensive movements). The stimulation intensity will be linearly increased/decreased with the slope rate 0.0062 (yielding a rise time of 15.7% per second in the normalized stimulation intensity) in each sampling instance until the desired angle is achieved. The following integral controller, which also includes an anti-windup strategy, is used:

$$v_b^j(k+1) \quad = \quad \underset{0,1}{\text{sat}}(v_b^j(k) + c_e \,\text{sgn}(r^j_{\vartheta_f} - \vartheta^j_f(k))), \qquad v_b^j(0) = v^j_{b,init}. \tag{71}$$

Herein, j represents the jth activation of the controller again. The initial stimulation intensity $v^j_{b,init}$ is adjusted to prevent the forearm from rapidly falling when the controller is activated and the brake released.[37]. Thus, before activating the controller, the stimulation intensity is increased up to 50% of the stimulation intensity achieved at the end of the previous activation phase of the elbow controller. The ramp-up phase lasts one second.

Conditions for the deactivation of the controller and the subsequent locking of the brake are in analogy to the ones given in Sec. 5.5.2.

5.6 Validation of the Control System

The control system was validated in five healthy subjects (three female and two male), aged 29-40 years old (mean 34.5 ± 5.3). Average weight was 61 ± 17 kg. The "Drinking" task was selected to evaluate the performance of the system. Each subject was asked to be completely relaxed during the arm movements, which were entirely generated by the system. He/she was asked to grasp and release the cup voluntarily. Each subject repeated the trial five times. Before the beginning of the trials, the exoskeleton, as well as the amount of gravity compensation, were adjusted to the anthropometric measures of each subject. Then, the system was calibrated performing the following steps:

- to set the stimulation parameters (Sec. 5.3),
- to determine the parameters of the kinematic model and coordinate transformation (Sec. 5.4),
- to tune the discrete-time controller of the shoulder flexion/extension by means of an experimental session aimed at model identification (Sec. 5.5), and
- to teach-in the rest position and the in-front-of-mouth position.

The experimental protocol was approved by the ethical committee of the Valduce Hospital (Italy) where the validation trials have been performed. All subjects signed a written informed consent.

[37] The stimulation intensity is only increased to 50% instead of 100% to ensure that the hereby induced muscle contraction does not lead to an unwanted flexion movement when releasing the brake. This behavior was observed in pre-investigations in which the stimulation intensity was initially set to 100 %.

TABLE 5: *Mean positioning errors along with their standard deviations in $x^g/y^g/z^g$-direction for five "Drinking" task sequences per subject measured via the exoskeleton sensors and via Kinect.*

subject	RMS [cm] error of kinematic model calibration	mean positioning errors (SD) in $x^g/y^g/z^g$-direction [cm] all positions		mouth		object	
(healthy)		via exo	via Kinect	via exo	via Kinect	via exo	via Kinect
A	0.4	0.4(1.8)/ -0.1(0.8)/ -0.1(2.1)	1.0(2.2)/ -0.0(1.2)/ 1.4(2.5)	-0.3(0.5)/ -1.3(0.2)/ 1.0(0.3)	1.3(0.6)/ -0.6(1.0)/ 0.8(1.0)	-0.4(0.9)/ -0.8(0.5)/ -2.5(1.6)	0.0(0.7)/ -0.9(0.7)/ -1.1(0.9)
B	1.8	0.6(7.9)/ 1.8(4.8)/ -0.2(3.2)	-1.4(6.7)/ 3.0(4.3)/ 2.0(3.9)	-4.8(5.9)/ -0.1(1.2)/ 0.8(2.0)	-0.38(1.3)/ 1.0 (1.3)/ -0.1(5.0)	-5.5(5.1)/ 0.4(0.7)/ 1.3(2.0)	-5.6(2.1)/ 2.1(0.6)/ 5.1(2.8)
C	1.4	-1.4(9.7)/ 1.3(3.9)/ -2.1(3.6)	-3.2(9.1)/ 1.5(3.9)/ 1.4(3.9)	1.3(1.2)/ -0.6(0.2)/ -0.3(0.3)	-5.0(1.0)/ 1.2 (1.4)/ -3.0(1.0)	-9.6(2.1)/ 1.8(1.4)/ -1.3(3.8)	-8.6(1.4)/ 2.0(1.1)/ 2.0(2.0)
D	1.4	-0.1(4.8)/ -0.6(1.4)/ -0.4(1.9)	-0.7(5.4)/ -1.5(3.5)/ 4.5(3.3)	-0.4(0.3)/ -2.1(0.4)/ 0.2(0.3)	-3.4(0.6)/ -8.9(0.9)/ 4.2(0.3)	-6.3(10.0)/ -0.8(0.4)/ -2.3(0.2)	-6.5(9.2)/ 0.1(0.3)/ 1.3(0.6)
E	1.7	-1.0(6.9)/ 1.3(4.0)/ 0.6(2.6)	-2.8(5.1)/ 2.4(3.8)/ 3.2(4.0)	2.5(1.3)/ -1.1(0.2)/ -0.7(0.1)	-5.5(1.5)/ -0.9(0.3)/ -3.7(0.1)	-12.6(0.5)/ 1.3(0.2)/ 2.1(0.3)	-7.0(3.1)/ 2.5(0.4)/ 5.1(0.5)

To evaluate the performance of the system, the positioning error between the target position and the entered position at the completion of each movement command was computed for the hand positions 1 to 8 shown in Fig. 64. Two sets of positioning errors were calculated since two different methods were used to derive the actual position in the global coordinate system: (1) the measured angles were applied to the forward kinematic model; (2) the actual position measured by the Kinect was transformed into the global coordinate system. Furthermore, the time needed to execute all movement commands during the "Drinking" task was computed.

5.7 RESULTS

Fig. 68 exemplarily shows the recorded angles together with their current references (bands), the applied stimulation intensities and the states of the brakes. Vertical, dashed lines separate the time periods of the controlled arm movements that have been introduced and numbered in Fig. 64. The control system is performing well in moving the arm such that the joint angles are close to the reference angles. However, in this example, an unwanted slipping of the horizontal shoulder brake can be observed after 43, 80, 92 and 106 seconds that causes the shoulder horizontal rotation angle φ_u to drift away from the previously realized target angle. Fig. 69 shows the desired arm posture at the end of every controlled arm movement in comparison to the real arm position achieved by the FES. The error caused by slipping is visible for the time points 2^*, 4^*, 6^* and 7^*, which represent the end time points of the corresponding movements defined in Fig. 64.

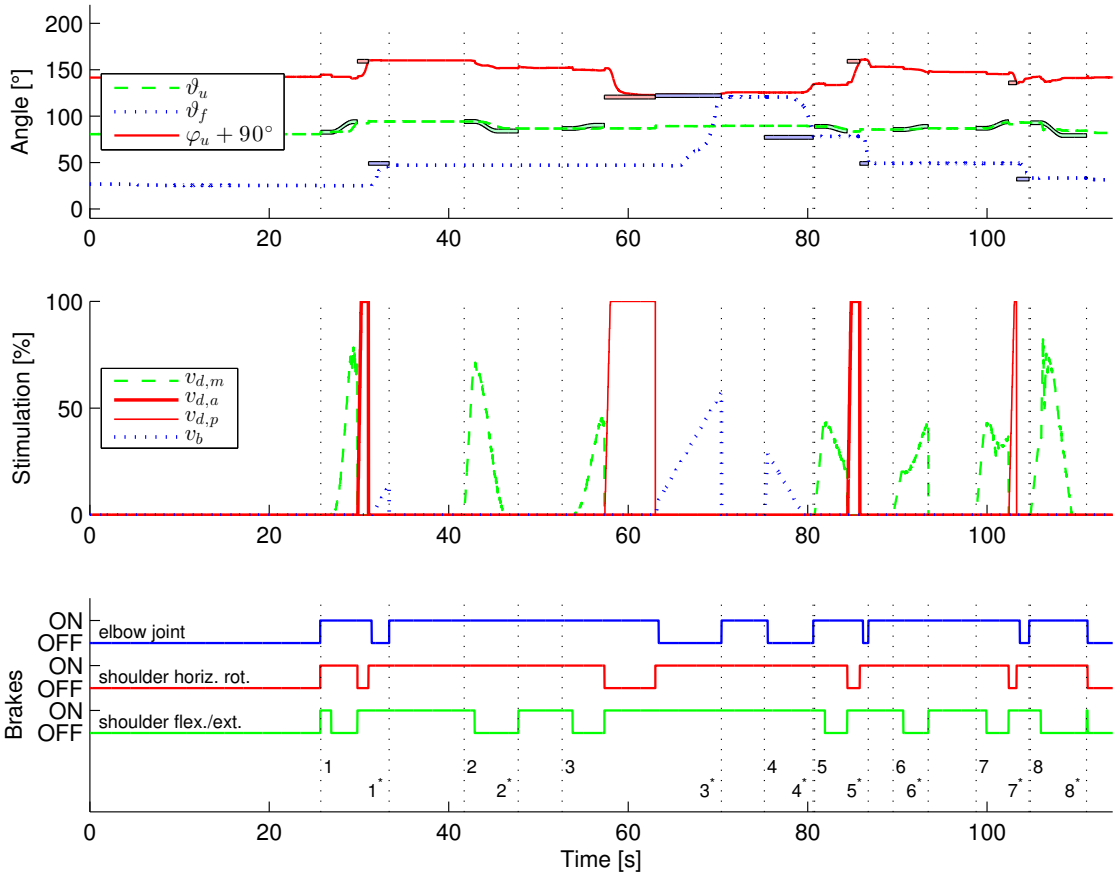

FIGURE 68: *Exemplary results of the application of the developed control system to one healthy subject. The transient behavior for one trial of the described "Drinking" task is shown. The numbers on the vertical dashed lines in the third subplot indicate the begin (without star) and end (with star) of the eight arm movements defined in Fig. 64. In the first subplot, the active reference angles (bold colored lines with black surrounding) are shown along with the measured angles. In the figure, the colors blue, green and red correspond to the elbow joint, shoulder flexion/extension and shoulder horizontal rotation, respectively. In the middle subplot, the applied stimulation intensities are presented. The state of each brake is plotted in the bottom subplot. An individual controller for one DoF is only active for time periods in which a reference trajectory is plotted for the corresponding angle. Theoretically, angles should not change in periods in which no corresponding reference trajectories are plotted due to active brakes.*

The five trials of the "Drinking" task were successfully performed by all subjects. For each subject, Table 5 reports the mean and standard deviation values of the position errors in x^g / y^g / z^g-directions obtained over the five trials of the "Drinking" task. The controller performance obtained in the two most important reaching subactions, i.e., reaching the object and reaching the mouth, and the overall performance obtained by averaging the results obtained in all of the eight target positions are shown in Table 5. The Euclidian norm (i.e., mean distance error) of the mean positioning error vectors has been calculated from data in Table 5 and is reported in Table 6. The mean distance error for all subjects and positions was less than two centimeters when using the exoskeleton angles to determine the hand position. Based on the Kinect measurements, the observed mean distance error is still smaller than five centimeters. For the majority of subjects

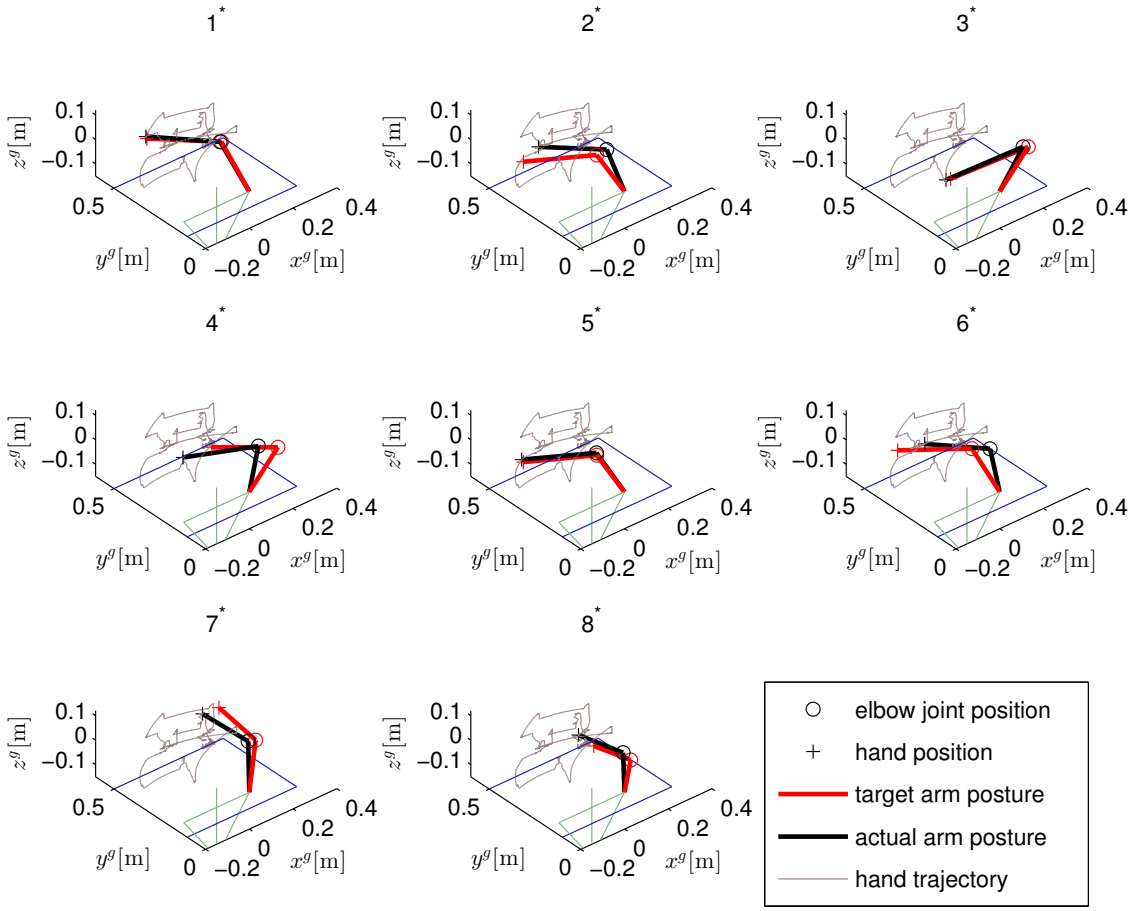

FIGURE 69: *Static arm postures for one trial of the described "Drinking" task. Shown are the desired arm postures and the obtained ones for the end of the eight arm movements defined in Fig. 64. The upper body is indicated in green while the right arm is pointing forwards. The table in front of the subject is illustrated in blue.*

(B-E), a relatively large mean (systematic) error in the x^g-direction of up to twelve centimeters can be observed for the object position (cf. Fig. 64), resulting in a mean distance of about eight centimeters (see Table 6). Subject D obtained a large standard deviation for the object positioning error in x^g-direction (see Table 5). A larger discrepancy between the errors based on the exoskeleton sensors and the Kinect can be observed for the mouth position for the subjects C-E.

In addition to the positioning error analysis, the model-fit of the identified kinematic model and coordinate transformation is investigated for each subject. For the twelve positions chosen during the kinematic model calibration, the RMS of the distance errors between the positions calculated by the identified kinematic model and those obtained by transforming the Kinect measurements into the global frame was calculated (see Table 5).

For the five trials, the mean values of the observed time durations for all submovements and each subject are reported in Table 7. Each submovement is indicated by a number previously introduced in Figure 64. Additionally, the mean values for the total time required to complete

TABLE 6: *Euclidean norm (distance) of the mean positioning error vector given in Table 5.*

subject (healthy)	Euclidean norm of the mean positioning error vector [cm] all positions via exo	all positions via Kinect	mouth via exo	mouth via Kinect	object via exo	object via Kinect
A	0.4	1.7	1.7	1.7	2.7	1.4
B	1.9	3.8	4.9	3.9	5.6	7.8
C	2.8	3.8	1.5	5.9	9.9	9.1
D	0.8	4.8	2.1	10.4	6.8	6.7
E	1.8	4.9	2.8	6.7	12.9	9.0
mean (SD)	1.5 (1.0)	3.8 (1.3)	2.6 (1.4)	5.7 (3.3)	7.6 (3.9)	6.8 (3.2)

TABLE 7: *Mean time durations along with their standard deviations for each submovement defined in Fig. 64 and each subject.*

sub movement	mean time durations (SD) [s] for the subjects A-E A	B	C	D	E	mean [s]
1	11.2 (0.16)	7.8 (0.22)	13.1 (1.08)	8.4 (0.17)	9.2 (0.27)	9.9
2	7.5 (0.24)	6.0 (0.35)	4.5 (0.05)	8.5 (0.50)	6.0 (0.11)	6.5
3	12.2 (0.39)	11.9 (1.26)	15.6 (0.60)	11.7 (0.14)	16.8 (0.90)	13.6
4	2.3 (0.05)	12.5 (0.49)	5.2 (0.79)	1.7 (0.04)	10.1 (0.40)	6.4
5	10.1 (0.76)	9.6 (0.51)	12.1 (0.71)	13.0 (0.81)	10.1 (0.73)	11.0
6	7.9 (0.57)	3.1 (0.93)	4.9 (0.51)	5.5 (0.29)	3.7 (0.25)	5.0
7	8.2 (0.20)	12.2 (0.61)	9.6 (0.57)	9.4 (0.22)	10.8 (0.91)	10.0
8	9.1 (0.42)	9.7 (0.61)	7.9 (0.15)	6.6 (0.29)	11.6 (0.78)	9.0
mean of total time duration (SD) for five trials [s]	68.3 (2.3)	72.8 (7.8)	73.1 (13.5)	64.8 (8.7)	78.3 (11.1)	**71.4 (5.1)**

a full "Drinking" task (including only time durations wherein the controller is activated) are reported per subject. The average time for the execution of all eight arm movement commands during the "Drinking" task was 71.4 seconds. The total time for donning the system on and for calibration was less than ten minutes for every subject (the calibration alone requires about two minutes).

5.8 Discussion and Conclusions

The experimental evaluation showed that the feedback control of the hybrid FES-exoskeleton system is feasible. Compared to the results presented in [49], no learning phase was required to achieve the desired functional movements. The evaluation shows that it is possible to support the user in performing the "Drinking" task.

The observed small positioning errors at the mouth might be corrected by minor head movements to allow the drinking from the cup by means of a straw. When positioning the hand above the object (i.e., the cup handle), larger deviations in y-direction were observed. But due to the large dimension of the cup handle, the ability to grasp the handle was not restricted. The limited accuracy for placing the hand at objects restricts the possible size and number of objects on the table. Reasons for the observed errors are diverse. One major problem observed is the limited braking torque of 2.5 Nm for the shoulder horizontal rotation that sometimes cannot prevent unwanted slipping for this DoF. Despite the careful placement of the stimulation electrodes, it cannot be avoided that a stimulation of the Deltoid, medial head, generates besides a desired shoulder extension moment also an unwanted shoulder horizontal rotation moment. If the latter exceeds the torque of the locked horizontal shoulder rotation brake then slipping for this DoF occurs. With the arm pointing forward, an error in the shoulder horizontal rotation leads to a large hand error in the x^8-direction, especially for the extended arm. In future, the use of more elaborated control systems, e.g., the one presented in Chapter 6 of this thesis might be used to reduce the limbs velocity when approaching the desired joint angle to prevent slipping. Another solution is to improve the brake torque by re-designing the exoskeleton. Even when moving to a position given in Cartesian coordinates, the real-time control system is based on angular control. The position errors determined by the exoskeleton angles, therefore, reveal errors purely related to the control system. The errors determined by the Kinect measurements take problems related to the used kinematic model and coordinate transformations additionally into account. The current controller design assumes that the exoskeleton/arm-combination represents a rigid body system. This is certainly not perfectly true in reality. Moreover, for the calibration of the kinematic model and the coordinate transformation, the arm/hand was moved by an assisting person to twelve arbitrary chosen different positions in the workspace. Compared to the later use with FES, no loading/deformation of the exoskeleton by the arm weight took place. Any deviation from the rigid body assumption causes a position error due to the use of an incorrect forward kinematics. Such errors can only be detected by an external measurement system, like the Kinect, and not by the exoskeleton's internal angle sensors. The larger errors computed from the Kinect measurements compared to the ones derived from the exoskeleton sensors are therefore an indicator that the rigid body system assumption is not perfectly true.

A shortcoming of the developed system is that elbow extension and shoulder flexion are only induced by gravity. This requires a carefully adjusted weight compensation. Any overcompensation of the weight could drive the arm movement into a deadlock.

Advantages of the used control strategy are its robustness and its simple adaptation to new users/sessions. Only a simple single-input single-output dynamical model needs to be identified for the adaptation of the controller. For all subjects, the same tuning parameters, like rise times and damping factors, have been used for the automatic design of the shoulder extension/flexion controller. In addition to this, the same gains have been applied to the controllers of shoulder horizontal rotation and elbow flexion/extension in all subjects. Due to automated and guided procedures, the system can be set up in a few minutes for the individual user allowing the operation by clinicians and caregivers. All individual FES controllers for the three DoFs include an integrator which allows for the compensation of muscular fatigue as long as the stimulation intensities do not saturate. No deterioration of control performance could be observed for the healthy subjects over the five performed trials and from day to day. All these advantages have to

be paid by the fact that the movements do not look very physiological and movement sequences are not time optimal (cf. Table 7). However, it is expected that this fact is not so crucial for final users and that the guaranteed functionality might overweight the timing issue for this assistive technology. The personal experience in performing all movements utilizing the own muscles is the major advantage compared to robotic approaches for the assistance of reaching function (e.g., [117]). Regular use of the proposed arm neuro-prosthesis and consequently of the patient's musculature is expected to be health promoting. It will increase muscle strength and might also improve cardio-vascular fitness.

In summary, a feedback-controlled hybrid FES-exoskeleton which does not require any residual function at the shoulder and arm level was developed. By combining FES with the passive exoskeleton for partial arm weight support, muscular fatigue can be significantly reduced as the required amount of muscular force is smaller compared to movements without weigh support. The use of electrically lockable joints reduces the onset of muscular fatigue even further as no muscle function is required to hold the desired position.

The presented study was focusing on the achievable control system performance, which was expected to be maximal for healthy individual due to non-atrophied muscles and the absence of spasticity. During the development of the system, a first test involving one incomplete SCI subject (C_4/C_5) was performed and showed that the system supported the subject in reaching a cup and bring it to the mouth. The results of this test have been previously published [135]. Tests of the feedback controller on a group of SCI subjects must be performed to observe the feasibility of the system in supporting daily life activities. To obtain successful results, an initial conditioning phase to assure that FES can induce some muscle force, and a longer familiarization phase with the system, are envisaged.

6

JOINT ANGLE CONTROL IN ANTAGONISTIC MUSCLE PAIRS

To improve the control of shoulder horizontal movements in completely paralyzed people, a non-linear, model-based control strategy for torque generation by antagonistic muscle pairs is presented. The controller is based on exact linearization methods and enables the tracking of reference joint torque profiles and the generation of pre-defined muscular co-contractions.

The static recruitment functions of both muscles in an antagonistic pair include a threshold at a certain stimulation level. In the control of movements not acting against gravity – like in the case of shoulder horizontal movements – typically small levels of muscle contractions are sufficient to generate even fast limb movements.[38] In such cases, this threshold level may be only marginally below the range of stimulation that a control system uses to generate these slight muscle contractions. As the threshold level may also vary in time due to muscle fatigue, the stimulation effect is difficult to predict for such low stimulation intensities. This variation in time especially reduces control performance, as this threshold enters the initially determined operational stimulation range of the controller, which renders the typical assumption of linearity to be invalid.

To also control small co-contraction forces, this activation threshold parameter has to be known exactly for both muscles, as otherwise, the control system has no information whether the muscle is contracted or whether the actuation variable is just acting below the threshold without any effect. Because this parameter is time-varying, an online identification would be required. However, this is rather difficult when only the resulting torque by both muscles is available indirectly through joint angle measurements. To compensate these effects and to linearize the uncertain recruitment behavior, recruitment control (cf. Chapter 3) is applied to both muscles.

In this chapter, a strategy for modulating the desired accelerating torque along with a co-contraction torque by a linearizing controller is presented. This controller acts on top of two recruitment (λ) control loops for each muscle respectively. The linearizing controller is based on system inversion for discrete-time systems. Since the signals for the actuation of each muscle are constrained to be positive, an extension to the linearizing controller is investigated that guarantees exact inversion with regard to the accelerating torque at the cost of a temporarily increased co-contraction torque. For demonstrating this concept, a linear joint angle controller acting on top of the linearizing controller is designed.

The methods and results presented in this chapter have been previously published as listed below.

- A model and the corresponding parameter identification for the shoulder horizontal rotation in combination with a passive exoskeleton for gravity compensation are published in

  [174] P. Spagnol, C. Klauer, F. Previdi, J. Raisch, and T. Schauer. "Modeling and Online-

[38] Please recap Fig. 8 that illustrates the described issues.

Identification of Electrically Stimulated Antagonistic Muscles for Horizontal Shoulder Abduction and Adduction". In: *Proc. of the European Control Conference 2013*. Zürich, Switzerland: IEEE, 2013, pp. 3979–3984. ISBN: 978-3-033-03962-9. The main work was performed by Pierfrancesco Spagnol, under my supervision.

- The control method, simulation results, and the results for one healthy subject are published in

  [86] C. Klauer, J. Raisch, and T. Schauer. "Nonlinear Joint-Angle Feedback Control of Electrically Stimulated and Lambda-Controlled Antagonistic Muscle Pairs". In: *Proc. of the European Control Conference 2013*. Zürich, Switzerland: IEEE, 2013, pp. 3101–3107. ISBN: 978-3-033-03962-9.

The following publications, in which I was involved, are related to this chapter:

- Pre-investigations (not described in this thesis) on shoulder horizontal movement control using antagonistic muscle pairs with PD-control without co-activation are presented in

  [184] C. Vidaurre, C. Klauer, T. Schauer, A. Ramos-Murguialday, and K.R. Müller. "EEG-based BCI for the Linear Control of an Upper-Limb Neuroprosthesis". In: *Medical Engineering & Physics* 38.11 (2016), pp. 1195–1204. DOI: 10.1016/j.medengphy.2016.06.010.

- Open-loop investigations (research going beyond the scope of this thesis) on how recruitment-controlled co-activations modulate joint impedances and improve the smoothness of motion are given in

  [153] M. Ruppel, C. Klauer, and T. Schauer. "Towards a High Motor-Precision Neuroprosthesis by Recruitment-Controlled Antagonistic Muscle Co-activation Strategies". In: *Abstract in Proc. of the 6th European Conference on Technically Assisted Rehabilitation – TAR 2017*. Berlin, Germany, 2017

  and

  [152] M. Ruppel, C. Klauer, and T. Schauer. "Enhancing the smoothness of joint motion induced by functional electrical stimulation using co-activation strategies". In: *Current Directions in Biomedical Engineering* 3.2 (2017), pp. 155–159. ISSN: 2364-5504. DOI: 10.1515/cdbme-2017-0033.

Copyright statement The text and the pictures in this section are based, with slight modifications, on the following publications: Sec. 6.1 to Sec. 6.6 are based on [86]. Slight modifications of the text and the figures were performed. The Figures 74 and 78 were added.

6.1 Experimental Set-up

The used set-up is shown in Fig. 70 and consists of a passive exoskeleton (Armeo Spring, Hocoma AG, Switzerland) for weight compensation that includes angle sensors, a stimulation system (RehaStim, Hasomed GmbH, Germany), a 24-bit EMG-amplifier (PhysioSense, developed at TU Berlin), an inertial motion unit (IMU) (RazorIMU 9DoF, Sparkfun, United Kingdom), and a PC running Linux with RT-Preemption-Patch. All devices are connected to the PC through USB interfaces.

The subject's arm is placed inside the exoskeleton as shown and the arm movement is limited to shoulder horizontal flexion and extension movements. The corresponding angle ϑ is defined as shown in Fig. 70. This angle and its first-time derivative are determined by fusing the outputs of the exoskeleton angle sensors and the IMU information.

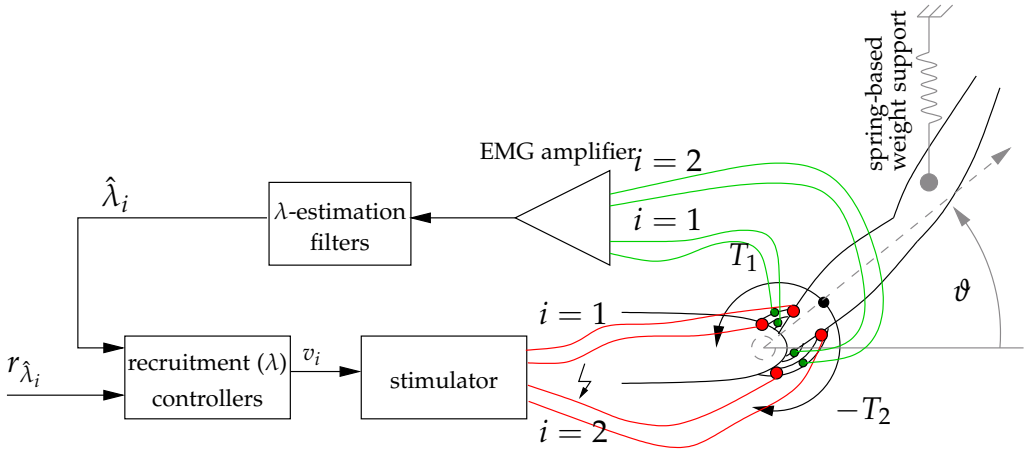

FIGURE 70: *The experimental set-up involving an exoskeleton (*ARMEO SPRING*, Hocoma AG, Switzerland; only the principle is shown in this figure) that keeps the arm elevated at approximately 90° by a spring-based weight compensation. The spring mechanism does not hinder movements in ϑ-direction. Recruitment controlled stimulation is applied to the anterior and posterior deltoid that produce the torques T_1 and T_2, respectively.*

Current-controlled stimulation impulses are applied through self-adhesive hydro-gel electrodes (VALUTRODE® CF4090 (4x6 cm), Axelgaard Manufacturing Co., USA) at a stimulation frequency of 28 Hz. The anterior part of the deltoid muscle is stimulated to cause shoulder horizontal extension. Horizontal flexion is produced by stimulation of the posterior part of the deltoid muscle. Signals related to flexion and extension will be denoted by the indices 1 and 2, respectively. For EMG measurement at the stimulated muscles, smaller AgCl electrodes (AMBU NEUROLINE 720, Ambu A/S, Denmark) are placed between each pair of stimulations electrodes. The FES-evoked EMG (eEMG) is recorded at a sampling rate of 4 kHz.

At the time when the experiments for the algorithms presented in this section were conducted, the automatic calibration routine for the recruitment controller has not been developed so far. Instead, a manual tuning of the filter parameters was performed.

For both muscles, the eEMG is filtered as described in Sec. 3.2.3 yielding $\hat{\lambda}_i, \quad i = 1,2,$. Herein, the filter parameters were not determined by the optimization procedure but instead fixed to $N_1 = 8$ and $N_2 = 20$ (cf. Sec.3.4.1). Two λ-controllers, as introduced in Sec. 3.3, automatically adjust the stimulation intensity (pulse charge) to generate the desired recruitment levels $r_{\lambda_i}, \quad i = 1,2$.[39] The parameter c_λ is manually tuned such that the step-response of the resulting closed-loop behavior yields a rise-time of approximately 6 sampling instants.

[39] Two-channel recruitment control as described in Sec. 3.7 was not available at the time the experiments yielding the presented results were performed. However, by placing the EMG electrodes in between the stimulation electrodes with small spacing, crosstalk between the individual muscle portions is reduced and, hence, the use of two separate recruitment controllers is at least feasible.

6.2 Neuro-Musculoskeletal Model

To describe the joint angle dynamics with FES actuation, the model as presented in Sec. 2.6 is extended to two muscles and a second-order mechanical system is assumed. This model along with methods for parameter estimation has been developed in corporation with Pierfrancesco Spagnol and is described in [174]. The used model is illustrated in Fig. 71 and includes the underlying closed-loop recruitment control system, the activation dynamics, the dependency muscle fiber stretching described by the functions f_1 and f_2, and a biomechanical system.

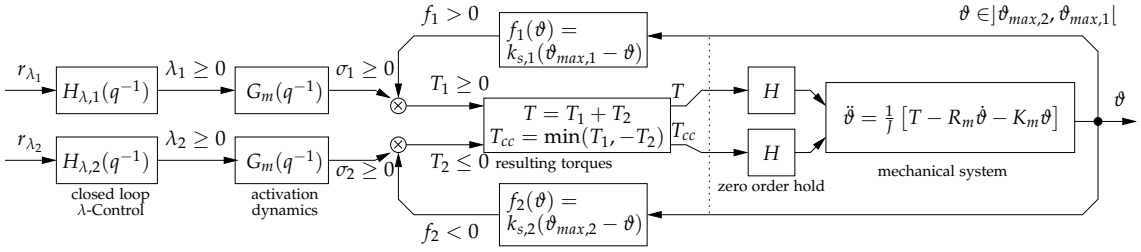

Figure 71: *The model used for controller design involving the closed loop dynamics of recruitment control, a model for each muscle, and a biomechanical model. Please note that the muscle recruitment function is internally compensated by recruitment control such that its determination might be skipped.*

6.2.1 Muscle model including λ-controller

The muscular model part, which also includes the closed loop of the λ-controller as shown in Fig. 72 describes the generated torque T_i for each muscle i, respectively. Because the muscles are λ-controlled, the inputs are the references for the recruitment levels. Internally, the λ-control systems adjust the stimulation intensities v_i of each muscle i such that the muscular recruitment levels λ_i follow their references r_{λ_i}. Hereby, integral controllers are used to control the one step delayed output of the recruitment functions rc_i (the estimated muscular recruitment $\hat{\lambda}$). These functions commonly consist of a threshold, a saturation, and an approximatively linear behavior in between. For the ongoing control design, the resulting closed-loop systems are assumed to be linear, whereby the reference to output behaviors are then described by the transfer functions H_{λ_i}[40].

Each λ-Controller gain is manually tuned to obtain a rise time of approximately 6 time-instants in the step response of the closed loop. The ability to compensate for muscular fatigue and time variant thresholds in rc_i was shown in Chapter 3.

The activation dynamics G_m models the dependency of the muscle activation σ_i on λ_i. The recruitment λ_i, its reference r_{λ_i}, the stimulation intensity v_i, and the muscular activation σ_i are constrained to be non-negative. The calcium dynamics can be approximated by a continuous-time transfer function of first order without zeros and a time delay T_{md} [174]. The transfer function is time discretized using Euler discretization:

$$G_m^*(q^{-1}) = 1/(sT_{ca} + 1)|_{s=(1-q^{-1})/T_a}\,.$$

[40] In contrast to the notation T for the closed loop of recruitment control as introduced in Chapter 3, within this chapter H_{λ_i} is preferred as it improves the readability.

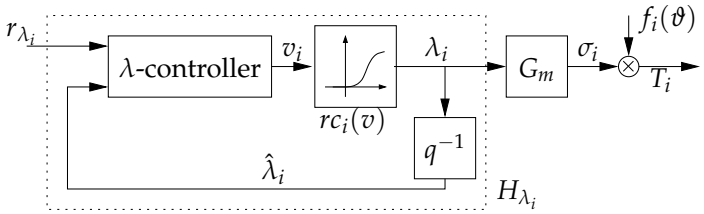

FIGURE 72: *The model for one λ-controlled muscle path. Given a reference r_{λ_i} for the muscular recruitment λ_i, the controller adjusts the stimulation intensity v_i. The nonlinear recruitment function rc_i describes the recruitment. The resulting closed loop H_{λ_i} has an approximatively linear dynamics. The calcium dynamics G_m models the dependency of the muscular activation σ_i on λ_i. The muscular torque T_i is then determined by the multiplication of the angle-dependent function f_i with σ_i.*

Herein, q^{-1} is the backward shift operator and $T_a = 36\,\text{ms}$ the sampling period. The approximative time constant $T_{ca} = 0.04\,\text{s}$ is chosen with reference to [149]. The time delay T_{md} of the calcium dynamics is approximated by a delay of two sampling steps (q^{-2}), which matches to measured data quite well. The closed loop systems H_{λ_i} are discrete-time first-order systems without dead time and zeros cf. Sec. 3.3.

Finally, the muscular torque T_i is then determined by the multiplication of the function f_i with σ_i. The function f_i linearly depends on the joint angle and is modeled by

$$f_i(k) = k_{s,i}(\vartheta_{max,i} - \vartheta(k)).$$

The parameters $\vartheta_{max,i}$ represent the boundaries of the operational angular space $\vartheta \in [\vartheta_{max,2}, \vartheta_{max,1}]$ and describe reachable joint angles. The gains $k_{s,1}$ and $k_{s,2}$ are strictly positive, which results in $f_1 \geq 0$ and $f_2 \leq 0$ and further in $T_1 \geq 0$ and $T_2 \leq 0$, respectively because of $\sigma_i \geq 0$.

Later on, for the linearizing controller designed, the slightly more conservative constraints $f_1 > 0$ and $f_2 < 0$ must be applied. Therefore, the valid range for the joint angle is reduced to $\vartheta \in]\vartheta_{max,2}, \vartheta_{max,1}[$.

The total muscle model is then described by

$$T_i(k) = \underbrace{k_{s,i}(\vartheta_{max,i} - \vartheta(k))}_{f_i(k)} \cdot \underbrace{\frac{q^{-2}(1-a)}{1-aq^{-1}}}_{q^{-2}G_m^*(q^{-1})} \cdot \underbrace{\frac{1-b_i}{1-b_iq^{-1}}}_{H_{\lambda_i}(q^{-1})} r_{\lambda_i}(k) \tag{72}$$

where k is the sampling index. The parameters $a \in [0, 1[$ and $b_i \in [0, 1[$ lead to an asymptotically stable system.

6.2.2 Resulting acceleration and co-contraction torque

For describing a torque T that leads to an acceleration of the mechanical system (arm) and to a co-contractive torque T_{cc}, which describes the amount of co-contracting torques in an antagonistic muscle pair, a transformation between both muscular induced torques T_i and the resulting torques T and T_{cc} is introduced.

The accelerating torque T is given by the operation

$$\mathcal{T}(T_1, T_2) := T_1 + T_2, \qquad T_1 \geq 0,\ T_2 \leq 0. \tag{73}$$

The co-contraction torque $T_{cc} \geq 0$ is obtained by the following operator:

$$\mathcal{T}_{cc}(T_1, T_2) := \min(T_1, -T_2). \tag{74}$$

The inverse transformation operator $\mathcal{T}_1^I$ is then

$$\mathcal{T}_1^I(T_{cc}, T) := \begin{cases} T_{cc} + T & T \geq 0 \\ T_{cc} & T < 0 \end{cases}, \tag{75}$$

and analog

$$\mathcal{T}_2^I(T_{cc}, T) := \begin{cases} -T_{cc} & T \geq 0 \\ -T_{cc} + T & T < 0 \end{cases}. \tag{76}$$

Using these operators, the torques T and T_{cc} are then described by

$$\begin{aligned} T(k) &= \mathcal{T}(T_1(k), T_2(k)), \\ T_{cc}(k) &= \mathcal{T}_{cc}(T_1(k), T_2(k)). \end{aligned}$$

6.2.3 Mechanical model

The inputs to the mechanical model are the resulting torques T and T_{cc}. Because of the one-dimensional movement, a second-order system including the viscous friction R_m and the elasticity K_m is used. The differential equation in terms of the joint angle ϑ is given by

$$\ddot{\vartheta} = \frac{1}{J}\left[T - R_m(T_{cc})\dot{\vartheta} - K_m(T_{cc})\vartheta\right]. \tag{77}$$

Herein, a modulation of the mechanical impedance by the co-contraction torque T_{cc} is assumed. In this case, the parameters for the viscous friction R_m and the elasticity K_m depend on T_{cc}. The design of a model for these functions would go beyond the scope of this thesis and forms future research topics. Therefore, for controller design, this modulation of the system properties is neglected, and only the constants obtained through system identification for zero co-contraction are used.

The complete model including the λ-controlled muscles and the mechanical system is presented in Fig. 71. The mechanical model as described in [174], also accounts for a static friction term, which is neglected in this work.

6.3 Linearizing Controller

The multiplication inside the muscle models with the internal feedback signal f_i leads to a non-linear system behavior. Since the mechanical system is already linear, only the muscular part that contains the multiplication is linearized. Therefore, a state-space representation of (72) is

derived with $\overline{\lambda}_i = q^{-1}\lambda_i$:

$$\begin{aligned}
\overline{\lambda}_i(k+1) &= b_i\overline{\lambda}_i(k) + (1-b_i)r_{\lambda,i}(k) && (78)\\
\sigma_i(k+1) &= a\sigma_i(k) + (1-a_i)\overline{\lambda}_i(k) && (79)\\
T_i(k) &= \sigma_i(k)f_i(k). && (80)
\end{aligned}$$

For describing the muscular torque induced by each muscle i with two time steps delay, two functions $\mathcal{T}_i$, $i = 1, 2$, are introduced that depend on the actuation variables $r_{\lambda_i}(k)$:

$$\mathcal{T}_i(r_{\lambda_i}) := f_i(k+2)\left[a\sigma_i(k+1) + (1-a_i)\left[b_i\lambda_i(k) + (1-b_i)r_{\lambda_i}(k)\right]\right]. \quad (81)$$

The modeled torque is then described by $T_i(k+2) = \mathcal{T}_i(r_{\lambda_i}(k))$. For the control law, two functions

$$\mathcal{R}_{\lambda_i}(u_i) := \frac{1}{1-b_i}\left[-b_i\lambda_i(k) + \frac{1}{1-a_i}\left[-a\sigma_i(k+1) + \frac{1}{f_i(k+2)}u_i\right]\right] \quad (82)$$

are introduced with $i = 1, 2$. By assigning them to the actuation variables $r_{\lambda_i} = \mathcal{R}_{\lambda_i}(u_i(k))$ the system (72) is exactly linearized. Eq. (82) depends on the future internal mechanical feedback variable $f_i(k+2)$ as well as on the state variables $\sigma_i(k+1)$ and $\lambda_i(k)$. The states are calculated by two internal models implementing (78) and (79) for $i \in 1, 2$, whereby the actuation variables $r_{\lambda_i}(k)$ are applied to this internal system. An estimation $\hat{f}_i(k+2)$ of $f_i(k+2)$ is used instead of the real signal[41], that is calculated by a two-step ahead prediction (described late on in Sec. 6.3.2) of the joint angle.

By applying the linearizing controllers Eq. (82) to Eq. (81), the virtual plants

$$T_i(k+2) = u_i(k),\ i = 1, 2$$

result. Each forms a delay of two sampling steps.

To control the joint angle or joint-stiffness by outer control loops, the virtual actuation variables T_d (desired resulting torque) and $T_{cc,d}$ (desired co-activation torque) are introduced using the operators introduced in Sec. 6.2.2. They relate to the torques produced by the individual muscle as described by

$$T_d = \mathcal{T}(T_{1,d}, T_{2,d}), \quad T_{cc,d} = \mathcal{T}_{cc}(T_{1,d}, T_{2,d}).$$

The inverse transformations $\mathcal{T}_1^I$ (Eq. (75)) and $\mathcal{T}_2^I$ (Eq. (76)) are then used to calculate the desired torque for each muscle $T_{1,d}$ and $T_{2,d}$, respectively by

$$T_{1,d} = \mathcal{T}_1^I(T_{cc,d}, T_d), \quad T_{2,d} = \mathcal{T}_2^I(T_{cc,d}, T_d).$$

In a case, where no constraints for the actuation variables are considered, $T_{i,d}$ are directly applied to the virtual inputs u_i of the linearization controller:

$$u_i(k) = T_{i,d}(k). \quad (83)$$

[41] As $f_i(k+2)$ is only available starting from the sampling instant $k+2$, meaning in the future, it must be predicted.

Again, by applying the linearizing controller to both muscles, the resulting torques

$$T_{cc}(k+2) = T_{cc,d}(k), \qquad T(k+2) = T_d(k)$$

are obtained. In practice, exact linearization in this form cannot always be achieved because the actuation variables must fulfill $r_{\lambda_1}(k) \geq 0 \wedge r_{\lambda_2}(k) \geq 0$.

6.3.1 Constrained actuation variables

Since both actuation variables are constrained by $r_{\lambda_i}(k) \geq 0$ for $i = 1, 2$, a possible improvement of linearization in case of violated constraints is investigated. For this analysis, different cases are considered:

Case 1: $\mathcal{R}_{\lambda_1,k}(T_{1,d}) \geq 0 \quad \text{and} \quad \mathcal{R}_{\lambda_2,k}(T_{2,d}) < 0$

Case 2: $\mathcal{R}_{\lambda_1,k}(T_{1,d}) < 0 \quad \text{and} \quad \mathcal{R}_{\lambda_2,k}(T_{2,d}) \geq 0$

Case 3: $\mathcal{R}_{\lambda_1,k}(T_{1,d}) < 0 \quad \text{and} \quad \mathcal{R}_{\lambda_2,k}(T_{2,d}) < 0.$

For each case, an individual extension to the linearizing controller is analyzed. By considering both paths at the same time, the behavior of the resulting accelerating torque T depending on the desired inputs T_d can be linearized – this time including the constraints. As it turns out in the analysis, this usually leads to the drawback of an increased co-contraction torque T_{cc} compared to the desired one $T_{cc,d}$.

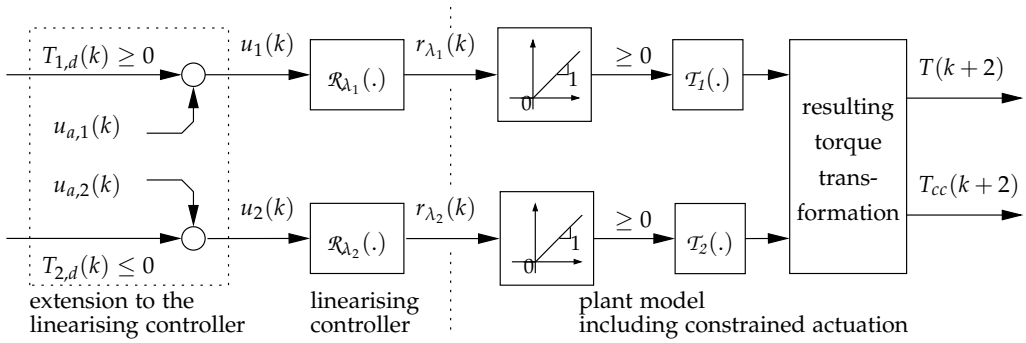

Figure 73: *An extension is applied to the linearizing controller in the presence of constrained actuation ($r_{\lambda_i}(k) \geq 0$) by modifying the signals u_1 and u_2. Herein, two additional variables $u_{a,1}$ and $u_{a,2}$ may be adjusted by the proposed extension, in case actuation constraints would be violated, such that these constraints are still fulfilled, while additionally realizing exact tracking. In case the constraints are not violated by the simple linearization strategy, $u_{a,1} = 0$ and $u_{a,2} = 0$ are applied. This strategy forms a switching control system.*

Fig. 73 shows the linearizing controller along with the nominal model including the constraints on the actuation variables $r_{\lambda_i}(k)$. Unlike equation (83), an extension is added, which feeds additive correction terms $u_{i,a}$ to the actuation variables u_i such that $T = T_d$ can be achieved:

$$u_1(k) = T_{1,d}(k) + u_{1,a}(k), \qquad u_2(k) = T_{2,d}(k) + u_{a,2}(k). \tag{84}$$

The basic principle of this extension is illustrated in Fig. 74. Because of the dynamics of the muscle contraction and the λ-control loop, the muscular activations $\sigma_i(k+1)$ are not necessarily zero

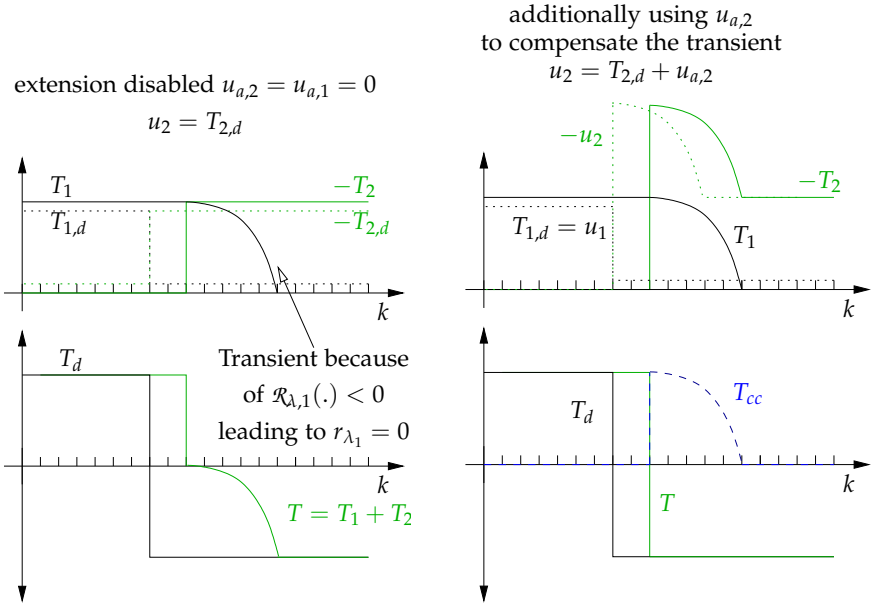

Case a) Case b)

Figure 74: *Illustration of the principle idea of the extension to the linearizing controller for the case of a switching of muscle torque from muscle 1 to muscle 2. Herein, the aim is to realize step-wise change the direction of the resulting torque T. Illustrated are the cases without and with the controller extension.* Case a) *Because of the saturation the actuation variable ($r_{\lambda_1} \geq 0$), the torque T_1 produced by muscle 1 cannot be controlled step-wise to zero within two sampling instants. Instead, a transient occurs that is caused by the activation and recruitment control dynamics. For T_2, perfect tracking can be achieved, though. In effect, about one half of the resulting torque's intensity $T = T_1 + T_2$ is also subjected to the maliciously introduced transient behavior.* Case b) *To compensate such effects that are visible in the resulting torque, an extension to the linearizing controller is applied: Instead of further decreasing the actuation variable r_{λ_1} below zero (which is impossible in reality), the desired torque $T_{2,d}$ is increased in its amplitude by applying $u_{a,2} < 0$ such that the effects of the transient behavior are compensated in the resulting torque trajectory. This yields a modified actuation variable u_2 and, further, causing r_{λ_2} to increase. However, a temporarily increased co-activation torque T_{cc} is caused.*

TABLE 8: *Properties of the functions $\mathcal{R}_{\lambda_1}$, $\mathcal{R}_{\lambda_2}$, $\mathcal{T}_1$, and $\mathcal{T}_2$.*

function	property	reason	description
$\mathcal{R}_{\lambda_1}(u_1)$, $\mathcal{T}_1(r_{\lambda_1})$	strictly monotonically increasing, $\nearrow$	$f_1 > 0$	Increasing the actuation u_1 results in a greater torque T_1.
$\mathcal{R}_{\lambda_2}(u_2)$, $\mathcal{T}_2(r_{\lambda_2})$	strictly monotonically decreasing, $\searrow$	$f_2 < 0$	Increasing the actuation u_2 results in a greater amplitude of the negative torque $-T_2$.

for zero actuation. Instead, because of the actuation-constraints, the smallest possible muscular activation can only be achieved by choosing $r_{\lambda_i}(k) = 0$. The torques produced by each muscle in these cases are called minimum torques:

$$\begin{aligned} T_{1,min} &:= \mathcal{T}_1(0) = f_1(k+2)(a\sigma_1(k+1) + (1-a)b_1\lambda_1(k)) \geq 0, \\ T_{2,min} &:= \mathcal{T}_2(0) = f_2(k+2)(a\sigma_2(k+1) + (1-a)b_2\lambda_2(k)) \leq 0. \end{aligned}$$

At first, monotonic properties of $\mathcal{R}_{\lambda_i}$ (defined in Eq. (82)) have been investigated. Therefore, the control law is rearranged:

$$\begin{aligned} \mathcal{R}_{\lambda_i}(u_i(k)) \quad := \quad & \underbrace{-\frac{1}{1-b_i}\left[b_i\lambda_i(k) + \frac{1}{1-a}a\sigma_i(k+1)\right]}_{>0} \\ & + \underbrace{\frac{1}{1-b_i}\frac{1}{1-a}}_{>0}\frac{1}{f_i(k+2)}u_i(k). \end{aligned}$$

Because of $f_1 > 0$, $\mathcal{R}_{\lambda_1}(u_1)$ is strictly monotonically increasing ($\mathcal{R}_{\lambda_1}(u_1^l) < \mathcal{R}_{\lambda_1}(u_1^h)$, *for* $u_1^l < u_1^h$), and $\mathcal{R}_{\lambda_2}(u_2)$ is strictly monotonically decreasing, since $f_2 < 0$.

Similar results are obtained for the functions $\mathcal{T}_1$ (strictly monotonically increasing) and $\mathcal{T}_2$ (strictly monotonically decreasing) with respect to the arguments r_{λ_1} and r_{λ_2}, respectively.

The obtained properties are summarized in Table 8.

CASE 1 $\mathcal{R}_{\lambda_1}(T_{1,d}) \geq 0 \wedge \mathcal{R}_{\lambda_2}(T_{2,d}) < 0$

In this case, the calculated actuation variable r_{λ_2} would[42] be negative and would be set to zero, because of saturation. Therefore, the requested torque for the second path $i = 2$ (always negative torques for this path) is bigger than the actually achievable torque $T_{2,min}$ (Please remind: The torque achieved for $r_{\lambda_2} = 0$):

$$T_{2,min}(k+2) = \mathcal{T}_2(0) < \mathcal{T}_2(\mathcal{R}_{\lambda_2}(T_{2,d}(k))) = T_{2,d}(k). \tag{85}$$

This is because of $\mathcal{R}_{\lambda_2}(T_{2,d}) < 0$, while $\mathcal{T}_2$ is monotonically decreasing. With active constraints and without additional measures ($u_{a,i} = 0, i = 1, 2$) the resulting acceleration torque would be smaller than the requested one T_d:

$$\mathcal{T}_1(\mathcal{R}_{\lambda_1}(T_{1,d}(k))) + T_{2,min}(k+2) < T_d(k). \tag{86}$$

[42] In case of $u_{a,2} = 0$

By choosing the modified actuation variable $u_1 = T_{1,d} + u_{a,1}$, while applying $u_2(k) = T_{2,min}(k+2)$ (yielding $r_{\lambda_2}(k) = 0$), the requirement on the resulting torque can be achieved if

$$\begin{aligned} & \mathcal{T}_1(\mathcal{R}_{\lambda,1}(\underbrace{T_{1,d}(k) + u_{a,1}(k)}_{u_1(k)})) + T_{2,min}(k+2) = T_d(k) \\ \Leftrightarrow \quad & T_{1,d}(k) + u_{a,1}(k) + T_{2,min}(k+2) = T_d(k) \end{aligned} \tag{87}$$

is true.

Using (86) and (87) it can be shown that $u_{a,1} > 0$ and, further, $\mathcal{R}_{\lambda_1}(T_{1,d} + u_{a,1}) > 0$ holds (meaning the constraint on the actuation variable is not violated in this case), because $T_{1,d} > 0$.

Now, Eq. (87) is solved with respect to $u_{a,1}$:

$$u_{a,1}(k) = T_d(k) - T_{2,min}(k+2) - T_{1,d}(k). \tag{88}$$

The variables u_i that fulfill the constraints for r_{λ_i} and yield $T(k+2) = T_d(k)$ are then given by

$$u_1(k) = T_d(k) - T_{2,min}(k+2), \quad u_2(k) = T_{2,min}(k+2).$$

Further, the corresponding activation variables are then given by

$$r_{\lambda_1}(k) = \mathcal{R}_{\lambda,1}(T_d(k) - T_{2,min}(k+2)), \quad r_{\lambda_2}(k) = 0.$$

Case 2 $\mathcal{R}_{\lambda_1}(T_{1,d}) < 0 \wedge \mathcal{R}_{\lambda_2}(T_{2,d}) \geq 0$

Because of symmetry reasons, the procedure is analog to Case 1. Here, the achieved torque for the muscle path 1 would be greater than the desired one (as the corresponding muscle cannot be deactivated fast enough). Therefore, the variable u_2 of the antagonistic path has to be decreased by choosing:

$$u_{a,2}(k) = T_d(k) - T_{1,min}(k+2) - T_{2,d}(k). \tag{89}$$

The variables u_i that fulfill the constraints for r_{λ_i} and yield $T(k+2) = T_d(k)$ are then given by

$$u_1(k) = T_{1,min}(k+2), \quad u_2(k) = T_d(k) - T_{1,min}(k+2).$$

The corresponding activation variables are then given by

$$r_{\lambda_1}(k) = 0, \quad r_{\lambda_2}(k) = \mathcal{R}_{\lambda,2}(T_d(k) - T_{1,min}(k+2)).$$

Case 3 $\mathcal{R}_{\lambda_1,k}(T_{1,d}) < 0 \wedge \mathcal{R}_{\lambda_2,k}(T_{2,d}) < 0$

Because both constraints for the actuation variables are violated within Case 3, the resulting accelerating torque would be $T_{1,min} + T_{2,min}$, which is not necessarily equal to the desired torque T_d. For determination of the compensation variables $u_{a,1}$ and $u_{a,2}$, two sub-cases are considered:

- Case 3.1 $T_d > T_{1,min} + T_{2,min}$ (actually produced torque would be too small)
- Case 3.2 $T_d < T_{1,min} + T_{2,min}$ (actually produced torque would be too big)

At first Case 3.1 is evaluated. In order to achieve the desired accelerating torque T_d, the torque T_1 needs to be increased. This can be fulfilled by applying the additional desired torque $u_{1,a}$ such that

$$T_d(k) = \mathcal{T}_1(\mathcal{R}_{\lambda_1}(T_{1,d}(k) + u_{1,a}(k))) + T_{2,min}(k+2). \tag{90}$$

Because of (90) and the condition for Case 3.1,

$$\mathcal{T}_1(\mathcal{R}_{\lambda_1}(T_{1,d}(k) + u_{1,a}(k))) \geq T_{1,min}(k+2) \geq 0$$

holds. Further, because $\mathcal{T}_1$ is monotonically increasing, also $\mathcal{R}_{\lambda_1}(T_{1,d} + u_{1,a}) \geq 0$ must hold, which means the constraint for the first actuation variable is satisfied. In this case, Eq. (90) becomes:

$$T_d(k) = T_{1,d}(k) + u_{1,a}(k) + T_{2,min}(k+2).$$

By rearranging $u_{1,a}$ can be calculated leading to

$$u_{1,a}(k) = T_d(k) - T_{1,d}(k) - T_{2,min}(k+2).$$

The variables u_i that fulfill the constraints for r_{λ_i} and yield $T(k+2) = T_d(k)$ are then given by

$$u_1(k) = T_d(k) - T_{2,min}(k+2), \quad u_2(k) = T_{2,min}(k+2).$$

The corresponding activation variables are then given by

$$r_{\lambda_1}(k) = \mathcal{R}_{\lambda,1}(T_d(k) - T_{2,min}(k+2)), \quad r_{\lambda_2}(k) = 0.$$

In Case 3.2, an analog procedure leads to the following result. The variables u_i that fulfill the constraints for r_{λ_i} and yield $T(k+2) = T_d(k)$ are then

$$u_1(k) = T_{1,min}(k+2), \quad u_2(k) = T_d(k) - T_{1,min}(k+2).$$

The corresponding activation variables are

$$r_{\lambda_1}(k) = 0, \quad r_{\lambda_2}(k) = \mathcal{R}_{\lambda_2}(T_d(k) - T_{1,min}(k+2)).$$

For all three cases, it is straightforward to show that exact tracking of T_d can only be achieved by increasing the level of co-contraction T_{cc}.

6.3.2 Two step ahead joint angle prediction

The mechanical system (77) is Euler-discretized yielding

$$x_1(k+1) = x_1(k) + T_a[x_2(k)] \tag{91}$$

$$x_2(k+1) = x_2(k) + \frac{T_a}{J}[-R_m x_2(k) - K_m x_1(k) + T(k)]. \tag{92}$$

Herein, x_1 and x_2 are the discrete-time representations of the joint angle and the joint angle velocity, respectively. By substituting $k \to k+1$ in Eq. (91), replacing $x_2(k+1)$ by Eq. (92), and further replacing $x_1(k+1)$ by the right hand side of Eq. (91), a two step ahead prediction

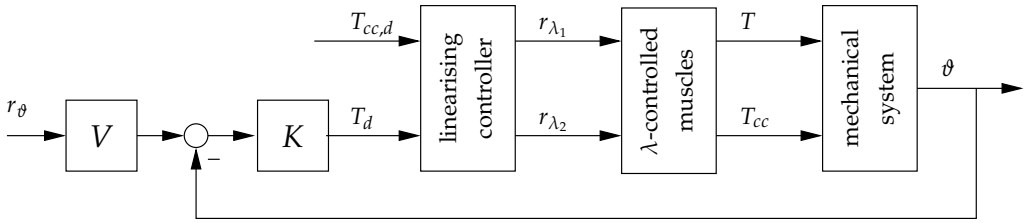

FIGURE 75: *The cascaded control scheme involving the joint angle controller, the linearization controller, and the recruitment controller.*

$\hat{x}_1(k+2)$ for the joint angle is derived:

$$\begin{aligned}\hat{x}_1(k+2) &= x_1(k) + T_a x_2(k) + T_a \Big[x_2(k) + \\ &\quad + \frac{T_a}{J} \left[-R_m x_2(k) - K_m x_1(k) + T(k) \right] \Big].\end{aligned} \tag{93}$$

The accelerating torque $T(k)$ is replaced by the desired one $T_d(k-2)$ since $T(k)$ cannot be measured and $T(k) = T_d(k-2)$ is enforced by the linearizing controller in the nominal case. The state variables $x_1(k)$ and $x_2(k)$, which refer to the joint angle ϑ and its derivation in time $\dot{\vartheta}$ are measured. Now, the estimates of $f_i(k+2)$, $i = 1, 2$, are determined by

$$\hat{f}_i(k+2) = k_{s,i}(\vartheta_{max,i} - \hat{x}_1(k+2)). \tag{94}$$

6.4 Linear Joint-Angle Feedback Control

As illustrated in Fig. 75, on top of the linearizing controller, a linear, time-discrete and two degrees of freedom joint angle controller is applied that uses the desired torque T_d as its actuation variable. The mechanical model Eq. (77) is Euler-discretized and used as transfer function for controller design:

$$G(z) = \frac{T_a^2/J}{z^2 + (\frac{R_m T_a}{J} - 2)z + (K_m T_a^2 - T_a R_m + 1)/J}.$$

The time delay of the system is neglected since it is assumed to be considerably lower than the rise time of G. The controller K cancels the asymptotically stable plant G and introduces a new second-order transfer function to the open loop:

$$K(z) = 1/G(z) \frac{a_0}{z^2 + b_1 z + b_0}.$$

The transfer function

$$G_{cl}(z) = \frac{a_0}{z^2 + b_1 z + b_0 + a_0} \tag{95}$$

describes the reference to output behavior and is considered for the specification of the closed-loop behavior (assuming at first no pre-filter for the reference).

The parameters a_0, b_0 and b_1 are determined by a pole-placement procedure for the denominator of G_{cl} and by claiming unity gain for G_{cl} ($G_{cl}(z = 1) = 1$). The latter condition leads to an integral

TABLE 9: *Summary of parameters.*

parameter	value
K_m/J	$4.015[s^{-2}]$
R_m/J	$1.28[s^{-1}]$
$\vartheta_{max,1}$	$0.52[rad]$
$\vartheta_{max,2}$	$-1.57[rad]$
$k_{s,1}/J$	$4.84[s^{-2}]$
$k_{s,2}/J$	$2.357[s^{-2}]$
a	0.678
b_1	0.811
b_2	0.845

(A) *simulation parameters*

parameter	value
K_m/J	$4.42[s^{-2}]$
R_m/J	$2.82[s^{-1}]$
$\vartheta_{max,1}$	$143[^\circ]$
$\vartheta_{max,2}$	$-67[^\circ]$
$k_{s,1}/J$	$1.188[s^{-2}]$
$k_{s,2}/J$	$0.846[s^{-2}]$
a	0.678
$b_1 = b_2$	0.65

(B) *real parameters*

parameter	value
d	0.5
T_r	$0.3[s]$
s_1	-3
s_2	-4

(C) *controller parameters*

controller. A desired-second order pole pair [12] described by a damping d and a rise time T_r is used for the pole-placement design.

A 2-DoF control design is preferred, wherein a fast feedback cancels disturbances. Further, step-wise changes in the joint angle reference shall not lead to an intensive excitation of the inner loop's actuation variables. Therefore, in addition to the feedback controller K, a reference pre-filter V is designed to cancel the reference to output behavior G_{cl} and to introduce a slower second-order dynamical system without conjugate complex poles:

$$V(z) = 1/G_{cl}(z) \cdot \frac{(1-\exp(-s_1 T_a)) \cdot (1-\exp(-s_2 T_a))}{(z-\exp(-s_1 T_a)) \cdot (z-\exp(-s_2 T_a))}.$$

6.5 RESULTS

For demonstrating the effectiveness of the linearizing controller along with its extension for the given constraints, a comparison of the controller with and without the extension was performed in form of a simulation study. Predefined trajectories were fed to the desired torques T_d and $T_{d,cc}$, while the torques of the plant model (cf. Sec. 6.2.) were evaluated. For the model and the linearizing controller, the parameters described in Table 9 (A) were used. In the Figs. 77 and 76 the results in form of a comparison of the desired torques (T_d, $T_{cc,d}$) and the actual torques (T, T_{cc}) are presented. Additionally, the actuation variables are shown.

For the linearizing controller without the extension, there is a considerable mismatch of T compared to the reference T_d. For an upper-level joint angle controller, this would lead to a decrease of the achievable performance. However, when the extension is enabled, T_d is matched (just leading to a time delay of two sampling steps). Small deviations (not visible in the plot) are due to the time-discretized plant model within the joint angle prediction (cf. Sec. 6.3.2).

The feasibility of the developed approach was further demonstrated by a joint angle control experiment in one healthy subject. Before the control experiment, the λ-control loops were tuned and the model (cf. Sec. 6.2) was identified using the procedure described in [174]. The resulting parameters are summarized in Table 9 (B) and the time-series for the used I/O data is shown in Fig. 78. The parameters for the joint angle controller are given in Table 9 (C).

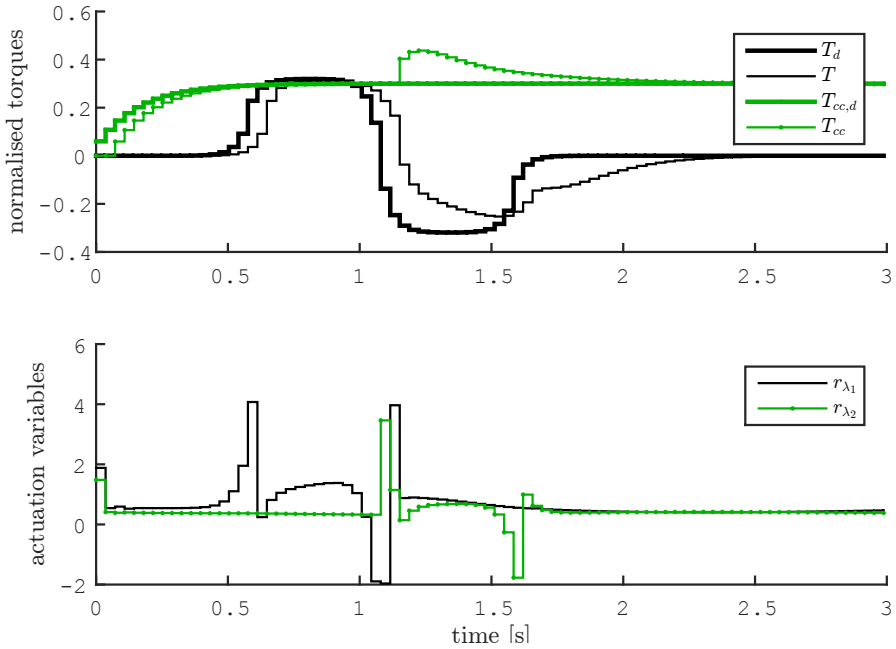

FIGURE 76: *Results for the linearization controller without taking constraints on the actuation variables into account. The actuation variables, given in the lower subplot, also show the computed negative values. However, for the simulated model the constraints $r_{\lambda_1} \geq 0$ and $r_{\lambda_2} \geq 0$ were applied, meaning that values violating these constraints were substituted by zero (saturation is applied).*

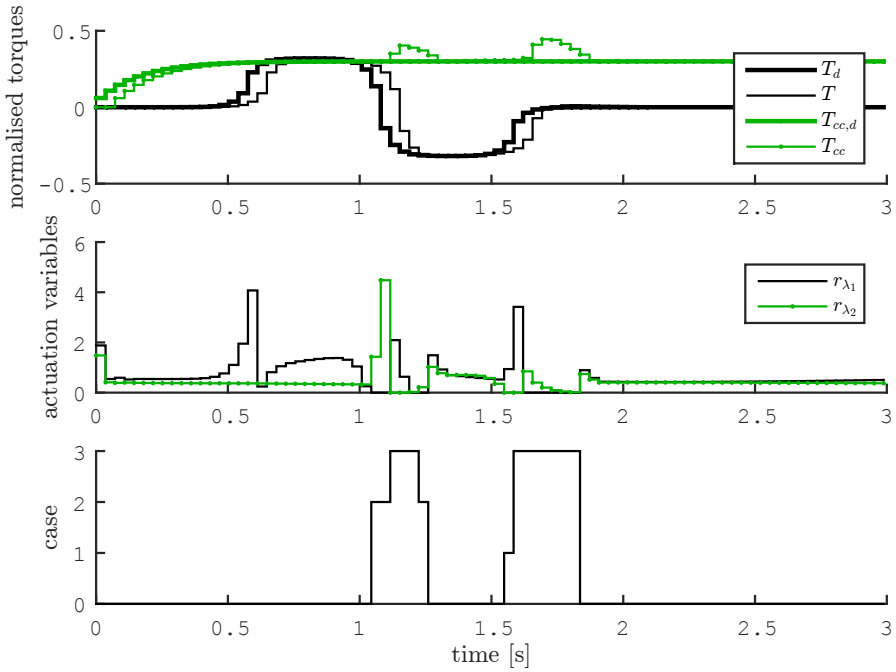

FIGURE 77: *Results for the extended linearization controller that additionally considers constrained actuation variables. During each sampling instance, measures are taken to prevent tracking errors as indicated by the case number. Herein,* CASE 0) *describes the case in which no additional measures were required as the constraints were not violated ($r_{\lambda_i} \geq 0\, i = 1, 2$). In comparison to the results shown in Fig. 76, the tracking performance of the resulting torque T improved significantly.*

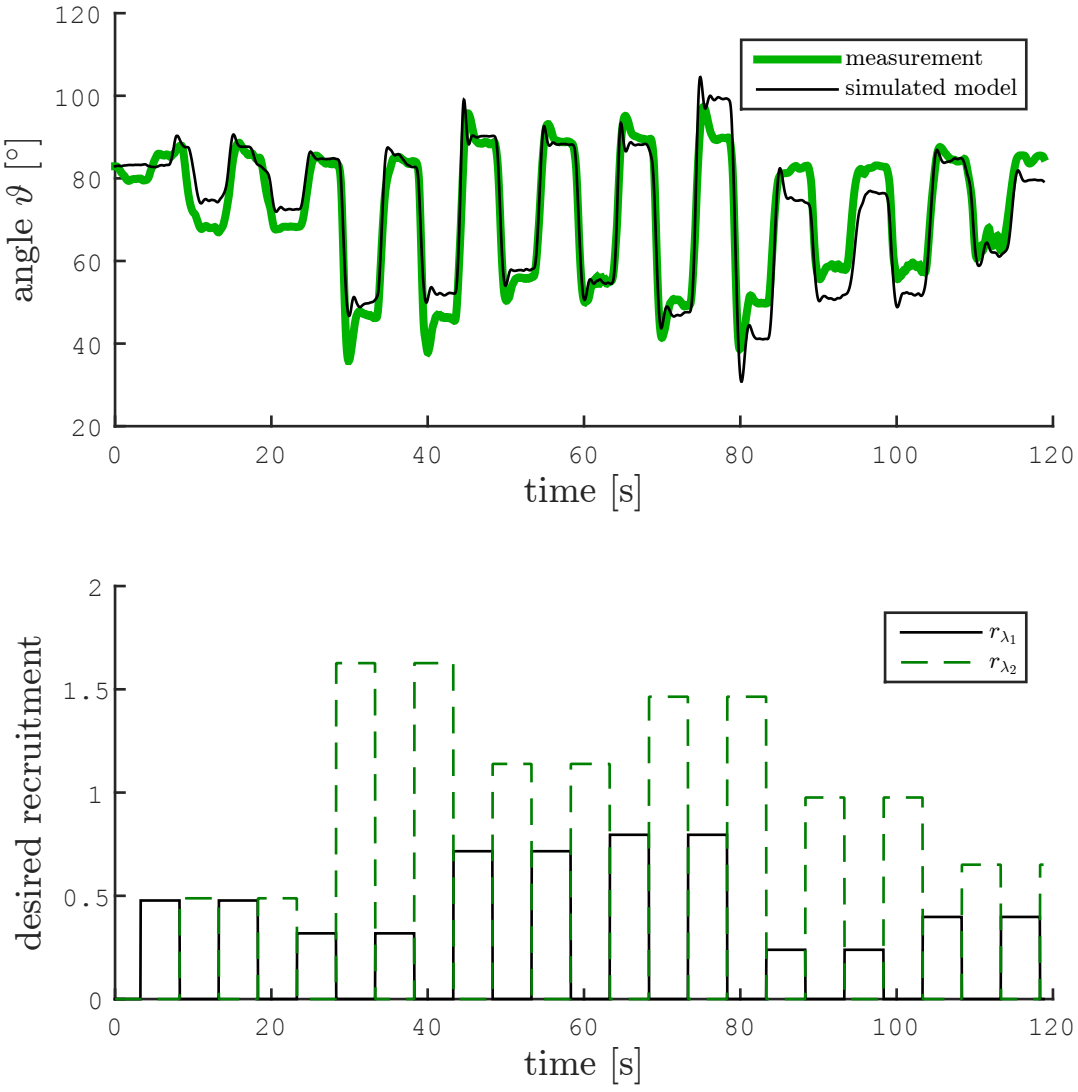

FIGURE 78: *I/O data used in the identification procedure. Further, the obtained model parameters were used to perform a simulation of the model by applying the input data. The resulting simulated joint angle is additionally shown.*

The results of the control experiment for a step-wise changing reference are shown in Fig. 79. In this test, no artificial co-activation was applied ($T_{cc,d} = 0$) as in the design of the linear positioning controller no co-activation and its influence on the controlled system was assumed.[43] In addition to the measured joint angle ϑ, the nominal behavior ϑ_{nom} (if the joint angle controller is applied to the linear plant model G) is shown. As the step size increases, the overshoot of the joint angle increases. Reason for this effect may be a decreased model-validity if the joint angle is not close to its equilibrium angle.

6.6 Conclusions and Outlook

The presented control strategy for antagonistic muscle pairs allows the control of accelerating torques along with the possibility to modulate the co-contraction strength. In a simulation study, the effectiveness of the proposed model inversion that takes actuation constraints into account was shown.

The entire control system, including the linearization and the upper-level joint angle controller, was successfully tested in one healthy subject. The low deviation between of ϑ and ϑ_{nom} shows the suitability of the proposed approach. The exact tracking is achieved at the cost of a temporarily increased level of co-activation. This increase, however, may even be beneficial concerning the smoothness of the obtained motion [153, 152].

Further, an investigation of the influence of co-contractions on the mechanical stiffness and elasticity is ongoing (e.g., [153, 152]), however, not included in this thesis. In this field, a great potential for the artificial control of limb movements is expected as described in Sec. 2.8.4.

[43] The investigation of the influence of co-activation and the respective controller design is not considered in this thesis.

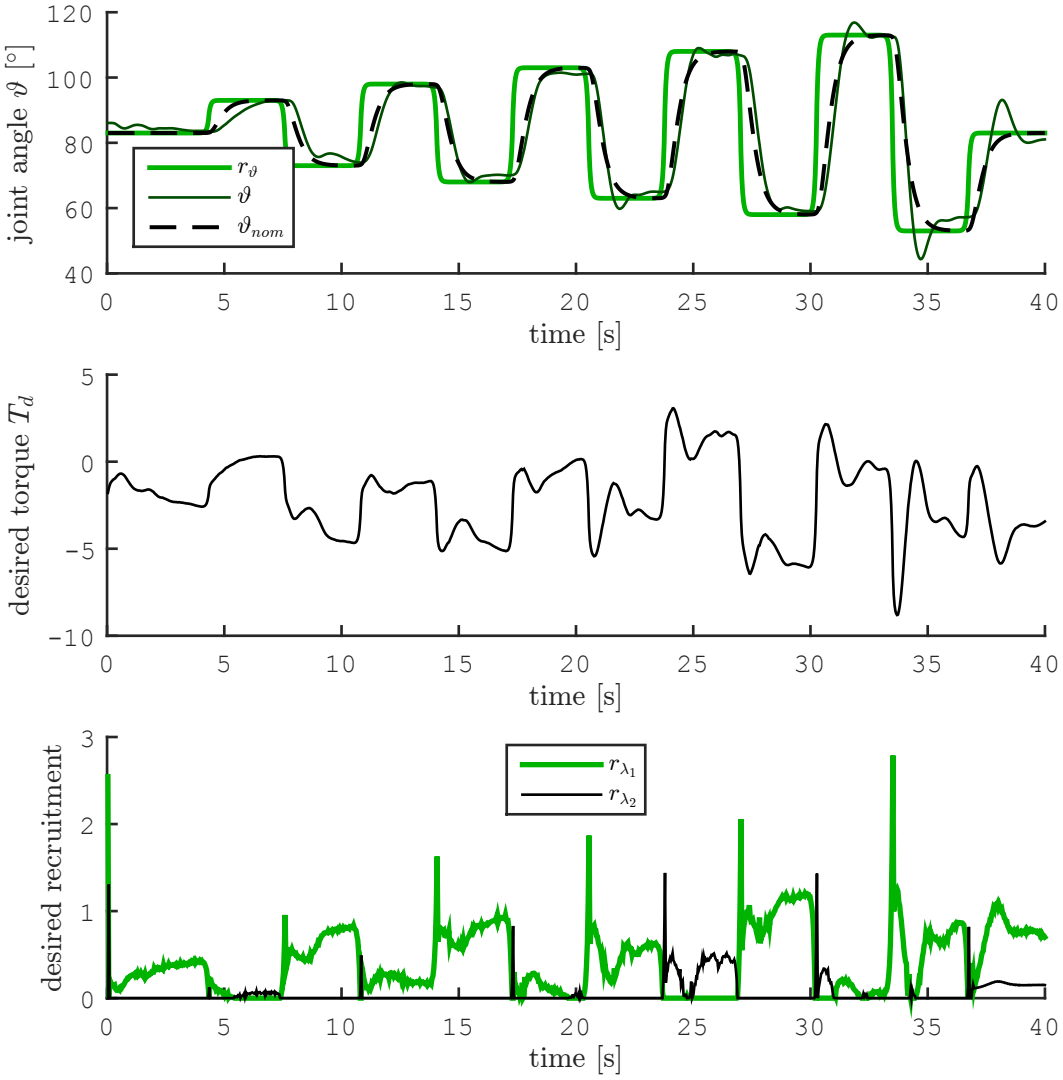

FIGURE 79: *Results of a joint angle control experiment for a healthy subject using the underlying linearization controller with extension and two λ-Control loops. The desired co-contraction torque $T_{cc,d}$ was zero.*

7

VARIABLE SAMPLING RATE CONTROLLED FES TO REDUCE THE PROGRESSION OF MUSCLE FATIGUE

To allow non-constant stimulation frequencies to be considered in feedback-controlled FES, a general method to design discrete-time controllers that consider variable sampling rates is presented in this chapter. This approach consists of a method for discretizing continuous linear time-invariant systems with irregular sampling and actuation time-instants to obtain discrete-time state-space representations of the systems to control. As these state-space models are nonlinear due to a dependency on the time-instants for sampling and actuation, a linearizing controller is applied that compensates for the influence of irregular sampling. Then, an augmented discrete-time system results that can be controlled by any traditional discrete-time control approach.

In the past, to obtain discrete-time models in FES, typically zero-order hold or Euler-based approaches were used. It is assumed, however, that models, which incorporate the application of Dirac-pulses to a continuous-time system are more suitable to describe the dynamics of the muscle's force (cf. Sec. 2.2) to electrical pulses as observed, e.g., in [150]. Therefore, unlike zero- or first-order hold discretization methods, the influence of the actuation sequence is described by intensity-modulated Dirac-pulses that are applied to the given continuous dynamical system. Zero- or first-order behavior can still easily be realized by extending the presented discretization method.

Other potential applications (not in the context of FES) include the estimation, e.g., using Kalman-filters under irregularly arriving measurements and the control of blood glucose concentration because the time intervals between glucose-concentration measurements and between the injections of insulin are typically not constant.

The methods and results presented in this chapter have been previously published in

- [89] C. Klauer and T. Schauer. "Discretisation & Control of Irregularly Actuated and Sampled LTI-Systems". In: *Proc. of the 19th International Conference on Methods and Models in Automation and Robotics, IEEE*. Międzyzdroje, Poland, 2014. ISBN: 978-1-4799-5081-2. DOI: 10.1109/MMAR.2014.6957394.

7.1 Overview

Typical time-discretization methods [57] assume a fixed duration of actuation- and sampling intervals. However, for the use case described above, a more general method is required that takes variable sampling and actuation times into account. Such a method is presented in this work (cf. Fig. 80). Variable and alternating time-points for actuation (actuation time) and sampling (sampling time) are described by the sequences t_δ and t_Δ, respectively. They represent inputs to the discretized system.

To match an output sequence $y_{\delta\Delta}$ according to a reference r_y, typical combinations of the three input variables and their applications (not only in FES) include:

a) While t_δ and t_Δ are given sequences, find a sequence u that leads to $y_{\delta\Delta} = r_y$. Typical applications include disturbed time periods in, e.g., networked control and soft real-time systems.

b) While u and t_Δ are a given sequences, find a sequence t_δ that leads to $y_{\delta\Delta} = r_y$. Application: Control of systems using PWM-modulation

c) Adjust u, t_δ and t_Δ such that $y_{\delta\Delta} = r_y$ and additional constraints on the relationship between u, t_δ and potentially t_Δ are fulfilled. Applications: Control of systems in which it is cost intensive to actuate or change the actuation intensity (e.g., FES, valves in process control).

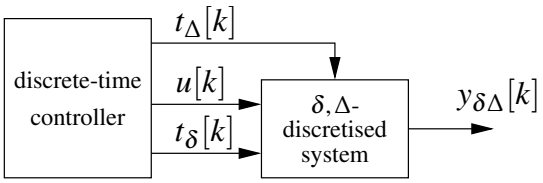

Figure 80: *The discrete-time system as obtained by the transformation incorporating variable actuation ($t_\delta[k]$) and sampling ($t_\Delta[k]$) times of a continuous system. In addition to the input sequence u, both time sequences are considered to be inputs to the discretized system. All variables may be adjusted by a control system.*

7.2 Definition and Properties

7.2.1 Delta-actuation and sampling

The continuous-time dynamical LTI SISO system

$$y(t) = \mathbb{S}[v(t)]\,(t), \qquad t \geq 0$$

is considered that maps an input signal $v(t) \in \mathbb{R}$ to an output signal $y(t) \in \mathbb{R}$ for $t \geq 0$. The I/O relationship between v and u is described by a state-space representation

$$\mathbb{S} \equiv \left\{ \begin{array}{ll} \dot{\boldsymbol{x}}(t) = \mathcal{A}\boldsymbol{x}(t) + \mathcal{B}v(t)), & \boldsymbol{x}(t) \in \mathbb{R}^n,\, v(t), y(t) \in \mathbb{R} \\ y(t) = \mathcal{C}\boldsymbol{x}(t), & \boldsymbol{x}(t=0) = \boldsymbol{x_0} \end{array} \right\}. \tag{96}$$

The continuous-domain δ-actuation input signal is defined as follows:

$$v_\delta(t) \coloneqq \sum_{j=0}^{\infty} u[j]\delta(t - t_\delta[j]), \qquad j \in \mathbb{N}, \tag{97}$$

whereby $\delta(t)$ is the Dirac delta distribution. The sequence $u = \{u[0], u[1], \cdots\}$ modulates the intensities of the δ-pulses. The time at which the k^{th} δ-pulse ($k \in \mathbb{N} \wedge k \geq 0$) is applied is denoted by the actuation time $t_\delta[k] \geq 0$ that is an element of the sequence $t_\delta = \{t_\delta[0], t_\delta[1], \cdots\}$. The first actuation is at time zero ($t_\delta[0] \coloneqq 0$).

This signal is applied to S ($v(t) = v_\delta$), while the output $y(t)$ is then sampled (denoted by Δ) at the sampling times $t_\Delta[k] > 0$ ($t_\Delta = \{t_\Delta[1], t_\Delta[2], \cdots\}$). The actuation and sampling is performed alternating, which is denoted by

$$t_\delta[k] < t_\Delta[k+1] < t_\delta[k+1] < t_\Delta[k+2] \quad \forall\, k \geq 0 \wedge k \in \mathbb{N}. \tag{98}$$

The described procedure is illustrated in Fig. 81 and called time-variable δ-actuation. By a formal definition the transformation $\boldsymbol{\mathcal{Z}_{\delta\Delta}}$ is introduced:

$$\begin{aligned} y_{\delta\Delta}[k] &= \boldsymbol{\mathcal{Z}_{\delta\Delta}}\left[\mathrm{S}, u, t_\delta, t_\Delta\right][k] \\ &\coloneqq \mathrm{S}\left[\sum_{j=0}^{\infty} u[j]\delta(t - t_\delta[j])\right](t_\Delta[k]). \end{aligned} \tag{99}$$

The time interval between an actuation pulse $k \geq 0$ and its subsequent measurement $k+1$ is defined as

$$T_\Delta[k] \coloneqq t_\Delta[k+1] - t_\delta[k] > 0, \qquad \forall k \geq 0. \tag{100}$$

Analog, the time interval between an actuation pulse k and a previous measurement k is defined (cf. Fig. 81) by

$$T_\delta[k-1] \coloneqq t_\delta[k] - t_\Delta[k] \geq 0, \qquad \forall k \geq 1. \tag{101}$$

By of these definitions, the following properties for calculating the time points $t_\Delta[k]$ and $t_\delta[k]$ from the time-differences derive: A relation for calculating the actuation time in dependence of sequences for the time intervals T_δ and T_Δ is

$$t_\delta[k] \coloneqq t_\delta[0] + \sum_{j=0}^{k-1} \left(T_\delta[j] + T_\Delta[j]\right), \qquad \forall k \geq 1 \tag{102}$$

The relation for the sampling time t_Δ is then:

$$t_\Delta[k+1] \coloneqq T_\Delta[k] + t_\delta[k], \qquad \forall k \geq 0 \tag{103}$$

7.2.2 Properties for linear time-invariant systems

If the system S is a linear system in the sense of

$$\mathrm{S}\left[av_1(t) + bv_2(t)\right](t) = a\,\mathrm{S}\left[v_1(t)\right](t) + b\,\mathrm{S}\left[v_2(t)\right](t), \tag{104}$$

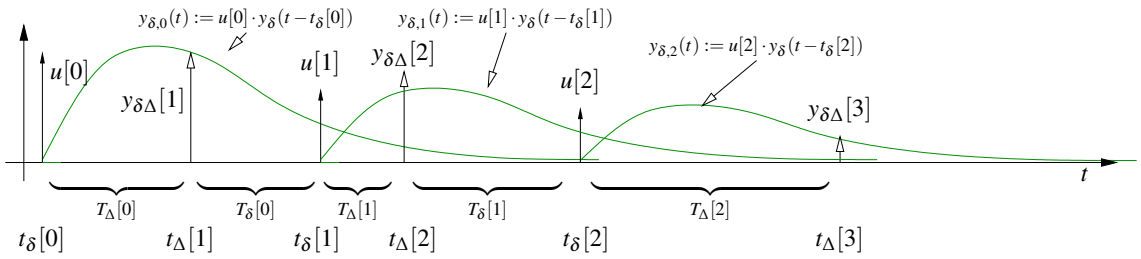

FIGURE 81: *Actuation of a LTI-system* $\mathbb{S}$ *using* δ*-actuation by applying* δ*-pulses at the actuation times* $t_\delta[k]$ *and sampling the output at* $t_\Delta[k]$*. The output of the continuous system is the superposition of the individual system responses* $y_{\delta,i}$ $(i = 0, 1, 2)$ *to each* δ*-pulse in addition to the transient caused by the initial states (not shown here).*

then the property of linearity also holds true for the dependency of y on u of the sampled system:

$$\begin{aligned} & \mathcal{Z}_{\delta\boldsymbol{\Delta}}\left[\mathbb{S}, au_1 + bu_2, t_\delta, t_\Delta\right][k] \\ = \quad & a\,\mathcal{Z}_{\delta\boldsymbol{\Delta}}\left[\mathbb{S}, u_1, t_\delta, t_\Delta\right][k] + b\,\mathcal{Z}_{\delta\boldsymbol{\Delta}}\left[\mathbb{S}, u_2, t_\delta, t_\Delta\right][k]. \end{aligned} \tag{105}$$

The prove is straightforward.

Remark: A System

$$\mathbb{S} \equiv \left\{ \; y(t) = \overline{\mathbb{S}}\left[u(t - T_d)\right](t) \; \right\}, \qquad T_d \geq 0$$

that incorporates an input delay T_d can be discretized by applying $\mathcal{Z}_{\delta\boldsymbol{\Delta}}$ to the system $\overline{\mathbb{S}}$ without delay while shifting the actuation times $t_\delta[k]$ by T_d such that $t_\delta + T_d$ is the new sequence for the actuation times. Herein, the time-interval $\overline{T}_\Delta[k] = t_\Delta[k+1] - (t_\delta[k] + T_d)$ between each shifted actuation pulse and next sampling time must be greater than zero to fulfill Eq. (98).

7.3 Discretization of Elementary Systems

In this section, $\mathcal{Z}_{\delta\boldsymbol{\Delta}}$ is applied to first- and second-order systems and analytical representations in form of discrete-time state-space systems to describe the I/O behavior result. For most higher-order systems, a decomposition into one or more of such basic systems can be performed (e.g., utilizing a Jordan normal form or a partial fraction decomposition) to apply $\mathcal{Z}_{\delta\boldsymbol{\Delta}}$ separately according to (105).

7.3.1 First-order LTI-System $\mathbb{S}^1$

Let the I/O-behavior of $\mathbb{S}^1$ for $t \geq 0$ (the dependency of $y(t)$ on $v(t)$) be described by the first-order state-space system:

$$\mathbb{S}^1 \equiv \left\{ \begin{array}{ll} \dot{x}(t) = s_\infty\, x(t) + v(t), & x, y, u, s_\infty, x_o \in \mathbb{C} \\ y(t) = x(t), & x(t=0) = x_0. \end{array} \right\}.$$

Please note that the output, the state, the initial state, and the parameter may be complex-valued in this case. This assumption is helpful when calculating $\mathcal{Z}_{\delta\boldsymbol{\Delta}}$ for a second-order system with

conjugated complex eigenvalues, which is then possible by applying the results obtained within this section.

To calculate the output y when applying the δ-actuation input $v_\delta(t)$, the Laplace-transform of this system is obtained and divided into a part P (particular solution) and a part H (homogeneous solution):

$$Y_\delta(s) = \underbrace{\frac{1}{s - s_\infty} x_0}_{:=Y_\delta^P(s)} + \underbrace{\frac{1}{s - s_\infty} V_\delta(s)}_{:=Y_\delta^H(s)}. \tag{106}$$

Herein, $Y_\delta^P(s)$ and $Y_\delta^H(s)$ are the Laplace-transformed output components $y_\delta^P(t)$ and $y_\delta^H(t)$ respectively. Further,

$$V_\delta(s) = \sum_{j=0}^{\infty} u[j] e^{-t_\delta[j]\, s}, \qquad j \in \mathbb{N} \tag{107}$$

is the Laplace-transform of the δ-actuation signal v_δ and $G^1(s) = 1/(s - s_\infty)$ the transfer function of S^1.

Particular part P: At first Y_δ^P is considered to calculate the output component y_δ^P. Hence, the time-domain impulse response ($v(t) = \delta(t)$) of G^1 is calculated:

$$\mathcal{L}^{-1}[G^1(s)](t) = y_\delta(t) = \begin{cases} 0 & if\, t < 0 \\ e^{s_\infty t} & if\, t \geq 0 \end{cases}. \tag{108}$$

The time-domain response of Y_δ^P is then given by

$$y_\delta^P(t) = x_0 \cdot y_\delta(t) = \begin{cases} 0 & if\, t < 0 \\ x_0 e^{s_\infty t} & if\, t \geq 0 \end{cases}.$$

As mentioned in (99) the output signal is sampled at $t_\Delta[k]$, $\forall k \geq 1$. Because $\boldsymbol{\mathcal{Z}_{\delta\Delta}}$ is I/O-linear (105), sampling y_δ is equivalent to calculating the sum of the sampled output components of H and P. Sampling y_δ^P at $t_\Delta[k] > 0$ yields:

$$y_{\delta\Delta}^P[k] = y_\delta^P(t_\Delta[k]) = x_0 e^{s_\infty t_\Delta[k]}, \qquad \forall k \geq 1. \tag{109}$$

Since the aim is to obtain a state-space description of the sampled system, a recursive representation of Eq. (109) is obtained, whereby $T_\delta[-1]$ is defined to be zero:

$$\begin{aligned} y_{\delta\Delta}^P[k+1] &= y_{\delta\Delta}^P[k] e^{s_\infty (T_\delta[k-1] + T_\Delta[k])} \qquad \forall k \geq 0 \\ y_{\delta\Delta}^P[0] &= x_0, \quad T_\delta[-1] := 0. \end{aligned} \tag{110}$$

Homogeneous part H: Now Y_δ^H is considered. Because S^1 is linear, the response $y_\delta^H(t)$ is the sum of all individual responses to each individual δ-pulse contained in v_δ:

$$y_\delta^H(t) = \sum_{j=0}^{\infty} \underbrace{u[j] y_\delta(t - t_\delta[j])}_{y_{\delta,j}(t)}.$$

Sampling the continuous signal y_δ^H at $t_\Delta[k]$ for $k \geq 1$ yields:

$$\begin{aligned} y_{\delta\Delta}^H[k] &= y_\delta^H(t_\Delta[k]) \\ &= \sum_{j=0}^{\infty} u[j] y_\delta(t_\Delta[k] - t_\delta[j]), \qquad \forall k \geq 1. \end{aligned}$$

Since $y_\delta(t)$ is zero for $t = t_\Delta[k] - t_\delta[j] < 0$ and because of (98), the elements $j \geq k$ of the sum are omitted and a finite sum is obtained:

$$\begin{aligned} y_{\delta\Delta}^H[k] &= \sum_{j=0}^{k-1} u[j] y_\delta(t_\Delta[k] - t_\delta[j]) \\ &= \sum_{j=0}^{k-1} u[j] e^{s_\infty (t_\Delta[k] - t_\delta[j])} \\ &= e^{s_\infty t_\Delta[k]} \cdot \sum_{j=0}^{k-1} u[j] e^{-s_\infty t_\delta[j]}, \qquad \forall k \geq 1. \end{aligned} \tag{111}$$

Recursion To calculate a recursive representation of (111), an index shift of one incremental step is performed:

$$y_{\delta\Delta}^H[k+1] = e^{s_\infty t_\Delta[k+1]} \cdot \left[u[k] e^{-s_\infty t_\delta[k]} + \sum_{j=0}^{k-1} u[j] e^{-s_\infty t_\delta[j]} \right], \tag{112}$$

whereby $\forall k \geq 0$. Decomposing the exponential factor using $t_\Delta[k+1] = t_\Delta[k] + T_\delta[k-1] + T_\Delta[k]$, which directly follows from Eq. (100) and (101) yields

$$e^{s_\infty t_\Delta[k+1]} = e^{s_\infty t_\Delta[k]} \cdot e^{s_\infty [T_\delta[k-1] + T_\Delta[k]]}.$$

Using this result, Eq. (112) can be rearranged yielding

$$\begin{aligned} y_{\delta a,\Delta}^H[k+1] &= e^{s_\infty [T_\delta[k-1] + T_\Delta[k]]} \cdot \underbrace{e^{s_\infty t_\Delta[k]} \cdot \sum_{j=0}^{k-1} u[j] e^{-s_\infty t_\delta[j]}}_{y_{\delta\Delta}^H[k]} \\ &+ e^{s_\infty t_\Delta[k]} \cdot e^{s_\infty [T_\delta[k-1] + T_\Delta[k]]} \cdot u[k] e^{-s_\infty t_\delta[k]}. \end{aligned} \tag{113}$$

By applying $t_\Delta[k] - t_\delta[k] = -T_\delta[k-1]$ following from Eq. (100) and Eq. (101), the resulting recursive equation for $y_{\delta a,\Delta}^H$ is then:

$$y_{\delta\Delta}^H[k+1] = e^{s_\infty [T_\delta[k-1] + T_\Delta[k]]} y_{\delta\Delta}^H[k] + u[k] e^{s_\infty T_\Delta[k]}. \tag{114}$$

The initial condition for $y_{\delta\Delta}^H[1]$ is obtained by evaluating Eq. (111) for $k = 1$:

$$y_{\delta\Delta}^H[1] = u[0] y_\delta(t_\Delta[1] - t_\delta[0]) = u[0] e^{s_\infty T_\Delta[0]}. \tag{115}$$

By defining $T_\delta[-1] := 0$ it is observed that the initial condition (115) turns into the more usual initial condition

$$y_{\delta\Delta}^H[0] := 0. \tag{116}$$

The variable $y^H_{\delta\Delta}[0]$ is hereby assigned and $y^H_{\delta\Delta}[1]$ results from (114) for $k = 0$.

Result The sampled output of $\mathbb{S}^1$ combines H and P:

$$y_{\delta\Delta}[k] = y^H_{\delta\Delta}[k] + y^P_{\delta\Delta}[k].$$

To obtain a resulting recursion formula, an index shift for k is performed, and the partial results described by Eq. (110) and (114) are combined yielding

$$y_{\delta\Delta}[k+1] = \underbrace{\left(y^H_{\delta\Delta}[k] + y^P_{\delta\Delta}[k]\right)}_{y_{\delta\Delta}[k]} \cdot e^{s_\infty [T_\delta[k-1]+T_\Delta[k]]} + u[k] e^{s_\infty T_\Delta[k]}.$$

The initial condition for $y_{\delta\Delta}[0]$ is then obtained using (116) and (110) yielding

$$y_{\delta\Delta}[0] = y^H_{\delta\Delta}[0] + y^P_{\delta\Delta}[0] = x_0.$$

Summarizing the analytical result for the discretization of $\mathbb{S}^1$ is described by

$$\begin{aligned} & \left\{ \; y_{\delta\Delta} = \boldsymbol{\mathcal{Z}}_{\boldsymbol{\delta\Delta}} \left[\mathbb{S}^1, u, t_\delta, t_\Delta\right][k] \; \right\} \\ \equiv \; & \left\{ \begin{array}{l} y_{\delta\Delta}[k+1] = y_{\delta\Delta}[k] \cdot e^{s_\infty [T_\delta[k-1]+T_\Delta[k]]} + u[k] e^{s_\infty T_\Delta[k]} \\ y_{\delta\Delta}[0] = x_0. \end{array} \right\}. \end{aligned} \tag{117}$$

This relationship describes a non-linear discrete-time system with the inputs u, T_δ and T_Δ. A scheduling of the system's coefficients based on the inputs for the time differences T_δ and T_Δ is herein performed.

7.3.2 SECOND-ORDER LTI-SYSTEMS WITH CONJUGATE COMPLEX EIGENVALUES

For second-order systems, only the case of a system $\mathbb{S}^{cc}$ incorporating conjugated complex eigenvalues ($\lambda_1 = \lambda = \sigma + j\omega$, $\lambda_2 = \overline{\lambda} = \sigma - j\omega$, j is the imaginary unit) is considered. Systems with non-equal and real-valued eigenvalues ($\lambda_1, \lambda_2 \in \mathbb{R} \wedge \lambda_1 \neq \lambda_2$), can be decomposed into two 1^{st}-order systems with superposed outputs that are then discretized separately by re-using (117).

Also for discretizing $\mathbb{S}^{cc}$ this principle is used in a first step, but as the resulting discrete-time systems have complex-valued states, a further effort for deriving real-valued systems is required. The I/O behavior of a strictly proper second-order system $\mathbb{S}^{cc}$ with conjugate complex eigenvalues can always be described by the following state-space representation:

$$\mathbb{S}^{cc} \equiv \left\{ \begin{array}{ll} \underbrace{\begin{pmatrix} \dot{x}_1 \\ \dot{x}_2 \end{pmatrix}}_{\dot{\boldsymbol{x}}(t)} = \underbrace{\begin{pmatrix} \lambda + \overline{\lambda} & -\lambda\overline{\lambda} \\ 1 & 0 \end{pmatrix}}_{\boldsymbol{A}} \underbrace{\begin{pmatrix} x_1 \\ x_2 \end{pmatrix}}_{\boldsymbol{x}(t)} + \boldsymbol{B} v(t), & \boldsymbol{B} \in \mathbb{R}^2 \\ y(t) = \underbrace{\begin{pmatrix} 0 & 1 \end{pmatrix}}_{\boldsymbol{C}} \boldsymbol{x}(t) & \boldsymbol{x}(0) = \begin{pmatrix} x_{1,0} \\ x_{2,0} \end{pmatrix} \end{array} \right\} \tag{118}$$

Ongoing, two different classes of systems are considered:

A) $\mathbb{S}_A^{cc}$ that derives from $\mathbb{S}^{cc}$ by choosing $\boldsymbol{B} = \boldsymbol{B_A} \coloneqq [1,0]^T$ and realizes the transfer function $1/((s-\lambda)(s-\overline{\lambda}))$.

B) $\mathbb{S}_B^{cc}$ as derived from $\mathbb{S}^{cc}$ by choosing $\boldsymbol{B} = \boldsymbol{B_B} \coloneqq [-a+\lambda+\overline{\lambda}, 1]^T$ that realizes $(s-a)/((s-\lambda)(s-\overline{\lambda}))$.

To perform a separation into two first-order systems, a diagonal form for describing $\boldsymbol{A}$ is calculated:

$$\begin{aligned} \boldsymbol{A} &= \boldsymbol{P}\boldsymbol{J}\boldsymbol{P}^{-1}, \qquad \boldsymbol{J} = \operatorname{diag}(\overline{\lambda}, \lambda) \\ \boldsymbol{P} &= \begin{pmatrix} \frac{\lambda}{2\omega} & \frac{\overline{\lambda}}{2\omega} \\ \frac{j}{2\omega} & -\frac{j}{2\omega} \end{pmatrix}, \qquad \boldsymbol{P}^{-1} = \begin{pmatrix} 1 & -\lambda \\ 1 & -\overline{\lambda} \end{pmatrix} \end{aligned} \tag{119}$$

By introducing the transformed state vector

$$\tilde{\boldsymbol{x}} = [\tilde{x}_1, \tilde{x}_2] = \boldsymbol{P}^{-1}\boldsymbol{x},$$

a representation with a diagonal system matrix $\boldsymbol{J}$ is obtained:

$$\mathbb{S}^{cc} \equiv \left\{ \begin{array}{ll} \underbrace{\boldsymbol{P}^{-1}\dot{\boldsymbol{x}}}_{\dot{\tilde{\boldsymbol{x}}}} = \boldsymbol{J}\underbrace{\boldsymbol{P}^{-1}\boldsymbol{x}}_{\tilde{\boldsymbol{x}}} + \underbrace{\boldsymbol{P}^{-1}\boldsymbol{B}}_{\tilde{\boldsymbol{B}}} v(t), & \tilde{\boldsymbol{B}} = [\tilde{b}_1, \tilde{b}_2]^T \\ y(t) = \boldsymbol{C}\boldsymbol{P}\tilde{\boldsymbol{x}} & \tilde{\boldsymbol{x}}(0) = \boldsymbol{P}^{-1}\begin{pmatrix} x_{1,0} \\ x_{2,0} \end{pmatrix} = \begin{pmatrix} x_{1,0} - \lambda x_{2,0} \\ x_{1,0} - \overline{\lambda} x_{2,0} \end{pmatrix} \end{array} \right\}.$$

For the systems $\mathbb{S}_A^{cc}$ and $\mathbb{S}_B^{cc}$, the input matrix $\boldsymbol{B}$ becomes

$$\tilde{\boldsymbol{B}}_{\boldsymbol{A}} = \begin{bmatrix} \tilde{b}_{A1} \\ \tilde{b}_{A2} \end{bmatrix} = \boldsymbol{P}^{-1}\boldsymbol{B}_{\boldsymbol{A}} = \begin{pmatrix} 1 \\ 1 \end{pmatrix} \text{ and } \tilde{\boldsymbol{B}}_{\boldsymbol{B}} = \begin{bmatrix} \tilde{b}_{B1} \\ \tilde{b}_{B2} \end{bmatrix} = \boldsymbol{P}^{-1}\boldsymbol{B}_{\boldsymbol{B}} = \begin{pmatrix} -a+\overline{\lambda} \\ -a+\lambda \end{pmatrix}, \tag{120}$$

respectively, whereby the vector elements are conjugated complex to each other ($\tilde{b}_{A1} = \overline{\tilde{b}_{A2}}$ and $\tilde{b}_{B1} = \overline{\tilde{b}_{B2}}$). To avoid redundant calculations in the ongoing analysis, the input gains $\tilde{b}_1$ and $\tilde{b}_2$ are shifted into the output matrix, which is easily possible because J is diagonal:

$$\mathbb{S}^{cc} \equiv \left\{ \begin{array}{ll} \begin{pmatrix} \dot{\tilde{x}}_1 \\ \dot{\tilde{x}}_2 \end{pmatrix} = \begin{pmatrix} \overline{\lambda} & 0 \\ 0 & \lambda \end{pmatrix}\begin{pmatrix} \tilde{x}_1 \\ \tilde{x}_2 \end{pmatrix} + \begin{pmatrix} 1 \\ 1 \end{pmatrix} v(t), & y(t) = \begin{pmatrix} \frac{j\tilde{b}_1}{2\omega} \\ -\frac{j\tilde{b}_2}{2\omega} \end{pmatrix}^T \begin{pmatrix} \tilde{x}_1 \\ \tilde{x}_2 \end{pmatrix} \\ \begin{pmatrix} \tilde{x}_1(0) \\ \tilde{x}_2(0) \end{pmatrix} = \begin{pmatrix} (x_{1,0} - \lambda x_{2,0})/\tilde{b}_1 \\ (x_{1,0} - \overline{\lambda} x_{2,0})/\tilde{b}_2 \end{pmatrix} & \end{array} \right\}.$$

Two decoupled first-order systems with the respective eigenvalues λ and $\overline{\lambda}$ result, whereby the original output y is the by complex-valued factors weighted sum of the states $\tilde{x}_1$ and $\tilde{x}_2$. Hence, the result for the first-order system (114) is re-used:

$$\begin{aligned} y_{\delta\Delta}[k] = {} & \underbrace{j\tilde{b}_1/(2\omega)}_{:=re^{j\phi}} \; \boldsymbol{\mathcal{Z}}_{\boldsymbol{\delta\Delta}} \left[\left\{ \begin{array}{l} \dot{y}(t) = \overline{\lambda} y(t) + v(t) \\ y(0) = (x_{1,0} - \lambda x_{2,0})/\tilde{b}_1 \end{array} \right\}, u, t_\delta, t_\Delta \right] \\ + \; & \underbrace{-j\tilde{b}_2/(2\omega)}_{:=re^{-j\phi}} \; \boldsymbol{\mathcal{Z}}_{\boldsymbol{\delta\Delta}} \left[\left\{ \begin{array}{l} \dot{y}(t) = \lambda y(t) + v(t) \\ y(0) = (x_{1,0} - \overline{\lambda} x_{2,0})/\tilde{b}_2 \end{array} \right\}, u, t_\delta, t_\Delta \right]. \end{aligned}$$

To reduce complexity, the weighting factors are described by the polar coordinates r and ϕ. For $\mathbb{S}_A^{cc}$ and $\mathbb{S}_B^{cc}$ they become:

$$\begin{aligned} r_A e^{\phi_A} &:= j\tilde{b}_{A,1}/(2\omega) \Rightarrow r_A = 1/(2\omega),\ \phi_A = \pi/2 \\ r_B e^{\phi_B} &:= j\tilde{b}_{B,1}/(2\omega) = \tfrac{1}{2} + j\tfrac{\sigma - a}{2\omega} \\ \Rightarrow r_B = \frac{1}{2}\sqrt{1 + [(\sigma - a)/\omega]^2},\ \phi_B &= \tan^{-1}\left[(\sigma - a)/\omega\right]. \end{aligned} \tag{121}$$

The sampling interval $T_s[k] := T_\delta[k-1] + T_\Delta[k]$ is defined for a compact representation. Evaluating $\boldsymbol{\mathcal{Z}}_{\boldsymbol{\delta\Delta}}$ for both 1^{st}-order systems with the eigenvalues λ and $\overline{\lambda}$ by using (117) yields the discrete-time state-space representation

$$\begin{pmatrix} z_1[k+1] \\ z_2[k+2] \end{pmatrix} = \underbrace{\begin{pmatrix} e^{\overline{\lambda} T_s[k]} & 0 \\ 0 & e^{\lambda T_s[k]} \end{pmatrix}}_{\underline{\boldsymbol{A}}^{cc}} \begin{pmatrix} z_1[k] \\ z_2[k] \end{pmatrix} + \underbrace{\begin{pmatrix} e^{\overline{\lambda} T_\Delta[k]} \\ e^{\lambda T_\Delta[k]} \end{pmatrix}}_{\underline{\boldsymbol{B}}^{cc}} u[k]$$

$$y_{\delta\Delta}[k] = \underbrace{\begin{pmatrix} re^{j\phi} & re^{-j\phi} \end{pmatrix}}_{\underline{\boldsymbol{C}}^{cc}} \begin{pmatrix} z_1[k] \\ z_2[k] \end{pmatrix} \quad \underbrace{\begin{pmatrix} z_1[0] \\ z_2[0] \end{pmatrix}}_{\underline{\boldsymbol{z_0}}^{cc}} = \begin{pmatrix} (x_{1,0} - \lambda x_{2,0})/\tilde{b}_1 \\ (x_{1,0} - \overline{\lambda} x_{2,0})/\tilde{b}_2 \end{pmatrix}.$$

Please note that the states z_1 and z_2 relate conjugated complex to each other ($\overline{z}_1 = z_2$). A state-space representation with purely real-valued states is desirable to reduce computational complexity in computer controlled systems. Therefore, a state transformation is performed such that the obtained states represent imaginary and real part of z_2:

$$\boldsymbol{z}^{cc}[k] = \begin{pmatrix} z^R[k] \\ z^I[k] \end{pmatrix} := \begin{pmatrix} \Re\{z_2[k]\} \\ \Im\{z_2[k]\} \end{pmatrix} = \underbrace{\begin{pmatrix} 0.5 & 0.5 \\ 0.5j & -0.5j \end{pmatrix}}_{:=\underline{\boldsymbol{T}}} \begin{pmatrix} z_1[k] \\ z_2[k] \end{pmatrix} \tag{122}$$

By applying this state transformation, a real-valued state-space system is obtained, and the resulting discretization is then

$$\begin{aligned} &\left\{\ y_{\delta\Delta} = \boldsymbol{\mathcal{Z}}_{\boldsymbol{\delta\Delta}}\left[\mathbb{S}^{cc}, u, t_\delta, t_\Delta\right][k]\ \right\} \\ \equiv\ &\left\{ \begin{array}{lcl} \boldsymbol{z}^{cc}[k+1] &=& \boldsymbol{A}^{cc} \cdot \boldsymbol{z}^{cc}[k] + \boldsymbol{B}^{cc} u[k] \\ y_{\delta\Delta}[k] &=& \boldsymbol{C}^{cc} \cdot \boldsymbol{z}^{cc}[k] \\ \boldsymbol{z}_{cc}[0] &=& \boldsymbol{z}_{\boldsymbol{0}}^{cc},\quad \boldsymbol{z}_{cc} \in \mathbb{R}^2 \end{array} \right\}, \end{aligned} \tag{123}$$

wherein the matrices $\boldsymbol{A}^{cc}$. $\boldsymbol{B}^{cc}$, $\boldsymbol{C}^{cc}$ and the initial state vector $\boldsymbol{z}_{\boldsymbol{0}}^{cc}$ are given by

$$\begin{aligned} \boldsymbol{A}^{cc} &= \boldsymbol{T}\underline{\boldsymbol{A}}^{cc}\boldsymbol{T}^{-1} = e^{\sigma T_s[k]} \begin{bmatrix} \cos(\omega T_s[k]) & -\sin(\omega T_s[k]) \\ \sin(\omega T_s[k]) & \cos(\omega T_s[k]) \end{bmatrix} \\ \boldsymbol{B}^{cc} &= \boldsymbol{T}\underline{\boldsymbol{B}}^{cc} = e^{\sigma T_\Delta[k]} \begin{bmatrix} \cos(\omega T_\Delta[k]) \\ \sin(\omega T_\Delta[k]) \end{bmatrix} \\ \boldsymbol{C}^{cc} &= \underline{\boldsymbol{C}}^{cc}\boldsymbol{T}^{-1} = [2r\cos\phi, 2r\sin\phi], \qquad T_s[k] := T_\delta[k-1] + T_\Delta[k] \\ \boldsymbol{z}_{\boldsymbol{0}}^{cc} &= \boldsymbol{T}\underline{\boldsymbol{z_0}}^{cc}. \end{aligned}$$

For case A) ($\tilde{b}_2 = 1$) the initial state vector $\boldsymbol{z}_{\boldsymbol{0}}^{cc}$ becomes

$$\boldsymbol{z}_{\boldsymbol{A,0}}^{cc} = \begin{bmatrix} x_{1,0} - \sigma x_{2,0} \\ \omega x_{2,0} \end{bmatrix} \tag{124}$$

and in case B) ($\tilde{b}_2 = \tilde{b}_{B2}$), using (121):

$$\boldsymbol{z}_{\boldsymbol{B,0}}^{cc} = \begin{bmatrix} z^R[0] \\ z^I[0] \end{bmatrix} = \begin{bmatrix} \sin\phi^B & \cos\phi^B \\ -\cos\phi^B & \sin\phi^B \end{bmatrix} \begin{bmatrix} x_{1,0} - \sigma x_{2,0} \\ \omega x_{2,0} \end{bmatrix} / (2\omega r_B). \tag{125}$$

For the discretization of $\mathbb{S}_A^{cc}$ by using (123), the parameters r, ϕ and $\boldsymbol{z}_{\boldsymbol{0}}^{cc}$ are respectively substituted by r_A, ϕ_A (121) and $\boldsymbol{z}_{\boldsymbol{A,0}}^{cc}$ (124), while using r_B, ϕ_B (121) and $\boldsymbol{z}_{\boldsymbol{B,0}}^{cc}$ (125) for $\mathbb{S}_B^{cc}$.

7.4 Simulation Results

A continuous system of second order Eq. (118) ($\lambda = -40 + j30$, $x_{1,0} = 2$, $x_{2,0} = 0.01$) is discretized using $\boldsymbol{\mathcal{Z}}_{\boldsymbol{\delta\Delta}}$. Predefined sequences for t_δ, t_Δ and u were applied as shown in Fig. 82. The continuous-time system output y in response to the δ-actuation was numerically calculated by superposing the responses to each δ-pulse and the dynamics caused by the initial states. The time-discrete state-space model (123) was evaluated, and the sampled values are shown.

7.5 Linearizing Controller

Since the resulting discrete-time representations are non-linear in their coefficients, the classic linear control theory cannot be directly applied. Therefore, an exact linearization approach (system inversion) is presented that leads – when combined with the system to control – to a linear augmented plant.

Most higher-order continuous system can be decomposed and discretized using $\boldsymbol{\mathcal{Z}}_{\boldsymbol{\delta\Delta}}$ such that the following state-space system

$$\begin{aligned} \boldsymbol{z}[k+1] &= \boldsymbol{A}_{\boldsymbol{\delta\Delta}} \boldsymbol{z}[k] + \boldsymbol{B}_{\boldsymbol{\delta\Delta}} u[k] && (126) \\ y_{\delta\Delta}[k] &= \boldsymbol{C}_{\boldsymbol{\delta\Delta}} \boldsymbol{z}[k] && (127) \end{aligned}$$

is obtained, whereby the matrices are given by

$$\boldsymbol{A}_{\boldsymbol{\delta\Delta}} = \operatorname{diag}\left[\boldsymbol{A}_{\boldsymbol{1}}^{cc}, \boldsymbol{A}_{\boldsymbol{2}}^{cc}, \cdots, a_1^1, a_2^1, \cdots\right] \tag{128}$$

$$\boldsymbol{z}[k] \coloneqq \begin{bmatrix} \boldsymbol{z}_{\boldsymbol{1}}^{cc}[k] \\ \boldsymbol{z}_{\boldsymbol{2}}^{cc}[k] \\ \vdots \\ z_1^1[k] \\ z_2^1[k] \\ \vdots \end{bmatrix} \qquad \boldsymbol{B}_{\boldsymbol{\delta\Delta}} = \begin{bmatrix} \boldsymbol{B}_{\boldsymbol{1}}^{cc} \\ \boldsymbol{B}_{\boldsymbol{2}}^{cc} \\ \vdots \\ b_1^1 \\ b_2^1 \\ \vdots \end{bmatrix} \qquad \boldsymbol{C}_{\boldsymbol{\delta\Delta}} = \begin{bmatrix} c_1^{cc} \boldsymbol{C}_{\boldsymbol{1}}^{cc\,T} \\ c_2^{cc} \boldsymbol{C}_{\boldsymbol{2}}^{cc\,T} \\ \vdots \\ c_1^1 \\ c_2^1 \\ \vdots \end{bmatrix}^T .$$

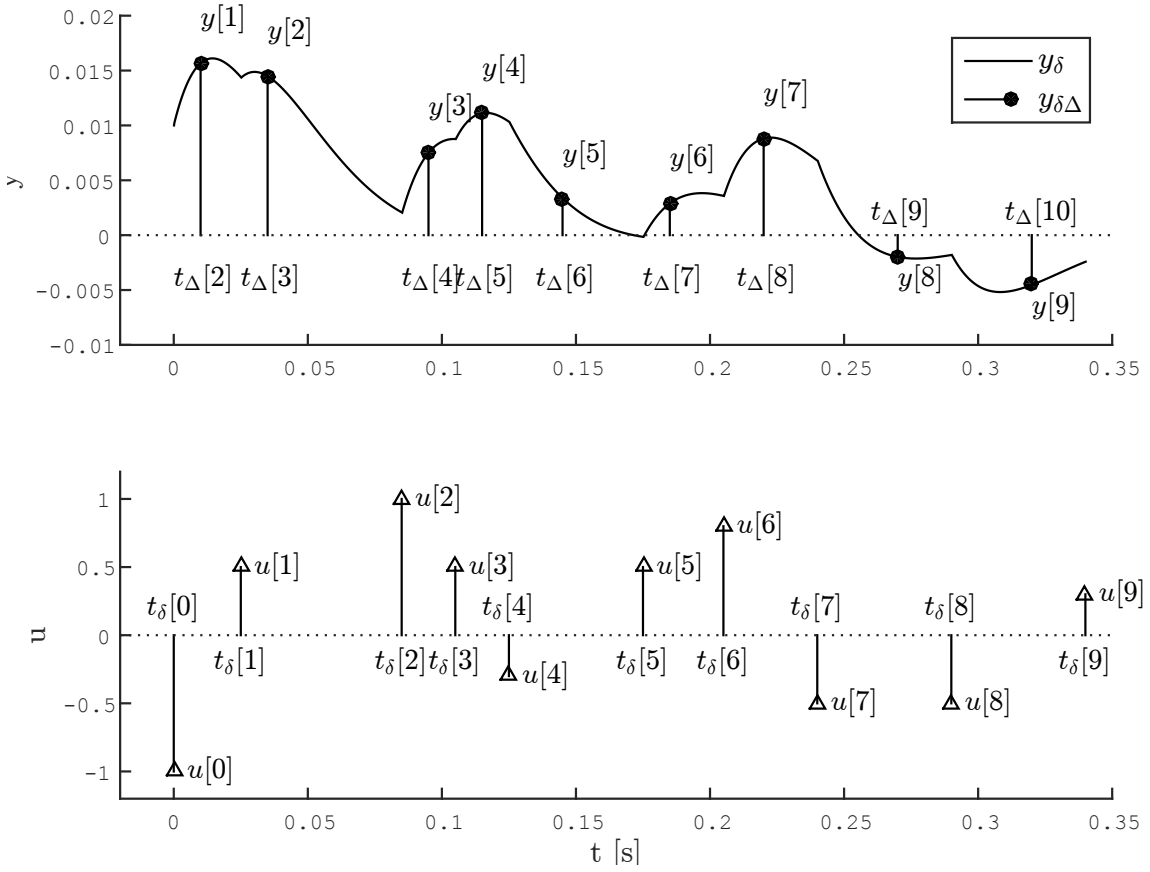

FIGURE 82: *The I/O sequences of the discrete-time system along with the continuous-time output for a second-order system.*

The matrices $\boldsymbol{A}_i^{cc}$, $\boldsymbol{B}_i^{cc}$, a_i^1, and b_i^1 are the coefficients of the discrete-time representations of all partial continuous-time systems obtained by the decomposition. They depend on the time interval $T_\Delta[k]$. The discrete-time states are $\boldsymbol{z}_i^{cc}$ and z_i^1, while c_i^{cc} and c_i^1 are the decomposition's weighting factors.

The overall output of the discrete-time system for the next time step is then:

$$y_{\delta\Delta}[k+1] = \boldsymbol{C}_{\delta\boldsymbol{\Delta}}\boldsymbol{A}_{\delta\boldsymbol{\Delta}}\boldsymbol{z}[k] + \boldsymbol{C}_{\delta\boldsymbol{\Delta}}\boldsymbol{B}_{\delta\boldsymbol{\Delta}}u[k]. \tag{129}$$

By applying the linearizing controller

$$u[k] = \frac{1}{\boldsymbol{C}_{\delta\boldsymbol{\Delta}}\boldsymbol{B}_{\delta\boldsymbol{\Delta}}}\left[-\boldsymbol{C}_{\delta\boldsymbol{\Delta}}\boldsymbol{A}_{\delta\boldsymbol{\Delta}}\boldsymbol{z}[k] + \overline{v}[k]\right], \tag{130}$$

an exact linearization $y_{\delta\Delta}[k+1] = \overline{v}[k]$ with regard to the virtual input (and new actuation variable) $\overline{v}$ is obtained. The herein required state information $\boldsymbol{z}[k]$ can be obtained either by Eq. (126) yielding in a feed-forward control (only possible for asymptotically stable plants) or utilizing an observer.

Internal dynamics Please note that a potentially unstable internal dynamics may be present. Such instabilities usually cause actuation signals suffering from high-frequency oscillations that continuously increase in their amplitude and are unfeasible to be applied in real-world control. A general investigation on a stability criterion has not been performed so far. Hence, stability must be investigated in the individual case. From observations in simulations, it was found that setting the time-interval T_δ to be zero ($T_\delta = 0$), which causes sampling and actuation to happen at the same time, may prevent such oscillations. Sampling times that are non-equal to the actuation time can still be considered in other ways, e.g., by a prediction of the system's output for the next actuation time.

Example for a FES-plant A continuous-time model described by the transfer function (rise time $0.3\,s$, $0.25\,\%$ overshoot)

$$\begin{aligned} G(s) &= \frac{c}{(s-s_\infty)(s^2-2\sigma s+\sigma^2+\omega^2)} \\ &= \frac{c}{(s-s_\infty)(s-\underbrace{(\sigma+j\omega)}_{:=\lambda})(s-\underbrace{(\sigma-j\omega)}_{:=\overline{\lambda}})}, \quad \begin{array}{l} s_\infty = -10,\ \sigma = -3, \\ \omega = 10,\ c = 1090 \end{array} \end{aligned}$$

is considered that describes the typical response of a joint angle (e.g., the shoulder elevation) to electrical stimulation. All initial values are assumed to be zero. The partial fraction decomposition is given by

$$\begin{aligned} G(s) &= A\frac{1}{s-s_\infty} + B\frac{1}{s-\lambda} + C\frac{1}{s-\overline{\lambda}} \\ A &= \frac{c}{(s_\infty-\lambda)(s_\infty-\overline{\lambda})},\ B = \frac{c}{(\lambda-s_\infty)(\lambda-\overline{\lambda})},\ C = \frac{c}{(\overline{\lambda}-s_\infty)(\overline{\lambda}-\lambda)}. \end{aligned}$$

Further, the system G is split into a first-order (G^1) and a second-order (G^{cc}) system with conjugate complex eigenvalues:

$$\begin{aligned} G(s) &= A\frac{1}{s-s_\infty} + \frac{s(B+C)+(-\lambda C-\overline{\lambda}B)}{(s-\lambda)(s-\overline{\lambda})} \\ &= \underbrace{A\frac{1}{s-s_\infty}}_{G^1(s)} + \underbrace{c^{cc}\frac{s-a}{(s-\lambda)(s-\overline{\lambda})}}_{G^{cc}(s)}, \quad a = 2\sigma - s_\infty, \quad c^{cc} = \frac{c}{-\omega^2 - s_\infty^2 + 2s_\infty\sigma - \sigma^2}. \end{aligned}$$

The corresponding state-space system that realizes the transfer function $G^1(s)$ (cf. Sec. 7.3.1) results in the following discrete-time state-space representation:

$$z^1[k+1] = z^1[k]\cdot\underbrace{e^{s_\infty[T_\delta[k-1]+T_\Delta[k]]}}_{a^1} + u[k]\underbrace{e^{s_\infty T_\Delta[k]}}_{b^1}, \quad y^1_{\delta\Delta}[k] = \underbrace{A}_{c^1}, z^1[0] = 0.$$

For the second-order system G^{cc} the following discrete-time state-space system is obtained (cf. Sec. 7.3.2, Case B):

$$\begin{aligned} \boldsymbol{z^{cc}}[k+1] &= \boldsymbol{A^{cc}}\cdot\boldsymbol{z^{cc}}[k] + \boldsymbol{B^{cc}}u[k] \\ y^{cc}_{\delta\Delta}[k] &= c^{cc}\cdot\boldsymbol{C^{cc}}\cdot\boldsymbol{z^{cc}}[k]. \end{aligned}$$

Herein, the matrices $\boldsymbol{A^{cc}}$. $\boldsymbol{B^{cc}}$, $\boldsymbol{C^{cc}}$ and the initial state vector $\boldsymbol{z^{cc}_0}$ are given by

$$\begin{aligned} \boldsymbol{A^{cc}} &= = e^{\sigma T_s[k]}\begin{bmatrix}\cos(\omega T_s[k]) & -\sin(\omega T_s[k])\\ \sin(\omega T_s[k]) & \cos(\omega T_s[k])\end{bmatrix} \\ \boldsymbol{B^{cc}} &= = e^{\sigma T_\Delta[k]}\begin{bmatrix}\cos(\omega T_\Delta[k])\\ \sin(\omega T_\Delta[k])\end{bmatrix} \\ \boldsymbol{C^{cc}} &= = [2r\cos\phi, 2r\sin\phi], \qquad T_s[k] \coloneqq T_\delta[k-1] + T_\Delta[k] \\ \boldsymbol{z^{cc}_0} &= [0,0]^T \end{aligned}$$

$$r = \frac{1}{2}\sqrt{1+[(\sigma-a)/\omega]^2},\ \phi = \tan^{-1}\left[(\sigma-a)/\omega\right].$$

The complete discretized model and its output variable $y_{\delta\Delta}[k] = y^{cc}_{\delta\Delta}[k] + y^1_{\delta\Delta}[k]$ is then brought into the form (126, 127) yielding

$$\boldsymbol{z}[k+1] = \boldsymbol{A_{\delta\Delta}}\boldsymbol{z}[k] + \boldsymbol{B_{\delta\Delta}}u[k] \tag{131}$$

$$y_{\delta\Delta}[k] = \boldsymbol{C_{\delta\Delta}}\boldsymbol{z}[k] \tag{132}$$

$$\boldsymbol{A_{\delta\Delta}} = \operatorname{diag}\left[\boldsymbol{A^{cc}}, a^1\right]$$

$$\boldsymbol{z}[k] \coloneqq \begin{bmatrix}\boldsymbol{z^{cc}}[k]\\ z^1[k]\end{bmatrix} \qquad \boldsymbol{B_{\delta\Delta}} = \begin{bmatrix}\boldsymbol{B^{cc}}\\ b^1\end{bmatrix} \qquad \boldsymbol{C_{\delta\Delta}} = \begin{bmatrix}c^{cc}\boldsymbol{C^{cc}}^T\\ c^1\end{bmatrix}^T.$$

Then, the linearizing controller (cf. 130)

$$u[k] = \frac{1}{\boldsymbol{C_{\delta\Delta}}\boldsymbol{B_{\delta\Delta}}}\left[-\boldsymbol{C_{\delta\Delta}}\boldsymbol{A_{\delta\Delta}}\hat{\boldsymbol{z}}[k] + \overline{v}[k]\right], \text{for } k \geq 0 \tag{133}$$

is applied to u, whereby the required state estimate $\hat{\boldsymbol{z}}$ is calculated by using (131):

$$\hat{\boldsymbol{z}}[k] = \boldsymbol{A}_{\delta\Delta}\hat{\boldsymbol{z}}[k-1] + \boldsymbol{B}_{\delta\Delta}u[k-1], \text{ for } k \geq 1 \tag{134}$$

$$\hat{\boldsymbol{z}}[0] = [0\ 0\ 0]^T. \tag{135}$$

Please note that the system described by Eqs. (133), (134), and (135) must be asymptotically stable to prevent, e.g., oscillations in the actuation variable u. In the considered example, this requirement could be achieved by setting the time-interval T_δ to zero ($T_\delta = 0$).[44] In this example, a fixed, cosine shaped sequence for the sampling frequency ranging from 20 to 50 Hz is defined yielding T_Δ ($T_\delta = 0$) and t_δ. Further, a continuous-time reference trajectory is defined by $r(t) = -(\cos(\pi t_\delta / T_r) - 1)/2$, $T_r = 1.5\,s$ and sampled at t_δ ($r(t_\delta[k])$. The resulting sequence is applied to the linearizing controller $\overline{v}[k] = r(t_\delta[k])$. The obtained I/O sequences, and the continuous-time output are shown in Fig. 83.

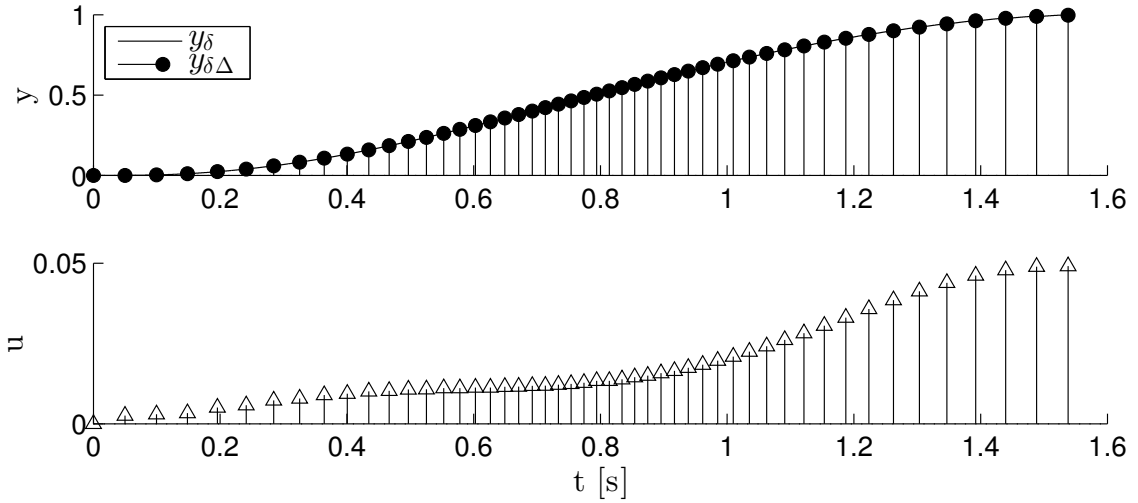

FIGURE 83: *The I/O sequences and the output $y_\delta(t)$ of the FES-system when applying the linearizing feed-forward controller using irregular sampling-times are shown. The sampled reference trajectory $\overline{v}[k] = r(t_\delta[k])\ \forall k$ is exactly tracked by $y_{\delta\Delta}$. Please note that the reference is not shown in this figure as an exact tracking (despite a delay of one sampling step) is achieved.*

7.6 Conclusions and Outlook

A method for the time-discretization of continuous systems under variable actuation and sampling times was presented and analytically evaluated yielding discrete-time state-space systems with non-constant, input dependent coefficients. By a simulation example relevant to the control of neuroprosthetic systems, it could be demonstrated that the obtained gain-scheduled systems can be controlled by an inversion approach that yields a linear dead-beat system. In this approach, the stability of the internal dynamics must be ensured, as otherwise, the actuation variable may become unfeasible to be applied to a real-world system. A systematic analysis is still missing. However, it is hypothesized that sampling and actuation are required to take place at the same time to prevent instabilities. If the output has to be sampled at other time instances, a prediction

[44] Please note that no systematic investigation has been performed on this topic so far.

of the system's output for the next actuation time might be used. Along with the investigations of possible aliasing-effects and the inter-sampling behavior, this is up to future investigations.

8

CONCLUSIONS AND FUTURE WORK

The general aim of this thesis is to improve the applicability of elaborated FES-based systems with a focus on the restoration and the support of arm reaching movements. Up to date, most practically relevant applications of FES use open-loop strategies – successfully in their dedicated application. However, applications like the support or the restoration of arm reaching may benefit from more elaborated FES feedback control that is still under active research. As a contribution to this topic, several approaches that aim to make sophisticated feedback control systems clinically feasible were investigated in this thesis.

Muscle recruitment control Usually one would expect that feedback control approaches applied to FES-based neuroprosthesis significantly enhance the functions of the individual system regarding motor precision, robustness, and adaptivity to the individual patient. The main reason why such approaches generally fail in practice was identified to be the uncertainty of the muscular behavior in response to FES. This uncertainty is commonly caused by the rapid progression of muscle fatigue under FES and the non-linear behavior of stimulated muscles. Therefore, an important topic considered in this thesis was the compensation of muscle fatigue and the linearization of the highly non-linear process of muscle recruitment as outlined in Chapter 3. Herein, a feedback of the stimulation-evoked EMG is used to detect the muscle's response to the applied stimulation that is adjusted to realize a given level of muscle recruitment. This approach cancels time-variances and some non-linearities in the process of motor unit recruitment. Tests in five healthy subjects have demonstrated the effectiveness of this approach. Further, the functionality was successfully tested in two stroke patients.

A neuroprosthesis for arm weight relief The concept of muscle-recruitment control was then applied in a neuroprosthesis to support the arm elevation in partially paralyzed stroke patients as described in Chapter 4. Based on the measured shoulder elevation angle, a FES-induced muscle recruitment – proportionally to this angle – is generated in the shoulder deltoid muscle. This yields an arm weight relief, which reduces the needed volitional activity. As shown in the results obtained from five healthy subjects, indeed less residual voluntary activity is required to perform functional tasks. An analytical investigation proves the asymptotic stability of the positive feedback loop for support factors less than 100%.

In the clinical tests of this approach in two stroke patients, the support factor was manually tuned to obtain the highest support of arm elevation. Herein, overcompensation of the arm weight has to be avoided as this typically causes difficulties for the patient in returning to his rest position. It was observed that the proposed concept is feasible to restore paretic arm elevation movements in stroke patients. In one patient, even the full restoration of the arm elevation was possible.

Automatic adaption of the weight-support level To automatically perform the adjustment of the support factor an adaptive control scheme has been presented in Sec. 4.7. This approach relies on repetitive movement trials as encountered in the rehabilitation of stroke patients. After each trial, the support factor is adapted. Tests in one healthy subject show the feasibility of the chosen approach. However, tests on patients have not been performed yet.

A model for hybrid muscle activation The controller for the support-factor adaptation relies on a model that describes the influence of FES-induced and volitional activity on the amount of arm elevation. In Sec. 4.7 a linear model is herein assumed. However, the actual behavior is non-linear (cf. Sec. 2.6). Hence, in a fist investigation, an ANN-based model was developed to obtain a more realistic representation for describing the resulting arm elevation (cf. Appendix A). The model-structure has been validated in two healthy subjects and yields a performance feasible to the targeted application.

Please note that the developed model is currently not suitable to be applied to the adaptation algorithm of the weight compensation controller since the level of muscle recruitment should be the model input instead of the stimulation intensity.

Combining FES with an exoskeleton The combination of a passive exoskeleton for gravity compensation with FES (Chapter 5) forms an interesting approach concerning fatigue reduction and the guidance of FES-induced motion. Normally, a precise positioning of the hand using only FES is difficult to achieve when the arm is completely paralyzed. In combination with the used exoskeleton that allows locking each degree of freedom individually, a positioning was possible as shown in tests involving five healthy subjects. To allow a daily-live application of the presented system, further integration steps must be performed as the system is currently immobile. This immobility is due to the large effort spent for sensor technology to detect the patient's intention and to further detect object positions.

Co-activation in antagonistic muscle pairs As the dynamic positioning performance in the previously investigated neuroprosthesis for restoring reaching functions with FES (Chapter 5) is significantly lower compared to physiologic movements, a potential improvement in terms of motor precision and movement speed was investigated in Chapter 6. The approach applies to the antagonistic muscle pair formed by the anterior and posterior deltoid muscle.

A linearization controller is proposed that allow realizing a given joint torque and a level of co-activation. In combination with a joint angle controller, an increased co-activation during the phases in which switching between muscles occurs is present. This effect potentially (among others) yielded a positioning performance much higher than the one obtained in Chapter 5. Though, a further, detailed investigation has not been performed yet. Also, the effects of an increased level of co-activation are not considered in the investigations. This approach may be extended by, e.g., increasing the co-activation level also for holding postures such that external disturbances only have a reduced influence on the maintained position.

Variable stimulation frequencies The effects of the fast progression of muscle fatigue can be compensated by the presented recruitment control strategy (cf. Chapter 3). This compensation is

accompanied, however, by a continuously increasing average stimulation level that can only be increased up to the maximally tolerated stimulation intensity. Once this is reached, the effects of muscle fatigue can no longer be compensated. By choosing lower stimulation frequencies, the progression of fatigue may be delayed. As lower stimulation frequencies also mean lower update rates of the control system, the motion performance likely decreases. Hence, it is suggested to adaptively vary the stimulation rate as needed, e.g., for repositioning a high rate may be used and once a posture is entered, the rate may be decreased. To allow variable sampling frequencies in discrete-time motion controllers, a new method to design discrete-time control systems that consider irregular sampling and actuation times has been developed. An open-loop control simulation example relevant to FES is given that shows how the actuation variable is modulated for a given sequence of inter-pulse interval durations to realize a given output trajectory. Though the principle has been demonstrated, there is still much further work left including investigations on the stability of the internal dynamics, closed-loop control, and the application to a real FES-neuroprosthesis. For the latter, decision algorithms must be developed that adjust the applied stimulation intensity. As described in the next section 8.1, this approach should be integrated with recruitment control and the generation of artificial co-activations.

8.1 Future Research

Muscle recruitment control The recruitment control system has been evaluated for the medial shoulder deltoid muscle. It is expected to perform sufficiently well when applied to other muscles as well. This should be investigated in future work. Especially, the optimal placement of the EMG electrodes must be investigated for each muscle type individually.

The combination of recruitment control with the estimation of the volitional activity is currently constrained to one stimulation channel or only possible in case of negligible crosstalk effects in multi-channel set-ups. This is because of the timing constraints in the time-multiplexed approach causing the estimation of the volitional EMG to be infeasible. Further, for a three-channel stimulation, the maximally possible effective stimulation frequency would be too low.

Even for muscles that are not close to each other, crosstalk effects can be observed in separated EMG-measurements. In such cases, the application of the time-multiplex extension for recruitment control is beneficial. For advanced neuroprosthesis, that might consider the restoration or support of arm elevation, elbow extension, and hand functions at the same time, a larger number of stimulated muscles are involved. Further, the acquisition of the volitional EMG is often beneficial for user control.

By weakening the requirement of updating the individual recruitment controller in a multi-channel setup after each stimulation pulse applied, the time-multiplexing approach could be extended to allow the stimulation of more than two muscles including the measurement of the volitional EMG.

Enhancing the detection of the patient's intention through the volitional activity The detection of the volitional activity is a key component to realize a user control of neuroprostheses. In case of the arm elevation support as presented in Chapter 4, the measurement of the volitional EMG is not

required as the volitional activity is detected indirectly via the joint angle measurement[45]. This is possible because movements are performed against gravity. For the support of other functions, e.g., the elbow-joint extension, measurements of the volitional EMG are still required. These, however, are subjected to a low signal to noise ratio rendering, e.g., threshold-based classification approaches difficult to implement. Last but not least, the relationship between the actual effect caused by a volitional component in hybrid muscle activations and the measured vEMG is difficult to model. A model for describing hybrid muscle activation as described in Appendix A may improve the control of hybrid neuroprosthesis. This model is currently describing the relation between the stimulation intensity, the estimated volitional activity, and a joint angle. It must be integrated into the recruitment control framework in future research.

Integrating (multi-channel) recruitment control, co-activation control strategies, user-intention detection, and variable stimulation frequencies In the recruitment control approach, it is assumed that the dynamics of the control loop do not depend on the stimulation frequency. Hence, it should be straightforward to combine recruitment control with the proposed concept of varying the stimulation frequency. Nevertheless, this assumption must be proven, of course. Further, the influence of the stimulation frequency on the muscle activation level, i.e., the contraction strength must be investigated. During holding postures, wherein an increased level of co-activation may be applied, the stimulation frequency can be decreased so that the progression of muscle fatigue becomes slower during these phases.

8.2 Résumé & Exploitation

Most approaches considered in this thesis can be categorized into *applied control* and *medical engineering*. Some of them, e.g., variable stimulation frequencies and the model for describing hybrid muscle activations, are currently of a more theoretical nature as they have not (yet) been applied to neuroprosthetic control systems.

However, they are expected to form a basis for future improvements in the control of neuroprosthetic systems. The control of antagonistic muscle pairs using co-activation is still in an early stage. However, it can be seen as a proof of concept to increase motion performance. These investigations may be applied in the restoration of reaching functions, for example. The most fundamental approach is likely the EMG-based control of the muscular recruitment. As an underlying control system to simplify modeling and control of FES-activated muscles, many potential applications in neuroprostheses are imaginable.

The approaches presented in Chapter 5 (Exoskeleton-based support of arm movements) and Chapter 4 (Arm weight relief) directly target the assistance of neurologically impaired patients. Because of its simplicity regarding required devices and electrodes to be placed, the latter has a higher potential to be used in daily-live situations by patients. However, an extension to support elbow-joint extension movements is often beneficial to additionally compensate for the effects of an increased muscle tone in the biceps.

[45] In case the adaptive control system is not used.

A

A MODEL TO DESCRIBE HYBRID MUSCLE ACTIVATION

The adaptive control scheme used to automatically tune the parameter (support factor) of the arm weight relief neuroprosthesis described in Chapter 4 relies on a model to describe muscle activation under hybrid conditions (FES and volitionally activated, cf. Sec. 2.6). Therefore, in the design of the controller, a linear model is assumed. However, the actual behavior is strongly non-linear. If trial-based movements are similar in their respective realization (e.g., regarding duration and movement trajectory), the assumption of linearity limits the applicability of the presented adaptation approach: The individual trials are required to be similar in their duration and movement paths. If they vary significantly (like in support of activities of daily living), the non-linearities may hinder the successful adaptation of the support factor.

Hence, a more sophisticated, non-linear model for describing joint motions induced by concurrently present voluntary- and FES-induced muscle activation is proposed. It is based on a Hammerstein model – as commonly used in feedback-controlled FES – and exemplarily applied to describe the shoulder elevation joint angle. One component of a Hammerstein muscle model is a static input non-linearity that depends on the stimulation intensity. To additionally incorporate voluntary contributions, the static non-linearity is extended by a second input describing the intensity of the voluntary contribution that is estimated by electromyography (EMG) measurements – even during active FES. An Artificial Neural Network (ANN) is used to describe the static input non-linearity. The output of the ANN drives a second-order linear dynamical system that describes the combined muscle activation and joint angle dynamics. The tunable parameters are adapted to the individual subject by a system identification approach using previously recorded I/O data. The model has been validated in two healthy subjects yielding RMS values for the joint angle error of 3.56° and 3.44°, respectively.

The methods and results presented in this chapter have been previously published in

- [81] C. Klauer, M. Irmer, and T. Schauer. "A muscle model for hybrid muscle activation". In: *Current Directions in Biomedical Engineering* 1.1 (2015), pp. 386–389. ISSN: 2364-5504. DOI: 10.1515/cdbme-2015-0094.

A.1 Methods

Typically, models describing FES-activated muscles (cf. Sec. 2.6) consider muscle recruitment in form of the static recruitment function that only depends on the stimulation intensity. To consider hybrid muscle activations, the static input function is extended by adding a second input – the normalized voluntary activity $\gamma^* \in [0,1]$. As shown in Fig. 84, this extended recruitment function is described by an Artificial Neural Network (ANN) that uses Local Linear Models (LLM) weighted by Radial Basis (RB) functions (cf. Fig. 85). Four normalized radial basis functions

$$\Phi_i(v,\gamma^*) = \frac{\mu_i(v,\gamma^*)}{\sum_{n=1}^{4} \mu_n(v,\gamma^*)},\ i = \{1,2,3,4\} \tag{136}$$

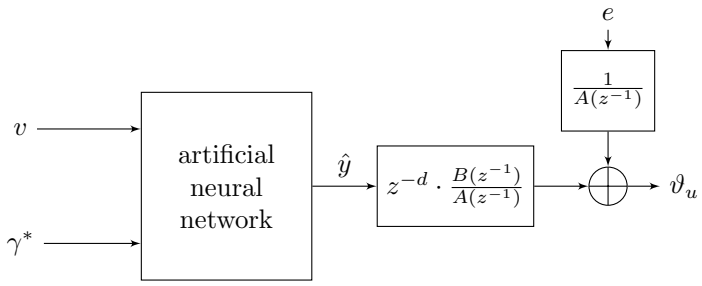

Figure 84: *The used model consists of a static input function (artificial neural network), that describes the motor unit recruitment, and a linear transfer function model (AutoRegressive model with eXogenous input (ARX)), that captures the muscle activation dynamics and the joint motion.*

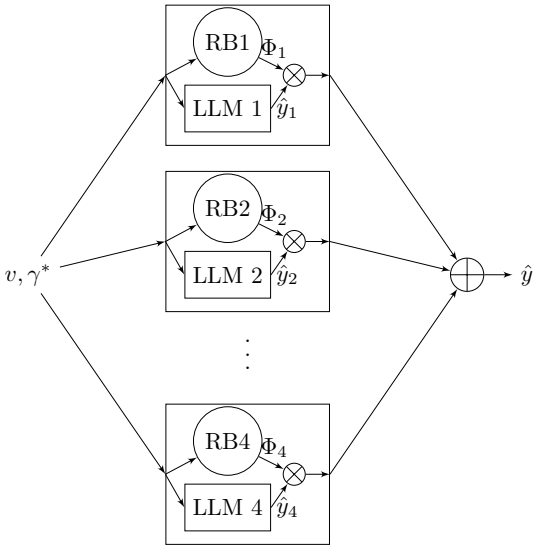

Figure 85: *The applied structure for the artificial neural network that involves four neurons.*

TABLE 11: *Parameters of the ANN.*

i (neuron)	$c_{i,v}$	c_{i,γ^*}	$\sigma_{i,\gamma^*} = \sigma_{i,v}$
1	0.25	0.25	0.2167
2	0.25	0.75	0.2167
3	0.75	0.25	0.2167
4	0.75	0.75	0.2167

based on standard radial basis functions

$$\mu_i(v, \gamma^*) = \exp\left(-\frac{1}{2}\left(\frac{(v - c_{i,v})^2}{\sigma_{i,v}^2} + \frac{(\gamma^* - c_{i,\gamma^*})^2}{\sigma_{i,\gamma^*}^2} \right) \right) \tag{137}$$

are used, which forms a compromise between model complexity and the ability to describe I/O data. The parameters of the radial basis functions are chosen concerning [130] and summarized in Tab. 11. The normalized RB functions are combined with four local linear models to yield the neurons whose outputs are superposed yielding the output of the ANN:

$$\hat{y} = \sum_{i=1}^{4} \underbrace{(w_{i,0} + w_{i,v} v + w_{i,\hat{\gamma}} \gamma^*)}_{\hat{y}_i} \cdot \Phi_i(v, \gamma^*). \tag{138}$$

To describe the combined muscle activation dynamics and joint motion, an AutoRegressive model with eXogenous input (ARX)) [130] (a linear dynamic transfer function model) is used:

$$\hat{\vartheta}[k] = \frac{q^{-m}}{1 + a_1 q^{-1} + a_2 q^{-2}} \hat{y}[k], \tag{139}$$

where $\hat{\vartheta}[k]$ is the joint angle at sampling instant k and q^{-1} is the one-step backwards shift operator ($q^{-1} s(k) = s(k-1)$). The time delay of $m = 1$ sampling instants matches the typically observed delay in the recorded I/O-data. The tunable parameters are combined in the parameter vector

$$\boldsymbol{\Theta} = [w_{1,0}, w_{1,v}, w_{1,\gamma^*}, \cdots, w_{4,0}, w_{4,v}, w_{4,\gamma^*}, a_1, a_2]. \tag{140}$$

To adapt them to the individual subject and muscle condition, I/O data are recorded during an identification experiment, and a linear least squares optimization is performed yielding the optimal parameter set $\boldsymbol{\Theta}^*$ that minimizes the cost function

$$J(\boldsymbol{\Theta}) = \sum_{k=0}^{N} (\hat{\vartheta}[k](\boldsymbol{\Theta}, \gamma^*[k], v[k]) - \vartheta[k])^2, \tag{141}$$

where $\vartheta[k]$ is the recorded joint angle.

To obtain I/O data, an experimental procedure is proposed in which the stimulation intensity is increased stepwise (five levels, linear increase of the level's intensity) to the upper well-tolerated intensity. During the time periods in which the stimulation intensity remains constant (always lasting 6 s), the subject is instructed to voluntarily elevate his arm to a given joint angle of approximately 50° for 2 s.

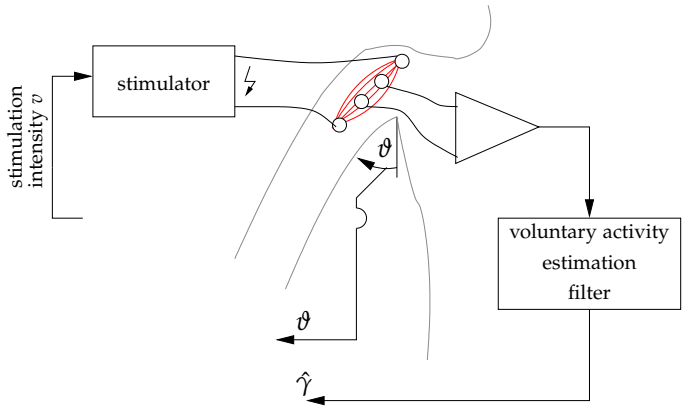

FIGURE 86: *Experimental Set-up.*

A.2 Experimental Set-up

To demonstrate the feasibility of the proposed hybrid model, it is exemplarily applied to the shoulder elevation movement against gravity, as shown in Fig. 86.

The raw EMG-measurements in-between two stimulation pulses are filtered using the approach described in Sec. 3.2.2 yielding $\hat{\gamma}$ for the intensity of the voluntary contribution. This estimate is normalized to the maximally occurring level of volitional muscle activity yielding the normalized estimate $\hat{\gamma}^*$ (range [0,1]). For later use in the model, this noisy volitional muscle activity is low-pass filtered using a non-causal fourth-order Butterworth filter with zero phase shift and a cut-off frequency of 27 Hz yielding the input γ^* (range [0,1]) to the neural network. The stimulation intensity v is applied in terms of a normalized charge yielding current amplitude and pulse width of the applied bi-phasic stimulation pulses as described in Sec. 2.4.

A.3 Results

The proposed experimental procedure has been performed twice for two healthy subjects yielding one training and one validation dataset for each subject. Herein, the subjects are asked to perform five trials of volitional arm elevation movements. In between these trials, the stimulation intensity v is increased stepwise and then held constant for a duration of 6 s.

The model parameters were identified, and the output ϑ of the obtained model was then simulated (not predicted) for the inputs of the training dataset and compared to the measured output to evaluate the model fit. The result in terms of the Root Mean Square (RMS) error is 3.3° for subject A and 2.67° for subject B.

To validate the model, the inputs of the validation dataset are used to simulate the output of the obtained model. The input signals as well as the simulated and measured output angle are shown in Fig. 87 and Fig. 88 for both subjects. In this validation, RMS errors of 3.56° and 3.44° for subject A and subject B have been obtained, respectively.

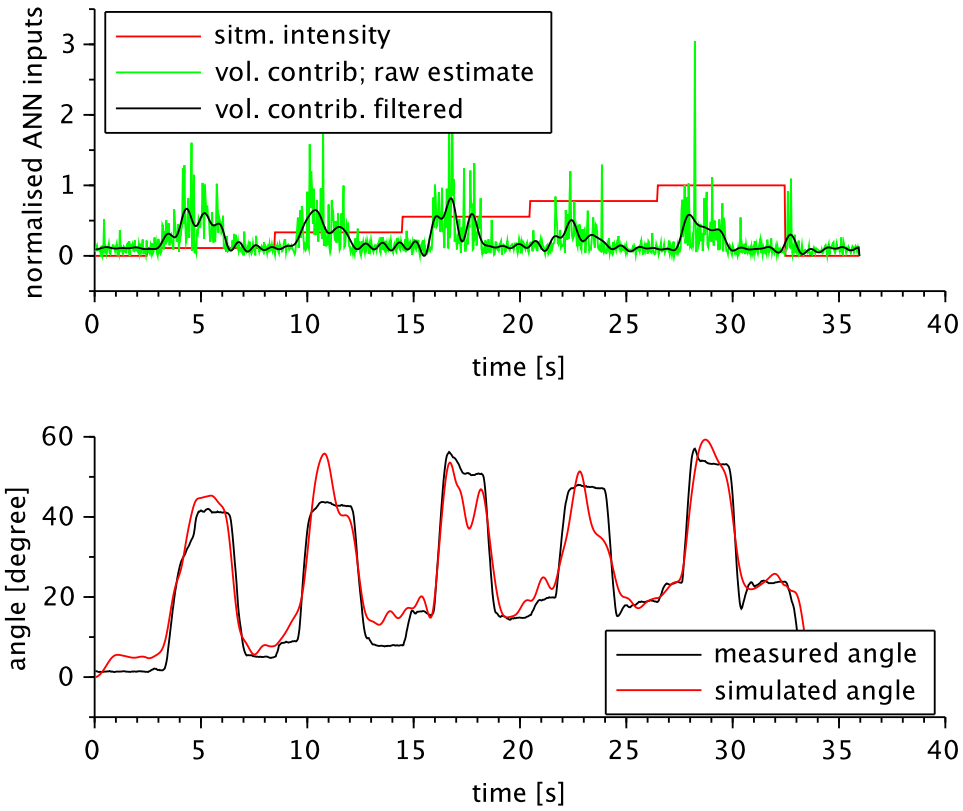

FIGURE 87: *The result of the model validation for subject A.*

A.4 CONCLUSIONS

For the prediction and simulation of joint angle movements, an ANN-based dynamical model has been developed and was tested in two healthy subjects. The obtained small RMS errors – both for model fit and validation – show the feasibility of the proposed joint angle prediction in the considered range of about 50°. The required time duration of approximately half a minute for the identification procedure is feasible to the time constraints in clinical environments. The observed model accuracy is high despite using a Hammerstein model structure that is usually applied to describe isometric muscle contractions only[46]. A Hill-type muscle model structure can be considered as an extension of this approach if the accuracy of the proposed model decreases for larger joint angle ranges.

This model forms an initial investigation of hybrid muscle activations as present in the arm weight-relief neuroprosthesis presented in Chapter 4. Herein, a linear model was assumed to describe the behavior of hybrid muscle activation. The described adaptive control loop uses measurements of the volitional activity and compares them to the resulting joint angle based on this linear assumption. A better understanding of the actual hybrid behavior may potentially lead to further improvements of the adaptive control loop as outlined in Sec. 4.8.

[46]Especially, the non-linear dependency of the muscle torque on the joint angle and velocity is neglected.

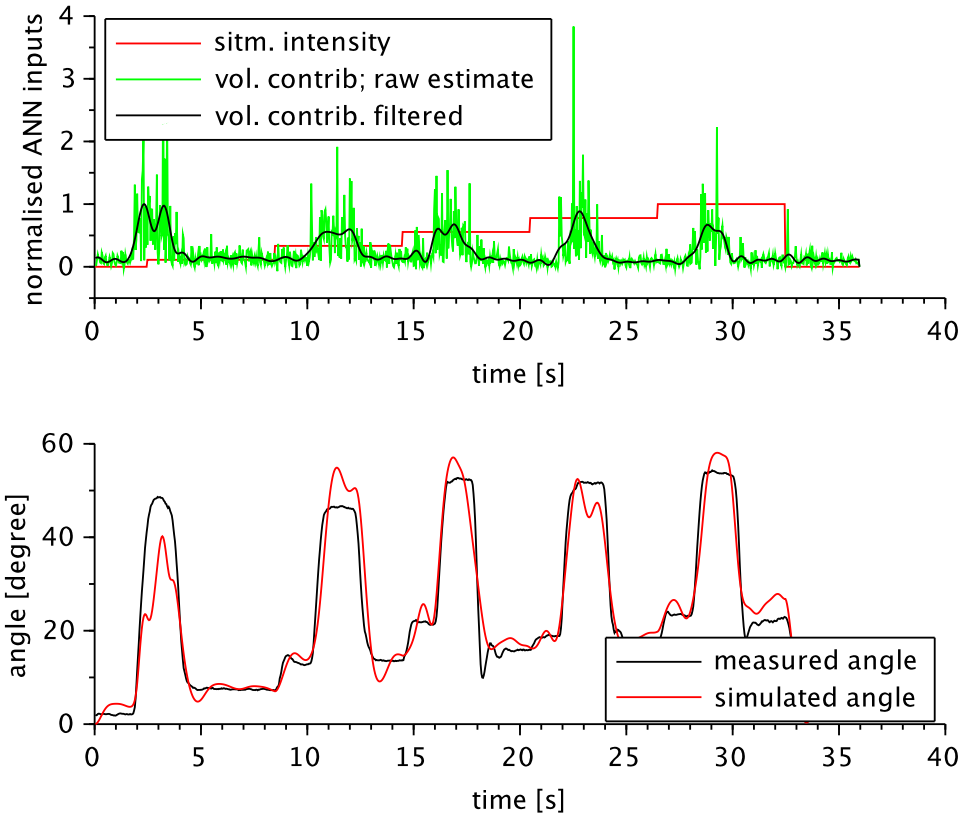

FIGURE 88: *The result of the model validation for subject B.*

Concerning the long-term accuracy, however, difficulties caused by time-variances in the muscle's behavior may be present. Herein, important factors are the rapidly progressing muscle fatigue under FES and in case of stroke patients, a potential time-variant spasticity. To tackle these issues, it is suggested to perform a periodic re-calibration of the model in trial to trial based training procedures. Herein, it is expected that I/O data obtained during FES-supported training for motor re-learning are also feasible to the parameter estimation. Another approach, worth to be investigated, would be a parameter estimation using Recursive Least Squares (RLS) during training. Both approaches would not require interventions or additional effort to be performed during training sessions.

Future work The proposed model describes the stimulation effect (joint angle) dependent on the stimulation intensity, whose influence on the muscle recruitment is known to be time-variant. The estimation of the stimulation-evoked muscle recruitment $\hat{\lambda}$ has been shown to be less dependent on such time-varying effects in Chapter 3. Therefore, it is likely beneficial to substitute the stimulation input of the ANN by the estimated recruitment-level $\hat{\lambda}$.

Future work should also consider multiple muscles that act on one joint and, finally, investigations in stroke patients.

B

REFERENCES

[1] J. J. Abbas and R. J. Triolo. "Experimental evaluation of an adaptive feedforward controller for use in functional neuromuscular stimulation systems". In: *IEEE Transactions on Rehabilitation Engineering* 5.1 (1997), pp. 12–22. ISSN: 1063-6528. DOI: 10.1109/86.559345.

[2] A. M. Acosta, R. F. Kirsch, and F. C. T Van der Helm. "Feasibility of restoring shoulder function in individuals with C3-C4 spinal cord injury". In: *Proc. of the 6th Annual International FES Society Conference*. Cleverland, Ohio, 2001.

[3] A Bolu Ajiboye, Francis R Willett, Daniel R Young, William D Memberg, Brian A Murphy, Jonathan P Miller, Benjamin L Walter, Jennifer A Sweet, Harry A Hoyen, Michael W Keith, et al. "Restoration of reaching and grasping movements through brain-controlled muscle stimulation in a person with tetraplegia: a proof-of-concept demonstration". In: *The Lancet* 389.10081 (2017), pp. 1821–1830.

[4] J. Allin and G. F. Inbar. "FNS Control Schemes for the Upper Limb". In: *IEEE Transactions on Biomedical Engineering* BME-33.9 (Sept. 1986), pp. 818–828. ISSN: 0018-9294. DOI: 10.1109/TBME.1986.325775.

[5] Naif B Almutairi, Mo-Yuen Chow, and Yodyium Tipsuwan. "Network-based controlled DC motor with fuzzy compensation". In: *Industrial Electronics Society, 2001. IECON'01. The 27th Annual Conference of the IEEE*. Vol. 3. IEEE. 2001, pp. 1844–1849.

[6] E. Ambrosini, S. Ferrante, T. Schauer, C. Klauer, M. Gaffuri, G. Ferrigno, and A. Pedrocchi. "A myocontrolled neuroprosthesis integrated with a passive exoskeleton to support upper limb activities". In: *Journal of Electromyography and Kinesiology* 24.2 (2014), pp. 307–317. ISSN: 1873-5711. DOI: 10.1016/j.jelekin.2014.01.006.

[7] E. Ambrosini, S. Ferrante, M. Tibiletti, T. Schauer, C. Klauer, G. Ferrigno, and A. Pedrocchi. "An EMG-controlled neuroprosthesis for daily upper limb support: A preliminary study". In: *Proc. of the 33rd Annual International Conference of the IEEE Engineering in Medicine and Biology Society (EMBC)*. 2011, pp. 4259–4262. DOI: 10.1109/IEMBS.2011.6091057.

[8] E. Ambrosini, T. Schauer, C. Klauer, A. Pedrocchi, G. Ferrigno, and S. Ferrante. "Control system for neuro-prostheses integrating induced and volitional effort". In: *IFAC-PapersOnLine*. 9th IFAC Symposium on Biological and Medical Systems BMS 2015, Berlin, Germany, 31 August-2 September 2015 48.20 (2015), pp. 327–332. ISSN: 2405-8963. DOI: 10.1016/j.ifacol.2015.10.160.

[9] E. Ambrosini, T. Schauer, C. Klauer, A. Pedrocchi, G. Ferrigno, and S. Ferrante. "Control system for neuro-prostheses integrating induced and volitional effort". In: *IFAC-PapersOnLine*. 9th IFAC Symposium on Biological and Medical Systems BMS 2015, Berlin, Germany, 31 August-2 September 2015 48.20 (2015), pp. 327–332. ISSN: 2405-8963. DOI: 10.1016/j.ifacol.2015.10.160.

[10] Adolfo Anta and Paulo Tabuada. "Self-triggered stabilization of homogeneous control systems". In: *American Control Conference, 2008*. IEEE. 2008, pp. 4129–4134.

[11] Karl-Erik Årzén. "A simple event-based PID controller". In: *Proc. 14th IFAC World Congress*. Vol. 18. 1999, pp. 423–428.

[12] K. J. Åström and B. Wittenmark. *Computer-Controlled Systems: Theory and Design*. Prentice Hall, 1997.

[13] Karl J Aström. "Event based control". In: *Analysis and design of nonlinear control systems*. Springer, 2008, pp. 127–147.

[14] Karl J Astrom and Bjorn Wittenmark. *Computer-Controlled Systems: Theory and Design*. 3rd. Prentice Hall, 1996.

[15] Richard V Baratta, Bing-He Zhou, Moshe Solomonow, and Robert D D'Ambrosia. "Force feedback control of motor unit recruitment in isometric muscle". In: *Journal of Biomechanics* 31.5 (1998), pp. 469–478. ISSN: 0021-9290. DOI: 10.1016/S0021-9290(98)00042-6. URL: http://www.sciencedirect.com/science/article/pii/S0021929098000426 (visited on 04/08/2013).

[16] Ruth N Barker, Sandra G Brauer, and Richard G Carson. "Training of reaching in stroke survivors with severe and chronic upper limb paresis using a novel nonrobotic device". In: *Stroke* 39.6 (2008), pp. 1800–1807.

[17] Gergely I Barsi, Dejan B Popovic, Ina M Tarkka, Thomas Sinkjær, and Michael J Grey. "Cortical excitability changes following grasping exercise augmented with electrical stimulation". In: *Experimental brain research* 191.1 (2008), pp. 57–66.

[18] Dimitra Blana, Robert F Kirsch, and Edward K Chadwick. "Combined feedforward and feedback control of a redundant, nonlinear, dynamic musculoskeletal system". In: *Medical & biological engineering & computing* 47.5 (2009), pp. 533–542.

[19] A.P.L. Bó and and P. Poignet. "Tremor attenuation using FES-based joint stiffness control". In: *Robotics and Automation (ICRA), 2010 IEEE International Conference on*. May 2010, pp. 2928–2933. DOI: 10.1109/ROBOT.2010.5509560.

[20] A. Bó, Lucas O. da Fonseca, and Ana Carolina C. de Sousa. "FES-induced co-activation of antagonist muscles for upper limb control and disturbance rejection". In: *Medical Engineering & Physics* 38.11 (2016), pp. 1176–1184. ISSN: 1350-4533. DOI: http://dx.doi.org/10.1016/j.medengphy.2016.07.004.

[21] Antonio P.L. Bo and Herlandson C. Moura. "Elbow Control using Functional Electrical Stimulation: an Experimental Comparison of Different Control Strategies". In: *IFAC-PapersOnLine, BMS 2015* 48.20 (2015), pp. 343–347. ISSN: 2405-8963. DOI: http://dx.doi.org/10.1016/j.ifacol.2015.10.163. URL: http://www.sciencedirect.com/science/article/pii/S2405896315020546.

[22] David AE Bolton, James H Cauraugh, and Heather A Hausenblas. "Electromyogram-triggered neuromuscular stimulation and stroke motor recovery of arm/hand functions: a meta-analysis". In: *Journal of the neurological sciences* 223.2 (2004), pp. 121–127.

[23] O. Brend, C. Freeman, and M. French. "Multiple-Model Adaptive Control of Functional Electrical Stimulation". In: *IEEE Transactions on Control Systems Technology* 23.5 (Sept. 2015), pp. 1901–1913. ISSN: 1063-6536. DOI: 10.1109/TCST.2015.2394508.

[24] Ida Bromley. *Tetraplegia and paraplegia: a guide for physiotherapists*. Elsevier Health Sciences, 2006.

[25] Anne M. Bryden, William D. Memberg, and Patrick E. Crago. "Electrically stimulated elbow extension in persons with C5/C6 tetraplegia: A functional and physiological evaluation". In: *Archives of Physical Medicine and Rehabilitation* 81.1 (Jan. 2000), pp. 80–88. ISSN: 0003-9993. DOI: 10.1016/S0003-9993(00)90226-0. URL: http://www.archives-pmr.org/article/S0003999300902260/abstract (visited on 07/16/2014).

[26] Etienne Burdet, Rieko Osu, David W Franklin, Theodore E Milner, and Mitsuo Kawato. "The central nervous system stabilizes unstable dynamics by learning optimal impedance". In: *Nature* 414.6862 (2001), pp. 446–449.

[27] J. Cauraugh, K. Light, S. Kim, M. Thigpen, and A. Behrman. "Chronic motor dysfunction after stroke: recovering wrist and finger extension by electromyography-triggered neuromuscular stimulation". In: *Stroke* 31.6 (June 2000), pp. 1360–4.

[28] Mauricio G Cea and Graham C Goodwin. "Event based sampling in non-linear filtering". In: *Control Engineering Practice* 20.10 (2012), pp. 963–971.

[29] EK Chadwick, D Blana, JD Simeral, J Lambrecht, Sung-Phil Kim, AS Cornwell, DM Taylor, LR Hochberg, JP Donoghue, and RF Kirsch. "Continuous neuronal ensemble control of simulated arm reaching by a human with tetraplegia". In: *Journal of neural engineering* 8.3 (2011), p. 034003.

[30] Gwo-Ching Chang, Jer-Junn Lub, Gon-Der Liao, Jin-Shin Lai, Cheng-Kung Cheng, Bor-Lin Kuo, and Te-Son Kuo. "A neuro-control system for the knee joint position control with quadriceps stimulation". In: *IEEE transactions on rehabilitation engineering* 5.1 (1997), pp. 2–11.

[31] JJ Chen and Nan-Ying Yu. "The validity of stimulus-evoked EMG for studying muscle fatigue characteristics of paraplegic subjects during dynamic cycling movement". In: *Rehabilitation Engineering, IEEE Transactions on* 5.2 (1997), pp. 170–178.

[32] Naomi C. Chesler and William K. Durfee. "Surface EMG as a fatigue indicator during FES-induced isometric muscle contractions". In: *Journal of Electromyography and Kinesiology* 7.1 (1997), pp. 27–37. URL: http://www.sciencedirect.com/science/article/pii/S1050641196000168.

[33] Edward A Clancy, Lukai Liu, Pu Liu, and Daniel V Zandt Moyer. "Identification of constant-posture EMG–torque relationship about the elbow using nonlinear dynamic models". In: *Biomedical Engineering, IEEE Transactions on* 59.1 (2012), pp. 205–212.

[34] P. E. Crago, N. Lan, P. H. Veltink, J. J. Abbas, and C. Kantor. "New control strategies for neuroprosthetic systems". In: *Journal of Rehabilitation Research & Development* 33.2 (1996), pp. 158–172.

[35] Jun Ding, Anthony S. Wexler, and Stuart A. Binder-Macleod. "A predictive model of fatigue in human skeletal muscles". In: *Journal of Applied Physiology* 89.4 (2000), pp. 1322–1332. ISSN: 8750-7587. eprint: http://jap.physiology.org/content/89/4/1322.full.pdf. URL: http://jap.physiology.org/content/89/4/1322.

[36] W. K. Durfee. "Task-based methods for evaluating electrically stimulated antagonist muscle controllers". In: *Transactions on Biomedical Engineering, IEEE*. IEEE 36.3 (1989), pp. 309–321. ISSN: 0018-9294. DOI: 10.1109/10.19852.

[37] W. K. Durfee and J. T. Dennerlein. "EMG as a feedback signal in surfaces FES applications: issues and preliminary results". In: *Proceedings of the Annual International Conference of the IEEE Engineering in Engineering in Medicine and Biology Society, 1989. Images of the Twenty-First Century*. 1989, 1009–1010 vol.3. DOI: 10.1109/IEMBS.1989.96059.

[38] W. K. Durfee and K. E. MacLean. "Methods for estimating isometric recruitment curves of electrically stimulated muscle". In: *Transactions on Biomedical Engineering, IEEE*. IEEE 36.7 (1989), pp. 654–667.

[39] A. Erfanian, H.J. Chizeck, and R.M. Hashemi. "Using evoked EMG as a synthetic force sensor of isometric electrically stimulated muscle". In: *IEEE Transactions on Biomedical Engineering* 45.2 (1998), pp. 188–202.

[40] Eduardo H. Estigoni, Ché Fornusek, Richard M. Smith, and Glen M. Davis. "Evoked EMG and Muscle Fatigue During Isokinetic FES-Cycling in Individuals With SCI". In: *Neuromodulation: Technology at the Neural Interface* 14.4 (2011), pp. 349–355. ISSN: 1525-1403. DOI: 10.1111/j.1525-1403.2011.00354.x. URL: http://dx.doi.org/10.1111/j.1525-1403.2011.00354.x.

[41] PD Faghri, MM Rodgers, RM Glaser, JG Bors, C Ho, and P Akuthota. "The effects of functional electrical stimulation on shoulder subluxation, arm function recovery, and shoulder pain in hemiplegic stroke patients". In: *Archives of physical medicine and rehabilitation* 75.1 (Jan. 1994), pp. 73–79. ISSN: 0003-9993. URL: http://europepmc.org/abstract/MED/8291967.

[42] M. Ferrarin, F. Palazzo, R. Riener, and J. Quintern. "Model-based control of FES-induced single joint movements". In: *IEEE Transactions on Neural Systems and Rehabilitation Engineering* 9.3 (2001), pp. 245–257.

[43] H. M. Franken, P. H. Veltink, G. Baardman, R. A. Redmeyer, and H. B. K. Boom. "Cycle-to-cycle control of swing phase of paraplegic gait induced by surface electrical stimulation". In: *Medical and Biological Engineering and Computing* 33.3 (May 1995), pp. 440–451. ISSN: 1741-0444. DOI: 10.1007/BF02510528.

[44] C. T Freeman, A. M Hughes, J. H Burridge, P. H Chappell, P. L Lewin, and E. Rogers. "A model of the upper extremity using FES for stroke rehabilitation". In: *Journal of Biomechanical Engineering* 131 (2009), p. 031011.

[45] C. T. Freeman, A. M Hughes, J. H. Burridge, P. H. Chappell, P. L. Lewin, and E. Rogers. "Iterative learning control of FES applied to the upper extremity for rehabilitation". In: *Control Engineering Practice* 17.3 (2009), pp. 368–381. DOI: 10.1016/j.conengprac.2008.08.003.

[46] C T Freeman, D Tong, K Meadmore, Z Cai, E Rogers, A M Hughes, and J H Burridge. "Phase-lead iterative learning control algorithms for functional electrical stimulation-based stroke rehabilitation". In: *Proceedings of the Institution of Mechanical Engineers, Part I: Journal of Systems and Control Engineering* 225.6 (2011), pp. 850–859. DOI: 10.1177/0959651811408976.

[47] Chris T Freeman, Eric Rogers, A Hughes, Jane H Burridge, and Katie L Meadmore. "Iterative learning control in health care: Electrical stimulation and robotic-assisted upper-limb stroke rehabilitation". In: *Control Systems, IEEE* 32.1 (2012), pp. 18–43.

[48] Chris Freeman, Eric Rogers, Jane H Burridge, Ann-Marie Hughes, and Katie L Meadmore. *Iterative Learning Control for Electrical Stimulation and Stroke Rehabilitation*. Springer, 2015.

[49] C.T. Freeman, E. Rogers, A Hughes, J.H. Burridge, and K.L. Meadmore. "Iterative Learning Control in Health Care: Electrical Stimulation and Robotic-Assisted Upper-Limb Stroke Rehabilitation". In: *IEEE Control Systems* 32.1 (Feb. 2012), pp. 18–43. ISSN: 1066-033X. DOI: 10.1109/MCS.2011.2173261.

[50] C. Fu and R. Wang. "The Influence of Co-Contraction to the Arm Impedance During Free Planar Movement". In: *2009 3rd International Conference on Bioinformatics and Biomedical Engineering*. June 2009, pp. 1–3. DOI: 10.1109/ICBBE.2009.5163625.

[51] T. Fujiwara, Y. Kasashima, K. Honaga, Y. Muraoka, T. Tsuji, R. Osu, K. Hase, Y. Masakado, and M. Liu. "Motor improvement and corticospinal modulation induced by hybrid assistive neuromuscular dynamic stimulation (HANDS) therapy in patients with chronic stroke". In: *Neurorehabil Neural Repair* 23.2 (Feb. 2009), pp. 125–32. DOI: 10.1177/1545968308321777.

[52] M. Gandolla, S. Ferrante, F. Molteni, E. Guanziroli, T. Frattini, A. Martegani, G. Ferrigno, K. Friston, A. Pedrocchi, and N.S. Ward. "Re-thinking the role of motor cortex: context-sensitive motor outputs?" In: *Neuroimage* 91 (May 2014), pp. 366–74. DOI: 10.1016/j.neuroimage.2014.01.011.

[53] Huijun Gao and Tongwen Chen. "Stabilization of nonlinear systems under variable sampling: a fuzzy control approach". In: *Fuzzy Systems, IEEE Transactions on* 15.5 (2007), pp. 972–983.

[54] J. P. Giuffrida and P. E. Crago. "Functional restoration of elbow extension after spinal-cord injury using a neural network-based synergistic FES controller". In: *IEEE Transactions on Neural Systems and Rehabilitation Engineering* 13.2 (June 2005), pp. 147–152. ISSN: 1534-4320. DOI: 10.1109/TNSRE.2005.847375.

[55] Joseph P Giuffrida and Patrick E Crago. "Reciprocal EMG control of elbow extension by FES". In: *Neural Systems and Rehabilitation Engineering, IEEE Transactions on* 9.4 (2001), pp. 338–345.

[56] Michela Goffredo, Ivan Bernabucci, Maurizio Schmid, and Silvia Conforto. "A neural tracking and motor control approach to improve rehabilitation of upper limb movements". In: *Journal of NeuroEngineering and Rehabilitation* 5.1 (Feb. 2008), p. 5. ISSN: 1743-0003. DOI: 10.1186/1743-0003-5-5. URL: https://doi.org/10.1186/1743-0003-5-5.

[57] G.C. Goodwin, J.C. Agüero, M. Garrido, and J.I. Yuz. "Sampling and Sampled-Data Models". In: *IEEE control systems magazine* 33.5 (2013), pp. 34–53.

[58] Yukihiro Hara. "Neurorehabilitation with new functional electrical stimulation for hemiparetic upper extremity in stroke patients". In: *Journal of Nippon Medical School* 75.1 (2008), pp. 4–14.

[59] Yukihiro Hara. "Rehabilitation with Functional Electrical Stimulation in Stroke Patients". In: *International Journal of Physical Medicine & Rehabilitation* 01.6 (2013). ISSN: 23299096. DOI: 10.4172/2329-9096.1000147. URL: http://omicsonline.org/rehabilitation-with-functional-electrical-stimulation-in-stroke-patients-2329-9096.1000147.php?aid=17939 (visited on 10/29/2014).

[60] Yukihiro Hara, Shinji Ogawa, and Yoshihiro Muraoka. "Hybrid power-assisted functional electrical stimulation to improve hemiparetic upper-extremity function". In: *American journal of physical medicine & rehabilitation* 85.12 (2006), pp. 977–985.

[61] Yukihiro Hara, Shinji Ogawa, Kazuhito Tsujiuchi, and Yoshihiro Muraoka. "A home-based rehabilitation program for the hemiplegic upper extremity by power-assisted functional electrical stimulation". In: *Disability and Rehabilitation* 30.4 (2008). PMID: 17852312, pp. 296–304. DOI: 10.1080/09638280701265539.

[62] Richard L Harvey, Richard F Macko, Joel Stein, Carolee J Winstein, Richard D Zorowitz, et al. *Stroke recovery and rehabilitation*. Demos Medical Publishing, 2008.

[63] Mitsuhiro Hayashibe. "Evoked Electromyographically Controlled Electrical Stimulation". In: *Frontiers in Neuroscience* 10 (2016).

[64] WPMH Heemels, JH Sandee, and PPJ Van Den Bosch. "Analysis of event-driven controllers for linear systems". In: *International journal of control* 81.4 (2008), pp. 571–590.

[65] Dan Henriksson and Anton Cervin. "Optimal on-line sampling period assignment for real-time control tasks based on plant state information". In: *Proc. of the 44th IEEE Conference on Decision and Control and in Proc. of the European Control Conference (CDC and ECC'05)*. IEEE. 2005, pp. 4469–4474.

[66] Joao P Hespanha, Payam Naghshtabrizi, and Yonggang Xu. "A survey of recent results in networked control systems". In: *Proceedings of the IEEE* 95.1 (2007), pp. 138–162.

[67] A. V Hill. *First and last experiments in muscle mechanics*. Cambridge UP, 1970.

[68] J.A. Hoffer. *Closed-loop, implanted-sensor, functional electrical stimulation system for partial restoration of motor functions*. US Patent 4,750,499. June 1988. URL: https://www.google.com/patents/US4750499.

[69] N Hogan. "Adaptive control of mechanical impedance by coactivation of antagonist muscles". In: *IEEE Transactions on Automatic Control* 29.8 (1984), pp. 681–690. URL: http://ieeexplore.ieee.org/lpdocs/epic03/wrapper.htm?arnumber=1103644.

[70] Kenneth Horch and Daryl Kipke. *Neuroprosthetics: theory and practice*. Vol. 8. World Scientific, 2017.

[71] N. Hoshimiya, A. Naito, M. Yajima, and Y. Handa. "A multichannel FES system for the restoration of motor functions in high spinal cord injury patients: a respiration-controlled system for multijoint upper extremity". In: *IEEE Transactions on Biomedical Engineering* 36.7 (1989), pp. 754–760.

[72] A.M. Hughes, C.T. Freeman, J.H. Burridge, P.H. Chappell, P.L. Lewin, and E. Rogers. "Feasibility of Iterative Learning Control Mediated by Functional Electrical Stimulation for Reaching After Stroke". In: *Neurorehabilitation and Neural Repair* 23.6 (2009), pp. 559–568. DOI: 10.1177/1545968308328718.

[73] K. J. Hunt, M. Munih, N. d. N. Donaldson, and F. M. D. Barr. "Investigation of the Hammerstein hypothesis in the modeling of electrically stimulated muscle". In: *IEEE Transactions on Biomedical Engineering* 45.8 (1998), pp. 998–1009. ISSN: 0018-9294. DOI: 10.1109/10.704868.

[74] Kathleen M. Jagodnik and Antonie J. van den Bogert. "Optimization and evaluation of a proportional derivative controller for planar arm movement". In: *Journal of Biomechanics* 43.6 (2010), pp. 1086–1091. ISSN: 0021-9290. DOI: http://dx.doi.org/10.1016/j.jbiomech.2009.12.017. URL: http://www.sciencedirect.com/science/article/pii/S002192900900726X.

[75] S. Jezernik, R.G.V. Wassink, and T. Keller. "Sliding mode closed-loop control of FES controlling the shank movement". In: *Biomedical Engineering, IEEE Transactions on* 51.2 (Feb. 2004), pp. 263–272. ISSN: 0018-9294. DOI: 10.1109/TBME.2003.820393.

[76] Junichi Kameyama, Yasunobu Handa, Nozomu Hoshimiya, and Minoru Sakurai. "Restoration of Shoulder Movement in Quadriplegic and Hemiplegic Patients by Functional Electrical Stimulation Using Percutaneous Multiple Electrodes". In: *The Tohoku Journal of Experimental Medicine* 187.4 (1999), pp. 329–337. DOI: 10.1620/tjem.187.329.

[77] Jakob Karner, Werner Reichenfelser, and Margit Gfoehler. "Kinematic and kinetic analysis of human motion as design input for an upper extremity bracing system". In: *Proc. of IASTED International Conference Biomedical Engineering - BioMed 2012*. 764-105. ACTA Press, 2012.

[78] Trisha Kesar and Stuart Binder-Macleod. "Effect of frequency and pulse duration on human muscle fatigue during repetitive electrical stimulation". In: *Experimental physiology* 91.6 (2006), pp. 967–976.

[79] Trisha Kesar, Li-Wei Chou, and Stuart A. Binder-Macleod. "Effects of stimulation frequency versus pulse duration modulation on muscle fatigue". In: *Journal of Electromyography and Kinesiology* 18.4 (2008), pp. 662–671. ISSN: 1050-6411. DOI: http://dx.doi.org/10.1016/j.jelekin.2007.01.001. URL: http://www.sciencedirect.com/science/article/pii/S1050641107000028.

[80] C. Klauer, S. Ferrante, E. Ambrosini, U. Shiri, F. Dähne, I. Schmehl, A. Pedrocchi, and T. Schauer. "A patient-controlled functional electrical stimulation system for arm weight relief". In: *Medical Engineering & Physics* 38.11 (2016), pp. 1232–1243. DOI: 10.1016/j.medengphy.2016.06.006.

[81] C. Klauer, M. Irmer, and T. Schauer. "A muscle model for hybrid muscle activation". In: *Current Directions in Biomedical Engineering* 1.1 (2015), pp. 386–389. ISSN: 2364-5504. DOI: 10.1515/cdbme-2015-0094.

[82] C. Klauer, A. Passon, J. Raisch, and T. Schauer. "Virtual Weight-Compensating Exoskeleton using λ-Controlled FES". In: *Proc. of Automed 2013*. Dresden, Germany, 2013.

[83] C. Klauer, J. Raisch, and T. Schauer. "Advanced Control Strategies for Neuro-Prosthetic Systems". In: *Proc. of the 4th European Conference on Technically Assisted Rehabilitation - TAR 2013*. Berlin, Germany, 2013.

[84] C. Klauer, J. Raisch, and T. Schauer. "Feedback Control of the Electrical Stimulation Induced Muscular Recruitment Determined by the Evoked Electromyogram". In: *Biomedical Engineering / Biomedizinische Technik* 57.Suppl. 1, Track-F (2012), pp. 639–639. ISSN: 1862-278X. DOI: 10.1515/bmt-2012-4417.

[85] C. Klauer, J. Raisch, and T. Schauer. "Linearisation of electrically stimulated muscles by feedback control of the muscular recruitment measured by evoked EMG". In: *Proc. of the 17th International Conference on Methods and Models in Automation and Robotics 2012*. Międzyzdroje, Poland: IEEE, 2012, pp. 108–113. ISBN: 978-1-4673-2124-2. DOI: 10.1109/MMAR.2012.6347902.

[86] C. Klauer, J. Raisch, and T. Schauer. "Nonlinear Joint-Angle Feedback Control of Electrically Stimulated and Lambda-Controlled Antagonistic Muscle Pairs". In: *Proc. of the European Control Conference 2013*. Zürich, Switzerland: IEEE, 2013, pp. 3101–3107. ISBN: 978-3-033-03962-9.

[87] C. Klauer, M. Ruppel, and T. Schauer. "FES-based arm weight relief: First investigations in stroke patients". In: *Abstract in Proc. of the 6th European Conference on Technically Assisted Rehabilitation – TAR 2017*. Berlin, Germany, 2017.

[88] C. Klauer and T. Schauer. "Adaptive Control of a Neuroprosthesis for Stroke Patients Amplifying Weak Residual Shoulder-Muscle Activity". In: *Proc. of the 20th World Congress of the International Federation of Automatic Control, 9-14 July 2017*. Toulouse, France, 2017.

[89] C. Klauer and T. Schauer. "Discretisation & Control of Irregularly Actuated and Sampled LTI-Systems". In: *Proc. of the 19th International Conference on Methods and Models in Automation and Robotics, IEEE*. Międzyzdroje, Poland, 2014. ISBN: 978-1-4799-5081-2. DOI: 10.1109/MMAR.2014.6957394.

[90] C. Klauer, T. Schauer, J. Karner, W. Reichenfelser, E. Ambrosisni, S. Ferrante, and J. Raisch. "Design of feedback control strategies for an arm neuroprothesis combined with an exoskeleton". In: *Converging Clinical and Engineering Reseach on Neurorehabilitation - Part II, ICNR 2012*. Springer, 2012, pp. 1189–1193. ISBN: 978-3-642-34545-6.

[91] C. Klauer, T. Schauer, and J. Raisch. "Joint-angle control by electrical stimulation of antagonistic muscles (in German)". In: *at - Automatisierungstechnik* 59.10 (2011), pp. 629–637. DOI: doi:10.1524/auto.2011.0955.

[92] C. Klauer, T. Schauer, W. Reichenfelser, J. Karner, S. Zwicker, M. Gandolla, E. Ambrosini, S. Ferrante, M. Hack, A Jedlitschenka, A. Duschau-Wicke, M. Gföhler, and A. Pedrocchi. "Feedback Control of arm movements using Neuro-Muscular Electrical Stimulation (NMES) combined with a lockable, passive exoskeleton for gravity compensation". In: *Frontiers in Neuroscience* 8.262 (2014). DOI: 10.3389/fnins.2014.00262.

[93] C. Klauer and Schauer T. "Two-Channel Muscle Recruitment (λ)-Control using the Evoked-EMG". In: *Proc. of the 20th Annual International FES Society Conference 2016*. La Grande Motte, France, 2016.

[94] JS Knutson and J Chae. "Functional electrical stimulation (FES) for upper limb function after stroke". In: *Implantable Neuroprostheses for Restoring Function*. Elsevier, 2015, pp. 307–329. DOI: 10.1016/B978-1-78242-101-6.00014-8.

[95] Hamid-Reza Kobravi and Abbas Erfanian. "Decentralized adaptive robust control based on sliding mode and nonlinear compensator for the control of ankle movement using functional electrical stimulation of agonist–antagonist muscles". In: *Journal of Neural Engineering* 6.4 (2009), p. 046007. URL: http://stacks.iop.org/1741-2552/6/i=4/a=046007.

[96] Engin Koyuncu, Güldal Funda Nakipoğlu-Yüzer, Asuman Doğan, and Neşe Özgirgin. "The effectiveness of functional electrical stimulation for the treatment of shoulder subluxation and shoulder pain in hemiplegic patients: A randomized controlled trial". In: *Disability and Rehabilitation* 32.7 (2010). PMID: 20136474, pp. 560–566. DOI: 10.3109/09638280903183811.

[97] M. Kutlu, C. T. Freeman, E. Hallewell, A. M. Hughes, and D. S. Laila. "FES-based upper-limb stroke rehabilitation with advanced sensing and control". In: *2015 IEEE International Conference on Rehabilitation Robotics (ICORR)*. 2015, pp. 253–258. DOI: 10.1109/ICORR.2015.7281208.

[98] M. Kutlu, C.T. Freeman, E. Hallewell, A-M. Hughes, and D.S. Laila. "Upper-limb stroke rehabilitation using electrode-array based functional electrical stimulation with sensing and control innovations". In: *Medical Engineering & Physics* 38.4 (2016), pp. 366–379. ISSN: 1350-4533. DOI: http://dx.doi.org/10.1016/j.medengphy.2016.01.004. URL: http://www.sciencedirect.com/science/article/pii/S1350453316000254.

[99] Gert Kwakkel, Boudewijn J. Kollen, and Hermano I. Krebs. "Effects of Robot-Assisted Therapy on Upper Limb Recovery After Stroke: A Systematic Review". In: *Neurorehabilitation and Neural Repair* 22.2 (2008), pp. 111–121. DOI: 10.1177/1545968307305457.

[100] Pierre P Lagasse and Michel-Andre Roy. "Functional electrical stimulation and the reduction of co-contraction in spastic biceps brachii". In: *Clinical Rehabilitation* 3.2 (1989), pp. 111–116. DOI: 10.1177/026921558900300205. eprint: http://dx.doi.org/10.1177/026921558900300205. URL: http://dx.doi.org/10.1177/026921558900300205.

[101] Mark L Latash. *Neurophysiological basis of movement*. Human Kinetics, 2008.

[102] Z. Li, M. Hayashibe, D. Andreu, and D. Guiraud. "Real-time closed-loop FES control of muscle activation with evoked EMG feedback". In: *2015 7th International IEEE/EMBS Conference on Neural Engineering (NER)*. Apr. 2015, pp. 623–626. DOI: 10.1109/NER.2015.7146700.

[103] Z Li, M Hayashibe, C Fattal, and D Guiraud. "Muscle Fatigue Tracking with Evoked EMG via Recurrent Neural Network: Toward Personalized Neuroprosthetics". In: *Computational Intelligence Magazine, IEEE* 9.2 (2014), pp. 38–46.

[104] Z. Li, M. Hayashibe, Q. Zhang, and D. Guiraud. "FES-induced muscular torque prediction with evoked EMG synthesized by NARX-type recurrent neural network". In: *2012 IEEE/RSJ International Conference on Intelligent Robots and Systems*. Oct. 2012, pp. 2198–2203. DOI: 10.1109/IROS.2012.6385602.

[105] Zhan Li, David Guiraud, David Andreu, Mourad Benoussaad, Charles Fattal, and Mitsuhiro Hayashibe. "Real-time estimation of FES-induced joint torque with evoked EMG". In: *Journal of NeuroEngineering and Rehabilitation* 13.1 (2016), p. 60.

[106] Zheng Li and Mo-Yuen Chow. "Adaptive multiple sampling rate scheduling of real-time networked supervisory control system-part ii". In: *IEEE Industrial Electronics, IECON 2006-32nd Annual Conference on*. IEEE. 2006, pp. 4615–4620.

[107] Yu-Wei Liao, Eric M. Schearer, Eric J. Perreault, Matthew C. Tresch, and Kevin M. Lynch. "Multi-muscle FES control of the human arm for interaction tasks—stabilizing with muscle co-contraction and postural adjustment: a simulation study". In: *Intelligent Robots and Systems (IROS 2014), 2014 IEEE/RSJ International Conference on*. IEEE. 2014, pp. 2134–2139.

[108] Jing Z. Liu, Robert W. Brown, and Guang H. Yue. "A Dynamical Model of Muscle Activation, Fatigue, and Recovery". In: *Biophysical Journal* 82.5 (2002), pp. 2344–2359. ISSN: 0006-3495. DOI: 10.1016/S0006-3495(02)75580-X. URL: http://www.sciencedirect.com/science/article/pii/S000634950275580X.

[109] L. Ljung. *System identification*. Prentice Hall, 1999.

[110] D. G. Lloyd and T. F. Besier. "An EMG-driven musculoskeletal model to estimate muscle forces and knee joint moments in vivo". In: *Journal of biomechanics* 36.6 (2003), pp. 765–776.

[111] Jan Lunze and Daniel Lehmann. "A state-feedback approach to event-based control". In: *Automatica* 46.1 (2010), pp. 211–215.

[112] C. L. Lynch and M. R. Popovic. "Functional Electrical Stimulation". In: *IEEE Control Systems* 28.2 (2008), pp. 40–50. ISSN: 1066-033X. DOI: 10.1109/MCS.2007.914689.

[113] C. L. Lynch, D. Sayenko, and M. R. Popovic. "Co-contraction of antagonist muscles during knee extension against gravity: Insights for functional electrical stimulation control design". In: *2012 Annual International Conference of the IEEE Engineering in Medicine and Biology Society*. Aug. 2012, pp. 1843–1846. DOI: 10.1109/EMBC.2012.6346310.

[114] CL Lynch and MR Popovic. "Closed-loop control for FES: Past work and future directions". In: *10th Annual Conference of the International FES Society*. 2005.

[115] G.M. Lyons, T. Sinkjær, J.H. Burridge, and D.J. Wilcox. "A review of portable FES-based neural orthoses for the correction of drop foot". In: *Neural Systems and Rehabilitation Engineering, IEEE*. IEEE (2002).

[116] Paweł Maciejasz, Jörg Eschweiler, Kurt Gerlach-Hahn, Arne Jansen-Troy, and Steffen Leonhardt. "A survey on robotic devices for upper limb rehabilitation". In: *Journal of NeuroEngineering and Rehabilitation* 11.1 (2014), p. 3. ISSN: 1743-0003. DOI: 10.1186/1743-0003-11-3. URL: http://dx.doi.org/10.1186/1743-0003-11-3.

[117] V. Maheu, J. Frappier, P.S. Archambault, and F. Routhier. "Evaluation of the JACO robotic arm: Clinico-economic study for powered wheelchair users with upper-extremity disabilities". In: *Proc. of IEEE International Conference on Rehabilitation Robotics (ICORR)*. 2011, pp. 1–5. DOI: http://dx.doi.org/10.1109/ICORR.2011.5975397.

[118] Sébastien Mariéthoz and Manfred Morari. "Explicit Model-Predictive Control of a PWM Inverter With an LCL Filter". In: *Industrial Electronics, IEEE Transactions on* 56.2 (2009), pp. 389–399.

[119] Winfried Mayr, Christian Hofer, Manfred Bijak, Dietmar Rafolt, Ewald Unger, S Sauermann, H Lanmueller, and H Kern. "Functional Electrical Stimulation (FES) of denervated muscles: existing and prospective technological solutions". In: *Basic and applied myology (BAM)* 12.6 (2002), pp. 287–290. ISSN: 1120-9992.

[120] Katie L. Meadmore, Timothy A. Exell, Emma Hallewell, Ann-Marie Hughes, Chris T. Freeman, Mustafa Kutlu, Valerie Benson, Eric Rogers, and Jane H. Burridge. "The application of precisely controlled functional electrical stimulation to the shoulder, elbow and wrist for upper limb stroke rehabilitation: a feasibility study". In: *Journal of NeuroEngineering and Rehabilitation* 11.1 (2014), pp. 1–11. DOI: 10.1186/1743-0003-11-105. URL: http://dx.doi.org/10.1186/1743-0003-11-105.

[121] Katie L. Meadmore, Ann-Marie Hughes, Chris T. Freeman, Zhonglun Cai, Daisy Tong, Jane H. Burridge, and Eric Rogers. "Functional electrical stimulation mediated by iterative learning control and 3D robotics reduces motor impairment in chronic stroke". In: *Journal of NeuroEngineering and Rehabilitation* 9.1 (2012), p. 32. ISSN: 1743-0003. DOI: 10.1186/1743-0003-9-32. URL: http://dx.doi.org/10.1186/1743-0003-9-32.

[122] A Meilink, B Hemmen, HAM Seelen, and G Kwakkel. "Impact of EMG-triggered neuromuscular stimulation of the wrist and finger extensors of the paretic hand after stroke: a systematic review of the literature". In: *Clinical rehabilitation* 22.4 (2008), pp. 291–305.

[123] R. Merletti, M. Knaflitz, and C. J. De Luca. "Myoelectric manifestations of fatigue in voluntary and electrically elicited contractions". In: *Journal of Applied Physiology* 69.5 (1990), pp. 1810–1820. ISSN: 8750-7587. eprint: http://jap.physiology.org/content/69/5/1810.full.pdf. URL: http://jap.physiology.org/content/69/5/1810.

[124] R. Merletti and P.A. Parker. *Electromyography: Physiology, engineering, and noninvasive applications*. Wiley-IEEE Press, 2004.

[125] P. Meyer-Rachner, A. Passon, C. Klauer, and T. Schauer. "Compensating the effects of FES-Induced Muscle Fatigue by Rehabilitation Robotics During Arm Weight Support". In: *Current Directions in Biomedical Engineering, Proc. of the 6th European Conference on Technically Assisted Rehabilitation – TAR 2017*. Berlin, Germany, 2017. DOI: 10.1515/cdbme-2017-0007.

[126] T. E. Milner and C. Cloutier. "The effect of antagonist muscle co-contraction on damping of the wrist joint during voluntary movement". In: *Engineering in Medicine and Biology Society, 1995., IEEE 17th Annual Conference*. Vol. 2. Sept. 1995, 1247–1248 vol.2. DOI: 10.1109/IEMBS.1995.579664.

[127] P. Müller, M. A. Begin, T. Schauer, and T. Seel. "Alignment-Free, Self-Calibrating Elbow Angles Measurement using Inertial Sensors". In: *IEEE Journal of Biomedical and Health Informatics* 21.2 (2017), pp. 312–319. ISSN: 2168-2194. DOI: 10.1109/JBHI.2016.2639537. URL: http://ieeexplore.ieee.org/document/7782745/.

[128] Nathan, R. H. and Ohry A. "Upper limb functions regained in quadriplegia: a hybrid computerized neuromuscular stimulation system." In: *Archives of physical medicine and rehabilitation* 71 (1990), pp. 415–421.

[129] V. Nekoukar and A. Erfanian. "A Decentralized Modular Control Framework for Robust Control of FES-Activated Walker-Assisted Paraplegic Walking Using Terminal Sliding Mode and Fuzzy Logic Control". In: *IEEE Transactions on Biomedical Engineering* 59.10 (2012), pp. 2818–2827. ISSN: 0018-9294. DOI: 10.1109/TBME.2012.2208963.

[130] O. Nelles. *Nonlinear system identification: from classical approaches to neural networks and fuzzy models*. Springer Verlag, 2001.

[131] D. A. Nowak, E Altenmüller, M Ameli, F Binkofski, R Blank, B Brandauer, JM Burgunder, K Campen, A Conrad, M Dafotakis, et al. *Handfunktionsstörungen in der Neurologie*. Springer, 2011.

[132] A. Passon, T. Klewe, T. Seel, and T. Schauer. "A new approach for a Patient-Cooperative Upper Limb FES Support based on Vector Fields". In: *Proc. of the 20th World Congress of the International Federation of Automatic Control, 9-14 July 2017*. Toulouse, France, 2017.

[133] P Hunter Peckham and Jayme S Knutson. "Functional electrical stimulation for neuromuscular applications". In: *Annual Review of Biomedical Engineering* 7 (2005), pp. 327–360. ISSN: 1523-9829.

[134] Alessandra Pedrocchi, Simona Ferrante, Emilia Ambrosini, Marta Gandolla, Claudia Casellato, Thomas Schauer, Christian Klauer, Javier Pascual, Carmen Vidaurre, Margit Gfoehler, Werner Reichenfelser, Jakob Karner, Silvestro Micera, Andrea Crema, Franco Molteni, Mauro Rossini, Giovanna Palumbo, Eleonora Guanziroli, Andreas Jedlitschka, Marco Hack, Maria Bulgheroni, Enrico D Amico, Peter Schenk, Sven Zwicker, Alexander Duschau-Wicke, Justinas Miseikis, Lina Graber, and Giancarlo Ferrigno. "MUNDUS project: MUltimodal Neuroprosthesis for daily Upper limb Support". In: *J Neuroeng Rehabil* 10.1 (2013), p. 66.

[135] A. Pedrocchi, S. Ferrante, E. Ambrosini, M. Gandolla, C. Casellato, T Schauer, C. Klauer, J. Pascual, C. Vidaurre, M. Gfoehler, et al. "MUNDUS project: MUltimodal Neuroprosthesis for daily Upper limb Support". In: *Journal of neuroengineering and rehabilitation* 10.66 (2013), pp. 1–20. DOI: 10.1186/1743-0003-10-66.

[136] Dejan Popovic and Thomas Sinkjaer. *Control of movement for the physically disabled: control for rehabilitation technology*. Springer Science & Business Media, 2012.

[137] Dejan Popovic, Richard B Stein, M Namik Oguztoreli, Maria Lebiedowska, and Slavica Jonic. "Optimal control of walking with functional electrical stimulation: a computer simulation study". In: *Rehabilitation Engineering, IEEE Transactions on* 7.1 (1999), pp. 69–79.

[138] M. Popovic and D. Popovic. "Cloning biological synergies improves control of elbow neuroprostheses". In: *IEEE Engineering in Medicine and Biology Magazine* 20.1 (2001), pp. 74–81. ISSN: 0739-5175. DOI: 10.1109/51.897830.

[139] M. Popović and D. Popović. "A new approach to reaching control for tetraplegic subjects". In: *Journal of Electromyography and Kinesiology* 4.4 (1994), pp. 242–253. ISSN: 1050-6411. DOI: 10.1016/1050-6411(94)90011-6.

[140] Mirjana B. Popovic, Dejan B. Popovic, Laszlo Schwirtlich, and Thomas Sinkjær. "Functional Electrical Therapy (FET): Clinical Trial in Chronic Hemiplegic Subjects". In: *Neuromodulation: Technology at the Neural Interface* 7.2 (2004), pp. 133–140. ISSN: 1525-1403. DOI: 10.1111/j.1094-7159.2004.04017.x. URL: http://dx.doi.org/10.1111/j.1094-7159.2004.04017.x.

[141] Mirjana B Popovic, Dejan B Popovic, Thomas Sinkjær, Aleksandra Stefanovic, and Laszlo Schwirtlich. "Clinical evaluation of functional electrical therapy in acute hemiplegic subjects". In: *Journal of rehabilitation research and development* 40.5 (2003), p. 443.

[142] Mirjana B Popovic, Dejan B Popovic, Thomas Sinkjær, Aleksandra Stefanovic, and Laszlo Schwirtlich. "Restitution of reaching and grasping promoted by functional electrical therapy". In: *Artificial organs* 26.3 (2002), pp. 271–275.

[143] E. Previdi, T. Schauer, A. Lecchini, S. M. Savaresi, and K. J. Hunt. "Virtual reference feedback tuning for knee joint position control using functional electrical stimulation". In: (2001), pp. 3923–3928.

[144] Fabio Previdi and Emanuele Carpanzano. "Design of a gain scheduling controller for knee-joint angle control by using functional electrical stimulation". In: *Control Systems Technology, IEEE Transactions on* 11.3 (2003), pp. 310–324.

[145] Werner Reichenfelser, Jakob Karner, and Margit Gföhler. "Modular Instrumented Arm Orthosis with Weight Support for Application with NMES". In: *Converging Clinical and Engineering Research on Neurorehabilitation*. Ed. by José Pons, Diego Torricelli, and Marta Pajaro. Vol. 2. Springer, 2013, pp. 1159–1163.

[146] F. Resquín, J. Gonzalez-Vargas, J. Ibáñez, F. Brunetti, and J. L. Pons. "Feedback error learning controller for functional electrical stimulation assistance in a hybrid robotic system for reaching rehabilitation". In: *European journal of translational myology* 26.3 (2016).

[147] Francisco Resquín, Alicia Cuesta Gómez, Jose Gonzalez-Vargas, Fernando Brunetti, Diego Torricelli, Francisco Molina Rueda, Roberto Cano de la Cuerda, Juan Carlos Miangolarra, and José Luis Pons. "Hybrid robotic systems for upper limb rehabilitation after stroke: A review". In: *Medical Engineering & Physics* 38.11 (2016), pp. 1279–1288. ISSN: 1350-4533. DOI: http://dx.doi.org/10.1016/j.medengphy.2016.09.001. URL: //www.sciencedirect.com/science/article/pii/S1350453316302016.

[148] R. Riener. "Model–based Development of Neuroprostheses for Paraplegic Patients". In: *Philosophical Transactions of the Royal Society of London. Series B: Biological Sciences* 354.1385 (1999), pp. 877–894. ISSN: 0962-8436, 1471-2970. DOI: 10.1098/rstb.1999.0440.

[149] R. Riener and T. Fuhr. "Patient-driven control of FES-supported standing up". In: *IEEE Trans. Rehabil. Eng* 6.2 (1998), pp. 113–124.

[150] Robert Riener and Jochen Quintern. "A physiologically based model of muscle activation verified by electrical stimulation". In: *Bioelectrochemistry and Bioenergetics* 43.2 (1997), pp. 257–264.

[151] M Rohm, GR Müller-Putz, A Kreilinger, A von Ascheberg, and R Rupp. "A hybrid-Brain Computer Interface for control of a reaching and grasping neuroprosthesis". In: *Biomed Tech* 55 (2010), pp. 1–4.

[152] M. Ruppel, C. Klauer, and T. Schauer. "Enhancing the smoothness of joint motion induced by functional electrical stimulation using co-activation strategies". In: *Current Directions in Biomedical Engineering* 3.2 (2017), pp. 155–159. ISSN: 2364-5504. DOI: 10.1515/cdbme-2017-0033.

[153] M. Ruppel, C. Klauer, and T. Schauer. "Towards a High Motor-Precision Neuroprosthesis by Recruitment-Controlled Antagonistic Muscle Co-activation Strategies". In: *Abstract in Proc. of the 6th European Conference on Technically Assisted Rehabilitation – TAR 2017*. Berlin, Germany, 2017.

[154] D N Rushton. "Functional electrical stimulation". In: *Physiological Measurement* 18 (Nov. 1997), pp. 241–275. ISSN: 0967-3334, 1361-6579. DOI: 10.1088/0967-3334/18/4/001. URL: http://iopscience.iop.org/0967-3334/18/4/001 (visited on 10/21/2011).

[155] S. H. Sadat-Hosseini and A. Erfanian. "Sliding mode control of intramuscular functional electrical stimulation using fuzzy neural network with terminal sliding mode learning". In: *2015 7th International IEEE/EMBS Conference on Neural Engineering (NER)*. Apr. 2015, pp. 775–778. DOI: 10.1109/NER.2015.7146738.

[156] S. Saxena, S. Nikolić, and D. Popović. "An EMG-controlled grasping system for tetraplegics". In: *J Rehabil Res Dev* 32.1 (Feb. 1995), pp. 17–24.

[157] T Schauer, William Holderbaum, and KJ Hunt. "Sliding-mode control of knee-joint angle: experimental results". In: *Proc. of the 7th Annual International FES Society Conference, Ljubljana, Slovenia*. 2002.

[158] T Schauer, N-O Negård, F Previdi, KJ Hunt, MH Fraser, E Ferchland, and J Raisch. "Online identification and nonlinear control of the electrically stimulated quadriceps muscle". In: *Control Engineering Practice* 13.9 (2005), pp. 1207–1219.

[159] Thomas Schauer and Kenneth J. Hunt. "Linear Controller Design for the Single Limb Movement of Paraplegics". In: *IFAC Proceedings Volumes* 33.3 (2000). 4th IFAC Symposium on Modelling and Control in Biomedical Systems 2000, Karlsburg/Greifswald, Germany, 30 March-1 April 2000, pp. 7–12. ISSN: 1474-6670. DOI: http://dx.doi.org/10.1016/S1474-6670(17)35480-0. URL: http://www.sciencedirect.com/science/article/pii/S1474667017354800.

[160] Eric M. Schearer, Yu-Wei Liao, Eric J. Perreault, Matthew C. Tresch, William D. Memberg, Robert F. Kirsch, and Kevin M. Lynch. "Identifying inverse human arm dynamics using a robotic testbed". In: *Intelligent Robots and Systems (IROS 2014), 2014 IEEE/RSJ International Conference on*. IEEE. 2014, pp. 3585–3591.

[161] Eric M. Schearer, Yu-Wei Liao, Eric J. Perreault, Matthew C. Tresch, William D. Memberg, Robert F. Kirsch, and Kevin M. Lynch. "Multi-muscle FES force control of the human arm for arbitrary goals". In: *IEEE Transactions on Neural Systems and Rehabilitation Engineering* 22.3 (2014), pp. 654–663.

[162] Eric M. Schearer, Derek N. Wolf, and Robert F. Kirsch. "Quasi-Static Control of Whole-Arm Motions with FES". In: *Converging Clinical and Engineering Research on Neurorehabilitation II: Proceedings of the 3rd International Conference on NeuroRehabilitation (ICNR2016), October 18-21, 2016, Segovia, Spain*. Ed. by Jaime Ibáñez, José González-Vargas, José María Azorín, Metin Akay, and José Luis Pons. Cham: Springer International Publishing, 2017, pp. 673–677. ISBN: 978-3-319-46669-9. DOI: 10.1007/978-3-319-46669-9_111. URL: http://dx.doi.org/10.1007/978-3-319-46669-9_111.

[163] Oliver Schill, Roland Wiegand, Bastian Schmitz, Richard Matthies, Ute Eck, Christian Pylatiuk, Markus Reischl, Stefan Schulz, and Rüdiger Rupp. "OrthoJacket: an active FES-hybrid orthosis for the paralysed upper extremity." In: *Biomed Tech* 56.1 (2011), pp. 35–44. ISSN: 1862-278X.

[164] Michael Schinkel, Wen-Hua Chen, and Anders Rantzer. "Optimal control for systems with varying sampling rate". In: *American Control Conference, 2002. Proceedings of the 2002*. Vol. 4. IEEE. 2002, pp. 2979–2984.

[165] Søren Sennels, F Biering-Sorensen, Ole Trier Andersen, and Steffen Duus Hansen. "Functional neuromuscular stimulation controlled by surface electromyographic signals produced by volitional activation of the same muscle: adaptive removal of the muscle response from the recorded EMG-signal". In: *IEEE Transactions on Rehabilitation Engineering* 5.2 (1997), pp. 195–206.

[166] R. Shalaby. "Development of an Electromyography Detection System for the Control of Functional Electrical Stimulation in Neurological Rehabilitation". Doctoral Thesis. TU Berlin, 2011. URL: http://opus.kobv.de/tuberlin/volltexte/2011/3177.

[167] L. R. Sheffler and J. Chae. "Neuromuscular electrical stimulation in neurorehabilitation". In: *Muscle & nerve* 35.5 (2007), pp. 562–590.

[168] Rui N Silva, Joao M Lemos, and Luis M Rato. "Variable sampling adaptive control of a distributed collector solar field". In: *Control Systems Technology, IEEE Transactions on* 11.5 (2003), pp. 765–772.

[169] B. T. Smith, M. J. Mulcahey, and R. R. Betz. "Development of an upper extremity FES system for individuals with C4 tetraplegia". In: *IEEE Transactions on Rehabilitation Engineering* 4.4 (1996), pp. 264–270.

[170] Moshe Solomonow, Richard V. Baratta, and Robert D'Ambrosia. "EMG-force relations of a single skeletal muscle acting across a joint: Dependence on joint angle". In: *Journal of Electromyography and Kinesiology* 1.1 (1991), pp. 58–67. ISSN: 1050-6411. DOI: http://dx.doi.org/10.1016/1050-6411(91)90027-3. URL: http://www.sciencedirect.com/science/article/pii/1050641191900273.

[171] Moshe Solomonow, Richard Baratta, Hiromu Shoji, and Robert D D'Ambrosia. "The Myoelectric Signal of Electrically Stimulated Muscle During Recruitment: An Inherent Feedback Pareter for a Closed-Loop Control Scheme". In: *Biomedical Engineering, IEEE Transactions on* 8 (1986), pp. 735–745.

[172] Moshe Solomonow, Richard Baratta, Bing He Zhou, Hiromu Shoji, and Robert D D'Ambrosia. "The EMG-force model of electrically stimulated muscle: dependence on control strategy and predominant fiber composition". In: *Biomedical Engineering, IEEE Transactions on* 9 (1987), pp. 692–703.

[173] Moshe Solomonow, Chris Baten, Jos Smit, Richard Baratta, Hermie Hermens, Robert D'Ambrosia, and Hiromu Shoji. "Electromyogram power spectra frequencies associated with motor unit recruitment strategies". In: *Journal of Applied Physiology* 68.3 (1990), pp. 1177–1185.

[174] P. Spagnol, C. Klauer, F. Previdi, J. Raisch, and T. Schauer. "Modeling and Online-Identification of Electrically Stimulated Antagonistic Muscles for Horizontal Shoulder Abduction and Adduction". In: *Proc. of the European Control Conference 2013*. Zürich, Switzerland: IEEE, 2013, pp. 3979–3984. ISBN: 978-3-033-03962-9.

[175] Ming Sun and J.O. Hill. "A method for measuring mechanical work and work efficiency during human activities". In: *Journal of Biomechanics* 26.3 (1993), pp. 229–241. ISSN: 0021-9290. DOI: http://dx.doi.org/10.1016/0021-9290(93)90361-H. URL: http://www.sciencedirect.com/science/article/pii/002192909390361H.

[176] P Taylor, J Esnouf, and J Hobby. "The functional impact of the Freehand System on tetraplegic hand function. Clinical Results". In: *Spinal Cord* 40.11 (2002), p. 560.

[177] Dejan Tepavac and Laszlo Schwirtlich. "Detection and prediction of FES-induced fatigue". In: *Journal of Electromyography and Kinesiology* 7.1 (1997), pp. 39–50. ISSN: 1050-6411. DOI: http://dx.doi.org/10.1016/S1050-6411(96)00008-9. URL: http://www.sciencedirect.com/science/article/pii/S1050641196000089.

[178] Rune Thorsen, Ilaria Carpinella, and Maurizio Ferrarin. "Can the F-Response be Volitionally Repressed during Functional Electrical Stimulation?" In: *Neuromodulation: Technology at the Neural Interface* 8.2 (2005), pp. 141–147. ISSN: 1525-1403. DOI: 10.1111/j.1525-1403.2005.00230.x. URL: http://dx.doi.org/10.1111/j.1525-1403.2005.00230.x.

[179] Rune Thorsen, Davide Dalla Costa, Sara Chiaramonte, Luca Binda, Ettore Beghi, Tiziana Redaelli, Eugenio Occhi, and Maurizio Ferrarin. "A noninvasive neuroprosthesis augments hand grasp force in individuals with cervical spinal cord injury: The functional and therapeutic effects". In: *The Scientific World Journal* 2013 (2013).

[180] Rune Thorsen, Raffaella Spadone, and Maurizio Ferrarin. "A pilot study of myoelectrically controlled FES of upper extremity". In: *IEEE Transactions on Neural Systems and Rehabilitation Engineering* 9.2 (2001), pp. 161–168.

[181] T Truelsen, B Piechowski-Jóźwiak, R Bonita, C Mathers, J Bogousslavsky, and G Boysen. "Stroke incidence and prevalence in Europe: a review of available data". In: *European journal of neurology* 13.6 (2006), pp. 581–598.

[182] M. Valtin, T. Schauer, C. Behling, M. Daniel, and M. Weber. "Combined stimulation and measurement system for array electrodes". In: *Proc. of the International Conference on Biomedical Electronics and Devices - Biodevices 2012*. Algarve, Portugal, 2012, pp. 345–349X.

[183] Markus Valtin, Kristian Kociemba, Carsten Behling, Björn Kuberski, Sebastian Becker, and Thomas Schauer. "RehaMovePro: A versatile mobile stimulation system for transcutaneous FES applications". In: *European Journal of Translational Myology* 26.3 (2016).

[184] C. Vidaurre, C. Klauer, T. Schauer, A. Ramos-Murguialday, and K.R. Müller. "EEG-based BCI for the Linear Control of an Upper-Limb Neuroprosthesis". In: *Medical Engineering & Physics* 38.11 (2016), pp. 1195–1204. DOI: 10.1016/j.medengphy.2016.06.010.

[185] T. Vukova, M. Vydevska-Chichova, and N. Radicheva. "Fatigue-induced changes in muscle fiber action potentials estimated by wavelet analysis". In: *Journal of Electromyography and Kinesiology* 18.3 (2008), pp. 397–409. ISSN: 1050-6411. DOI: http://dx.doi.org/10.1016/j.jelekin.2006.09.014. URL: http://www.sciencedirect.com/science/article/pii/S105064110600126X.

[186] A. J. Westerveld, A. C. Schouten, P. H. Veltink, and H. van der Kooij. "Passive reach and grasp with functional electrical stimulation and robotic arm support". In: *2014 36th Annual International Conference of the IEEE Engineering in Medicine and Biology Society*. 2014, pp. 3085–3089. DOI: 10.1109/EMBC.2014.6944275.

[187] Jeffrey Winslow, Patrick L. Jacobs, and Dejan Tepavac. "Fatigue compensation during {FES} using surface {EMG}". In: *Journal of Electromyography and Kinesiology* 13.6 (2003), pp. 555–568. ISSN: 1050-6411. DOI: http://dx.doi.org/10.1016/S1050-6411(03)00055-5. URL: http://www.sciencedirect.com/science/article/pii/S1050641103000555.

[188] David A Winter. *Biomechanics and motor control of human movement*. John Wiley & Sons, 2009.

[189] F. C. Wu, Y. T. Lin, T. S. Kuo, J. J. Luh, and J. S. Lai. "Clinical effects of combined bilateral arm training with functional electrical stimulation in patients with stroke". In: *2011 IEEE International Conference on Rehabilitation Robotics*. June 2011, pp. 1–7. DOI: 10.1109/ICORR.2011.5975367.

[190] M. Yochum, T. Bakir, R. Lepers, and S. Binczak. "QUANTIFICATION OF MUSCLE FATIGUE WITH WAVELET ANALYSIS BASED ON EMG DURING MYOELECTRICAL STIMULATION". In: *Biostec 2012 - BIODEVICES 2012* 5.1 (2012), pp. 53–58.

[191] Dingguo Zhang, Tan Hock Guan, Ferdinan Widjaja, and Wei Tech Ang. "Functional electrical stimulation in rehabilitation engineering: A survey". In: *Proceedings of the 1st international convention on Rehabilitation engineering & assistive technology: in conjunction with 1st Tan Tock Seng Hospital Neurorehabilitation Meeting*. i-CREATe '07. New York, NY, USA: ACM, 2007, pp. 221–226. ISBN: 978-1-59593-852-7. DOI: 10.1145/1328491.1328546. URL: http://doi.acm.org/10.1145/1328491.1328546 (visited on 08/27/2013).

[192] Dingguo Zhang and Kuanyi Zhu. "Modeling biological motor control for human locomotion with functional electrical stimulation". In: *Biological cybernetics* 96.1 (2007), pp. 79–97.

[193] Q. Zhang, M. Hayashibe, and C. Azevedo-Coste. "Evoked Electromyography-Based Closed-Loop Torque Control in Functional Electrical Stimulation". In: *IEEE Transactions on Biomedical Engineering* 60.8 (Aug. 2013), pp. 2299–2307. ISSN: 0018-9294. DOI: 10.1109/TBME.2013.2253777.

[194] Q. Zhang, M. Hayashibe, P. Fraisse, and D. Guiraud. "FES-Induced Torque Prediction With Evoked EMG Sensing for Muscle Fatigue Tracking". In: *IEEE/ASME Transactions on Mechatronics* 16.5 (Oct. 2011), pp. 816–826. ISSN: 1083-4435. DOI: 10.1109/TMECH.2011.2160809.

[195] Q. Zhang, M. Hayashibe, and D. Guiraud. "Muscle fatigue tracking based on stimulus evoked EMG and adaptive torque prediction". In: *Proc. of IEEE ICRA 2011*. IEEE. 2011, pp. 1433–1438.

[196] Bing He Zhou, RV Baratta, M Solomonow, LJ Olivier, GT Nguyen, and RD D'Ambrosia. "Evaluation of isometric antagonist coactivation strategies of electrically stimulated muscles". In: *IEEE transactions on biomedical engineering* 43.2 (1996), pp. 150–160.